UNIVERSITÀ
DEGLI STUDI
DI PADOVA

Host Institution: Università degli Studi di Padova

Dipartimento di Geoscienze

DOCTORAL COURSE IN EARTH SCIENCES
SERIES XXIX

ARCHAEOMETRY OF TRACHYTE OF THE EUGANEAN HILLS (NE ITALY): PROVENANCE QUARRY RECOGNITION AND WEATHERING ANALYSIS

Coordinator: Prof. Fabrizio Nestola
Supervisor: Prof. Claudio Mazzoli
Co-Supervisor: Dr. Lara Maritan

PhD candidate: Luigi Germinario

Contents

Reviewers

An early version of this PhD dissertation has been subjected to revision, and approved for the final examination, by:

Prof. Giuseppe Cultrone

Departamento de Mineralogía y Petrología
Universidad de Granada, Spain
Email: cultrone@ugr.es

Prof. Siegfried Siegesmund

Geowissenschaftliches Zentrum,
Georg-August-Universität Göttingen, Germany
Email: ssieges@gwdg.de

according to the official procedure for admission to the doctoral defense at the University of Padova and for getting the additional qualification of *Doctor Europaeus* (European PhD).

Preface

This dissertation is structured in five independent and complete papers. For this reason, some inevitable repetitions are present throughout the text, mainly concerning the geological and historical background of the studied material. Each paper constitutes a separate chapter, and it is being (or will be) submitted for publication in international peer-reviewed journals, with me as first author. The last supplementary chapter, written after an early exploratory phase of experimentation, has been already published with the following reference:

Germinario L., Cossio R., Maritan L., Borghi A., Mazzoli C. (2016). Textural and mineralogical analysis of volcanic rocks by μ-XRF mapping. *Microscopy and Microanalysis*, 22, 690–697. doi: 10.1017/S1431927616000714

Supplementary digital material, mostly including large datasets, is referred to as "appendices" in the text. These are freely available for download on the following website:

http://geo.geoscienze.unipd.it/phd-dissertation

or can be requested by email:

luigi.germinario@gmail.com

This thesis contains the research I have carried out from 2014 to 2016, supervised by Prof. Claudio Mazzoli and co-supervised by Dr. Lara Maritan. This work has also benefitted by the research periods I spent abroad collaborating with Prof. Siegfried Siegesmund (Georg-August-Universität Göttingen, Germany) and Prof. John M. Hanchar (Memorial University of Newfoundland, Canada). Further research collaborations were arranged with Dr. Arturo Zara, Prof. Jacopo Bonetto, Prof. Raffaele Sassi (University of Padova), Prof. Alessandro Borghi and Dr. Roberto Cossio (University of Torino, Italy). I would like to express my most sincere thanks and gratitude to all of them, for their valued contributions and support.

Padova, January 2017

Luigi Germinario

Abstract

The Euganean Hills (Veneto, NE Italy) are the most important quarry district in Italy for the extraction of trachyte, which has been carried out in tens of quarries all through the centuries, from Pre-Protohistory and, more intensely, from the Roman age onwards. Trachyte of the Euganean Hills has an age-old tradition of usage as carving and building stone, mainly in northern and central Italy, e.g., for manufacturing diverse everyday items and funerary and votive artifacts, as well as for building infrastructure, monuments, and in public and private construction. An archaeometric study of Euganean trachyte is here presented following two main research directions.

The first involves the identification of criteria for recognizing provenance quarry of trachyte used in archaeological and historical materials, supported by a petrographic and geochemical database obtained from samples collected in the entire area of the Euganean Hills. The petrographic provenance tracers involve mineralogical composition and textural features of phenocrysts and groundmass, whereas the geochemical tracers comprise major- and trace-element composition of bulk rock and phenocrysts, in particular of mafic minerals. Trachyte provenance can be most precisely determined by applying multivariate relations based on phenocryst chemistry, which can be analyzed even on small, altered archaeological samples. The provenance markers were tested in a provenance study of Euganean trachyte used in Roman public infrastructure in Veneto, including roads, bridges and forum squares. The results provide insights into the commercial, political and economic dimension of the management of trachyte quarries and development of extraction activities in the Roman times, as well as into ancient trades in northern Italy and the main routes of stone circulation.

The second research topic addresses the investigation of weathering and durability of Euganean trachyte used as building stone. Weathering crusts and patinas were detected on trachyte in urban environment, and their mineralogical and microstructural characteristics, major- and trace-element chemical composition were analyzed. The alteration products, mainly involving surface enrichment in carbonates, heavy metals, and carbon, represent an informative indicator of environmental conditions, in particular air quality, and chemical stability of the rock-forming minerals of trachyte and neighboring jointing mortars. Trachyte durability was also examined by a petrophysical and mechanical characterization of quarry samples, providing elements for aiding quality assessment by conservators-restorers and building companies. Particular emphasis is placed on the properties related to absorption, transport, and retention of water and aqueous solutions, in liquid and vapor state. Depending on porosimetric characteristics, i.e., pore volume, size, size distribution, shape, and degree of interconnection, different trachyte varieties exhibit a relatively wide array of technical performances, diversely affecting their decay behavior.

Riassunto

I Colli Euganei (Veneto) rappresentano il più importante distretto di cava in Italia per l'estrazione di rocce trachitiche, attività storicamente condotta in decine di cave e iniziata già in epoca pre-protostorica, poi intensificatasi a partire dall'età romana. L'importanza della trachite dei Colli Euganei nel patrimonio culturale, soprattutto del nord e centro Italia, si collega ad una tradizione millenaria di impiego nella manifattura di utensili e manufatti votivi e funerari, nella costruzione di infrastrutture e monumenti e nell'edilizia pubblica e privata. In questa tesi, si presentano i risultati di uno studio archeometrico della trachite euganea incanalato in due linee di ricerca principali.

La prima riguarda l'identificazione di criteri per riconoscere la cava di provenienza della trachite usata in materiali di interesse archeologico e storico, supportata da un database petrografico e geochimico costruito su campioni prelevati nell'intero territorio dei Colli Euganei. I traccianti petrografici di provenienza comprendono la composizione mineralogica e le caratteristiche tessiturali dei fenocristalli e della matrice, mentre i traccianti geochimici considerano la composizione degli elementi maggiori e in traccia della roccia totale e dei fenocristalli, in particolare dei minerali femici. La maggior precisione nella determinazione della provenienza si ottiene applicando relazioni multivariate basate sulla composizione chimica dei fenocristalli, che può essere analizzata anche su campioni archeologici, spesso di dimensioni limitate e alterati. L'efficacia di questi indicatori è stata poi verificata in uno studio di provenienza della trachite euganea impiegata in Veneto in infrastrutture pubbliche di età romana, quali strade basolate, ponti e piazze forensi. I risultati di tale studio restituiscono un'idea della dimensione commerciale, politica ed economica in cui si inseriva la gestione delle cave romane e l'evoluzione delle attività estrattive, oltre a fornire informazioni sui traffici commerciali antichi sviluppatisi nel nord Italia.

La seconda tematica di ricerca è impostata sullo studio del degrado e della durevolezza della trachite euganea usata come pietra da costruzione. Inizialmente, si sono individuate croste e patine di alterazione della trachite in ambiente urbano e se ne sono analizzate le caratteristiche mineralogiche e strutturali e la composizione chimica degli elementi maggiori e in traccia. I prodotti di alterazione, che si rilevano spesso come arricchimenti superficiali in carbonati, metalli pesanti e carbonio, rappresentano degli interessanti indicatori del contesto ambientale, in particolare della qualità dell'aria, e della stabilità chimica delle fasi mineralogiche della trachite e delle malte di allettamento usate sulla pietra. Infine, la durevolezza della trachite è stata esaminata attraverso una caratterizzazione petrofisica e meccanica di campioni di cava, fornendo elementi utili alla valutazione della qualità da parte di restauratori, conservatori e compagnie edili. Particolare attenzione è stata riservata alla valutazione delle proprietà legate all'assorbimento, movimento e permanenza nella pietra dell'acqua e di soluzioni acquose, allo stato liquido e gassoso. I risultati sperimentali suggeriscono che la variabilità nella resa fisico-meccanica di diversi tipi di trachite dipende primariamente dalle peculiari caratteristiche porosimetriche (volume, dimensione, distribuzione dimensionale, morfologia e grado di interconnessione dei pori), che contribuiscono quindi a determinare diversi gradi di resistenza al degrado.

Chapter 1

New petrographic and geochemical tracers for recognizing provenance quarry

Abstract

Trachyte from the Euganean Hills (northeastern Italy) is a subvolcanic porphyritic rock widely used in cultural heritage of northern and central Italy, primarily from the Roman times onwards, with first evidences dating back to Prehistory. Stoneworks in Euganean trachyte historically include querns, steles, roads, bridges, churches, public buildings, private residences and much more, all through the centuries. The numerous quarries and trachyte varieties with very similar characteristics, as well as the widespread use of this stone, entail several problems in defining its provenance for materials of archaeological and historical significance.

New petrographic and geochemical tracers for recognizing trachyte quarry localities in the Euganean district are presented and discussed here. The petrographic markers principally involve quantitative data about mineralogical composition and textural features of phenocrysts and groundmass, determined by image analysis of X-ray chemical maps acquired by μ-XRF and SEM-EDS. The most useful parameters are: abundance of feldspars, phenocrysts-groundmass ratio, grain size distribution of feldspar phenocrysts, content of SiO_2 phases in the groundmass, arrangement and grain size of microlites in the matrix. On the other hand, the geochemical tracers comprise composition of bulk rock and phenocrysts, determined by XRF and LA-ICPMS, respectively; quarry recognition can be achieved using binary plots built from concentrations of major and trace elements, with mineral-scale chemistry being the most effective and precise discriminant parameter, especially referring to biotite and, secondarily, augite, kaersutite and magnetite.

The aim of this paper is to provide a comprehensive reference database for future provenance studies of Euganean trachyte in archaeometry, by an alternative and more reliable approach to that applied in the previously published literature.

1. The Euganean Hills

The Euganean Hills are a group of hills South-West of the city of Padova (Veneto) in northeastern Italy, covering an area of about 110 km^2 entirely surrounded by the Venetian Plain. Here, the landscape is typically characterized by dome- and cone-shaped reliefs (Fig. 1) rising up to a maximum elevation of 601 m amsl (M. Venda). These were mainly produced by magmas that intruded into pre-existing sedimentary sequences and creating laccoliths, domes, or dikes; the igneous bodies emplaced at shallow depths were eventually exhumed in a subaerial environment, and their base was later buried by fluvial deposits (Cucato & Mozzi 2011).

Specifically, the geology of the region is characterized by a deep-water sedimentary succession of limestones and marls dated to the upper Jurassic–lower Oligocene, followed by a Paleogene volcanic and hypabyssal series, and by Quaternary deposits of alluvial origin or derived from weathering of the igneous rocks (Cucato et al. 2011).

Fig. 1. Panoramic view of the Euganean Hills from the top of M. Grande, facing Rocca Pendice and M. Venda.

The volcanic activity in the Euganean region was part of the Veneto Volcanic Province (VVP). This formed in the upper Paleocene to Oligocene over an area of about 2,000 km^2 between the Garda Lake and Bassano del Grappa-Padova axis, in response to the extensional tectonics of the Southern Alps foreland related to the collision between the Adria and European plates. The Euganean volcanic activity was the latest within the VVP, and included two main events. The first one, upper Eocene in age, was associated with submarine basic and ultrabasic products with alkaline and subalkaline affinity, encompassing pillow and flow lavas, breccias, hyaloclastites and tuffs, known as the Castelnuovo di Teolo formation. The second one, lower Oligocene in age, yielded mostly acid and intermediate subvolcanic rocks, at times combined with effusive and explosive products. Rhyolites and trachytes with moderate Na-alkaline affinity are the most recurring rock types, while latites and basalts subordinately occur, all being included in the M. Venda formation (De Vecchi et al. 1976a, 1976b; De Pieri et al. 1983; Zantedeschi 1994; Cucato et al. 2011; Bartoli et al. 2015) (Fig. 2). This last differentiation was primarily connected to processes of low-pressure fractional crystallization of mantle-derived basic melts, which took place in multiple shallow magma chambers formed due to block-faulting tectonics, with modest crustal contamination (Milani et al. 1999).

2. Quarrying activity

Euganean trachyte – denomination actually comprising trachytes s.s., quartz-trachytes and less common rhyolites and trachyandesites – is a subvolcanic rock with porphyritic texture and a grey color, often ranging to brown and yellow shades (Fig. 3a). It is characterized by excellent durability and technical properties, in particular high resistance to mechanical abrasion and chemical alteration (Calvino 1969; Zantedeschi & Zanco 1993; Valluzzi et al. 2005; Graue et al. 2011; Graue 2013).
Trachyte outcrops have been widely exploited in the course of time, making the Euganean Hills the most important district in Italy for the extraction of this material. Indeed, trachyte also occurs in other Italian regions (Sardinia, Lazio, Tuscany, Campania), in some cases with a notable tradition of use and exploitation (Calvino 1966; Williams-Thorpe & Thorpe 1989; De Gennaro et al. 2000; Frulio et al. 2004; Langella et al. 2009), but to a much lesser extent if compared to the commercial relevance of the Euganean district.
Trachyte quarrying in this region is lost to history and started with the first populations settled in the Prehistory, but dramatically increased during the Roman times. The ancient extraction methods

involved the use of wedges, inserted into holes in the rock or natural fractures; metallic wedges were hammered inwards, whereas wooden wedges were soaked with water, causing their swelling (Buonopane 1987; Vergani 1994). The resulting rock splitting was made easier by columnar, tabular or prismatic jointing that trachyte often displays (Fig. 3b). Quarrying methods remained almost unchanged all through the centuries, until introduction of explosives and blasting technology,

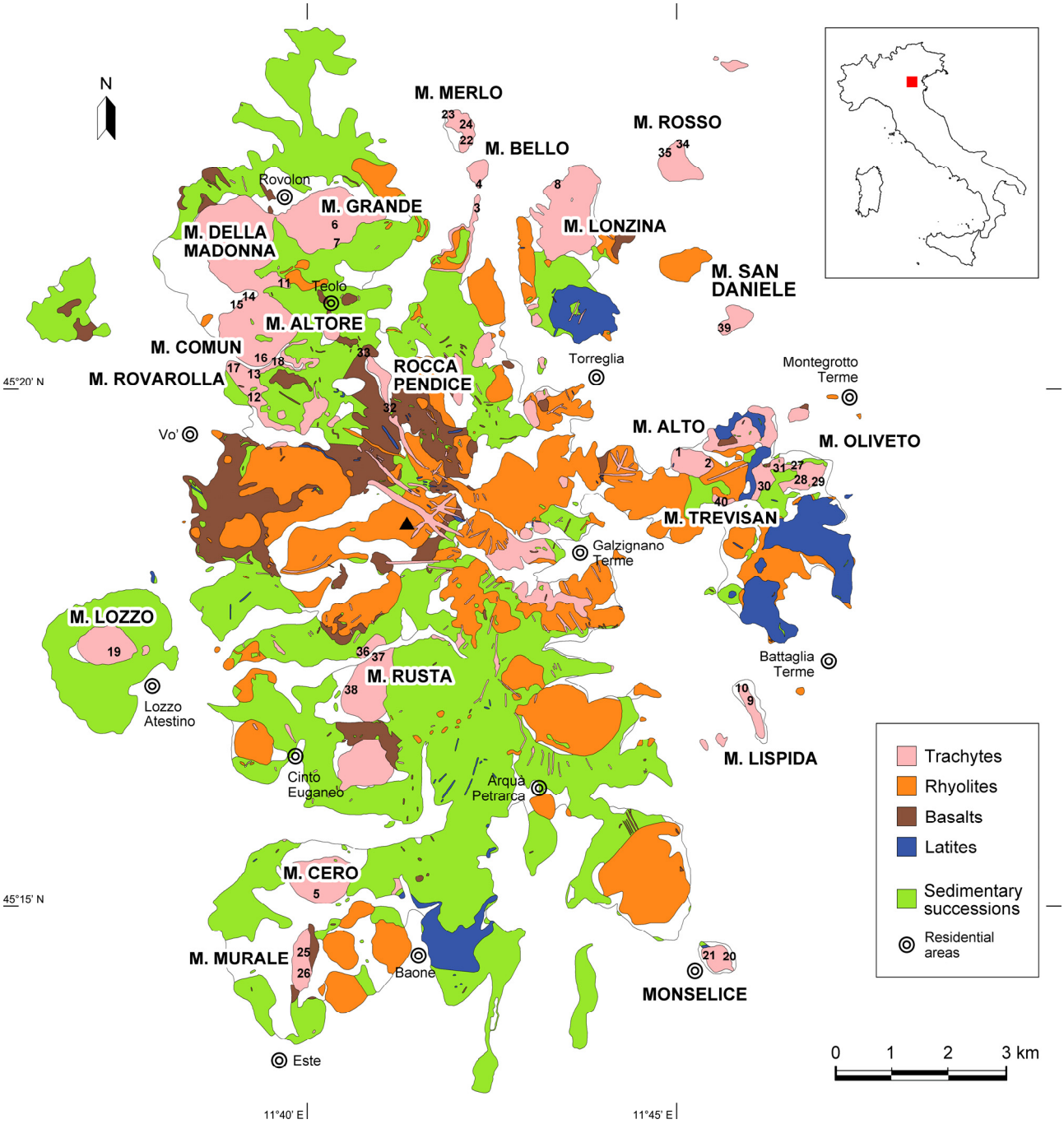

Fig. 2. Geological map of the Euganean Hills (modified after Piccoli et al. 1981). The named hills represent the sampled quarry localities, and each of the 40 sampled quarries is marked and localized with a reference progressive number (coordinates of each sampling point in Appendix 1). "M." in the proper name of the hills stands for "Monte" (mount). The peak of the highest hill, M. Venda (601 m a.m.s.l.), is indicated with a black triangle.

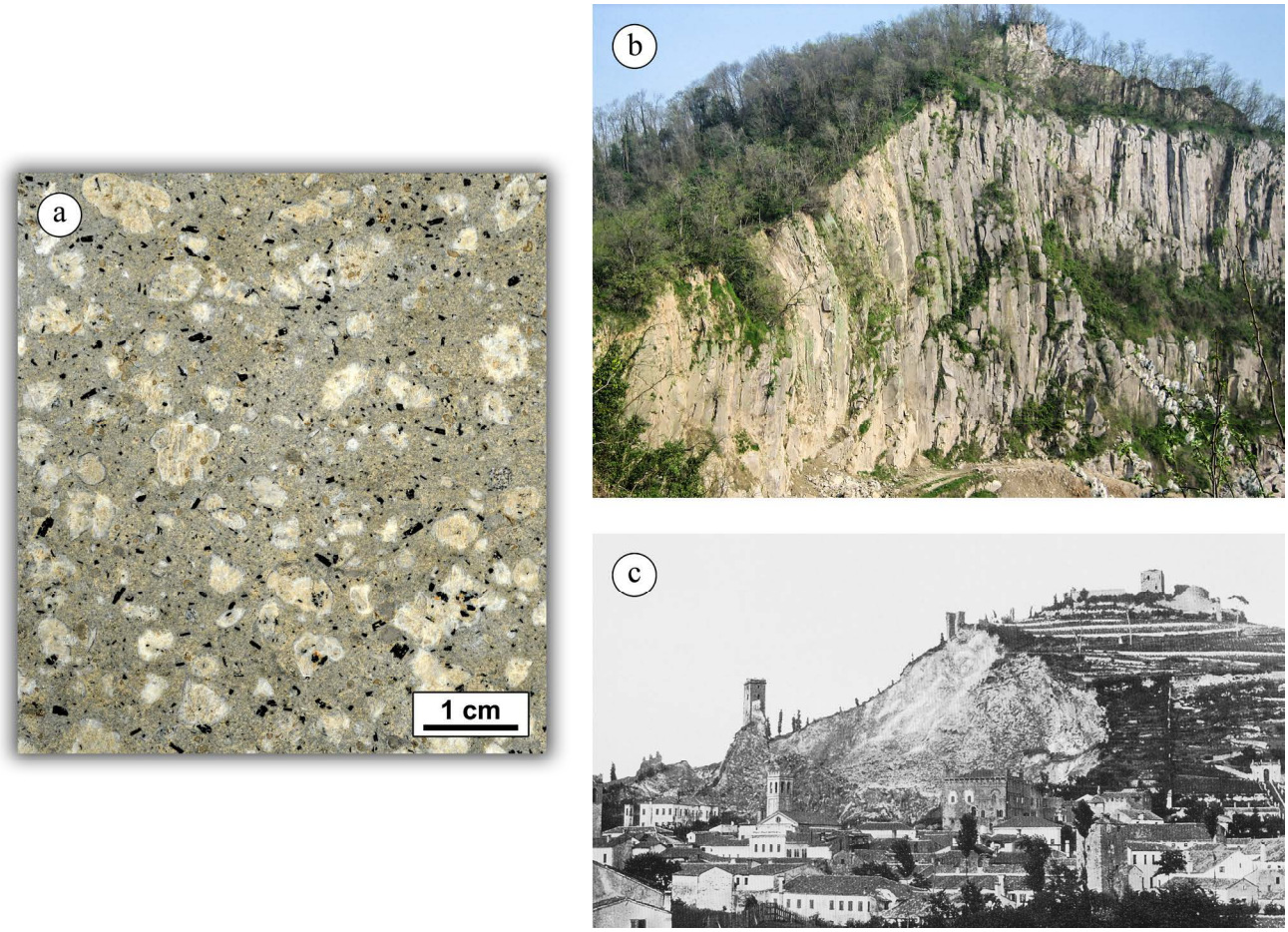

Fig. 3. a) Macroscopic appearance of Euganean trachyte (sample from M. Rovarolla); **b)** quarry face of M. Merlo in 2009, displaying columnar and prismatic jointing (courtesy of Michelangelo Dalla Francesca); **c)** quarry of Monselice in late 19th-early 20th century (Selmin 2005): part of the Medieval architectonic complex on the hill has been lost due to excavation activity.

experimented already in the 18th century but more frequently from the end of the 19th century onwards. Quarrying continued to be particularly intense at least until the 1960s, then a series of legislative measures (in 1971 and then in 2001) led to a gradual drop in extraction activities, in order to prevent further damage that millennia of excavation caused to the local landscape (Fig. 3c). Among the approximately 100 open pits in this area for the extraction of trachyte – 75 of which giving dimension stones (Calvino 1966) – only four are still active to date (one on M. Merlo and the others on M. Rovarolla).

Most quarries were developed on the edges of hills, which were more easily accessible and closer to residential zones and former settlements. The northwestern hills (M. Altore, M. Comun and M. Rovarolla, near the village Zovon di Vo') have the highest concentration of quarries, but historically the most exploited localities seem to have been those of Monselice, M. Oliveto and M. Merlo, according to the archaeometric literature (Previato et al. 2014).

3. Archaeometric background

3.1. Historical outline

The diverse use of Euganean trachyte in cultural heritage of northern and central Italy has an age-old tradition (Fig. 4), with its first traces dating back to Prehistory (Neolithic, 5th millennium BCE). A higher number of records, however, has been attested from Protohistory and pre-Roman period, within the territories controlled by the Venetic civilization as well as the Etruscans, thanks to mutual trades of raw and finished materials; crafting of querns has been principally reported, but trachyte was also used in buildings, necropolises, for funerary and votive cippi and steles (Cattani et al. 1997, Antonelli et al. 2004; Bianchin Citton & De Vecchi 2009), even as temper in pottery production (Calogero & Lazzarini 1984; Maritan 2004; Maritan et al. 2006).

Subsequently, Roman domination led to a considerable widespread usage of Euganean trachyte (Lazzaro 1992; Zara 2016), which was frequently transported by ship along the numerous waterways of the Venetian Plain, the Po river, and in the Adriatic Sea (Renzulli et al. 1999, 2002b); this system was often preferred to small-load transports by animal-drawn carts and sleds. Beside the manufacture of mortars and querns (Cattani et al. 1997; Renzulli et al. 2002a; Antonelli et al. 2004; Antonelli & Lazzarini 2010, 2012; Santi & Renzulli 2006), the Romans widely used trachyte for flagstones in paving urban and extra-urban roads – e.g., *Via Flaminia*, *Via Aemilia*, *Via Annia* – as well as for bridges, aqueducts, harbor structures, and milestones (Renzulli et al. 1999, 2002b; Capedri et al. 2000, 2003; Grossi & Zanco 2003; Santi & Renzulli 2006; Grossi 2007; Maritan et al. 2013; Previato et al. 2014). Moreover, the stone was used in private buildings and monuments, especially with structural function, and in funerary contexts, for sarcophagi, tombstones, cippi, urns and steles (Capedri et al. 2003; Capedri & Venturelli 2003; Previato et al. 2014). According to these findings, the network of trachyte circulation from the Euganean Hills, and therefore from the cities of *Patavium* (Padova) and *Ateste* (Este), extended at distances above 250 km, over a broad, almost quadrilateral area traced by the Roman settlements of *Mediolanum* (Milano)-*Ticinum* (Pavia), Bressanone, *Tergeste* (Trieste)-*Aquileia* and *Ancona-Urbs Salvia* (Urbisaglia) (Fig. 4). The Romans often adjusted the selection of the quarries based on their position with respect to transport routes.

Use and trade of Euganean trachyte continued also through the Middle Ages and Renaissance, with the extraction of huge volumes of stone, in addition to the reuse of material from Roman artefacts (Renzulli et al. 1999; Capedri et al. 2000; Capedri & Venturelli 2005; Marocchi et al. 2009). Especially with the rise of *Serenissima Repubblica di Venezia* (697–1797), stone construction was given a substantial boost, and trachyte was largely employed in public buildings, churches, monasteries, monumental gates, defensive walls, and private residences, as well as for paving squares and streets. The most striking examples can be admired in Venezia and Padova (Negri 1966; Lazzarini et al. 2008), but stone trades often went as far as the Po Valley and beyond (Capedri et al. 2000). Diverse applications in urban environments continued in the 19th and 20th century as well (Negri 1966; Borghi et al. 2015; Lugli et al. 2016).

Today, spread of Euganean trachyte and its use in construction are not limited to northern and central Italy, but also involve central and eastern Europe (e.g., Germany, Austria, Switzerland, Croatia, Netherlands, Russia). Trachyte is mostly used for cladding and paving, but also for restoration of historical architecture, in Italy and abroad, as in the case of excellence of Cologne Cathedral (Graue et al. 2011).

Fig. 4. Historical use of Euganean trachyte: **a)** indication of the area of trachyte circulation in the Roman times (shaded) and principal extra-urban roads; **b)** Roman road with trachyte flagstones in Classe, the ancient port of Ravenna, 4–6th c. CE (Maioli & Stoppioni 1987); **c)** funerary stele of Oppi family, Padova, 1st c. CE (courtesy of Musei Civici di Padova, Gabinetto Fotografico); **d)** Roman rotary querns, Padova (courtesy of Musei Civici di Padova, Gabinetto Fotografico); **e)** arcade of Palazzo della Ragione, Padova, 13–14th c. CE; **f)** Basilica of Sant'Antonio of Padova, 13–14th c. CE, with trachyte pillars and buttresses, and on the left the equestrian statue of Gattamelata by Donatello, 15th c. CE, with trachyte base; **g)** Basilica of San Marco, Venezia, 11th–17th c. CE, in Piazza San Marco, 12th–19th c. CE, paved with trachyte; **h)** Cologne Cathedral, 13–19th c. CE, with replacing ashlars in Euganean trachyte.

Less noble applications comprise street furniture, breakwaters, cladding of structures for industrial treatment of acids and, in the form of aggregate, road foundations and temper in brick production.

3.2. The provenance problem

Identifying the provenance quarry of stones used in archaeological or historical objects is a common task in archaeometry. This may involve tracing the ancient trades and circulation routes of raw materials and finished artifacts, reveal historical development of quarrying activities and location of the main sources of stone supply, and guide the choice of proper materials for restoration.
In the case of trachyte of the Euganean Hills, determining the provenance is even more challenging, since this involves a large number of quarries within a single extraction basin, which are very close, in some cases only a few hundred meters apart. This entails the need for carrying out provenance studies at high spatial resolution, in order to cast new light on the following issues: territorial organization of settlements; their areas of political influence; ownership and competition of quarries; localization of extraction and production sites; access to the main trade routes; connection to destination centers and preferred ways of material transport; construction relative chronology within single sites where materials from different quarries were used (e.g., Capedri et al. 2000); use of stone from specific quarries for specific applications.
An additional reason why archaeometry of Euganean trachyte is often essential to historical studies is that written sources about quarrying activities are available only from the 13th century, sporadically though, becoming more frequent and reliable from the end of the 17th century, due to fiscal policy of the *Serenissima* (Vergani 1994); moreover, the intense exploitation has prevented ancient traces of excavation to be preserved and ancient semi-finished products or artifacts have been found only occasionally on site, for example in the quarries of M. Merlo and M. Oliveto.
From an archaeometric point of view, Euganean trachyte can be easily discriminated from volcanic rocks of other important Italian quarry districts exploited in the antiquity, such as the leucite phonolite and tephritic phonolite of the Vulsini Mounts and Vico volcano in Umbria-Lazio, the basaltic trachyandesite and phonolitic tephrite of Somma-Vesuvius in Campania and the hawaiite and mugearite of the Etna volcano in Sicily. This can be achieved by considering the Na-alkaline affinity of Euganean trachyte and distribution of incompatible trace elements (Santi & Renzulli 2006), besides petrographic features.
Concerning the differences within the Euganean district itself, a first detailed census of some varieties of Euganean trachyte based on their petrographic and geochemical characteristics was made by Schiavinato (1944). Later on, several datasets reporting bulk-rock chemical compositions (e.g., Calvino 1969; De Vecchi et al. 1976; De Pieri et al. 1983) and chemistry of phenocrysts (De Pieri et al. 1977, 1978; De Pieri & Molin 1980; De Pieri & Gregnanin 1982) were published, although generally referred to few selected sites, until a collection of parameters useful for discriminating Euganean quarries was proposed by Zantedeschi & Zanco (1993). However, the first comprehensive database, which encompasses a higher number of quarry sites and currently represents the reference for archaeometric provenance studies of Euganean trachyte, is that set up by Capedri et al. (2000). Those authors proposed a distinction among the most important trachyte quarries based on textural features, modal composition, bulk chemical composition, and magnetic susceptibility. Despite its accuracy and com-

prehensiveness, the database has several limitations, discussed later in this paper. Since detailed petrographic characterization turned out to be still essential, in a recent study Germinario et al. (2016) explored the effectiveness of quantitative petrographic parameters as provenance markers.
In the present paper, new petrographic and geochemical tracers for discriminating and recognizing trachyte quarry localities in the Euganean district are illustrated, building an updated database containing quantitative data about mineralogy, textural features of phenocrysts and groundmass, bulk-rock chemistry and major- and trace-element composition of phenocrysts. The data were treated by means of a robust multivariate statistical approach. The aim is to provide a complete reference support for future provenance studies of Euganean trachyte in archaeometry, by an alternative and more reliable approach than what is currently available in the literature.

4. Sampling and experimental setup

A set of 86 trachyte samples (Table 1) were collected covering the entire area of the Euganean Hills, in 40 different outcrops and quarries, most of them inactive and abandoned, localized on 20 different hills (Fig. 2). The number of samples from each quarry was chosen depending on its size, presence of other extraction sites in the same quarry locality (i.e., hill) and lithological variability observed in the field. Most of these quarries, where exploitation has been most important or intense, were already sampled by Capedri et al. (2000). All of the analyses aimed at petrographic and geochemical characterization were done on thin sections with a thickness of 45 μm, unless indicated otherwise.

Table 1. List of the sampled localities and all the 86 samples collected, with relevant quarry specified (identification numbers as in Fig. 2; the coordinates of each sampling point are listed in Appendix 1). Each locality is assigned with an identification symbol, used further ahead for plots.

Quarry locality (Hill)	Town	Quarry ID	Sample ID (Quarry)
M. Alto	Torreglia	1; 2	ALT-01, 02 (1); ALT-03, 04 (2)
M. Altore	Zovon di Vo'	14; 15	LTR-06, 07, 08 (14); LTR-09, 10 (15)
M. Bello	Treponti di Teolo	3; 4	BLL-01, 02 (3); BLL-03, 04 (4)
M. Cero	Calaone di Baone	5	CER-01, 02, 03 (5)
M. Comun	Zovon di Vo'	16; 18	LTR-11 (16); LTR-15, 16 (18)
M. della Madonna	Teolo	11	LTR-01 (11)
M. Grande	Rovolon	6; 7	GRN-01 (6); GRN-02, 03 (7)
M. Lispida	Battaglia Terme	9; 10	LSP-01 (9); LSP-02, 03 (10)
M. Lonzina	Luvigliano di Torreglia	8	LNZ-01, 02 (8)
M. Lozzo	Lozzo Atestino	19	LZZ-01, 02, 03 (19)
M. Merlo	Montemerlo di Cervarese S. Croce	22; 23; 24	MRL-01, 02 (22); MRL-03, 04 (23); MRL-05, 06, 07 (24)
M. Murale	Calaone di Baone	25; 26	MUR-01, 02 (25); MUR-03, 04, 05 (26)
M. Oliveto	Montegrotto Terme	27; 28; 29; 30; 31	OLV-01, 02 (27); OLV-03, 04 (28); OLV-05, 06, 07 (29); OLV-08 (30); OLV-09, 10, 11, 12 (31)
M. Rosso	Monterosso di Abano Terme	34; 35	RSS-01, 02 (34); RSS-03, 04 (35)
M. Rovarolla	Zovon di Vo'	12; 13; 17	LTR-02, 03 (12); LTR-04, 05 (13); LTR-12, 13, 14 (17)
M. Rusta	Fontanafredda di Cinto Euganeo	36; 37; 38	RST-01, 02 (36); RST-03, 04, 05 (37); RST-06, 07, 08 (38)
M. San Daniele	Abano Terme	39	SND-01, 02 (39)
M. Trevisan	Montegrotto Terme	40	TRV-01, 02 (40)
Monselice	Monselice	20; 21	MNS-01, 02, 03 (20); MNS-04, 05 (21)
Rocca Pendice	Castelnuovo di Teolo	32; 33	PND-01 (32); PND-02, 03 (33)

- The quarry area of Zovon (M. Altore, M. Comun and M. Rovarolla) is assigned with the same identification symbol, for reasons of high petrographic and chemical homogeneity of the samples and according to Capedri et al. (2000).
- The sample from M. della Madonna turned out to be a petrographic and chemical outlier and has no symbol.

Petrographic investigations were done with a polarized-light optical microscope and a CamScan MX2500 scanning electron microscope (SEM) equipped with a LaB_6 cathode, an EDAX energy-dispersive X-ray spectroscopy (EDS) system and an electron backscattered diffraction (EBSD) detector, at the Department of Geosciences, University of Padova. In addition to standard observations and phase identification, high-resolution X-ray elemental maps were acquired on selected regions of the rock groundmass, having an area of 0.05 to 1.20 mm^2, depending on the grain size. Operating conditions were 20 kV acceleration voltage and 150 nA beam current and, during map acquisition, a grid of 512 x 400 pixels was scanned using a dwell time of 150 ms per pixel and a time constant of 2.5 μs, applying standard ZAF corrections. The resulting maps were processed by digital image analysis (DIA) through ImageJ and Multispec softwares, as described in Germinario et al. (2016), in order to extract the relative abundances of mineral phases and the following textural features of crystals in the groundmass: area, perimeter, Feret diameter, circularity and aspect ratio.

X-ray elemental maps were also acquired by micro X-ray fluorescence (μ-XRF), but on smoothed stone tiles and large areas of 20 cm^2, using an EDAX Eagle III XPL bench-top spectrometer, at the Department of Earth Sciences, University of Torino. Operating conditions were 40 kV acceleration voltage and 1 mA beam current and, during map acquisition, a grid of 512 x 400 pixels was scanned using a dwell time of 200 ms per pixel, a time constant of 2.5 μs, a spot size of 30 μm and a resolution (step size) of 103.5 μm. The resulting maps were processed by DIA as noted above. Considering the size of the area investigated and the resolution used, mineralogical and textural information was given about phenocrysts and relative abundance of groundmass was calculated, providing the porphyritic index (P.I.). Further details on this method are described in Germinario et al. (2016).

Bulk-rock chemical analyses for major and trace elements were done by X-ray fluorescence (XRF) on glass beads – prepared with calcined samples diluted with $Li_2B_4O_7$ flux in a 1:10 ratio – using a Philips PW2400 spectrometer operating in WD (wavelength dispersive) mode, at the Department of Geosciences, University of Padova. Loss on ignition (LOI) was also determined separately before the XRF analyses.

Finally, the chemical composition of phenocrysts was measured *in situ* on crystals of anorthoclase, plagioclase, sanidine, biotite, augite, kaersutite, Ti-magnetite, and apatite.

The major-element composition was determined by a Cameca Camebax SX 50 electron probe microanalyzer (EPMA), operating in WD mode, using a 15 kV acceleration voltage and a 10 nA beam current, at the Institute for Geosciences and Earth Resources of CNR (CNR-IGG, Padova).

The major- and trace-element composition of the same phenocrysts was also determined by laser ablation inductively-coupled plasma mass spectrometry (LA-ICPMS), using a Thermo Scientific Element XR double-focusing magnetic-sector spectrometer coupled to a GeoLas 193 nm Ar-F excimer laser, at the Micro Analysis Facility of the Bruneau Centre for Research and Innovation, Memorial University of Newfoundland. The laser energy density used for all the analyses was 3 J/cm^2 with a pulse frequency of 8 Hz and a spot size of 40 μm. For each analysis, the background was measured for 30 s, followed by 60 s of laser ablation, and wash out was monitored for 30 s after each ablation, analyzing 2 to 5 spots for each phase on each sample. NIST 610 glass reference material was used as primary calibrant, and analyzed every 10 measurements on the samples; USGS BCR-2G basalt glass reference material and Slyudyanka apatite were also analyzed with the same frequency as secondary standards. Element concentrations were calculated with Iolite v2.5 software package (Paton et al. 2011), based on the NIST 610 signal and the concentrations of selected major elements previously

determined by EPMA and used as internal standards[1]: ^{27}Al for anorthoclase, plagioclase, sanidine and biotite, ^{43}Ca for augite, kaersutite and apatite, ^{57}Fe for magnetite.
All the quantitative information obtained with the techniques above was subjected to univariate, bivariate, and multivariate statistical analysis, in particular principal component analysis (PCA) and discriminant analysis, using Statgraphics Centurion XVI software package, in order to identify the most distinctive petrographic and geochemical parameters among the trachyte quarries.

5. Petrographic tracers

5.1. General characterization

Based on the results of the analyses by optical microscopy, SEM, and EPMA, a general petrographic description will first be provided.
Euganean trachyte is a holocrystalline to hypocrystalline rock with porphyritic texture (Fig. 5), often glomeroporphyritic or cumuloporphyritic due to the occurrence of feldspar polycrystalline aggregates, frequently displaying consertal or radiate intergrowths.
The distribution of feldspars consists of anorthoclase, plagioclase, and sanidine, in diverse combinations and proportions. Anorthoclase can be pure end member or calcic, plagioclase has a prevalent oligoclase-andesine composition, while sanidine is mainly pure end member or sodic. Feldspar phenocrysts may be characterized by intracrystalline pores and minute inclusions of glass and feldspar microlites, sometimes zonally arranged, giving a spongy-like appearance; another common feature is overgrowth texture, e.g., plagioclase mantled by an alkali-feldspar corona, or anorthoclase by sanidine. Among mafic minerals, biotite is ubiquitous, often showing Fe-Ti oxide-rich reaction rims and resorbed edges (Fig. 6). Clinopyroxene with augite and Fe-augite composition and amphibole with kaersutite composition are sometimes present. In trachytes from several quarries, large crystals of quartz and cristobalite, and occasionally tridymite (verified by SEM-EBSD), also occur. Magnetite, ilmenite, apatite and zircon are the other most recurring accessory minerals, with the first having a Ti-magnetite composition, at times closer to ulvöspinel. Exceptionally, titanite, epidote, calcite, dolomite, monazite and pyrite are present, while siderite – displaying distinctive overgrowths with rhythmic Mg/Ca enrichments – occurs only in the Zovon area (i.e., M. Altore, M. Comun and M. Rovarolla).
Black-greyish xenoliths are common, having a porphyritic, granitoid or weakly schistose texture with usually a trachyandesitic, gabbroic or cornubianitic composition respectively, rich in mafic minerals and magnetite (Sassi et al. 2004; Lazzarini et al. 2008), and are likely derived from the basement

[1] For each mineral phase in each sample, a single EPMA analysis was used as internal standard, considered as mean value for data reduction of the 2 to 5 corresponding spots analyzed by LA-ICPMS. This was considered reliable for the following reasons: exploratory EPMA analyses showed negligible chemical variability of a given mineral phase within the same sample; the crystals analyzed displayed no or very slight zoning under the optical microscope and with cathodoluminescence, or chemical zoning involved elements not used as internal standard; in addition, a set of representative LA-ICPMS analyses was reduced again using as internal standard, for a given phase, the farthest from the average EPMA composition, producing in some cases sensible differences in element concentrations, but maintaining the same relative ratios and basically not affecting sample classification.

rocks through which trachyte intruded. Pervasive oxidation surfaces, constituted by brownish-yellowish migration fronts of Fe oxides and hydroxides, are sometimes visible as well, whereas the content in clay minerals from post-crystallization alteration is generally rather low or negligible.
The groundmass of Euganean trachyte has a microcrystalline to cryptocrystalline grain size, with a composition mainly given by prismatic alkali-feldspar microlites, frequently with fine-grained anhedral SiO_2 minerals (cristobalite and quartz, occasionally tridymite) and glass-bearing domains filling intercrystalline spaces. The texture is usually felty, with microlites being randomly arranged, although preferred orientations are observable also, i.e., trachytic texture, which is hyalopilitic or pilotaxitic depending on whether intercrystalline glass is present or not.
Further details and data useful for provenance determination of Euganean trachyte will be given in the next paragraphs, excluding from the discussion the petrographic outliers detected (in particular the single sample from M. della Madonna).

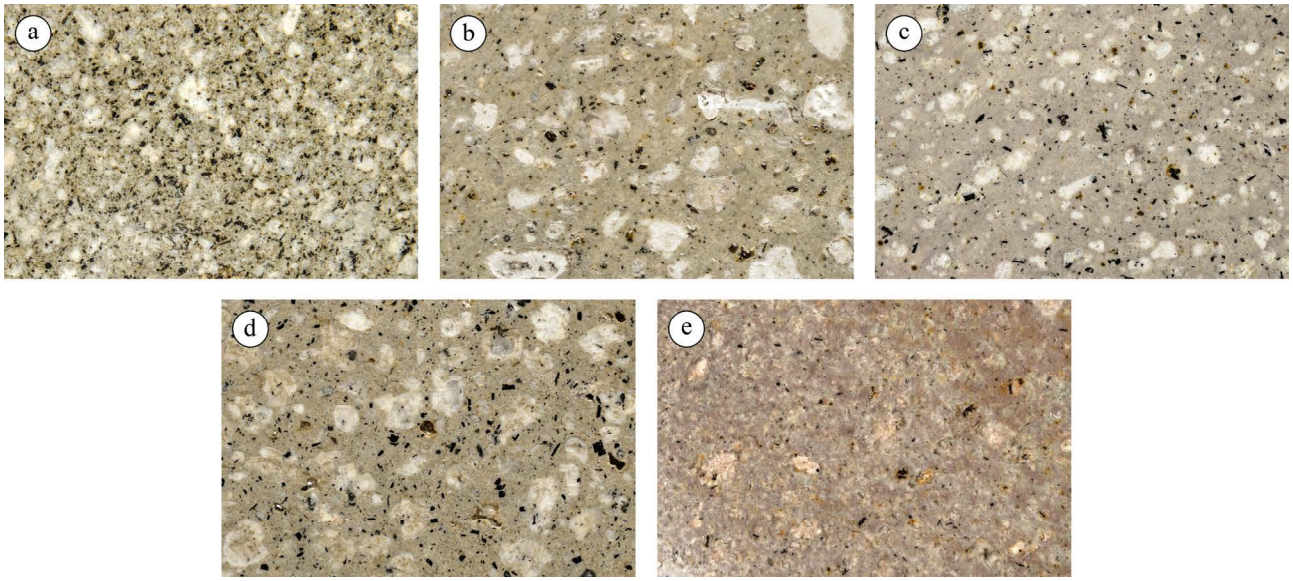

Fig. 5. Hand-specimen photos (5.8 x 3.8 cm) showing the macroscopic appearance of representative varieties of Euganean trachyte from M. Merlo **(a)**, Monselice **(b)**, M. Oliveto **(c)**, M. Rovarolla **(d)**, and M. Rusta **(e)**.

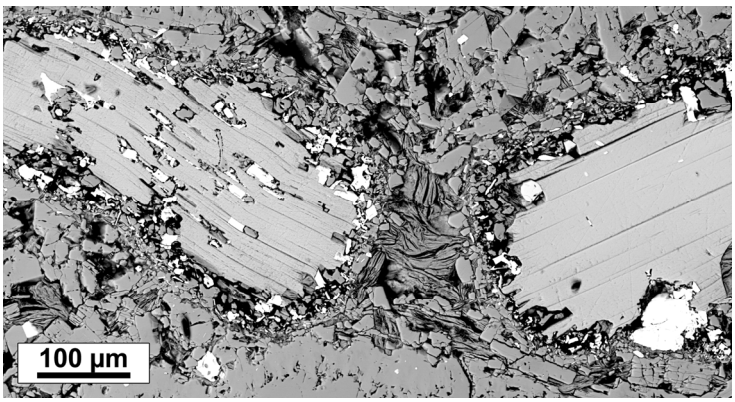

Fig. 6. Back-scattered electron map acquired by SEM-EDS of a sample of Euganean trachyte showing two biotite crystals with reaction rims rich in Fe-Ti oxides (the white fine-grained crystals in the image).

5.2. Modal composition

Data about mineralogy and phenocrysts-groundmass ratio obtained by DIA of µ-XRF maps are presented in Table 2, while Fig. 7 includes some illustrative phase maps obtained after X-ray map processing[2].

A first discriminant parameter among quarries is represented by quantitative ratios of the different feldspar phases in each trachyte variety. PCA performed on the concentrations of anorthoclase, plagioclase, and sanidine, clearly identifies four main groups (Fig. 8a). The first one includes trachytes from the Zovon area, Rocca Pendice and quarry 20 of Monselice, which have high amounts of anorthoclase, from 21 to 29%, and minor quantities of plagioclase (missing in Rocca Pendice and Monselice) and sanidine (missing in Zovon). The second group comprises trachytes from M. Rusta, M. Grande, M. San Daniele, quarry 2 of M. Alto and quarry 21 of Monselice: they all have the highest concentration of sanidine, up to 17%, the lowest concentration on average of plagioclase (totally absent in M. Rusta, M. Grande and Monselice) and often subordinate amounts of anorthoclase. The third group includes only trachytes from M. Bello and M. Lonzina, with the highest quantity of plagioclase, about 20%, the other feldspars being absent or very low. All the other localities are grouped in a fourth large cluster, characterized by negligible amounts of sanidine and an anorthoclase-plagioclase ratio mostly comprised from 1:1 to 3:1.

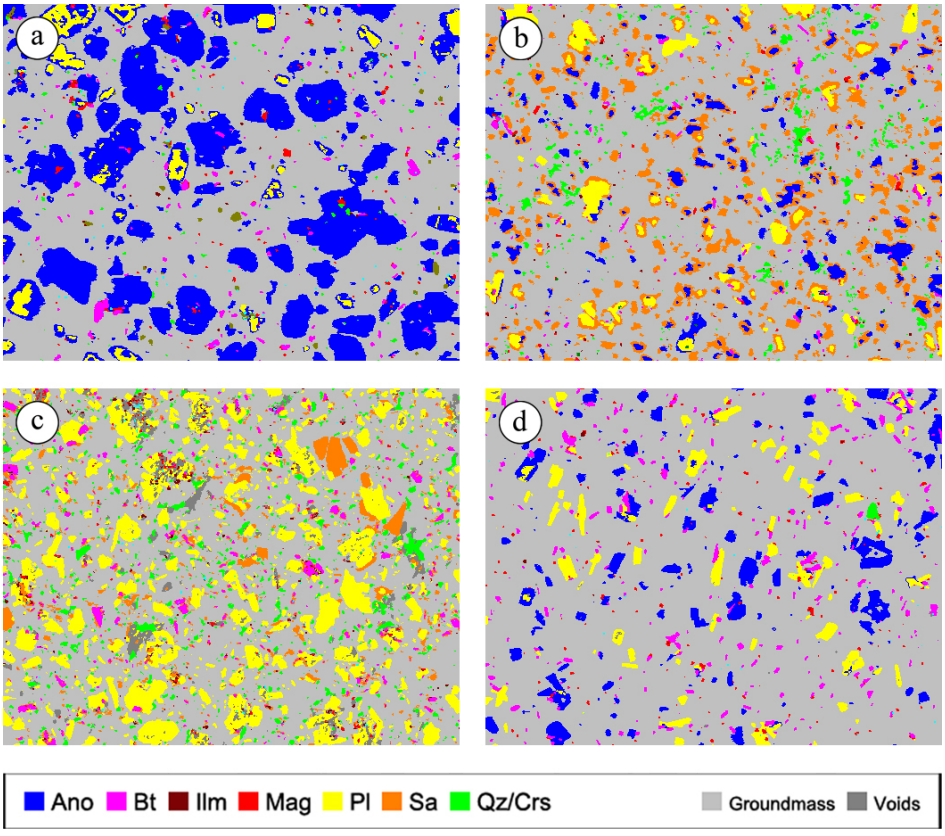

Fig. 7. Phase maps of Euganean trachyte processed from X-ray maps acquired by µ-XRF, on a surface of 5.30x4.14 cm of samples from: **a)** M. Altore, quarry 14, characterized by high concentration of anorthoclase, high P.I. and coarse grain size; **b)** M. San Daniele, quarry 39, with high amount of sanidine and fine grain size; **c)** M. Bello, quarry 3, displaying high content of plagioclase and medium-high P.I.; **d)** M. Cero, quarry 5, with an anorthoclase-plagioclase ratio of ~1:1, low P.I. and fine grain size. Mineral abbreviations as in Table 2, colors not in the legend indicate minor phases.

[2] Only some slight variability in mineral ratios, or absence/presence of minor mineral phases (e.g., plagioclase and augite in Monselice), have been observed in other historical samples of known provenance (unpublished data), so that the data of modal composition of this paper can be considered valid, or at least vey indicative, for ancient quarry faces too.

Table 2. Modal composition (percentage of mineral phases), groundmass percentage (GM) and porphyritic index (P.I.) determined by μ-XRF mapping and digital image analysis. For each quarry (number and localization as in Fig. 2), values are averaged among different samples.

Quarry	Locality	Feldspars				Mafic minerals			Accessory minerals				GM	P.I.
		Ano	Pl	Sa	Σ Fsp	Bt	Aug	Krs	Qz/Crs	Ti-Mag	Ilm	Others		
1	M. Alto	9.44	10.14	-	19.58	2.05	-	0.38	0.38	0.89	0.08	0.44	76.20	23.80
2	M. Alto	3.64	0.36	5.23	9.23	0.37	-	-	1.56	0.27	0.13	0.05	88.39	11.61
3	M. Bello	-	19.33	4.85	24.18	2.07	-	-	4.17	0.47	0.53	0.22	68.35	31.65
4	M. Bello	-	19.75	1.96	21.70	3.09	-	-	2.11	0.12	0.29	0.20	72.49	27.51
5	M. Cero	6.26	4.85	-	11.11	2.57	-	-	0.09	0.67	0.03	0.07	85.45	14.55
6	M. Grande	5.53	-	5.46	10.99	0.50	-	-	3.71	0.63	0.04	0.03	84.09	15.91
7	M. Grande	6.88	-	12.91	19.79	0.65	-	-	1.21	0.28	0.17	0.02	77.88	22.12
8	M. Lonzina	-	17.87	-	17.87	2.24	0.18	-	0.20	1.16	0.30	0.40	77.65	22.35
9	M. Lispida	11.23	4.50	-	15.73	1.49	-	-	0.35	0.41	0.07	0.01	81.94	18.06
10	M. Lispida	12.14	3.75	-	15.88	1.18	-	-	1.70	1.61	0.02	0.04	79.56	20.44
11	M. della Madonna	-	2.89	23.82	26.71	0.91	-	-	4.57	0.38	0.29	0.02	67.12	32.88
12	M. Rovarolla	25.86	2.88	-	28.75	1.60	0.02	-	1.10	0.29	0.07	0.54	67.62	32.38
13	M. Rovarolla	26.99	4.09	-	31.08	1.74	0.53	-	0.19	0.40	0.08	0.95	65.03	34.97
14	M. Altore	28.44	2.81	-	31.25	1.29	0.02	-	0.30	0.62	0.09	0.58	65.85	34.15
15	M. Altore	24.83	3.81	-	28.64	2.18	-	-	0.63	1.02	0.20	0.27	67.07	32.93
16	M. Comun	27.78	5.16	-	32.94	1.57	-	-	1.17	0.22	0.24	0.05	63.82	36.18
17	M. Rovarolla	25.47	4.16	-	29.63	1.58	0.62	-	0.71	0.13	0.34	0.37	66.62	33.38
18	M. Comun	23.84	2.85	-	26.70	1.31	-	-	0.89	0.40	0.16	0.04	70.50	29.50
19	M. Lozzo	16.57	8.51	0.43	25.52	1.59	0.02	0.51	1.80	1.39	0.50	0.21	68.46	31.54
20	Monselice	29.08	-	2.39	31.47	0.25	-	0.15	1.04	1.48	0.37	0.04	65.19	34.81
21	Monselice	12.76	-	9.43	22.19	0.33	-	0.14	0.03	0.74	0.31	0.11	76.15	23.85
22	M. Merlo	14.52	6.88	0.65	22.05	2.15	0.04	0.03	1.29	1.82	0.40	0.23	71.99	28.01
23	M. Merlo	15.93	4.46	6.01	26.41	1.03	0.30	0.32	0.23	0.75	0.31	0.05	70.59	29.41
24	M. Merlo	19.42	5.47	0.96	25.85	1.11	0.69	0.37	0.33	1.10	0.38	0.06	70.09	29.91
25	M. Murale	5.68	2.53	-	8.21	1.43	-	-	0.91	0.62	0.11	0.43	88.30	11.70
26	M. Murale	6.42	4.24	-	10.65	1.46	-	-	0.02	0.42	0.08	0.05	87.31	12.69
27	M. Oliveto	10.00	2.04	0.80	12.83	0.79	-	0.02	0.71	1.09	0.12	0.14	84.31	15.69
28	M. Oliveto	12.52	2.82	0.27	15.60	1.17	-	0.02	1.79	0.50	0.18	0.12	80.62	19.38
29	M. Oliveto	13.52	3.49	0.66	17.68	0.97	-	0.03	4.36	0.31	0.20	0.20	76.24	23.76
30	M. Oliveto	15.99	5.06	-	21.05	1.19	-	-	0.62	0.19	0.25	0.11	76.59	23.41
31	M. Oliveto	7.30	1.21	3.65	12.16	0.62	0.03	0.02	0.67	0.22	0.06	0.08	86.14	13.86
32	Rocca Pendice	21.17	-	0.19	21.36	1.75	1.14	-	0.16	0.57	0.15	0.09	74.77	25.23
33	Rocca Pendice	29.31	-	0.71	30.02	1.31	-	-	0.13	0.86	0.12	0.14	67.43	32.57
34	M. Rosso	14.54	7.94	1.28	23.75	2.17	0.64	-	1.52	1.29	0.31	0.08	70.24	29.76
35	M. Rosso	16.22	6.58	1.18	23.98	2.39	1.23	-	0.86	0.99	0.41	0.07	70.07	29.93
36	M. Rusta	-	-	13.64	13.64	0.71	-	-	2.59	0.36	0.62	0.04	82.05	17.95
37	M. Rusta	2.00	-	16.59	18.59	0.48	-	-	3.79	0.28	0.08	0.01	76.78	23.22
38	M. Rusta	4.14	-	10.31	14.45	0.56	-	-	0.45	0.28	0.10	0.01	84.16	15.84
39	M. San Daniele	4.68	4.04	11.82	20.54	0.86	-	-	2.14	0.42	0.18	0.09	75.78	24.22
40	M. Trevisan	1.56	5.50	-	7.06	0.64	-	0.89	0.65	0.53	0.04	0.38	89.80	10.20

- Abbreviations of minerals according to Whitney & Evans (2010): Ano = anorthoclase; Pl = plagioclase; Sa = sanidine; Bt = biotite; Aug = augite; Krs = kaersutite; Qz = quartz; Crs = cristobalite; Mag = magnetite; Ilm = ilmenite.
- Σ Fsp = percentage sum of all feldspars.
- "Others" include apatite, zircon, titanite, epidote, calcite, dolomite, pyrite and siderite.

A second parameter for distinguishing quarries is P.I., which is proportional to the total sum of the feldspar fraction. Trachytes from the Zovon area, quarry 20 of Monselice, Rocca Pendice, M. Bello, M. Lozzo, M. Rosso and M. Merlo are characterized by a P.I. higher than 25%, with groundmass percentage being particularly low (down to about 65%) for the first three localities. On the contrary, the lowest values of P.I., down to 10-15%, are related to M. Cero, M. Murale and M. Trevisan, together with some samples from M. Oliveto and quarry 2 of M. Alto, whereas trachytes from all the other localities are scattered among intermediate values (Fig. 9a).

Other mineralogical features are less effective as discriminant markers, but some complementary indications can be derived from the concentration of mafic minerals and SiO_2 phases. Total abundance of biotite, augite, and kaersutite is the lowest (under about 1%) in Monselice, M. Rusta, M. Grande, M. San Daniele, M. Oliveto and quarry 2 of M. Alto, and the highest (from 2 to over 3%) in M. Rosso, M. Bello, M. Cero, M. Merlo, M. Lonzina, M. Lozzo and quarry 1 of M. Alto; the simple presence/absence of augite and kaersutite can provide additional clues for discrimination. Concentration of quartz and cristobalite is noticeably high (from 2 to over 5%) only in trachytes from M. Bello, M. San Daniele and single quarries of M. Rusta, M. Oliveto and M. Grande.

5.3. Texture

The most interesting textural feature for quarry clustering derived from the µ-XRF imaging is size of feldspars and feldspar glomeroporphyries, and grain size distribution (Table 3, and qualitatively inferable from Fig. 7). PCA of the data of feldspar area indicates that trachytes from the Zovon area, Monselice and Rocca Pendice are clearly grouped by their coarse grain size (Fig. 8b): the coarsest feldspars exceed 10 mm in diameter, reaching a maximum value of 16 mm, with the highest frequency of crystals above 10 mm^2 in area, and up to 70 mm^2. On the other hand, fine-grained trachytes from M. Murale, M. San Daniele, M. Cero, M. Oliveto and quarry 2 of M. Alto are characterized by nearly all of the feldspar phenocrysts (over 90%) finer than 5 mm^2, often with no crystals in the size classes above 10 mm^2 (Fig. 9b) and with maximum diameter usually of 5-7 mm. Samples from the other localities range as in Fig. 9b, mostly in mid grain size classes.
Another discriminant parameter involving grain size distribution can be qualitatively provided through simple optical microscopic observations. Indeed, trachytes from M. Merlo and M. Lozzo

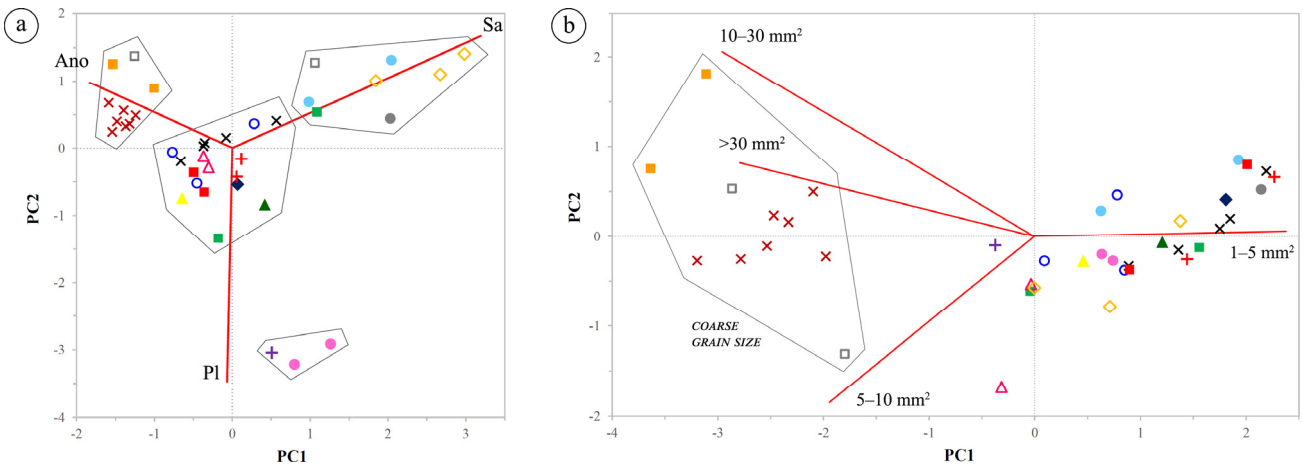

Fig. 8. Results of PCA performed on µ-XRF data of trachyte quarries, with score and loading plots built on the following parameters: **a)** average concentration of feldspars (anorthoclase, plagioclase and sanidine), with PC1 and PC2 covering 49% and 41% of total variance, respectively; **b)** frequency size classes of feldspars expressed as area, with PC1 and PC2 covering 83% and 10% of total variance, respectively. Quarry symbols as in Table 1.

have a seriate distribution, and so have those from M. Bello and M. Rosso, together with few samples from M. Oliveto, although to a lesser extent; in contrast, rocks from all the other quarries display an evident hiatal grain size distribution[3] (Fig. 10).

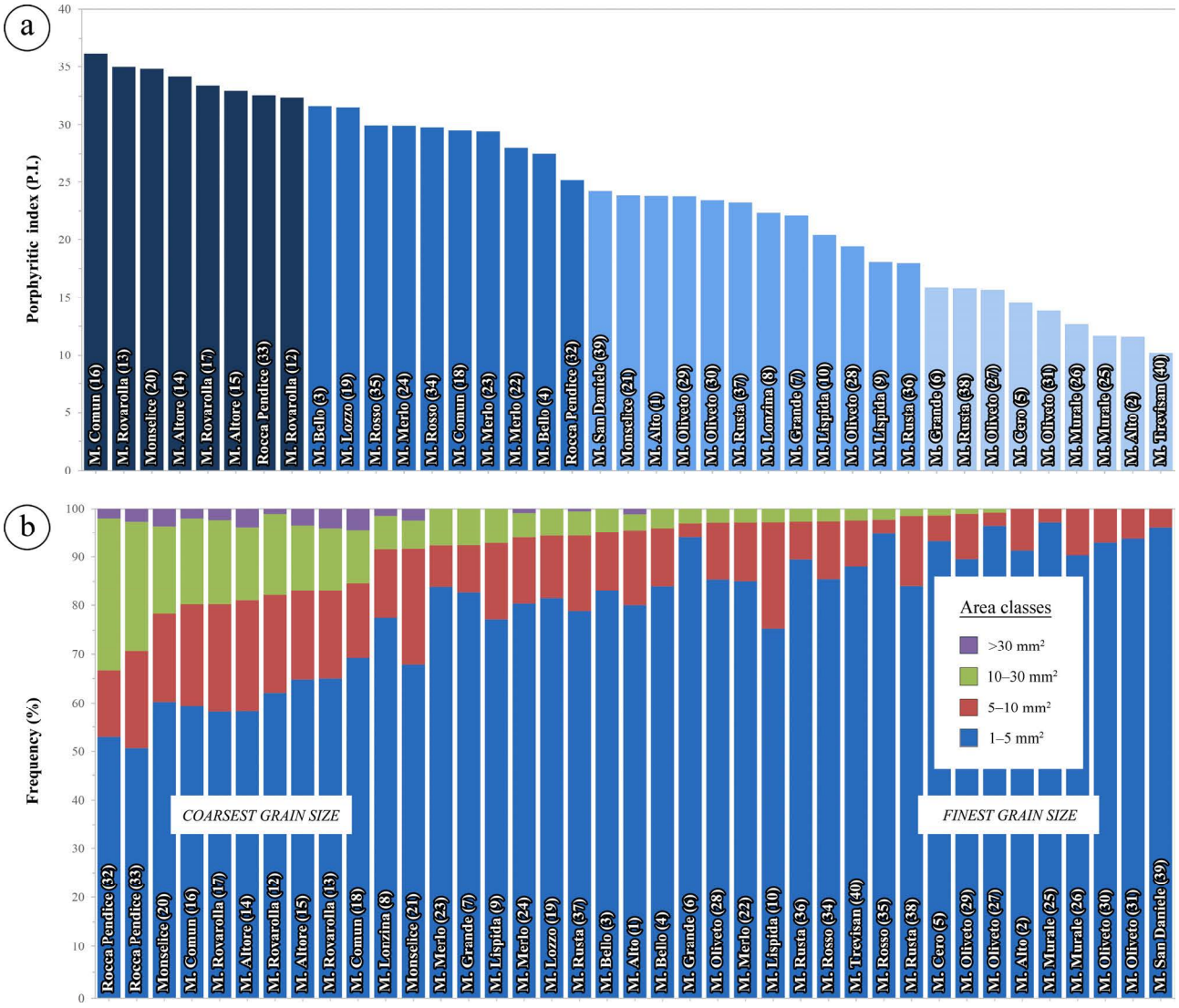

Fig. 9. Histograms of textural parameters determined by DIA of the μ-XRF maps for each trachyte quarry, considering **a)** porphyritic index (P.I.) and **b)** frequency size classes of feldspars expressed as area. Quarries are indicated with locality name and ID number in parentheses.

[3] Texture is said to be seriate if crystals of the main mineral phases are distributed within a continuous range of sizes, whereas hiatal texture involves crystals showing few, noticeably different sizes. In this paper, texture with intermediate characteristics is defined as weakly seriate, e.g., in trachytes from M. Bello and M. Rosso: their grain size is distributed in a continuous range only from the fine to the medium size classes (usually up to about 10 mm² in area and 5 mm in diameter, according to the μ-XRF results), while one or more hiatuses break the series from the medium to the coarse classes, so that coarse phenocrysts display only few different sizes.

Table 3. Texture expressed by grain size distribution, observed under the microscope, and size of feldspars (anorthoclase, plagioclase and sanidine considered together) and feldspar glomeroporphyries determined by μ-XRF mapping and digital image analysis. For each quarry (number and localization as in Fig. 2), values are averaged among different samples, except for maxima.

Quarry	Locality	Grain size distribution	Feldspars area (mm^2)						Feldspars Feret diameter (mm)				
			Mean	Max	1–5 (%)	5–10 (%)	10–30 (%)	>30 (%)	Mean	Max	≤2 (%)	2–8 (%)	>8 (%)
1	M. Alto	Hiatal	0.78	34.75	80.00	15.56	3.33	1.11	1.19	9.78	83.36	16.09	0.55
2	M. Alto	Hiatal	0.29	9.13	91.30	8.70	0.00	0.00	0.73	6.58	94.11	5.89	0.00
3	M. Bello	± Seriate	0.33	12.17	83.00	12.00	5.00	0.00	0.69	6.29	93.96	6.04	0.00
4	M. Bello	± Seriate	0.57	20.57	84.00	12.00	4.00	0.00	0.96	7.40	89.36	10.64	0.00
5	M. Cero	Hiatal	0.99	10.19	93.24	5.41	1.35	0.00	1.43	5.37	76.92	23.08	0.00
6	M. Grande	Hiatal	0.52	20.99	94.03	2.99	2.99	0.00	0.89	7.56	87.64	12.36	0.00
7	M. Grande	Hiatal	0.56	16.98	82.61	9.78	7.61	0.00	0.97	7.71	89.41	10.59	0.00
8	M. Lonzina	Hiatal	0.98	41.55	77.46	14.08	7.04	1.41	1.15	11.68	85.79	13.96	0.25
9	M. Lispida	Hiatal	0.74	24.19	77.14	15.71	7.14	0.00	1.17	6.98	83.11	16.89	0.00
10	M. Lispida	Hiatal	0.81	13.99	75.34	21.92	2.74	0.00	1.22	6.64	81.78	18.22	0.00
11	M. della Madonna	± Seriate	0.94	23.03	75.44	17.54	7.02	0.00	1.19	8.38	83.00	16.67	0.33
12	M. Rovarolla	Hiatal	1.66	32.51	62.11	20.00	16.84	1.05	1.51	9.77	77.04	22.16	0.79
13	M. Rovarolla	Hiatal	2.21	42.27	65.00	18.00	13.00	4.00	1.73	10.47	71.90	26.14	1.96
14	M. Altore	Hiatal	2.34	70.42	58.23	22.78	15.19	3.80	1.73	15.90	74.74	23.89	1.37
15	M. Altore	Hiatal	1.60	39.06	64.77	18.18	13.64	3.41	1.43	8.84	80.98	17.99	1.03
16	M. Comun	Hiatal	1.63	44.60	59.41	20.79	17.82	1.98	1.47	10.69	78.00	20.63	1.36
17	M. Rovarolla	Hiatal	1.87	42.61	58.14	22.09	17.44	2.33	1.54	11.92	78.67	19.60	1.73
18	M. Comun	Hiatal	1.53	34.35	69.23	15.38	10.99	4.40	1.49	11.04	77.51	20.11	2.38
19	M. Lozzo	Seriate	1.01	29.45	81.45	12.90	5.65	0.00	1.36	10.38	81.33	18.31	0.36
20	Monselice	Hiatal	1.17	40.00	60.24	18.07	18.07	3.61	1.04	10.77	85.56	13.73	0.71
21	Monselice	Hiatal	1.06	41.15	67.86	23.81	5.95	2.38	1.24	10.37	82.67	16.67	0.67
22	M. Merlo	Seriate	0.42	15.37	85.05	12.15	2.80	0.00	0.86	6.15	90.63	9.37	0.00
23	M. Merlo	Seriate	0.62	26.96	83.90	8.47	7.63	0.00	1.01	7.99	87.96	12.04	0.00
24	M. Merlo	Seriate	0.76	34.94	80.34	13.68	5.13	0.85	1.19	9.69	84.72	15.15	0.13
25	M. Murale	Hiatal	0.30	5.60	97.22	2.78	0.00	0.00	0.86	6.23	92.27	7.73	0.00
26	M. Murale	Hiatal	0.47	7.81	90.32	9.68	0.00	0.00	0.88	5.62	89.66	10.34	0.00
27	M. Oliveto	Hiatal	0.40	10.21	96.49	2.73	0.78	0.00	0.88	6.95	91.21	8.79	0.00
28	M. Oliveto	Hiatal	0.40	13.86	85.39	11.80	2.81	0.00	0.84	7.46	92.71	7.29	0.00
29	M. Oliveto	Hiatal; ± Seriate	0.34	13.28	89.53	9.45	1.02	0.00	0.76	8.53	93.23	6.74	0.04
30	M. Oliveto	Hiatal	0.43	9.61	92.92	7.08	0.00	0.00	0.88	7.83	91.10	8.90	0.00
31	M. Oliveto	Hiatal; ± Seriate	0.46	7.22	93.74	6.26	0.00	0.00	0.91	5.51	90.38	9.62	0.00
32	Rocca Pendice	Hiatal	2.23	48.88	52.94	13.73	31.37	1.96	1.67	12.90	77.07	21.95	0.98
33	Rocca Pendice	Hiatal	1.60	44.86	50.67	20.00	26.67	2.67	1.35	12.74	83.04	15.21	1.75
34	M. Rosso	± Seriate	0.52	28.03	85.47	11.97	2.56	0.00	0.93	10.46	89.88	9.92	0.20
35	M. Rosso	± Seriate	0.52	23.55	94.81	2.96	2.22	0.00	1.01	10.83	88.68	11.22	0.10
36	M. Rusta	Hiatal	0.61	15.75	89.47	7.89	2.63	0.00	0.97	7.25	88.33	11.67	0.00
37	M. Rusta	Hiatal	1.23	33.79	78.83	15.55	5.09	0.53	1.51	10.16	76.14	23.41	0.45
38	M. Rusta	Hiatal	0.51	23.93	84.06	14.49	1.45	0.00	0.87	10.04	89.62	10.21	0.16
39	M. San Daniele	Hiatal	0.56	8.89	96.18	3.82	0.00	0.00	1.15	5.15	86.48	13.52	0.00
40	M. Trevisan	Hiatal	0.71	11.88	88.10	9.52	2.38	0.00	1.15	5.45	85.78	14.22	0.00

- Grain size distribution showing intermediate characteristics between hiatal and seriate is marked with "±" (i.e., weakly seriate).
- Area distribution is represented through four classes (with limits at 5, 10, and 30mm^2), Feret diameter distribution through three classes (with limits at 2 and 8 mm) and frequencies within each class are expressed as relative percentage.

5.4. Groundmass

Additional elements for separating and distinguishing the different quarries are composition and texture of the groundmass, studied through SEM-EDS mapping, DIA and optical microscopy (Table 4). Only a few features turned out to be rather variable within the same sample, i.e., more strictly dependent on the specific mapped portion of the groundmass, such as presence and abundance of glass,

iron oxides, other accessory minerals, or microphenocrysts.
On the other hand, the abundance of quartz and cristobalite in the groundmass can be used for identifying a few large quarry clusters (Fig. 11). Trachytes from M. Rosso, M. Bello, quarry 2 of M. Alto and quarry 16 of M. Comun are characterized by the highest percentages of the SiO_2 phases, exceeding 20%, while the other quarries of the Zovon area are associated with values from 15 to 20%. At the other extreme are M. Lispida, M. Lozzo, Monselice, M. Cero and M. Murale, which display increasingly lower concentrations, from 10 to nearly 0%. The other localities are scattered over an intermediate or undefined/broad interval.

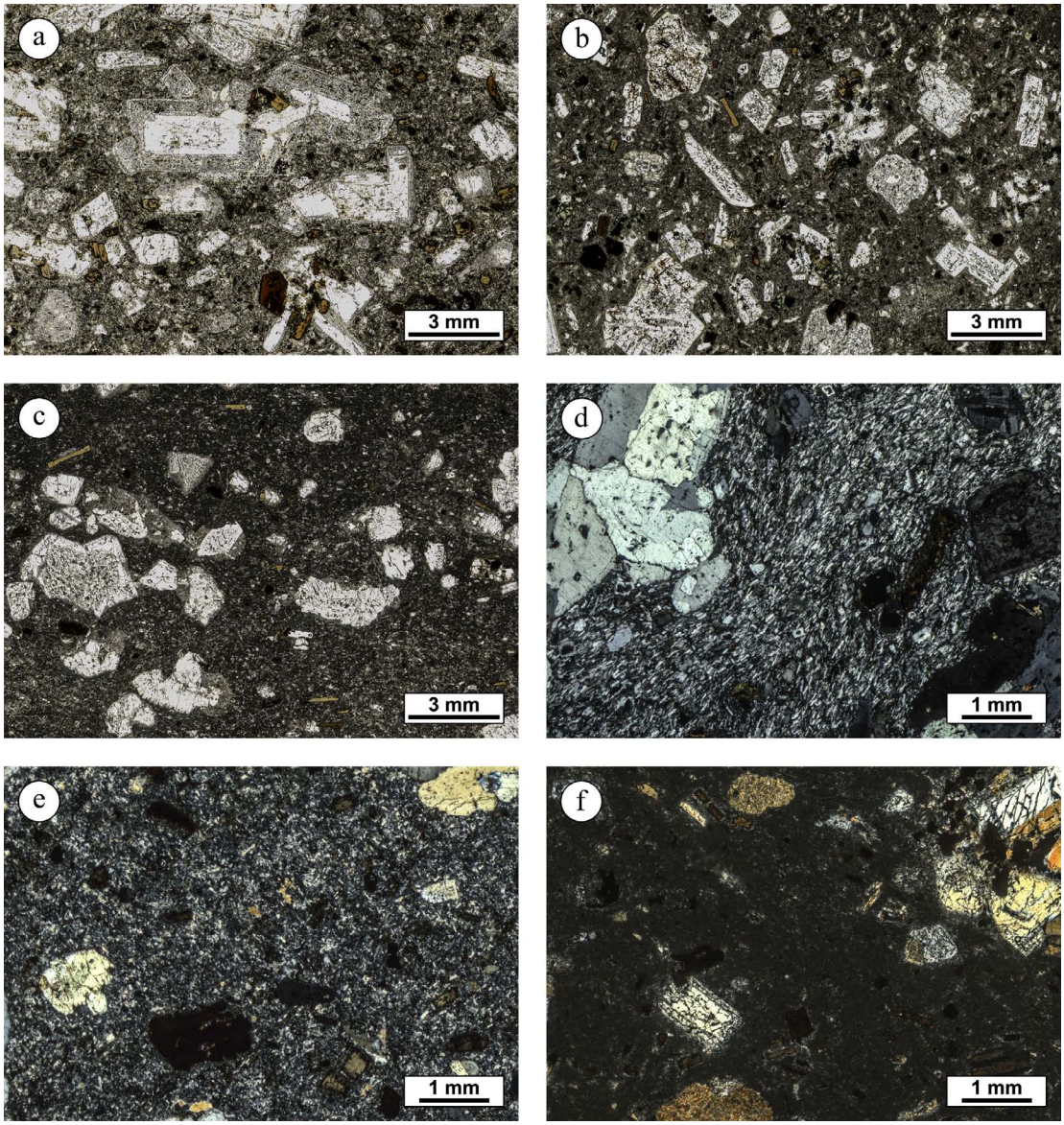

Fig. 10. Thin-section photomicrographs of Euganean trachyte, with samples from: **a)** M. Merlo, quarry 22, showing a seriate grain size distribution (plane-polarized light); **b)** M. Rosso, quarry 34, displaying a weakly seriate grain size distribution (plane-polarized light); **c)** M. Oliveto, quarry 31, with a hiatal distribution (plane-polarized light); **d)** Monselice, quarry 20, having a microcrystalline groundmass with trachytic texture (crossed-polarized light); **e)** M. Rovarolla, quarry 12, with a microcrystalline felty groundmass (crossed-polarized light); **f)** M. Oliveto, quarry 30, characterized by a cryptocrystalline groundmass (crossed-polarized light). Anomalous colors are due to the 45 μm thickness of the sections.

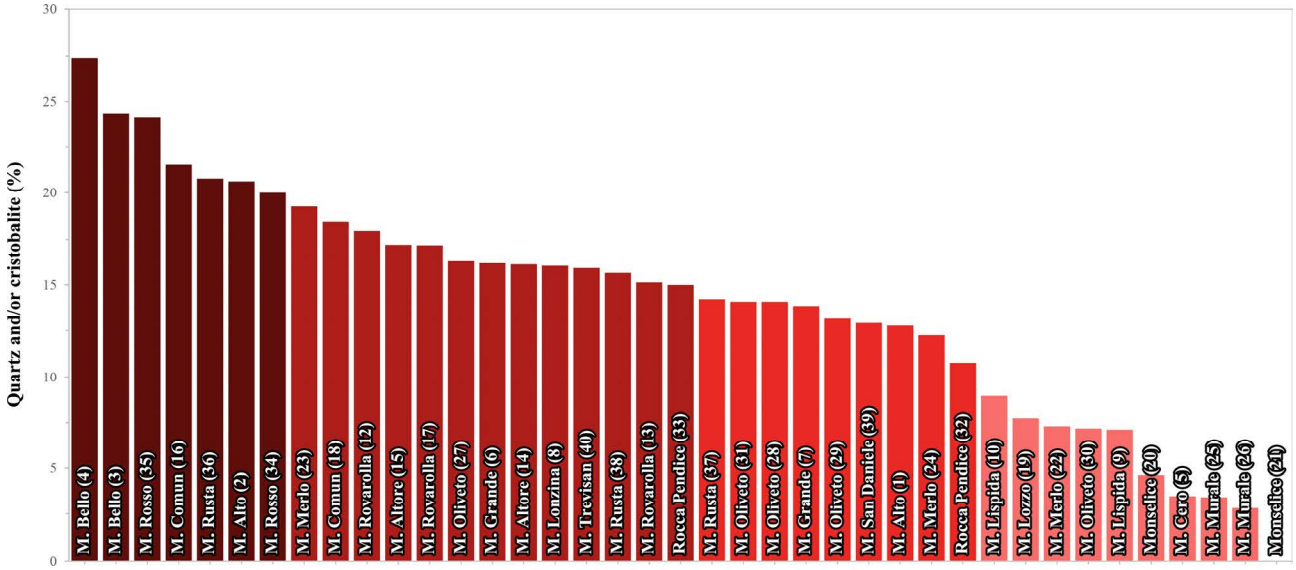

Fig. 11. Histogram of concentration of quartz and/or cristobalite in trachyte groundmass for each quarry, determined by SEM-EDS imaging. Quarries are indicated with locality name and ID number in parentheses.

Another informative mineralogical parameter is the presence and abundance of plagioclase or Ca enriched alkali-feldspars in the rock matrix. Concentration of Ca-rich feldspars ranges from 7 to 13% in quarry 1 of M. Alto, M. Lozzo, M. Murale, M. San Daniele, M. Trevisan and M. Merlo. Slightly lower percentages can be detected for Monselice, M. Rosso and M. Lonzina, whereas for M. Lispida, M. Bello and M. Cero values approach 0%. Ca-rich feldspars are absent in the groundmass of trachytes from all the other localities.

With regard to the groundmass texture, relative arrangement of crystals and grain size can be best analyzed qualitatively under the optical microscope (Fig. 10). Since the matrix is almost entirely constituted of alkali-feldspars, the correct separation of single microlites in mutual contact and with the same composition is virtually impossible from X-ray chemical maps.

The groundmass texture is felty in most quarries, while a trachytic texture can be seen in Monselice, M. Cero, M. Murale and M. Trevisan. A mixed felty-trachytic texture can be observed in M. Grande, as well as in few samples from Monselice, M. Oliveto and M. Trevisan, in these last cases being linked to weak isorientation of microlites in domains surrounding the phenocrysts.

As for grain size, a rough distinction among microcrystalline, cryptocrystalline and intermediate matrix is presented in Table 4, where it is worth noting that, on a qualitative basis, the finest-grained groundmass is that of trachytes from M. Oliveto, M. Lonzina and M. Lispida; conversely, the coarsest grain size is typical of M. Merlo, M. Lozzo, Monselice, and quarry 1 of M. Alto. These considerations are partly validated by quantitative data about grain size of the SiO_2 phases; indeed, mean area of the intercrystalline particles of quartz and cristobalite is proportional to pore-free intercrystalline spaces and, indirectly, to microlite size. This approximation matches in several cases microscopic observations, with the positive correlation between quartz/cristobalite grain size – calculated by SEM-EDS imaging – and related groundmass grain size – observed under the optical microscope.

Table 4. Groundmass properties: textural arrangement and size of microlites, observed under the microscope, modal composition/glass content expressed in percentage and grain size of SiO_2 phases determined by μ-XRF mapping and digital image analysis. For each quarry (number and localization as in Fig. 2), values are averaged among different samples, except for maxima.

Quarry	Locality	Texture	Grain size	Composition							Qz/Crs grain size	
				Afs	Pl	Qz/ Crs	Ti-Mag	Ilm	Glass	Others	Mean area (μm²)	Mean diameter (μm)
1	M. Alto	Felty	M	72.64	13.27	12.76	0.86	0.07	-	0.39	123.31	15.72
2	M. Alto	Felty	M/C	78.37	-	20.62	0.60	0.23	-	0.18	64.67	10.47
3	M. Bello	Felty	C	74.64	0.38	24.35	0.46	0.14	-	0.03	95.73	15.16
4	M. Bello	Felty	C	69.32	1.24	27.39	0.41	0.28	1.27	0.08	127.39	15.90
5	M. Cero	Trachytic	M	95.01	0.54	3.46	0.77	-	-	0.22	79.97	13.28
6	M. Grande	± Felty	M	81.67	-	16.18	0.43	0.03	1.67	0.01	81.60	12.90
7	M. Grande	± Felty	M	82.70	-	13.84	0.92	0.09	2.42	0.03	102.77	15.62
8	M. Lonzina	Felty	C	78.25	4.81	16.05	0.50	0.33	-	0.07	26.46	7.75
9	M. Lispida	Felty	C	85.59	1.46	7.11	0.99	0.19	4.65	0.01	116.31	11.30
10	M. Lispida	Felty	C/M	86.96	2.38	8.94	0.46	0.12	1.01	0.13	132.00	15.84
11	M. della Madonna	Felty	M	80.27	-	14.43	0.49	0.17	4.35	0.29	49.19	8.15
12	M. Rovarolla	Felty	M	80.71	-	17.96	0.95	0.19	-	0.20	193.55	19.84
13	M. Rovarolla	Felty	M/C	82.22	-	15.13	0.99	0.29	-	1.38	162.17	18.12
14	M. Altore	Felty	M/C	82.09	-	16.13	1.00	0.20	0.29	0.29	179.46	20.05
15	M. Altore	Felty	M/C	80.48	-	17.19	0.80	0.22	1.18	0.13	170.22	19.01
16	M. Comun	Felty	M/C	76.85	-	21.56	0.74	0.24	0.50	0.12	211.26	19.99
17	M. Rovarolla	Felty	M/C	80.31	-	17.17	0.57	0.31	-	1.64	252.77	20.95
18	M. Comun	Felty	M/C	78.30	-	18.42	0.81	0.18	1.81	0.48	184.53	19.92
19	M. Lozzo	Felty	M	78.25	12.38	7.75	0.76	0.36	-	0.51	295.86	19.68
20	Monselice	Trachytic	M	87.47	5.14	4.62	0.66	-	1.21	0.90	176.27	18.35
21	Monselice	Trachytic	M	94.70	2.85	0.03	0.80	-	1.00	0.62	42.53	7.85
22	M. Merlo	Felty	M	74.95	7.36	7.30	0.68	0.34	8.75	0.64	318.03	21.39
23	M. Merlo	Felty	M	72.42	7.08	19.25	0.33	0.57	-	0.34	176.79	18.42
24	M. Merlo	Felty	M	77.03	9.40	12.25	0.61	0.40	-	0.31	425.55	27.02
25	M. Murale	Trachytic	M/C	82.80	11.05	3.39	0.66	0.24	1.73	0.13	30.78	7.39
26	M. Murale	Trachytic	M/C	87.41	8.18	2.81	0.47	-	1.13	0.01	15.61	6.19
27	M. Oliveto	± Felty	C	82.51	-	16.29	0.78	0.25	-	0.17	60.44	12.28
28	M. Oliveto	Felty	C	84.75	-	14.07	0.89	0.17	-	0.12	76.59	11.28
29	M. Oliveto	Felty	C/M	85.81	-	13.14	0.54	0.24	-	0.27	104.72	16.02
30	M. Oliveto	± Felty	C	89.61	-	7.17	0.86	0.23	1.98	0.14	52.48	10.86
31	M. Oliveto	Felty	C/M	85.27	-	14.08	0.36	0.14	-	0.16	35.72	9.13
32	Rocca Pendice	Felty	M/C	88.22	-	10.76	0.78	0.10	-	0.14	106.64	15.47
33	Rocca Pendice	Felty	M/C	81.82	-	14.98	0.56	0.20	2.16	0.27	90.60	12.38
34	M. Rosso	Felty	M	73.85	4.86	20.00	0.64	0.48	-	0.16	127.84	15.93
35	M. Rosso	Felty	M	70.50	4.20	24.15	0.59	0.37	-	0.19	174.72	17.15
36	M. Rusta	Felty	M/C	77.70	-	20.78	0.69	0.17	0.65	-	86.59	13.74
37	M. Rusta	Felty	M/C	84.49	-	14.22	0.62	0.45	0.19	0.03	74.66	13.75
38	M. Rusta	Felty	M/C	83.40	-	15.65	0.33	0.41	0.19	0.02	41.36	9.34
39	M. San Daniele	Felty	M/C	73.37	10.95	12.91	1.23	0.19	1.30	0.05	50.56	10.22
40	M. Trevisan	Trachytic	C/M	72.58	10.83	15.91	0.45	0.04	-	0.20	129.11	14.20

- Texture showing intermediate characteristics between felty and trachytic is marked with "±".
- Grain size is marked with "M" and "C" standing for microcrystalline or cryptocrystalline, respectively.
- Abbreviations of minerals according to Whitney & Evans (2010): Afs = alkali-feldspar; Pl = plagioclase; Qz = quartz; Crs = cristobalite; Mag = magnetite; Ilm = ilmenite.
- Discrimination between alkali-feldspar and plagioclase is uncertain due to their compositions with variable K:Ca ratios.

5.5. Step-by-step provenance recognition

Provenance recognition of Euganean trachyte based on petrography can be accomplished multiple ways, taking into account the parameters described above. Here, a simplified and synthetic procedure,

considering one at a time the main petrographic criteria, is suggested and schematically represented in Fig. 12. It is possible to start with simple qualitative features easily detectable under the optical microscope, describing grain size distribution and groundmass texture. Image analysis – not necessarily on X-ray maps – is strongly recommended in support of microscopic observations, while going deeper into characterization. In case high uncertainty of provenance attribution of a particular sample arises, the minor petrographic tracers specified in the previous paragraphs will help.
However, contrary to what has been previously stated in the literature, petrographic features alone are not infallible for determining trachyte provenance, especially if a high degree of precision is required, qualitative parameters are mainly considered or a reference collection of quarry samples of known provenance is not available. Indeed, different quarry localities, even far away, can share very similar petrographic features. In addition, within the same quarry or locality, some samples can display a misleading variability in mineralogical and textural characteristics. This is the case, as an instance, of M. Alto, M. Oliveto and Monselice.

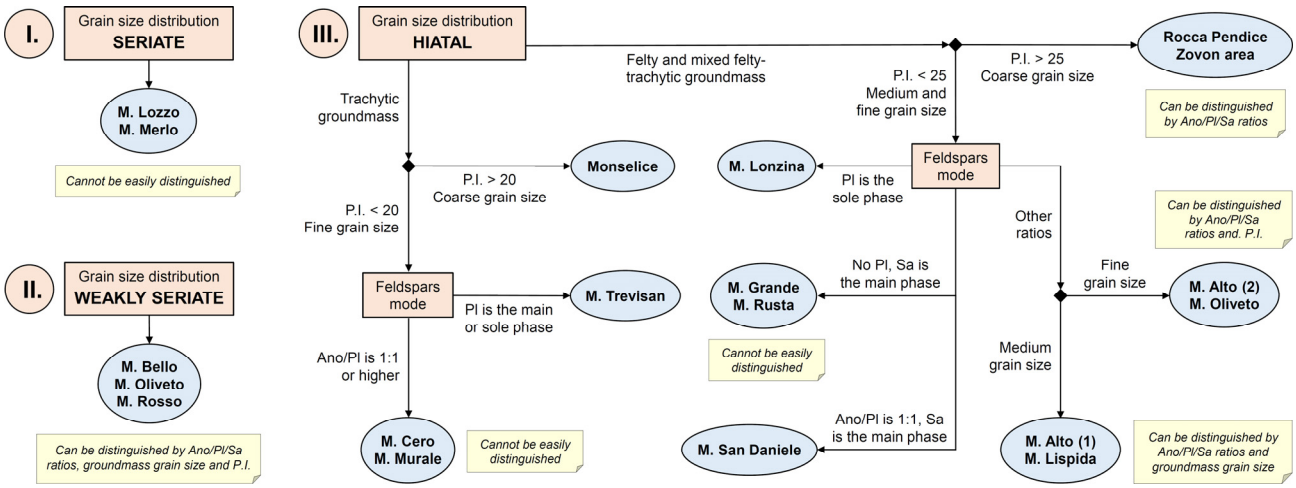

Fig. 12. Practical flowchart-like scheme for recognizing quarry locality of provenance of Euganean trachyte, starting from one of the three kinds of grain size distribution. Only few, significant petrographic parameters are considered here, so that it is necessary to refer to the text and tables (Table 2, 3, 4) for precise attribution, quantitative data and to try discriminating analogous sites. Feldspars abbreviations according to Whitney & Evans (2010).

5.6. Comparison with literature data

The petrographic markers discussed so far have proven to be the most effective for provenancing purposes. Other criteria suggested in the former literature (Zantedeschi & Zanco 1993; Capedri et al. 2000) turned out not to have the same reliability.
Rock color is not a useful parameter: besides being rather similar for most trachytes, it can be heavily affected by weathering and Fe oxides/hydroxides migration, the extent of which is independent on the quarry considered.

Determination of modal composition and phenocrysts-groundmass ratio has been previously done by either visual assessment or point counting on thin section, revealing significant inaccuracy especially with regard to correct identification of the different mineral phases and calculation of their quantitative relationships.
Magnetic susceptibility is another parameter suggested as an indirect indicator of mineralogical composition, in particular the abundance of Fe oxides, which however is never uniquely distinctive.
Finally, texture has been previously studied in a qualitative way mostly. Specific features such as feldspar microstructures (e.g., overgrown coronas, internal zoning) and shape are not unequivocally typical of the different quarries, as also confirmed by data of circularity and aspect ratio of phenocrysts acquired by DIA in the present study. Even former determinations of grain size in the literature, performed by naked eye on hand specimens, are less precise and representative than those done by DIA.
The framework of the petrographic analysis proposed here aims at reducing subjectivity and inaccuracy linked to qualitative methods, providing more strict and precise elements for quarry recognition and introducing new criteria.

6. Geochemical tracers

6.1. General characterization

According to the total alkali-silica (TAS) classification (Le Maitre 2002), most samples of Euganean trachyte can be defined as trachyte s.s., based on XRF data of bulk chemical composition. Some of the samples plot in the field of rhyolite, i.e., almost the totality of trachyte samples from M. Rusta and few others from M. Oliveto, M. Alto, M. Grande and M. della Madonna; others more from these localities and M. San Daniele plot very close to the boundary between the two fields (Fig. 13). Combining the data of the modal composition determined on phenocrysts and groundmass by μ-XRF and

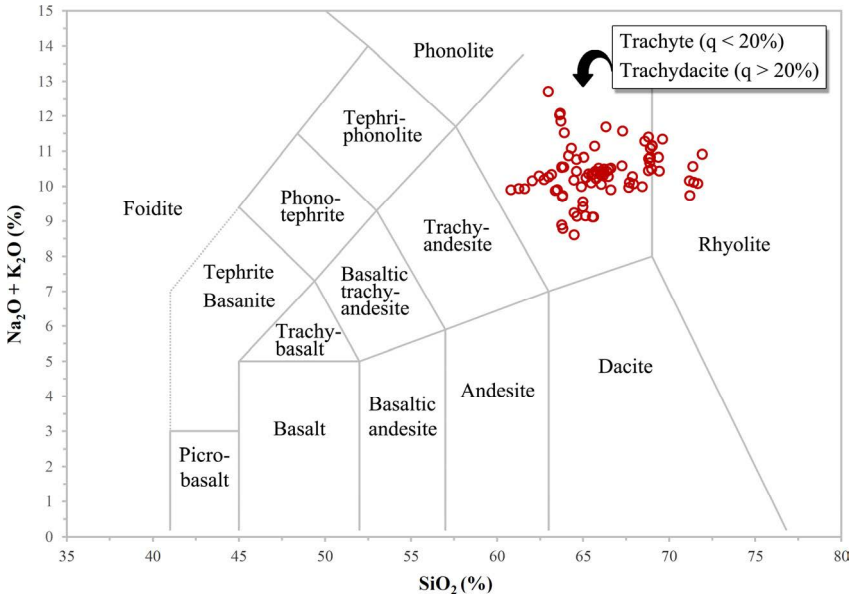

Fig. 13. Disposition of the samples of Euganean trachyte in the TAS (total alkali-silica) classification diagram (Le Maitre 2002), based on bulk-rock chemical composition determined by XRF.

SEM-EDS, and considering the "q" factor (total quartz percentage normalized to the sum of quartz and feldspars), only few samples (from M. Bello, quarry 2 of M. Alto and quarry 36 of M. Rusta) display a value higher than 20%, and then can be classified as trachydacite.
In the following paragraphs, information and plots useful for recognizing provenance quarry of Euganean trachyte will be provided. Few samples (including those previously identified as outliers on petrographic basis, e.g., from M. della Madonna and M. Murale) were recognized as outliers through univariate and multivariate statistical methods applied to their bulk chemical composition, and excluded from the calculations.

6.2. Bulk-rock composition

Bulk-rock chemical composition calculated by XRF is reported for all the samples in Appendix 2. These data were used to build binary plots and, among all the possible combinations, select the pairs of major and trace elements showing the best separations among the Euganean quarry localities; the selection was supported by an explorative PCA done on all the chemical elements analyzed (Appendix 3), then refined by bivariate statistical analysis. The most informative binary plot is V/Nb, in which the quarry localities of Monselice, M. Rosso, M. Trevisan and M. Merlo (quarry 21 and 23) cluster separately, while the couples M. Bello-M. Lonzina and Zovon area-Rocca Pendice form two mixed clusters (Fig. 14); other useful binary plots are TiO_2/Zr, TiO_2/K_2O, Na_2O/Zr, Rb/Zr, Al_2O_3/Sr and Ce/Nd (Fig. 15). Few sites can be easily distinguished in multiple binary plots, others cannot be isolated at all, i.e., M. Cero, M. Lispida and quarry 22 of M. Merlo, while the Zovon area and Rocca Pendice cannot be uniquely differentiated from each other. In general, clustering is often not very satisfactory, and attribution of correct provenance may be affected by great uncertainty. This may further increase when analyzing small and altered archaeological objects, instead of fresh quarry samples. For these reasons, in order to minimize possible errors, it is suggested not to rely on single plots

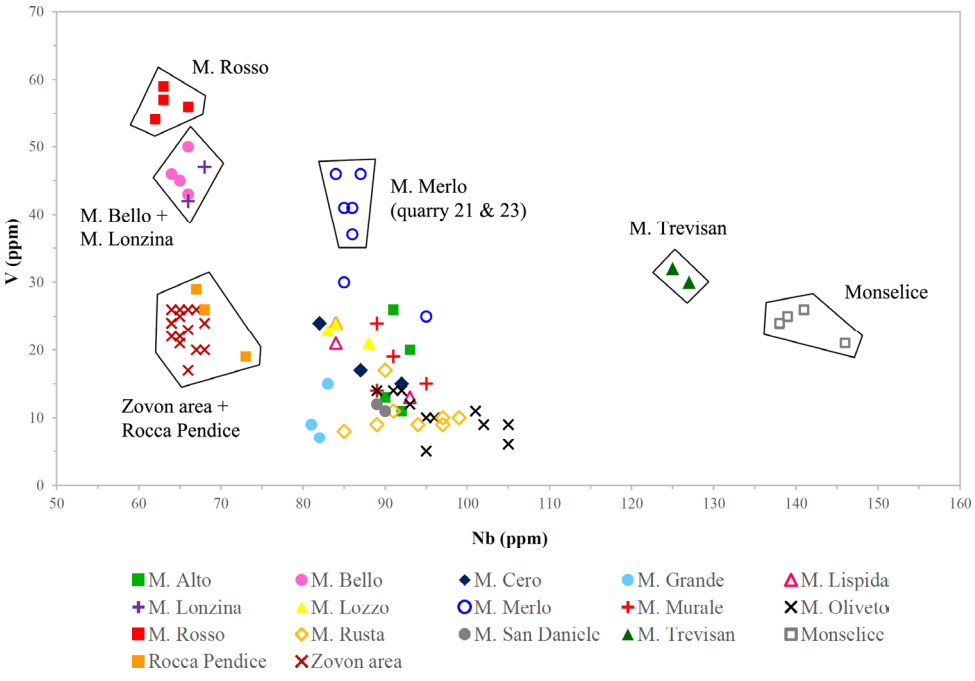

Fig. 14. V vs. Nb scatterplot from bulk-rock chemical composition determined by XRF for all the samples of Euganean trachyte.

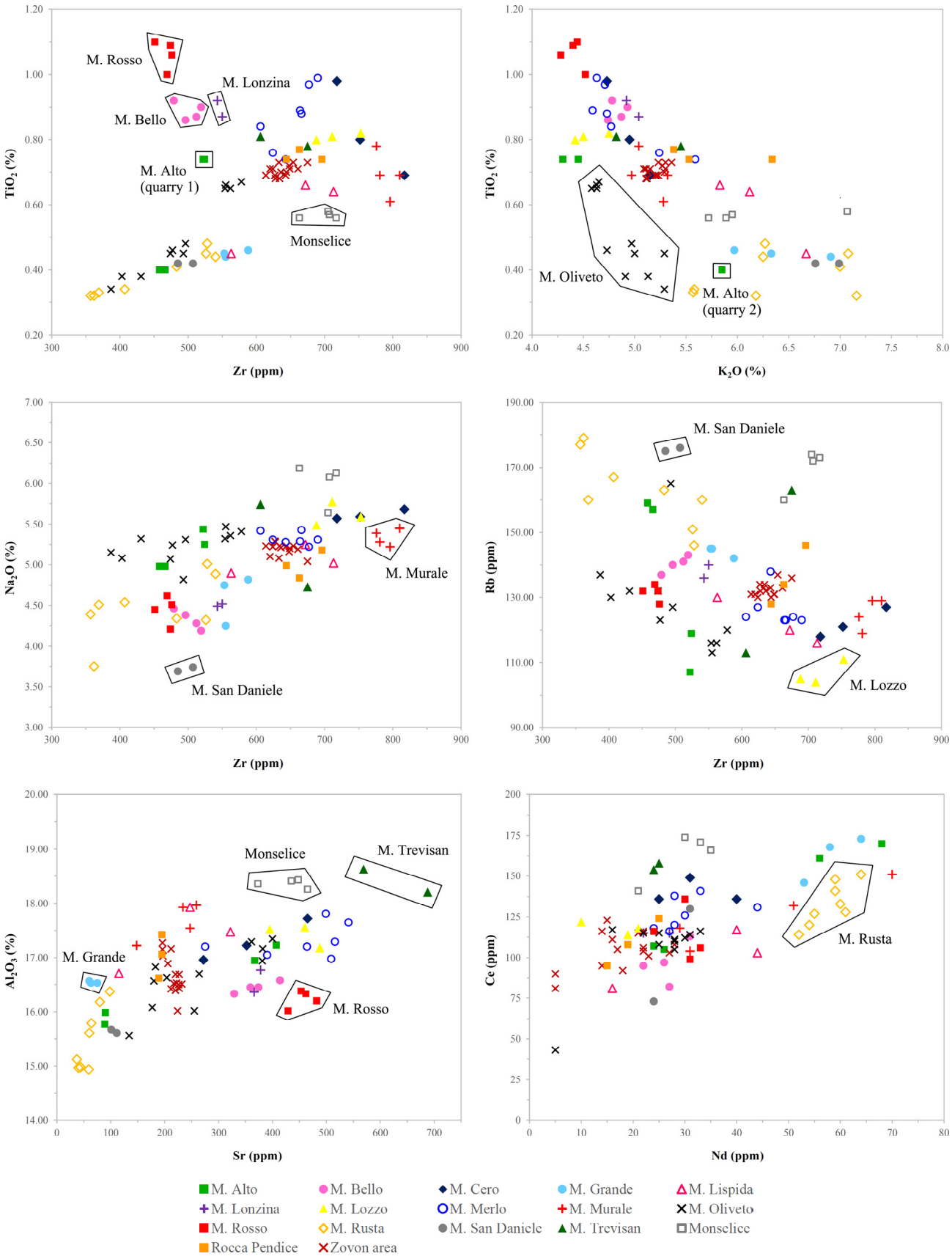

Fig. 15. Binary scatterplots from bulk-rock chemical composition determined by XRF for all the samples of Euganean trachyte.

and clusters only, but to check the disposition of a study sample using all of the diagrams proposed, and verify which group of reference quarry samples provides the best fit. An alternative could be accomplished by doing a statistical discriminant analysis, using all the data in Appendix 2 in order to classify trachytes from the different quarry localities based on their composition and known provenance, and verifying which locality is attributed by default to the study sample based on multivariate chemical correlations.

6.3. Mineral-scale composition

Major-element chemistry of phenocrysts in Euganean trachyte determined by EPMA does not provide useful hints for provenancing after a bivariate and multivariate statistical analysis, since major-element composition of a given phase is rather homogeneous among all the samples, as indicated by the generally low values of the standard deviations from the mean concentrations in Table 5.
The same does not apply to LA-ICPMS results and to major elements when combined with trace elements. All the data obtained from each analyzed spot are included in Appendix 4, subdivided by mineral phase, together with average values measured on 610 and BCR-2G standards.
Initially, the LA-ICPMS data were processed normalizing all the concentrations of rare earth elements (REE) and incompatible elements to CI chondrites and primitive mantle compositions (Sun & McDonough 1989; McDonough & Sun 1995). The resulting REE patterns and spider diagrams show negligible variations among the samples and very similar trends for each mineral phase.
The next step was identifying the most informative elements to be used in simple scatterplots for separating quarry localities. A statistical discriminant analysis was performed and all the samples were classified *a priori* according to their known provenance, then the best discriminating multivariate correlations were selected, i.e., linear combinations of major- and trace-element concentrations. These functions were eventually used to build the binary and ternary plots presented below. Traditional binary plots based on concentration values of single elements, similarly to what was done for the XRF data, are also provided in Appendix 5; they can be useful in case of anomalous concentrations obtained for particular elements, which would compromise the efficacy of multivariate correlations.

Table 5. Major-element chemical composition of the main mineral phases in Euganean trachyte determined by EPMA and averaged among all the samples with standard deviations (~500 crystals in total); concentrations are expressed as oxide weight percent.

	Anorthoclase	**Apatite**	**Augite**	**Biotite**	**Kaersutite**	**Plagioclase**	**Sanidine**	**Ti-magnetite**
Na_2O	7.68 ± 0.54	0.30 ± 0.12	0.84 ± 0.26	0.73 ± 0.15	2.76 ± 0.12	7.40 ± 0.73	5.64 ± 0.69	0.03 ± 0.04
MgO	0.01 ± 0.01	0.17 ± 0.11	13.62 ± 1.25	14.21 ± 1.27	12.59 ± 0.70	0.02 ± 0.02	0.01 ± 0.01	0.83 ± 0.77
Al_2O_3	20.79 ± 0.87	0.01 ± 0.02	1.41 ± 0.45	13.84 ± 0.49	12.39 ± 0.61	24.33 ± 1.32	19.13 ± 0.30	1.10 ± 0.66
SiO_2	65.34 ± 1.24	0.29 ± 0.17	51.62 ± 0.68	36.43 ± 0.62	40.39 ± 0.62	60.72 ± 2.09	66.55 ± 0.61	0.75 ± 1.03
P_2O_5	*n/a*	41.77 ± 0.78	*n/a*	*n/a*	*n/a*	*n/a*	*n/a*	*n/a*
Cl_2O	*n/a*	1.12 ± 0.70	*n/a*	*n/a*	*n/a*	*n/a*	*n/a*	*n/a*
K_2O	3.81 ± 1.12	0.02 ± 0.03	0.01 ± 0.01	8.39 ± 0.42	1.05 ± 0.16	1.01 ± 0.29	8.08 ± 0.95	0.01 ± 0.02
CaO	2.25 ± 0.83	53.33 ± 0.62	20.74 ± 0.77	0.03 ± 0.07	10.63 ± 0.29	6.22 ± 1.55	0.54 ± 0.17	0.19 ± 1.12
TiO_2	0.04 ± 0.03	0.01 ± 0.02	0.37 ± 0.14	6.25 ± 0.64	4.83 ± 0.58	0.04 ± 0.03	0.02 ± 0.02	10.83 ± 4.75
Cr_2O_3	0.01 ± 0.02	0.01 ± 0.02	0.01 ± 0.02	0.01 ± 0.02	0.01 ± 0.02	0.01 ± 0.02	0.01 ± 0.01	0.02 ± 0.02
MnO	0.01 ± 0.02	0.26 ± 0.09	1.00 ± 0.33	0.31 ± 0.16	0.26 ± 0.09	0.02 ± 0.02	0.01 ± 0.01	1.03 ± 0.71
Fe_2O_3	0.29 ± 0.08	0.44 ± 0.29	11.04 ± 1.42	16.81 ± 2.27	14.56 ± 1.12	0.38 ± 0.07	0.20 ± 0.05	84.40 ± 6.60

Biotite is by far the most informative phase, especially considering correlations among Li, Sc, TiO_2, V, MnO and Co, used for the plots in Fig. 16, in which a large number of quarry localities cluster separately in a rather well-defined fashion: M. Lispida, M. Lonzina, M. Merlo, M. Rusta, M. San Daniele, M. Trevisan, Monselice and quarry 2 of M. Alto. In addition, the couples Bello-M. Rosso and M. Cero-M. Murale are included in two different mixed clusters; the last two localities can be distinguished in a Co/Zr plot (Appendix 5). The other sites are scattered over broader intervals of

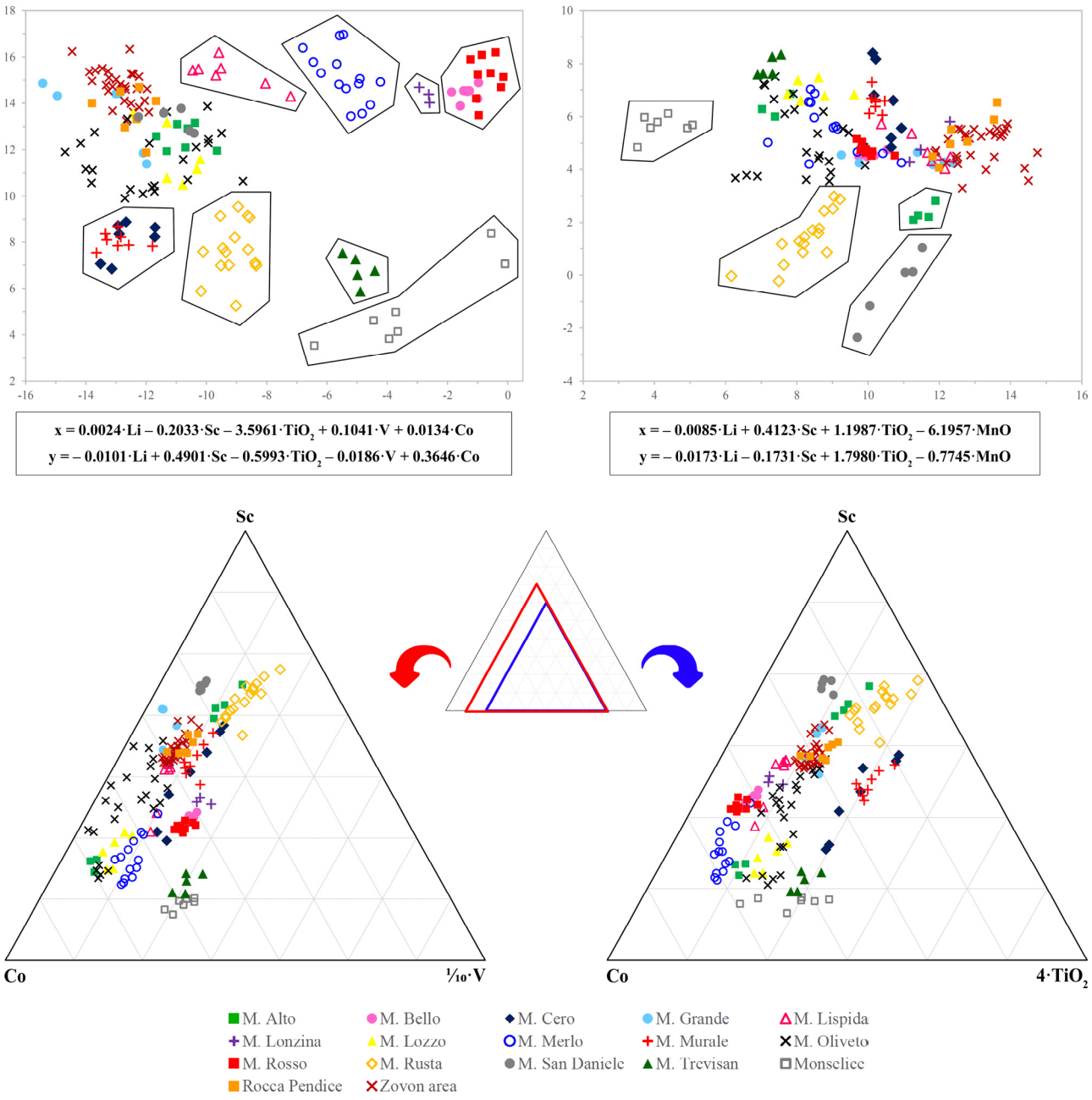

Fig. 16. Plots from chemical composition of biotite in Euganean trachyte determined by LA-ICPMS, with major elements expressed as oxide weight percent and trace elements as ppm, using the isotopes in Appendix 4: **top)** scatterplots after statistical discriminant analysis, with variables calculated from multivariate combinations of element concentrations, indicated under each relevant graph; **bottom)** ternary plots, scaled up as indicated in the miniature.

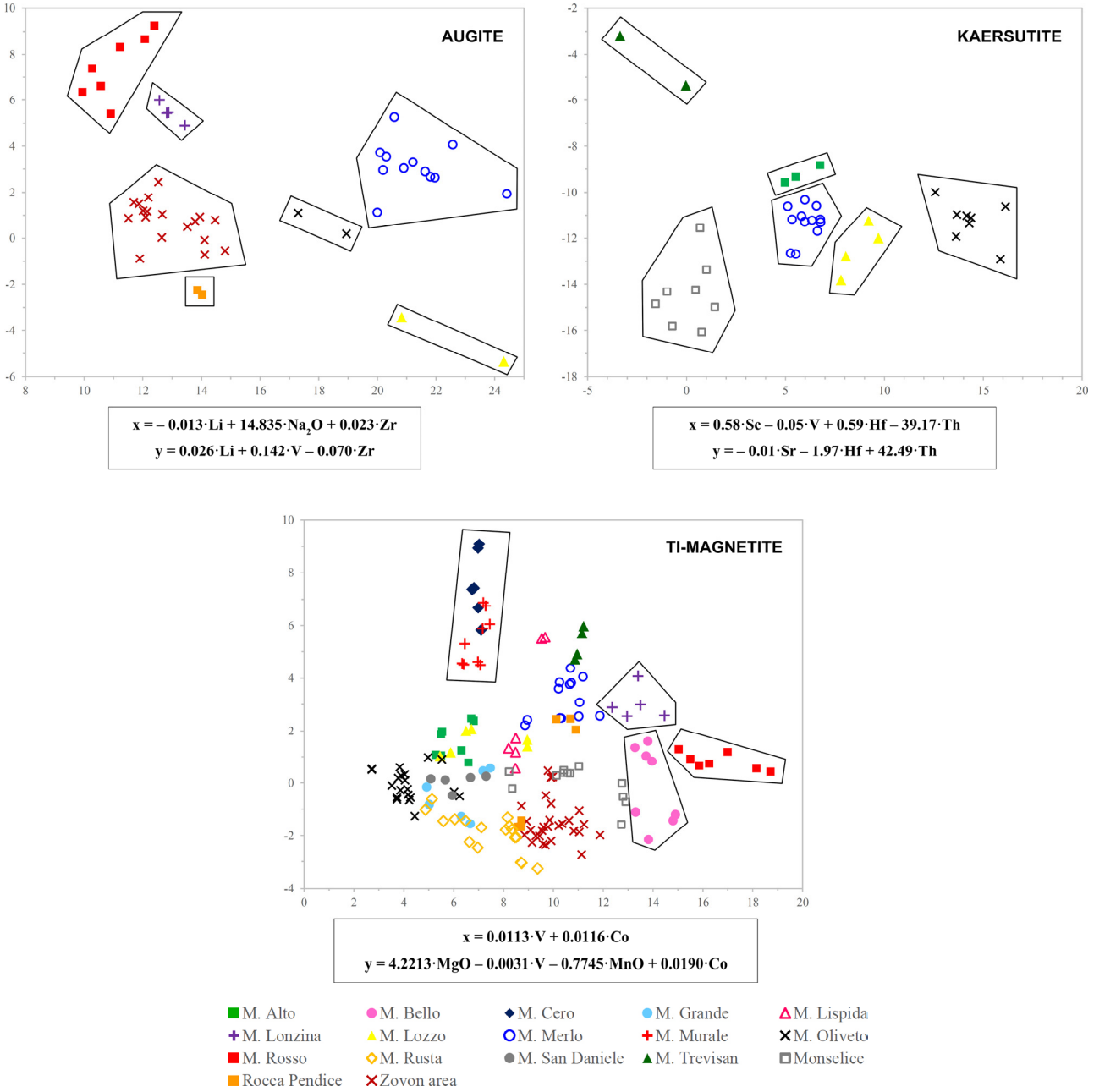

Fig. 17. Scatterplots from chemical composition of augite, kaersutite and Ti-magnetite in Euganean trachyte determined by LA-ICPMS, with major elements expressed as oxide weight percent and trace elements as ppm, using the isotopes in Appendix 4; variables are calculated from multivariate combinations of element concentrations, indicated under each relevant graph, after statistical discriminant analysis.

elemental concentration, although their dispersion in the ternary plots is more limited (e.g., for M. Oliveto) and might serve as an indicative guide to try provenance attribution; in this case, however, relying also on other mineral phases is more effective.

When the trachyte to be studied also contains other mafic minerals, one can try to exploit the concentrations of Li, Na_2O, V, Zr in the case of pyroxenes, and Sc, V, Sr, Hf, Th for amphiboles (Fig. 17). The relevant discriminant plots are particularly effective, as all the localities in which these mafic minerals were observed on thin section are well separated. Concerning augite, M. Lonzina, M. Lozzo,

M. Merlo, M. Rosso, Zovon, quarry 31 of M. Oliveto and quarry 32 of Rocca Pendice. Concerning kaersutite, M. Lozzo, M. Merlo, M. Oliveto, M. Trevisan, Monselice and quarry 1 of M. Alto. Complementary traditional binary plots are reported in Appendix 5.

Among the accessory minerals, apatite composition does not show any systematic variation related to provenance quarry, whereas magnetite chemistry represents a valid support for aiding quarry attribution when the results obtained on mafic minerals are still questionable. As shown in Fig. 17, several quarry sites cluster separately in a plot based on linear combinations of MgO, V, MnO and Co concentrations, although with some ambiguous groups and overlapping. Nevertheless, the advantage of considering magnetite is that – contrary to augite or kaersutite – it is ubiquitous in Euganean trachyte, and provides better separations for M. Bello, M. Oliveto, M. Rosso and Zovon. Again, additional supporting plots can be consulted in Appendix 5.

Finally, and somewhat surprisingly, feldspars turned out to be source of only a limited amount of information for provenancing, and discriminant analysis was more complex, requiring and involving a larger number of elements to produce some sort of quarry clustering (Fig. 18). Indeed, analysis of feldspars should be generally unnecessary, or considered only in a final step, for further confirming previous findings or when provenance achieved with the other phases is still undetermined. Considering anorthoclase, combinations of Li, Sc, TiO_2, Sr, La, Eu and Pb allow separating the quarry localities of M. Grande, M. Rosso, M. San Daniele, M. Trevisan, Rocca Pendice and Zovon, but with a partial overlapping. For sanidine, combinations of Li, TiO_2, Rb, Sr, Ce, Eu and Pb lead to distinguish quarry groups for M. Grande, M. Lozzo, M. San Daniele, Rocca Pendice and quarry 2 of M. Alto, while M. Bello and M. Rosso plot in the same field. Finally, plagioclase results to be suitable only for recognizing the localities of Zovon, M. Trevisan and quarry 2 of M. Alto, applying the concentrations of Li, Sc, TiO_2, Sr, La and Eu. For all the feldspars, as for all the other mineral phases, additional binary plots, built with pairs of the chemical elements mentioned before, are provided in Appendix 5.

Globally, quarry clustering achieved at the mineral scale with LA-ICPMS data is definitely more precise and effective than that obtained on bulk rock with XRF, and this applies to nearly all the Euganean quarry localities, especially if analyses of different phases are cross-matched. As already suggested previously, however, it is advisable to plot concentrations on multiple discriminant diagrams, even when only a single phase is analyzed.

6.4. Comparison with literature data

As the LA-ICPMS data are introduced here for the first time referring to Euganean trachyte, the only possible comparison with previously published geochemical data involves the XRF results of this paper and those from the database by Capedri et al. (2000), the most complete collection of bulk-compositional data of Euganean trachyte so far.

Maritan et al. (2013) already outlined a discrepancy between the concentrations of some elements (e.g., Ti, Th, Sr, Zr) reported in the reference database and those published later, determined by either XRF or ICP-MS, even by the same authors of the database (Renzulli et al. 2002b; Capedri et al. 2003; Capedri & Venturelli 2003, 2005; Antonelli et al. 2004; Antonelli & Lazzarini 2012). This is further confirmed here and illustrated in Fig. 19 in the Sr/Th plot, the main discriminant diagram by Capedri

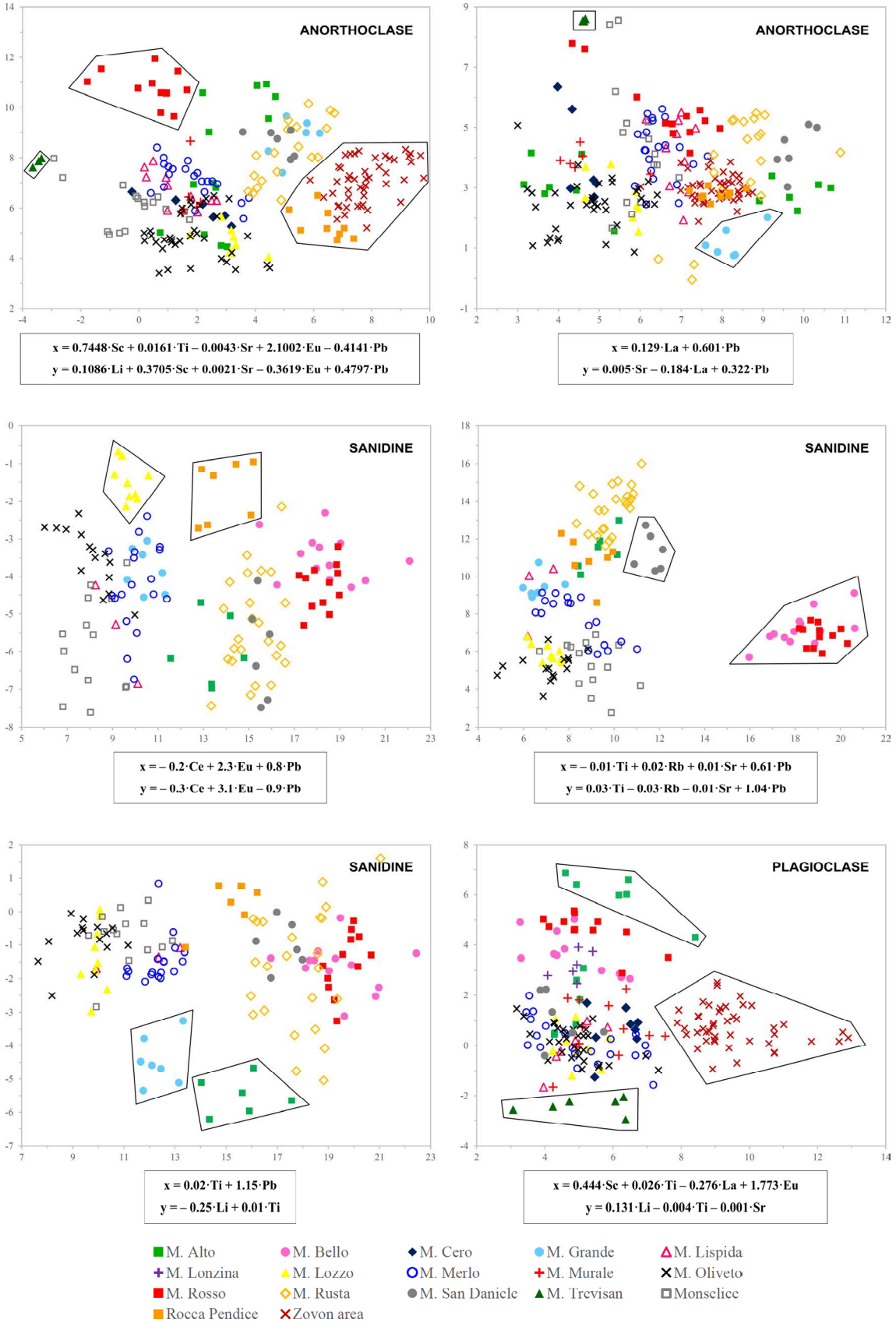

Fig. 18. Scatterplots from chemical composition of feldspars in Euganean trachyte determined by LA-ICPMS, with trace elements expressed as ppm, using the isotopes in Appendix 4; variables are calculated from multivariate combinations of element concentrations, indicated under each relevant graph, after statistical discriminant analysis.

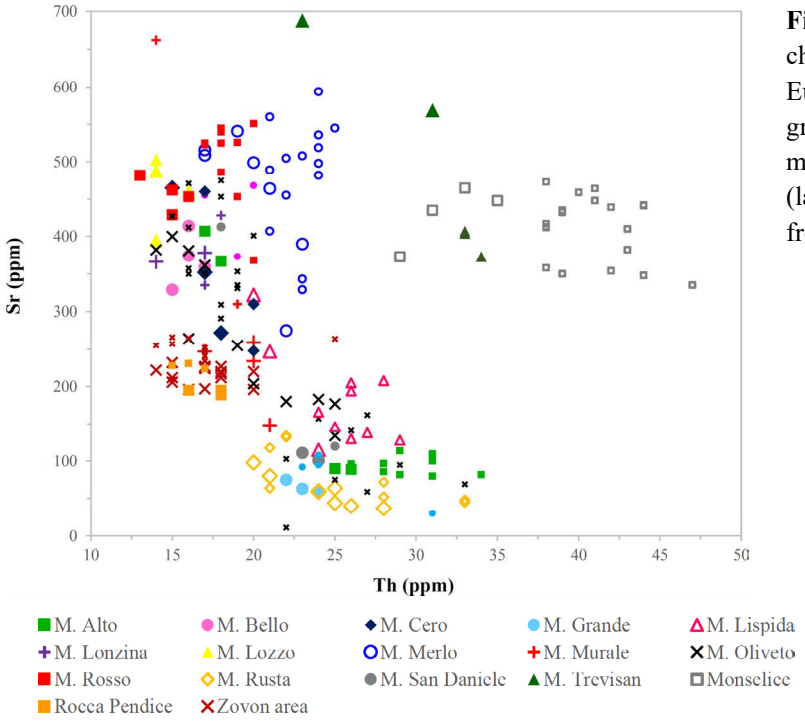

Fig. 19. Sr vs. Th scatterplot from bulk-rock chemical composition determined by XRF on Euganean trachyte – the main discriminant diagram by Capedri et al. (2000) – showing the mismatch among the samples from this work (large indicators) and the corresponding ones from the reference database (small indicators).

et al. (2000), in which the mismatch between the samples of the reference database and those studied in this paper is evident. The same applies to the other reference binary plots. This seems to confirm the hypothesis of Maritan et al. (2013) that powder grain size in the pellets prepared by Capedri et al. (2000) was not fine enough to prevent matrix, microabsorption and enhancement effects, leading to low data accuracy of the XRF analyses.
Therefore, besides the fact that discrimination of Euganean trachyte based exclusively on bulk composition is not fully reliable, it is recommended to use the new discriminant binary plots here proposed, when only XRF data are available.

7. Conclusions

A new reference database of petrographic and geochemical data for trachyte of the Euganean Hills, based on samples from 40 different quarries, has been established in support of archaeometric studies aimed at understanding stone provenance in artifacts and structures of archaeological and historical significance. Proposing an alternative and more reliable approach than that presently available from the literature, this paper describes several provenance markers referred to mineralogy, texture, bulk-rock and mineral-scale chemistry of Euganean trachyte, providing mainly quantitative data and objective criteria for quarry recognition.
This study discriminates among hills and quarry localities, but not among single quarries within the same locality. In fact, trachytes from different quarries but belonging to the same geological body are obviously extremely hard to distinguish. Moreover, such a high-resolution investigation, in this case, would be of scarce significance for archaeometric purposes.

Standard petrographic observations of thin sections, and analysis of bulk chemical composition, the most traditional methodologies previously used, might both be applied to solve provenance problems of Euganean trachyte. However, in most cases, differences of petrographic features and bulk composition among different quarry sites are subtle, and provenancing may be accurate only combining the two techniques, although still not univocal. The use of quantitative petrographic parameters from image analysis of X-ray elemental maps – or even optical images – considerably improves attribution reliability. On the other hand, success of a study based on XRF (or bulk ICP-MS) can be compromised by insufficient compositional representativeness of samples, a major drawback when dealing with archaeological materials, the sampling of which may be restricted to very small portions, in some cases also having altered surfaces.

Alternatively, *in situ* LA-ICPMS analysis at the mineral scale has proven to be a precise, accurate, and highly sensitive method for autonomously recognizing virtually all the Euganean quarry localities, using major- and trace-element composition of phenocrysts. Besides higher reliability of provenance attribution, the amount of material required for the analyses is very limited: at best, even few fine-grained crystals – for representativeness reasons – of a single diagnostic phase might be sufficient, and this is a great advantage in the study of cultural heritage, when non-destructive or micro-destructive techniques are mandatory. Moreover, although LA-ICPMS may work as a stand-alone technique, one could choose to couple a petrographic examination, in this case a single thin section of suitable thickness (40-50 μm) would be needed (to avoid drilling through the sample during the LA-ICPMS analyses).

In summary, although a standard petrographic study is fast and cost-effective, interpretation is complex and may lead to some degree of uncertainty in quarry identification. On the other hand, mineral-scale chemical analysis of major and trace elements is undoubtedly more expensive and requires greater effort in data processing, but provides univocal results and can be applied to considerably smaller samples.

The improved precision of the novel methodology proposed here might call into question some of the provenance determinations made in the past, which might have introduced a misleading bias in the following provenance studies, with possible consequences on the global archaeometric record of Euganean trachyte.

Acknowledgements

The author thanks Anne Westhues (MUN, St. John's), Raul Carampin (CNR-IGG, Padova), Richard Spiess and Leonardo Tauro (Uni. Padova) for their support during the LA-ICPMS, EPMA and SEM analyses, respectively. The author is very grateful to Arturo Zara and Jacopo Bonetto (Uni. Padova) for the constant exchange of information and ideas concerning the archaeological background. Thanks are due to the owners of the quarries of Zovon (Martini Costruzioni s.r.l., Toniolo s.r.l., Trachite Euganea s.r.l.) and Montemerlo (Cave Pietra Montemerlo s.r.l.) and, in particular, to Michelangelo Dalla Francesca, for providing trachyte samples and information about quarry activities. Musei Civici di Padova and, in particular, Francesca Veronese are also thanked for photographic material and information about trachyte artifacts in Padova. Finally, the author is grateful to Silvio Capedri, Riccardo Grandi (Uni. Modena-Reggio Emilia) and Gianpiero Venturelli (Uni. Parma) for their previous inspiring work on the same topic.

References

Antonelli F., Bernardini F., Capedri S., Lazzarini L., Montagnari Kokelj E. (2004). Archaeometric study of protohistoric grinding tools of volcanic rocks found in the Karst (Italy-Slovenia) and Istria (Croatia). *Archaeometry*, 46 (4), 537–552

Antonelli F., Lazzarini L. (2010). Mediterranean trade of the most widespread Roman volcanic millstones from Italy and petrochemical markers of their raw materials. *Journal of Archaeological Science*, 37, 2081–2092

Antonelli F., Lazzarini L. (2012). The first archaeometric characterization of Roman millstones found in the Aquileia archaeological site (Udine, Italy). *Archaeometry*, 54 (1), 1–17

Bartoli O., Meli S., Bergomi M.A., Sassi R., Magaraci D., Liu D.Y. (2015). Geochemistry and zircon U-Pb geochronology of magmatic enclaves in trachytes from the Euganean Hills (NE Italy): further constraints on Oligocene magmatism in the eastern Southern Alps. *European Journal of Mineralogy*, 27, 161–174

Bianchin Citton E., De Vecchi G. (2009). L'impiego della trachite euganea nella fabbricazione di macine in età preromana. In: Bianchin Citton E., Rossi S., Zanovello P., eds, *Dinamiche insediative nel territorio dei Colli Euganei dal Paleolitico al Medioevo. Atti del convegno di studi*, Este & Monselice, Italy, 27–28 November 2009, 139–150

Borghi A., Berra V., D'Atri A., Dino G.A., Gallo L.M., Giacobino E., Martire L., Massaro G., Vaggelli G., Bertok C., Castelli D., Costa E., Ferrando S., Groppo C., Rolfo F. (2015). Stone materials used for monumental buildings in the historical centre of Turin (NW Italy): architectonical survey and petrographic characterization of Via Roma. In: Pereira D. et al., eds, *Global heritage stone: towards international recognition of building and ornamental stones*. Geological Society, London, Special Publications, 407, 201–218

Buonopane A. (1987). Estrazione, lavorazione e commercio dei materiali lapidei. In: Buchi E., ed., *Il Veneto nell'età romana*. Banca Popolare di Verona, s.l., 1, 186–218

Buxeda i Garrigós J. (1999). Alteration and contamination of archaeological ceramics: the perturbation problem. *Journal of Archaeological Science*, 26, 295–313.

Buxeda i Garrigós J., Kilikoglou V. (2003). Total variation as a measure of variability in chemical data sets. In: van Zelst L., ed., *Patterns and process*. Smithsonian Center for Materials Research and Education, Suitland, MD, 185–198

Calogero S., Lazzarini L. (1984). Caratterizzazione chimico-fisica di ceramiche grigie dallo scavo dell'area ex Pilsen a Padova. *Archeologia Veneta*, 7, 81–97

Calvino F. (1966). *Le cave dei Colli Euganei*. Consorzio per la valorizzazione dei Colli Euganei, Padova

Calvino F. (1969). Studi sulle proprietà tecniche della trachite da taglio di Montemerlo (Colli Euganei). *Memorie degli Istituti di Geologia e Mineralogia dell'Università di Padova*, 27, 3–39

Capedri S., Grandi R., Venturelli G. (2003). Trachytes used for paving Roman roads in the Po Plain: characterization by petrographic and chemical parameters and provenance of flagstones. *Journal of Archaeological Science*, 30, 491–509

Capedri S., Venturelli G. (2003). Trachytes employed for funerary artefacts in the Roman Colonies Regium Lepidi (Reggio Emilia) and Mutina (Modena) (Italy): provenance inferred by petrographic and chemical parameters and by magnetic susceptibility. *Journal of Cultural Heritage*, 4, 319–328

Capedri S., Venturelli G. (2005). Provenance determination of trachytic lavas, employed as blocks in the Romanesque cathedral of Modena (Northern Italy), using magnetic susceptibility, and petrographic and chemical parameters. *Journal of Cultural Heritage*, 6, 7–19

Capedri S., Venturelli G., Grandi R. (2000). Euganean trachytes: discrimination of quarried sites by petrographic and chemical parameters and by magnetic susceptibility and its bearing on the provenance of stones of ancient artefacts. *Journal of Cultural Heritage*, 1, 341–364

Cattani M., Lazzarini L., Falcone R. (1997). Macine protostoriche dall'Emilia e dal Veneto: note archeologiche, caratterizzazione chimico-petrografica e determinazione della provenienza. *Padusa*, 31, 105–137

Cucato M., De Vecchi G., Sedea R. (2011). Inquadramento geologico. In: Cucato M. et al., eds, *Note illustrative della Carta Geologica d'Italia alla scala 1:50.000, Foglio 147, Padova sud*. ISPRA, Padova, 27–31

Cucato M., Mozzi P. (2011). Inquadramento geomorfologico. In: Cucato M. et al., eds, *Note illustrative della Carta Geologica d'Italia alla scala 1:50.000, Foglio 147, Padova sud*. ISPRA, Padova, 17–25

De Gennaro M., Calcaterra D., Cappelletti P., Langella A., Morra V. (2000). Building stone and related weathering in the architecture of the ancient city of Naples. *Journal of Cultural Heritage*, 1, 399–414

De Pieri R., De Vecchi G., Gregnanin A., Piccirillo E.M. (1977). Trachyte and rhyolite feldspars in the Euganean Hills (Northern Italy). *Memorie di Scienze Geologiche*, 32, 1–22

De Pieri R., Gregnanin A. (1982). Trachyte amphiboles in the Euganean Hills (North-eastern Italy). *Rendiconti della Società Italiana di Mineralogia e Petrologia*, 38 (2), 657–666

De Pieri R., Gregnanin A., Piccirillo E.M. (1978). Trachyte and rhyolite biotites in the Euganean Hills (North-eastern Italy). *Neues Jahrbuch für Mineralogie Abhandlungen*, 132 (3), 309–328

De Pieri R., Gregnanin A., Sedea R. (1983). Guida alla escursione sui Colli Euganei. *Memorie della Società Geologica Italiana*, 26, 371–381

De Pieri R., Molin G.M. (1980). Trachyte pyroxenes in the Euganean Hills (North-eastern Italy). *Neues Jahrbuch für Mineralogie Abhandlungen*, 138 (1), 64–80

De Vecchi G., Gregnanin A., Piccirillo E.M. (1976a). Aspetti petrogenetici del vulcanesimo terziario veneto. *Memorie degli Istituti di Geologia e Mineralogia dell'Università di Padova*, 30, 1–32

De Vecchi G., Gregnanin A., Piccirillo E.M. (1976b). Tertiary volcanism in the Veneto: magmatology, petrogenesis and geodynamic implications. *Geologische Rundschau*, 65 (1), 701–710

Frulio G., Langiu M.R., Mameli P. (2004). L'impiego della trachite nelle architetture tra gli anni Venti e Cinquanta in Sardegna: tecniche costruttive e materiali tradizionali tra nuove tecnologie e modernità. In: Biscontin G., Driussi G., eds, *Architettura e materiali del Novecento: conservazione, restauro, manutenzione. Atti del convegno di studi*, Bressanone, Italy, 13–16 July 2004, 465–476

Germinario L., Cossio R., Maritan L., Borghi A., Mazzoli C. (2016). Textural and mineralogical analysis of volcanic rocks by μ-XRF mapping. *Microscopy and Microanalysis*, 22, 690–697. doi: 10.1017/S1431927616000714

Graue B. (2013). *Stone deterioration and replacement of natural building stones at the Cologne cathedral. A contribution to the preservation of cultural heritage*, PhD dissertation. Geowissenschaftliches Zentrum, Georg-August-Universität Göttingen, Germany

Graue B., Siegesmund S., Middendorf B. (2011). Quality assessment of replacement stones for the Cologne Cathedral: mineralogical and petrophysical requirements. *Environmental Earth Sciences*, 63, 1799–1822

Grossi P., Zanco A. (2003). Miliari romani nel Nord Italia: materiali, provenienza, lavorazione. L'esempio dell'area Veneta e Friulana. *Quaderni di archeologia del Veneto*, 19, 192–202

Grossi P. (2007). Pietre miliari della VIII Regio: analisi litologiche, provenienza dei materiali e loro distribuzione. *Epigraphica*, 69, 181–207

Langella A., Calcaterra D., Cappelletti P., Colella A., D'Albora M.P., Morra V., De Gennaro M. (2009). Lava stones from Neapolitan volcanic districts in the architecture of Campania region, Italy. *Environmental Earth Sciences*, 59, 145–160

Lazzarini L., Antonelli F., Cancelliere S., Conventi A. (2008). The deterioration of Euganean trachyte in Venice. In: Lukaszewicz J.W., Niemcewicz P., eds, *Proceedings of the 11th International Congress on Deterioration and Conservation of Stone*, Torun, Poland, 15–20 September 2008, 153–163

Lazzaro L. (1992). Cave di trachite ed uso della pietra trachitica in età romana. *Padova e il suo territorio*, 37, 38–40

Le Maitre R.W., ed. (2002). *Igneous rocks: a classification and glossary of terms*. 2nd ed. Cambridge University Press, Cambridge

Lugli S., Caroselli M., Marchetti Dori S., Vandelli V., Marzani G., Segattini R., Bianchi C., Weber J. (2016). Building materials and degradation phenomena of the Finale Emilia Town Hall (Modena): an archaeometric study for the restoration project after the 2012 earthquake. *Periodico di Mineralogia*, 85, 59–67

Maioli M.G., Stoppioni M.L. (1987). *Classe e Ravenna fra terra e mare*. Sirri, Ravenna

Maritan L. (2004). Archaeometric study of Etruscan-Padan type pottery from the Veneto region: petrographic, mineralogical and geochemical-physical characterisation. *European Journal of Mineralogy*, 16, 297–307

Maritan L., Mazzoli C., Rigaldo P., Pesavento Mattioli S., Mazzocchin S. (2006). Le olle romane dello scavo di via Neroniana (Montegrotto Terme – Padova): indagini preliminari. In: D'Amico C., ed., *Atti del Convegno AIAr*, Caserta, Italy, 16–18 February 2005, 253–260

Maritan L., Mazzoli C., Sassi R., Speranza F., Zanco A., Zanovello P. (2013). Trachyte from the Roman aqueducts of Padua and Este (north-east Italy): a provenance study based on petrography, chemistry and magnetic susceptibility. *European Journal of Mineralogy*, 25, 415–427

Marocchi M., Dellisanti F., Bargossi G.M., Gasparotto G., Grillini G.C., Rossi P.L. (2009). Mineralogical-petrographic characterisation and provenance of "Porta Nuova" stones: a XVI century gate in Ravenna (Italy). *Periodico di Mineralogia*, 78, 13–28

McDonough W.F., Sun S.-s. (1995). The composition of the Earth. *Chemical Geology*, 120, 223–253

Milani L., Beccaluva L., Coltorti M. (1999). Petrogenesis and evolution of the Euganean Magmatic Complex, Veneto Region, North-East Italy. *European Journal of Mineralogy*, 11, 379–399

Negri A. (1966). L'impiego della trachite euganea nei monumenti storici in Padova. *Marmo Tecnica Architettura*, 7, 89–100

Paton C., Hellstrom J., Paul B., Woodhead J., Hergt J. (2011). Iolite: Freeware for the visualisation and processing of mass spectrometric data. *Journal of Analytical Atomic Spectrometry*, 26, 2508–2518

Piccoli G., Sedea R., Bellati R., Di Lallo E., Medizza F., Girardi A., De Pieri R., De Vecchi G., Gregnanin A., Piccirillo E.M., Norinelli A., Dal Prà A. (1981). Note illustrative della Carta geologica dei Colli Euganei alla scala 1:25000 – II edizione. *Memore di Scienze Geologiche*, 34, 523–566

Previato C., Bonetto J., Mazzoli C., Maritan L. (2014). Aquileia e le cave delle regioni alto-adriatiche: il caso della trachite euganea. In: Bonetto J., Camporeale S., Pizzo A., eds, *Arqueología de la construcción IV. Las canteras en el mundo antiguo: sistemas de explotación y procesos productivos*. CSIC, Mérida, 149–166

Renzulli A., Antonelli F., Santi P., Busdraghi P., Luni M. (1999). Provenance determination of lava flagstones from the Roman 'Via Consolare Flaminia' pavement (central Italy) using petrological investigations. *Archaeometry*, 41 (2), 209–226

Renzulli A., Santi P., Nappi G., Luni M., Vitali D. (2002a). Provenance and trade of volcanic rock millstones from Etruscan-Celtic and Roman archaeological sites in Central Italy. *European Journal of Mineralogy*, 14, 175–183

Renzulli A., Santi P., Serri G., Luni M. (2002b). The Euganean trachyte flagstones ("basoli") used by the Romans along the mid-Adriatic coast (Marche, central Italy): an archaeometric study. *Periodico di Mineralogia*, 71, 189–201

Santi P., Renzulli A. (2006). Italian volcanoes as landmarks for the spreading of trade networks during the Etruscan and Roman periods: the millstones and flagstones case study. *Acta Vulcanologica*, 18 (1-2), 133–140

Sassi R., Mazzoli C., Spiess R., Cester T. (2004). Towards a better understanding of the fibrolite problem: the effect of reaction overstepping and surface energy anisotropy. *Journal of Petrology*, 45 (7), 1467–1479

Schiavinato G. (1944). Studio chimico-petrografico dei Colli Euganei. *Memorie dell'Istituto Geologico dell'Università di Padova*, 15, 1–59

Selmin F., ed. (2005). *I Colli Euganei*. Cierre, Sommacampagna

Sun S.-s., McDonough W.F. (1989). Chemical and isotopic systematics of oceanic basalts: implications for mantle composition and processes. In: Saunders A.D., Norry M.J., eds, *Magmatism in the Ocean Basins*. Geological Society, Oxford, Special Publication, 42, 313–345

Valluzzi M.R., Mazzoli C., Maritan L., Bianchini G., Andreoli F. (2005). Experimental analyses for the preservation of trachyte pavings in salt-controlled weathering conditions. In: Banthia N., Uomoto T., Bentur A., Shah S.P., eds, *Construction materials: proceedings of ConMat '05 and Mindness Symposium*, Vancouver, Canada, 22–24 August 2005, 1–10

Vergani R. (1994). Masegne e calchere: secoli di attività estrattiva. In: Rigon A., ed., *Monselice. Storia, cultura e arte di un centro "minore" del Veneto*. Canova, Monselice, 403–413

Whitney D.L., Evans B.W. (2010). Abbreviations for names of rock-forming minerals. *American Mineralogist*, 95, 185–187

Williams-Thorpe O., Thorpe R.S. (1989). Provenancing and archaeology of Roman millstones from Sardinia (Italy). *Oxford Journal of Archaeology*, 8 (1), 89–117

Zantedeschi C. (1994). New Rb-Sr radiometric data from Colli Euganei (North-Eastern Italy). *Memorie di Scienze Geologiche*, 46, 17–22

Zantedeschi C., Zanco A. (1993). Distinctive characteristics of euganean trachytes for their identification in ancient monuments. *Science and Technology for Cultural Heritage*, 2, 1–10

Zara A. (2016). *La trachite euganea: approvvigionamento, impiego e diffusione in età romana*, PhD dissertation. Dipartimento dei Beni Culturali, Università degli Studi di Padova, Italy

Chapter 2

Provenance study of Roman infrastructure and insights into ancient trades in northern Italy

Abstract

Roman colonization of northern Italy during the late Republican Age brought a significant building activity in the new acquired territories, especially involving the construction of new infrastructure, which demanded huge amounts of stone. Trachyte of the Euganean Hills was one of the most used materials for building infrastructure, in particular roads, and even bridges, forum squares and aqueducts. This paper addresses the recognition of the provenance quarry of Euganean trachyte used in Roman public infrastructure in northeastern Italy, mostly built from the 1st century BCE to the 1st century CE. Petrographic features and major- and trace-element composition of bulk rock and phenocrysts, analyzed by XRF and LA-ICPMS, were used as provenance tracers. The provenance determinations allow exploring the management of trachyte quarries and the development of extraction activities in the Roman times, as well as the related commercial and economic dynamics involving stone supply for public works. Moreover, indications are given with regard to the territorial organization of Roman settlements, their areas of political influence and ownership and competition of quarries. Finally, broad insights into ancient trades in northern Italy and the main routes of stone circulation are provided.

1. Introduction

The outstanding construction skills of the Romans were well known in the classical antiquity, and their great care in building infrastructure, in particular roads, aqueducts, and sewers, was admired even in the ancient Greece by Strabo (*Geōgraphiká*, V, 3, 8). Realization of infrastructure was a fundamental step in the Roman colonization process, for controlling and reorganizing new territories and promoting their development and integration. The Roman road network can be considered the longest monument in the world, globally spanning over 80,000 km on three continents, with such a complexity never seen before, in the other ancient civilizations of Egypt, Persia, or India (Chevallier 1976; Witcher 1998; Staccioli 2003; Davies 2008).

The building boom brought by the Romans in new acquired territories demanded enormous quantities of stone. In northern Italy, and particularly in the easternmost regions, trachyte of the Euganean Hills was one of the most commonly used materials for infrastructure. Broad interest has been given to trachyte quarry recognition in the archaeometric literature, especially applied to flagstones used in urban and extra-urban roads, the renowned *viae publicae* (Fig. 1). In northern Italy, infrastructure building was initiated during the Republican Age, but Emperor Augustus was the main promoter of a general renewal that, according to Titus Livius (*Ab Urbe Condita*, XLI, 27, 5), also led to a wide usage of flagstones in roads, especially in urban areas (Matteazzi 2009).

Several provenance studies of Euganean trachyte have focused on Roman road stretches on the mid-Adriatic coast and in the Po Plain, in particular *Via Flaminia* (Renzulli et al. 1999, 2002b) and *Via Aemilia* (Capedri et al. 2000, 2003); these roads, dated from 220 and 187 BCE respectively, connected *Roma* to *Ariminum* (present-day Rimini), and the latter to *Placentia* (Piacenza).

Only few provenance studies have considered the territories of northeastern Italy, where the quarry district of the Euganean Hills is localized and the concentration of trachyte infrastructure is the highest. These researches have dealt with the aqueducts of *Patavium* (Padova) and *Ateste* (Este) (Maritan et al. 2013), and the roads and harbor structures in *Aquileia* (Previato et al. 2014; Previato 2015).

Fig. 1. Area of Euganean trachyte circulation in the Roman times (shaded) and the main Roman roads, also known as *viae publicae*.

Other than in infrastructure, the usage of Euganean trachyte by the Romans has been also attested in private buildings and monuments, especially with structural functions, as well as in diverse artifacts, such as querns, mortars, milestones, sarcophagi, tombstones, cippi, urns and steles (Cattani et al. 1997; Renzulli et al. 2002a; Capedri et al. 2003; Capedri & Venturelli 2003; Grossi & Zanco 2003; Antonelli et al. 2004; Capedri & Venturelli 2005; Grossi 2007; Antonelli & Lazzarini 2010, 2012; Santi & Renzulli 2006; Previato et al. 2014; Previato 2015; Zara 2016).

Generally, the network of trachyte circulation from the Euganean Hills extended within a radius of over 250 km, approximately corresponding to a broad, ideal quadrilateral traced by the Roman settlements of *Mediolanum* (Milano)-*Ticinum* (Pavia), Bressanone, *Tergeste* (Trieste)-*Aquileia* and *Ancona-Urbs Salvia* (Urbisaglia) (Fig. 1). Archaeometric literature reveals that the most exploited Euganean quarry localities were Monselice, M. Oliveto and M. Merlo; several artifacts have also been attributed to trachyte from M. Rosso, whereas the recurrence of other sites, such as M. San Daniele, M. Lispida, M. Trevisan and M. Altore, is occasional (Fig. 2).

This paper presents the results of a provenance study of Roman public infrastructures built in the Veneto region (NE Italy) using trachyte of the Euganean Hills, namely roads, bridges, and forum squares. Provenance was determined according to the petrographic and geochemical tracers discussed in Ch. 1, involving mineralogical composition, texture of phenocrysts and groundmass, major- and trace-element composition of bulk rock and phenocrysts, which were analyzed on trachyte samples collected in six former Roman settlements. The goal is to explore the management of trachyte quarries and development of extraction activities in the Roman times, as well as the related commercial and economic dynamics involving stone supply for public works. Finally, the ancient trades of trachyte in northern Italy and the possible routes of stone circulation are examined.

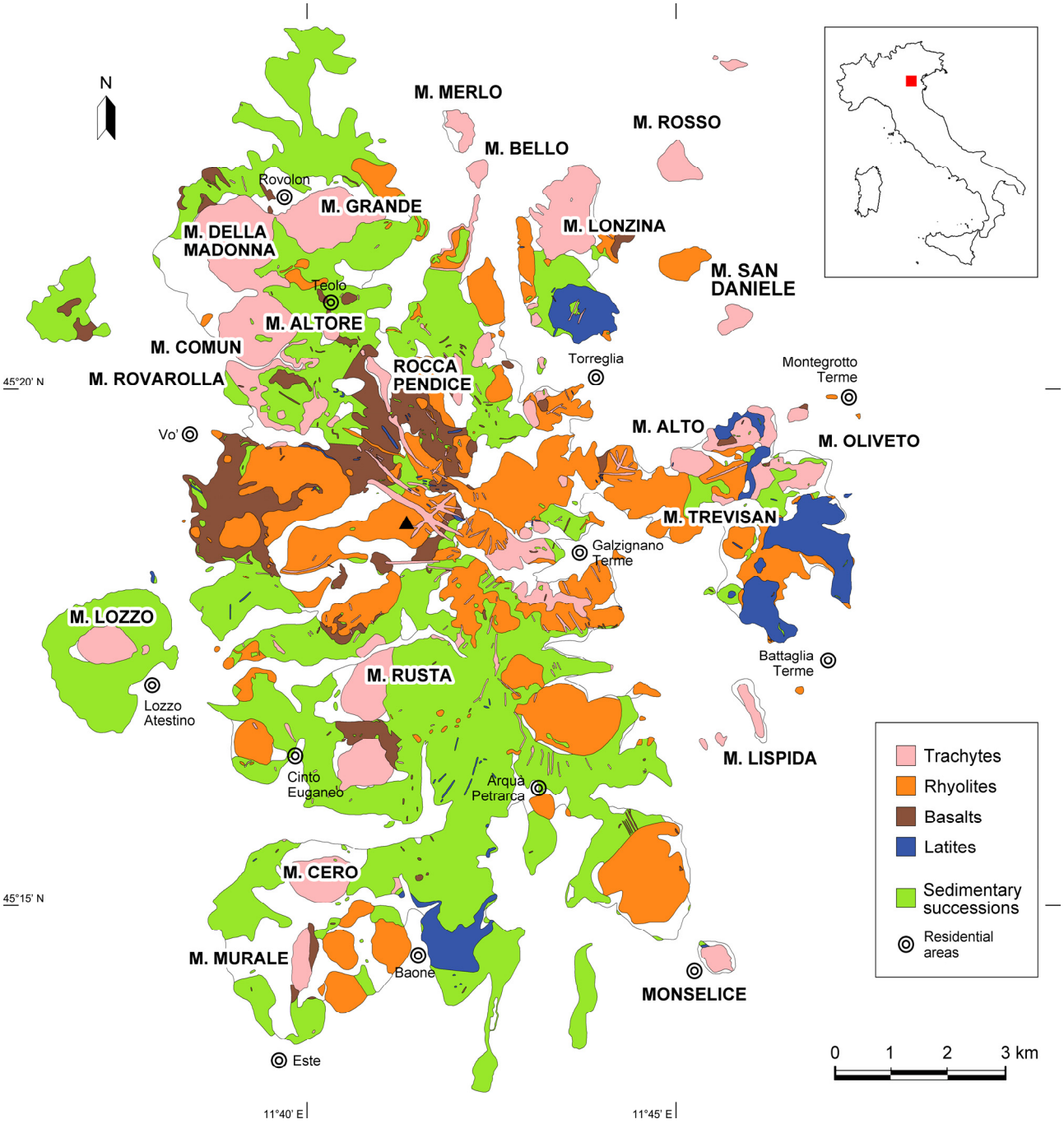

Fig. 2. Geological map of the Euganean Hills (modified after Piccoli et al. 1981). "M." in the proper name of the hills stands for "Monte" (mount).

2. The Euganean quarry district

The Euganean Hills are a hill complex near Padova (Veneto, northeastern Italy), covering an area of about 110 km^2 entirely surrounded by the Venetian Plain. Here, a deep-water sedimentary succession of limestones and marls dated to the upper Jurassic–lower Oligocene is followed by a Paleogene

volcanic and hypabyssal series and by Quaternary sedimentary deposits. The subvolcanic series, dated to the lower Oligocene and having an acid to intermediate composition, mostly includes rhyolites and trachytes with moderate Na-alkaline affinity, while latites and basalts subordinately occur (Milani et al. 1999; Sassi et al. 2004; Bartoli et al. 2015 and references therein) (Fig. 2).
The Euganean Hills are the most important district in Italy for the extraction of trachyte, which also historically occurs in other regions, such as Sardinia, Lazio, Tuscany, and Campania, however on a minor commercial scale. The earliest quarrying of Euganean trachyte is lost to history and started with the first populations settled in the Neolithic, but dramatically increased during the Roman times. The ancient extraction methods involved the use of wedges, inserted into holes in the rock or natural fractures; metallic wedges were hammered inwards, whereas wooden wedges were soaked with water, causing their swelling (Buonopane 1987; Vergani 1994). The resulting rock splitting was made easier by columnar, tabular or prismatic joints that trachyte often displays. The Romans exploited trachyte in tens of quarries, and many others have been opened in the course of time, so that about 100 different extraction sites can be recognized. The numerous quarries – often very close to each other, in some cases a few hundred meters – and trachyte varieties with very similar characteristics greatly complicate the identification of provenance quarry of archaeological stone (Ch. 1).

3. Sampling and experimental methods

Euganean trachyte used as building stone in Roman infrastructures in Veneto was sampled in six former Roman cities: *Patavium* (Padova), *Ateste* (Este), *Vicetia* (Vicenza), the closest to the Euganean Hills, and *Altinum* (Altino), *Opitergium* (Oderzo) and *Iulia Concordia* (Concordia Sagittaria), about 60, 80 and 100 km far, respectively, from the Euganean quarries. A set of 63 samples were collected from 20 infrastructures including roads, bridges and forum squares (Fig. 3), mostly dated to the 1st century BCE–1st century CE, in which Euganean trachyte was used for flagstones, ashlars, voussoirs, and other applications. Detailed information about the sampling sites and sample dating is provided in Appendix 1.
The archaeological samples were subjected to a petrographic and geochemical investigation.
Petrographic observations were done with a polarized-light microscope on thin sections with a 45 μm thickness, at the Department of Geosciences, University of Padova.
Bulk-rock chemical analyses for major and trace elements were done by X-ray fluorescence (XRF) on glass beads – prepared with calcined samples diluted with $Li_2B_4O_7$ flux in a 1:10 ratio – using a Philips PW2400 spectrometer operating in WD (wavelength dispersive) mode, at the Department of Geosciences, University of Padova. Loss on ignition (LOI) was also determined separately before the XRF analyses.
Finally, crystals of biotite, augite, kaersutite, Ti-magnetite, sanidine and anorthoclase were selected to determine their major- and trace-element chemical composition. The selection was carried out under the optical microscope, except for Ti-magnetite, identified by micro-Raman with a Horiba Jobin Yvon Labram HR800-UV spectrometer equipped with a 488 nm diode laser, at the Geoscience Center of Georg-August-Universität Göttingen.
The chemical analyses were done on the thin sections by laser ablation inductively-coupled plasma mass spectrometry (LA-ICPMS), at the Geoscience Center of Georg-August-Universität Göttingen.

Fig. 3. Two of the sampled Roman infrastructures in Veneto: the road of *Altinum* (Altino), dated to the 2nd c. CE **(left)**; the bridge of *Iulia Concordia* (Concordia Sagittaria), dated to the Augustan Age **(right)**. The insets show details of the sampling points of Euganean trachyte (courtesy of Arturo Zara).

A Thermo Scientific Element 2 double-focusing magnetic-sector spectrometer coupled to a Resonetics Resolution 193 nm Ar-F excimer laser was used. The laser operated with a 8 Hz repetition rate, 3 J/cm^2 fluence, and using a spot size of 40 µm. For each analysis, an initial 20 s background acquisition was set, followed by a 50 s ablation and, finally, a further 15 s background acquisition, analyzing on each sample 3 to 6 spots per phase on different crystals. NIST 610 glass reference material was used as primary calibrant, and analyzed every 10 measurements on the samples; USGS BCR-2G basalt glass reference material was also analyzed with the same frequency as secondary standard. Element concentrations were calculated with Iolite v2.5 software package (Paton et al. 2011), by a script based on the following procedure: the LA-ICPMS signal is first smoothed by ratioing to an appropriate denominator isotope present in the sample and standard (^{29}Si was used); the element ratios are standardized with NIST 610 glass reference material; then, they are normalized to oxides sum to reach 100%, including all the elements (Simon 2015). Preliminary determination of the concentration of an internal standard is not needed with this procedure.

4. Petrographic features

A detailed summary of the petrographic features of all the archaeological samples is included in Appendix 2. Four main petrographic types can be identified, with slightly different mineralogical and textural features but having in common the porphyritic texture (often glomeroporphyritic and/or cumuloporphyritic due to occurrence of feldspar aggregates) and the ubiquitous presence of biotite, apatite and opaque minerals, i.e., Ti-magnetite and ilmenite.

Type I is distinguished by a seriate[1] grain size distribution and a microcrystalline felty groundmass, with anorthoclase and plagioclase being the most abundant phenocrysts, and sanidine in secondary amounts; augite and kaersutite are usually present, and cristobalite may often occur too (Fig. 4a).

[1] Texture is said to be seriate if crystals of the main mineral phases are distributed within a continuous range of sizes, whereas hiatal texture involves crystals showing few, noticeably different sizes.

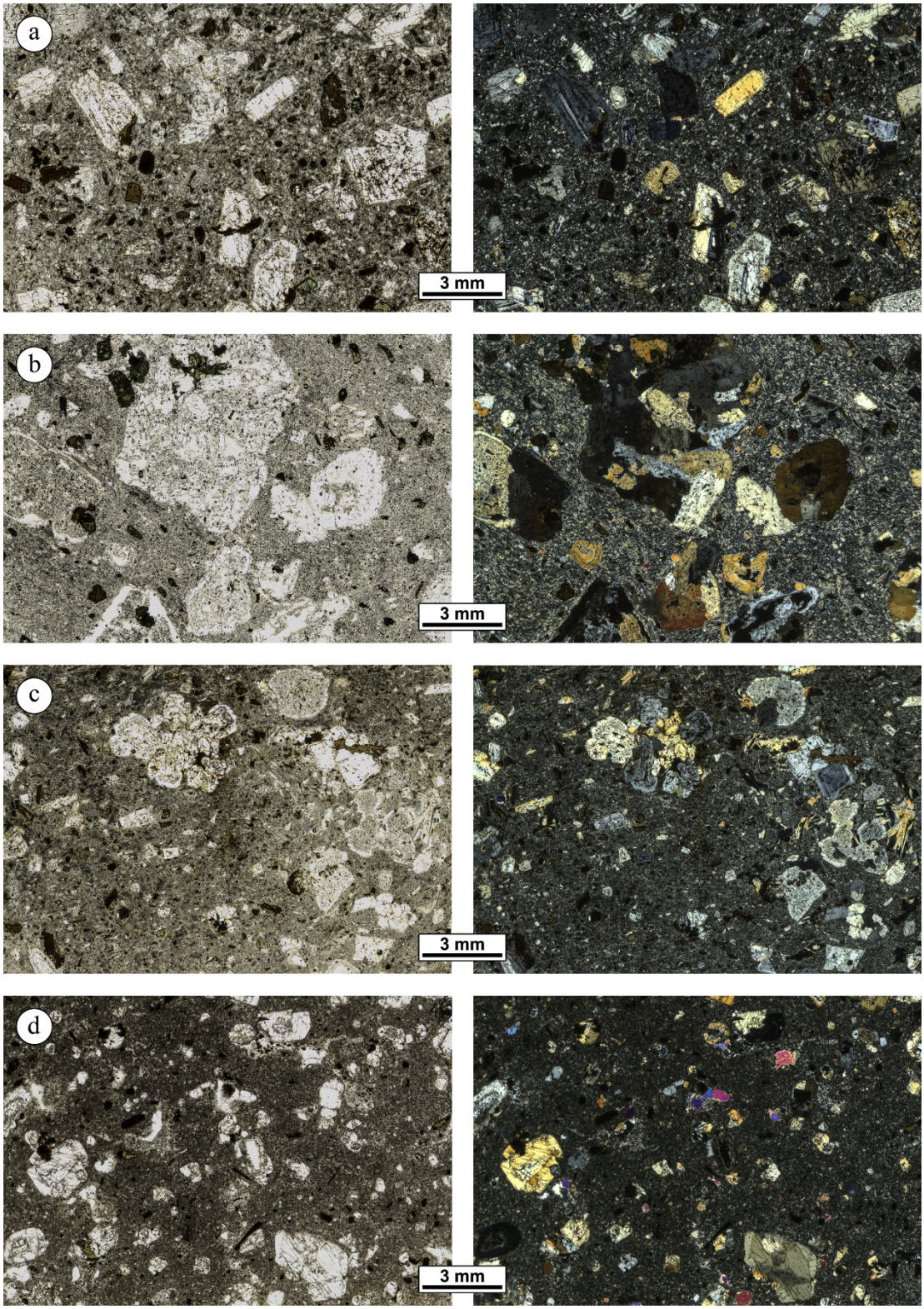

Fig. 4. Thin-section photomicrographs, in plane- and crossed-polarized light, of the main petrographic types of Euganean trachyte observed on the archaeological samples: **a)** Type I, sample VI7 from Vicenza; **b)** Type II, sample AL9 from Altino; **c)** Type III, sample OD6 from Oderzo; **d)** Type IV, sample CS11 from Concordia Sagittaria. Anomalously higher interference colors are determined by the 45 μm thickness of the sections.

Type II has a hiatal grain size distribution and a microcrystalline groundmass characterized by preferred orientations of the feldspar microlites (trachytic texture); anorthoclase is the main phase, and sanidine, kaersutite, augite and titanite are often also detected (Fig. 4b).
Type III has a hiatal grain size distribution and a micro- to cryptocrystalline felty groundmass, with phenocrysts mostly of anorthoclase and plagioclase, the possible presence of sanidine and kaersutite and the highest concentration of cristobalite observed (Fig. 4c).
Type IV is characterized by a hiatal grain size distribution and a micro- to cryptocrystalline felty groundmass; sanidine is the main phase among the phenocrysts, with subordinate anorthoclase and plagioclase and a high concentration of quartz (Fig. 4d).
This rough discrimination is just indicative, since several samples show mineralogical and textural features being ambiguous, or diverse, or mixed among the different trachyte types. This may be dependent on the natural petrographic variability of Euganean trachyte – as outlined in Ch. 1, especially within certain quarries – also due to quarry face advancing with ongoing exploitation, which was intense and fast in the Roman times. Another reason lies in the small size of some samples, which did not allow examining a rock section representative, and large enough, for a comprehensive petrographic investigation.
Taking into account these limitations, the sole petrographic observations allow proposing the following attributions, according to the provenance tracers in Ch. 1 and after a comparison with the relevant thin-section collection of quarry trachytes. Type I can be referred to the quarry localities of M. Merlo or M. Lozzo, with few uncertainties (involving the possible provenance from M. Rosso, M. Oliveto, M. Alto or M. Lispida). Type II denotes a provenance from Monselice (in some cases mistakable with M. Oliveto, M. Cero, M. Murale or Zovon[2]). Type III can be associated with M. Oliveto or M. Alto, although some samples display ambiguous characteristics (related to M. Rosso, M. Cero, M. Murale, M. Lispida, M. Bello or M. Merlo). Finally, provenance of Type IV is the most difficult to achieve, since its petrographic features are shared among several quarry localities: M. San Daniele, M. Grande, M. Rusta, M. Alto and M. Bello.
Generally, the petrographic examinations do not turn out to be sufficient to define with accuracy the provenance quarry localities, although some main trends can be identified.

5. Geochemical composition

5.1. Bulk rock

On the basis of bulk-rock chemical composition, most archaeological samples fall into the compositional field of trachytes, according to the total alkali-silica (TAS) classification (Le Maitre 2002), except for a group with higher content of SiO_2 in the field of rhyolites or very close to it (Fig. 5). These last samples have been all defined previously as belonging to petrographic Type IV. Another

[2] According to Ch. 1, the quarry localities of M. Altore, M. Comun and M. Rovarolla are grouped under the denomination of Zovon area (Zovon di Vo' is a nearby village), since petrographic and geochemical characteristics of the outcrop are not distinguishable.

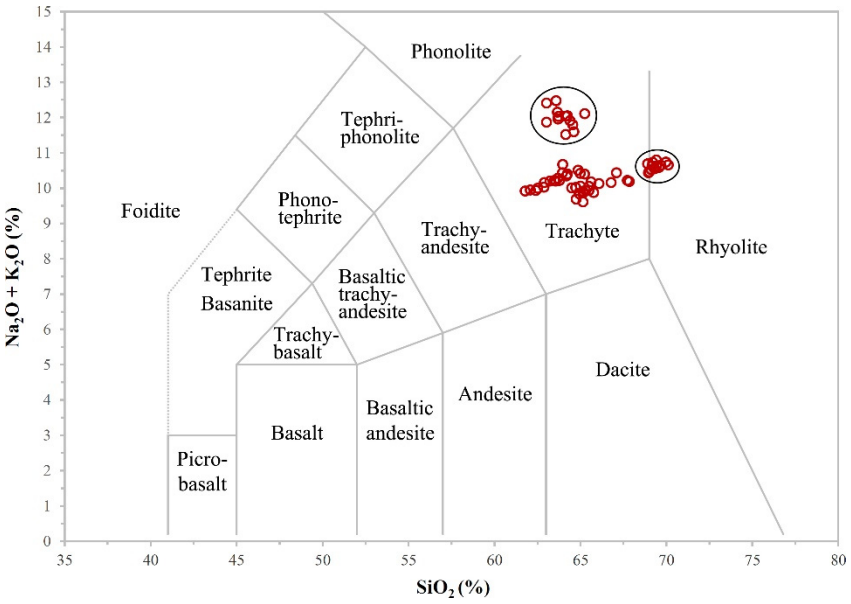

Fig. 5. Chemical composition of the archaeological samples of Euganean trachyte projected within the TAS (total alkali-silica) classification diagram, based on bulk-rock XRF analyses. Two clusters of samples with higher contents in alkali metals and SiO_2 are indicated, mostly referable to the petrographic Type II and Type IV, respectively, as previously defined.

separate cluster can be observed, with higher content of alkali metals, comprising the samples classified as petrographic Type II.

The bulk-rock XRF data were analyzed using bivariate and multivariate statistical methods.

The position of the archaeological samples was verified in relation to the reference quarry clusters of Euganean trachyte in the binary plots proposed in Ch. 1, i.e., V/Nb, TiO_2/Zr, TiO_2/K_2O, Na_2O/Zr, Rb/Zr, Al_2O_3/Sr, and Ce/Nd. Some of these are presented in Fig. 6. Several samples do not precisely match the reference fields, although valid indications about possible provenance are provided in any case. As suggested in Ch. 1, disposition of each sample was checked in all the discriminant plots, verifying which group of reference quarry trachytes it approached most and how often.

Concerning the statistical multivariate approach, a discriminant analysis was done with Statgraphics Centurion XVI software package: concentration of all major and trace elements of the quarry samples of Euganean trachyte reported in Ch. 1 was used for *a priori* classification of the different quarry localities. Subsequently, each archaeological sample was automatically assigned to a possible quarry locality based on its bulk-rock chemistry. In many cases, this procedure confirms the findings of the bivariate analysis, but also introduces further uncertainty in provenance attribution for several samples.

According to the results of both the statistical methods, four main provenance groups are confirmed, encompassing most samples: M. Merlo/M. Lozzo, Monselice, M. Oliveto/M.Alto and M. San Daniele/M. Rusta. The first term of each pair represents the most likely provenance. Zovon/Rocca Pendice and M. Lispida are also recognized for few samples.

It is worth mentioning that provenance determination has a higher degree of uncertainty for the smaller samples, due to low chemical representativeness, possibly further complicated by former processes of surface weathering.

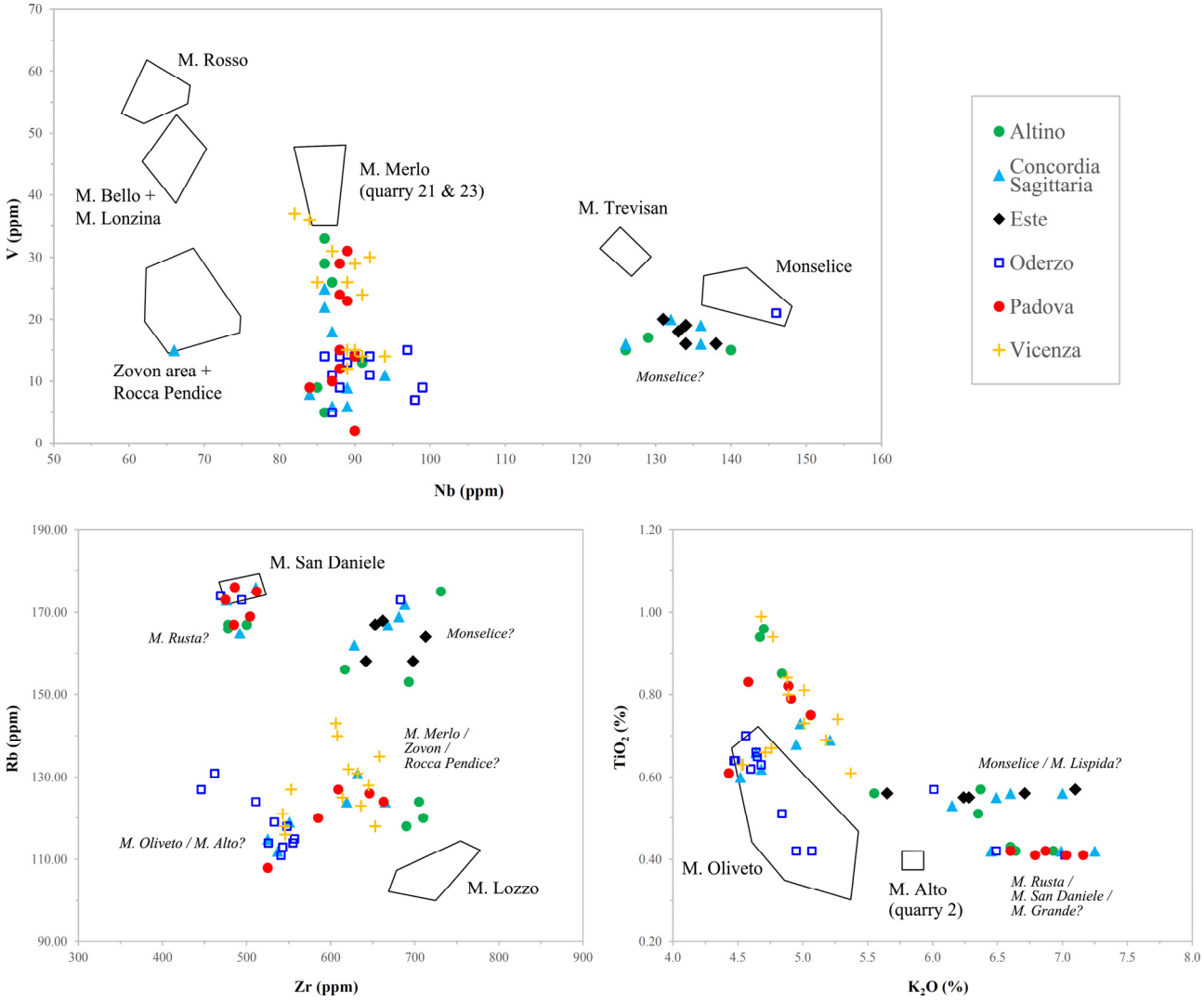

Fig. 6. V/Nb, Rb/Zr and TiO_2/K_2O scatterplots for provenance recognition of Euganean trachyte using bulk-rock chemical composition (Ch. 1), determined on the archaeological samples by XRF. The reference fields of quarry clusters of Ch. 1 are indicated by solid lines and the name of the relevant quarry locality. Possible provenance of the archaeological samples outside the reference fields is also specified, based on the relative position of other overlapping and indefinite clusters of different quarry localities.

5.2. Phenocrysts

Major- and trace-element composition of phenocrysts determined by LA-ICPMS allows solving all the uncertainties described so far, assigning univocally and independently every archaeological sample to a determined, single quarry locality.

The first analyses were done on biotite crystals on the entire set of trachytes, while for selected samples further measurements were done on the other mineral phases, i.e., augite, kaersutite, Ti-magnetite, sanidine and anorthoclase. The results are listed in Appendix 4, excluding the non-representative measures or those disturbed by inclusions (usually of apatite, zircon, and monazite) affecting the concentration of the elements of interest. For provenance determination, the LA-ICPMS diagrams proposed in Ch. 1 were applied, considering all the multivariate, binary and ternary plots.

The sole results of the biotite analyses provide most of the information required, based on multivariate correlations among the concentrations of Li, Sc, TiO_2, V, MnO and Co (Fig. 7). Three main provenance localities, namely M. Merlo, Monselice and M. San Daniele, are revealed by the samples clustering into the reference quarry fields; those plotting outside, but still nearby, cannot be referred to any other provenance, considering the relevant ranges of elemental concentrations. Other than using

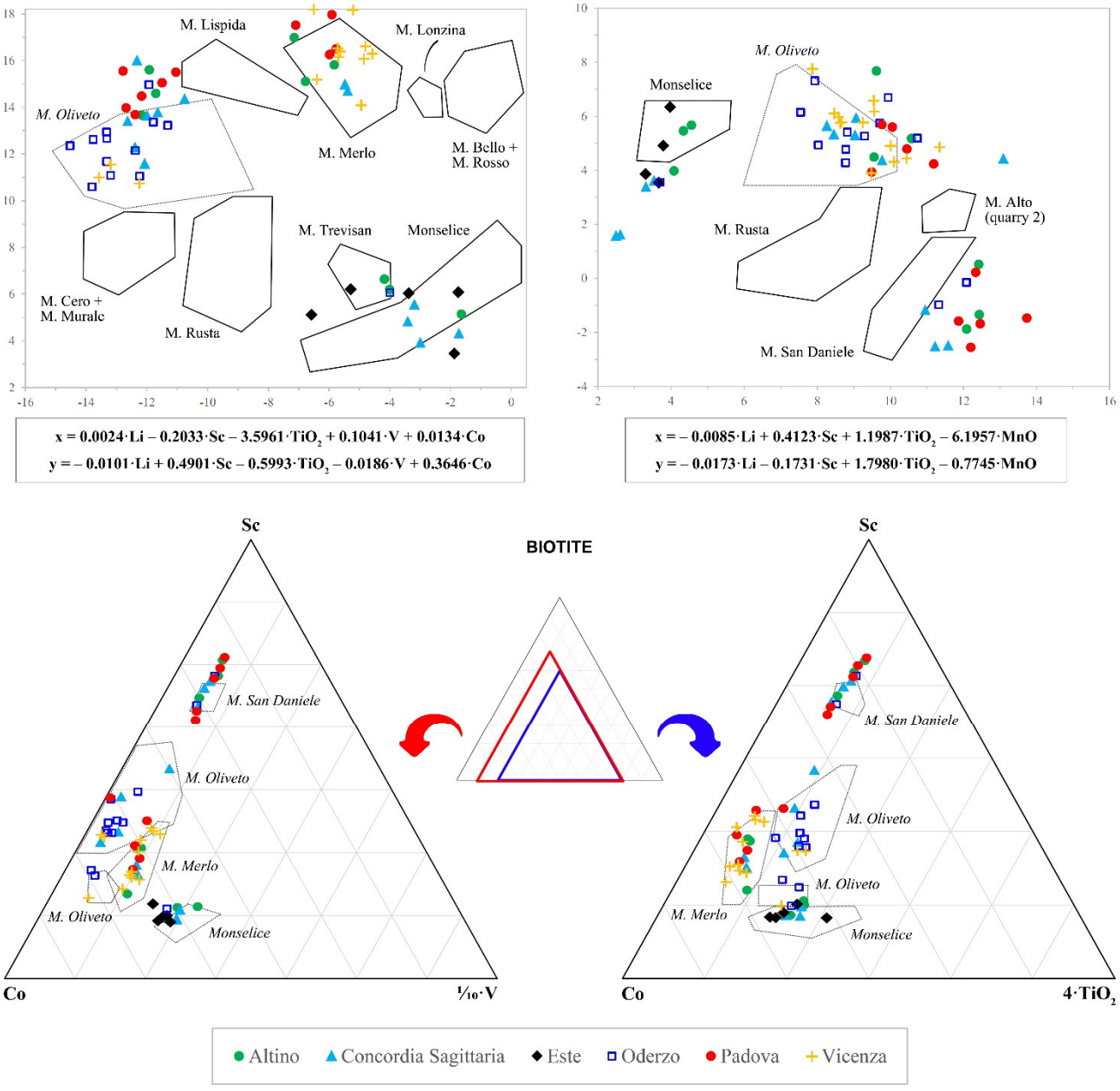

Fig. 7. Plots for provenance recognition of Euganean trachyte using chemical composition of biotite (Ch. 1), determined on the archaeological samples by LA-ICPMS, with major elements expressed as oxide weight percent and trace elements as ppm, using the isotopes in Appendix 4. For each sample, concentrations are averaged from multiple analyses. Solid lines indicate the reference fields of quarry clusters of Ch. 1, the names of which are also reported. The fields indicated by dotted lines and the name of the quarry locality in italics, drawn according to the position of the relevant quarry samples in Ch. 1, overlap or are very close to those of other localities: they cannot be used for univocal provenance attribution, but serve as reference for checking the position of unknown samples in multiple plots.

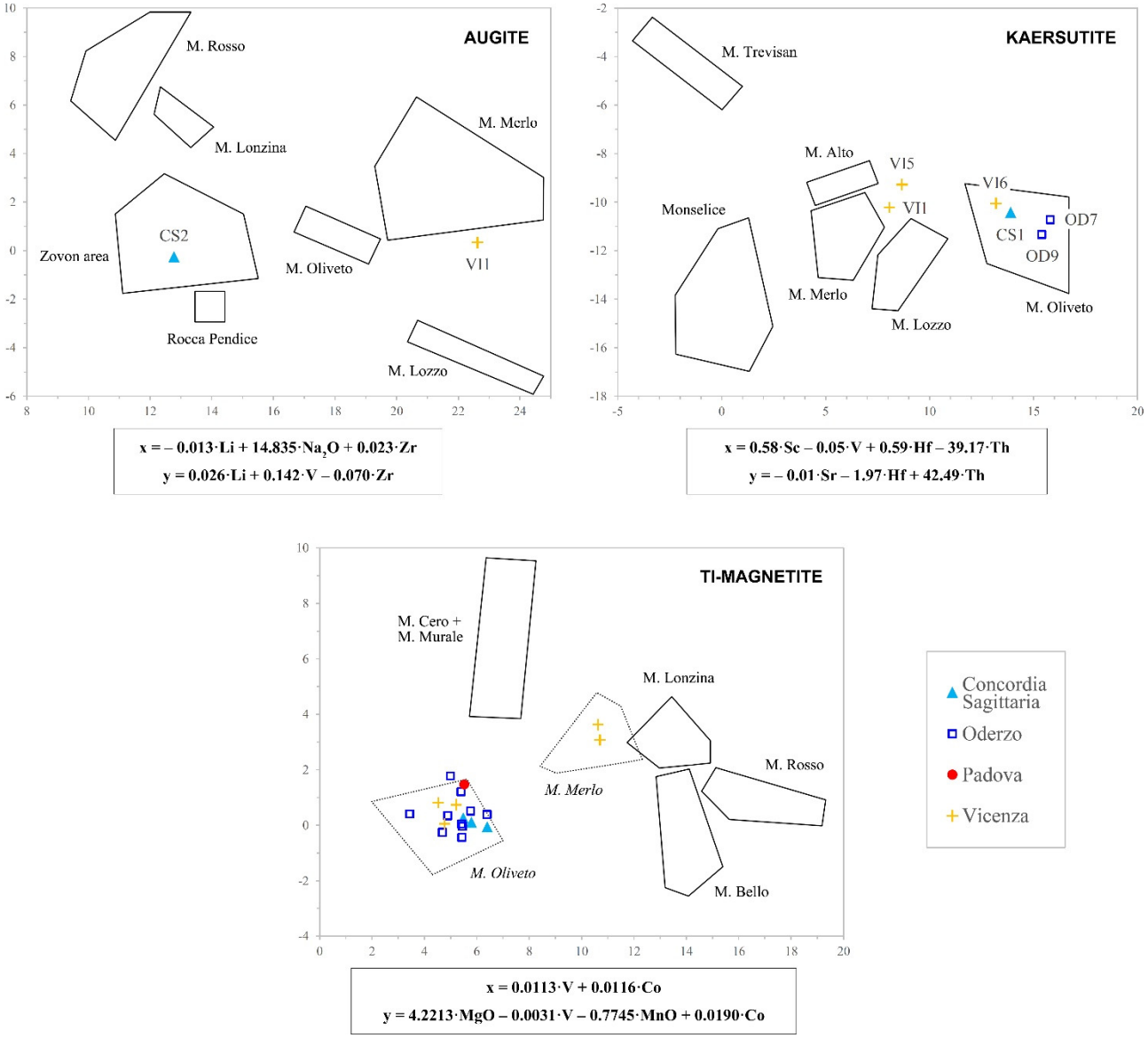

Fig. 8. Plots for provenance recognition of Euganean trachyte using chemical composition of augite, kaersutite and Ti-magnetite (Ch. 1), determined on the archaeological samples by LA-ICPMS, with major elements expressed as oxide weight percent and trace elements as ppm, using the isotopes in Appendix 4. For each sample, concentrations are averaged from multiple analyses. Solid lines indicate the reference fields of quarry clusters of Ch. 1, the names of which are also reported. The fields indicated by dotted lines and the name of the quarry locality in italics, drawn according to the position of the relevant quarry samples in Ch. 1, overlap or are very close to those of other localities: they cannot be used for univocal provenance attribution, but serve as reference for checking the position of unknown samples in multiple plots.

the diagrams in Fig. 7, the LA-ICPMS data were also plotted in the complementary reference binary plots suggested in Ch. 1, in order to definitively solve any possible doubt of provenance determination. This combined check also allows for assigning all the remaining unknown samples to the quarry locality of M. Oliveto (the ternary plots, as well as the binary plots V/Sc and Co/Sc showed in Appendix 5 are particularly useful for that). Only a single sample (CS2) shows a frequent deviation from the predefined quarry clusters.

This sample can be definitively attributed to the locality of Zovon, taking into account the analysis of augite and the correlation among Li, Na_2O, V and Zr (Fig. 8). The occurrence of M. Merlo and M. Oliveto is also confirmed cross-matching the results obtained on biotite with those on augite, kaersutite and Ti-magnetite (Fig. 8).
The few feldspar analyses, after a comparison with those of the reference quarry materials in Ch. 1, further validate the findings above.
Generally, the LA-ICPMS results confirm part of the previous attributions defined by the combined approach involving petrography and bulk-rock chemistry, but allow distinguishing trachytes of different provenance having very similar mineralogical, textural and bulk-chemical characteristics. This is not possible by either optical microscopy or XRF. Moreover, sometimes provenance determined only with these last methods turns out to be incorrect. Therefore, provenance identification by LA-ICPMS analysis of phenocrysts is more precise and effective, providing reliable and univocal results even on very limited amounts of sampled material (i.e., on thin sections of few mm^2 or cm^2). In addition, it is an independent technique, not requiring any other preliminary exploratory analysis.

6. Management of the Roman quarries

Based on the final provenance determinations (Table 1), four main provenances of Euganean trachyte used in the Roman infrastructures are recognized: M. Merlo (19 samples), M. Oliveto (17), Monselice (13) and M. San Daniele (13); a single sample also comes from the quarries of the Zovon area (Fig. 9).
These determinations are consistent with the Roman quarry localities most frequently reported in the literature, except for M. San Daniele that, in this study, results to have greater importance. Including also the previous archaeometric studies, involving the analysis of over 500 archaeological samples, Monselice quarries turn out to be the most exploited, with more than 40% of Roman trachyte samples coming from that locality, followed by M. Oliveto and M. Merlo (about 25%) (Zara 2016). All these sites are localized in the outermost part of the hill complex, more easily accessible from the surrounding plain.

Table 1. Provenance quarry locality determined for the samples of Euganean trachyte from the Roman infrastructures, grouped by the sampling locality.

Locality	Sample	Provenance	Locality	Sample	Provenance
Altino	AL1, 5, 7	M. San Daniele	Oderzo	OD1	Monselice
	AL2, 3, 4	M. Merlo		OD2, 3	M. San Daniele
	AL6, 8, 9	Monselice		OD4, 5, 6, 7, 8, 9, 10, 11, 12, 13	M. Oliveto
Concordia Sagittaria	CS1, 8, 12	M. Oliveto	Padova	PD1, 3, 4, 7	M. Merlo
	CS2	Zovon area		PD2, 5, 8, 10, 11	M. San Daniele
	CS3, 4	M. Merlo		PD6	M. Oliveto
	CS7, 9, 10, 14	Monselice			
	CS11, 13, 15	M. San Daniele	Vicenza	VI1, 2, 3, 4, 5, 7, 9, 10, 12, 13	M. Merlo
				VI6, 8, 11	M. Oliveto
Este	ES1, 2, 3, 4, 5	Monselice			

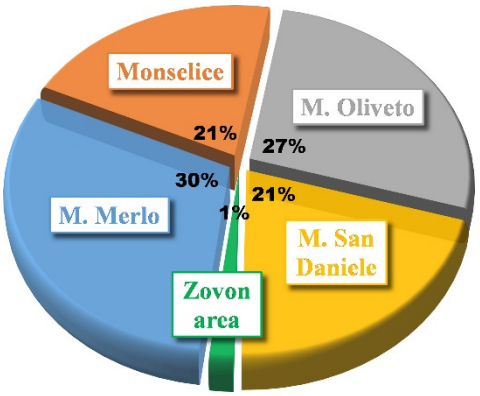

Fig. 9. Pie chart showing the occurrence frequency of the provenance quarry localities determined for the archaeological samples of Euganean trachyte.

No trend in the use of different trachytes from the localities listed above is noticed in relation to the time period or kind of infrastructure, but their geographic distribution is diverse. Considering the centers closest to the Euganean district, Monselice trachyte, cropping out south of the hill complex, is the sole variety identified in *Ateste*, few km nearby; conversely, it is totally missing in *Patavium* and *Vicetia*, closer to the northernmost area of the Euganean Hills and to M. Merlo and M. San Daniele quarries, where most of the trachytes sampled in the two cities come from. This cannot be considered accidental, especially in view of the widespread use of Monselice trachyte. Conversely, a separate management of the Euganean quarries by different cities may be argued. Monselice quarries were probably controlled by the nearby *Ateste*, whereas *Patavium* and *Vicetia* were not allowed to exploit that resource, or did not intentionally; it can be argued that these two centers could have obtained material from other owned quarries, closer to their territory, perhaps just those of M. Merlo, M. San Daniele and M. Oliveto; this applies in particular to *Patavium*, the most important settlement. It is worth pointing out that the quarries were presumably owned by the city authority but conceded as usufructuary properties to single private citizens or societies of publicans (Buonopane 1987), i.e., the cities kept indirect control of the quarrying activities while being relieved of the management commitments.

This subdivision of the Euganean region is supported by the territorial claims that the local communities advanced in the Republican Age, which were solved in the second half of the 2nd century BCE with the emplacement, by order of the Roman Senate, of two cippi and a rock inscription marking the borders between *Ateste* and *Patavium*, and another cippus defining the boundary between *Ateste* and *Vicetia* (Buonopane 1992). These claims are well comprehensible, considering the massive economic benefits that trachyte extraction and commercialization brought.

The provenance determinations presented here also reveal that different trachyte types are frequently used in the same infrastructure. This is probably due to periodic maintenances, which were necessary, for example, for substituting worn-out flagstones on roads, especially in the most important and populated cities; for these interventions, probably different quarries supplied the raw material. This could also happen for great public works, requiring tens of thousands of tons of stone, which could not be easily provided by a single quarry without slowing down the building process. One last option concerns the activity of intermediaries, who purchased and managed the transport and stockpiling of stone sets from different extraction localities, and then organizing one-off resales to the clients; in this way, big stone orders could be fulfilled more rapidly.

Only in few cases, a sole trachyte variety is recognized in a single infrastructure (e.g., the forum of *Opitergium*, completely paved with M. Oliveto trachyte). That probably represents the expressed choice of conferring aesthetic homogeneity on a specific complex, or the necessity of buying the material being the most economically convenient or coming from a quarry controlled by the relevant city.

7. The ancient trades of trachyte

Roman colonization in northeastern Italy started in the 2nd century BCE, but the territories of Veneto were fully annexed with the concession of Roman citizenship and the establishment of *municipia* from 49 BCE and, finally, with the institution by Augustus of the territorial entity of *Regio X Venetia et Histria*, in 7 CE. This resulted in a general urban and monumental renovation according to the Roman standards, with the realization of numerous great public works, for which stone demand progressively grew. Indeed, most of the dateable Roman infrastructures made of Euganean trachyte were built between the 1st century BCE and 1st century CE, so from the late Republican Age to the early Imperial Age (Zara 2016) (Fig. 10).

In that period, commercial activities involving fluvial routes were also strengthened, with the creation of littoral channels along the Adriatic coast and reorganization of harbors in cities like *Ravenna*, *Mediolanum* and *Altinum* (Cera 1995).

Indeed, trachyte circulation was mostly dependent on ship transport, taking advantage of the favorable position of the Euganean Hills in the network of waterways going through northern Italy (Fig. 11). Inland trades exploited the many rivers and channels of the Venetian Plain, in particular the Bacchiglione and the Adige, flowing north and south of the Euganean Hills, respectively. The occurrence of ships transporting stones along the Bacchiglione mainly from/to *Patavium* is confirmed by the discovery of a shipwreck and its stone load (Previato & Zara 2014); although it presently flows at a distance of about 4 km from the northernmost quarries of M. Merlo, the Bacchiglione was well connected to the Euganean district by a complex network of drainage channels (Bondesan et al. 2010; Primon et al. 2012). On the contrary, in the Roman times, the Adige flew very close to the southernmost side of the Euganean Hills, lapping the cities of *Ateste* and *Mons Silicis* (Monselice), before flowing into the Adriatic Sea (Piovan et al. 2012). Further nearby communication ways were represented by the Brenta river to the north, and possibly by the *Togisonus*, a channel lapping the eastern side of the Euganean Hills and joining the territory of *Patavium* to the Adige, according to Pliny the Elder (*Naturalis Historia*, III, 20, 121); this might justify the higher concentration of Roman quarries on the eastern side of the Euganean Hills. On the other hand, longer-range transports of trachyte relied on alternative routes. The Po river was the main waterway to the west – and so was for northern Italy,

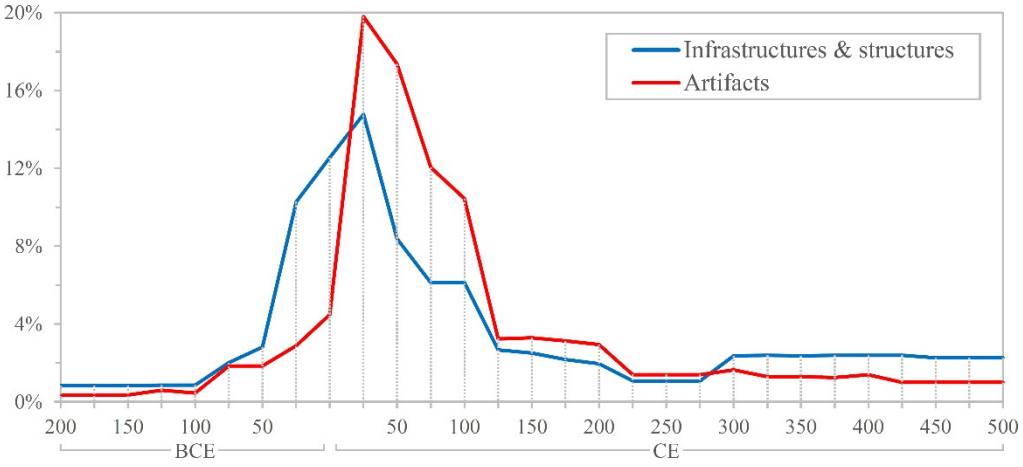

Fig. 10. Frequency distribution of all the known dated Roman finds made of Euganean trachyte in relation to their dating (from Zara 2016, encompassing 740 infrastructures and structures, and 505 artifacts out of a total of about 2500 finds).

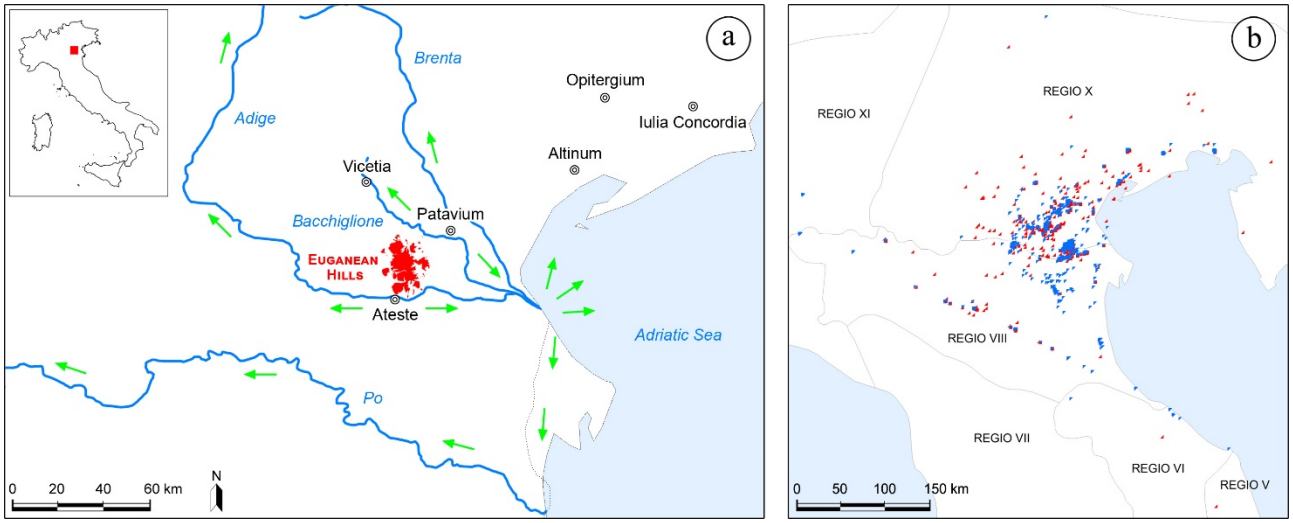

Fig. 11. (a) Localization of the Roman cities considered in this study and the Euganean district in relation to the main water routes and lines of trachyte trading. The rivers are indicated by their most probable main flow during the Roman times, together with the ancient coastline (dotted line) (Stefani & Vincenzi 2005; Mozzi et al. 2010; Stefani & Zuppiroli 2010; Piovan et al. 2012). The channel network connecting the rivers nowadays and in the past is not represented. **(b)** Geographic distribution in the *Regiones Augustee* of all the known Roman finds made of Euganean trachyte: the blue indicators are for infrastructures and structures, the red ones are for artifacts (after Zara 2016).

crossing its entire territory from one side to the other – allowing trading with centers along *Via Aemilia* and as far as *Mediolanum*. The discovery of trachyte milestones emplaced along *Via Aemilia* in the second half of the 2nd century BCE (Donati 2000) suggests that long-range trading was already active during the early phase of Roman colonization. Finally, the centers close to the Adriatic coast, from *Ancona* to *Aquileia* and even further, were reached by the system of sea and lagoon navigation. In general, water routes were often preferred to land ways, which were still necessary for short-range transports, or for reaching sites of stone extraction or processing, or even the northernmost destinations, e.g., those in the Alpine area. For land transport, animal-drawn carts and sleds were used: if compared to ships – able to bear several tens of tons of material – these means could carry smaller loads, were slower and more expensive; indeed, the advantages of trades afforded by waterways were well known in the classical antiquity, as attested by Pliny the Younger (*Epistulae*, X, 41, 2) and Strabo (*Geōgraphiká*, V, 3, 11).

The final validation of these theories comes from a reconstruction by Zara (2016) of the load capacity of different means of transport in line with the actual stone needs for Roman public works. Considering the example of the forum square of *Opitergium*, having a surface of about 100 x 40 m, almost 1,000 m^3 of M. Oliveto trachyte were needed for the paving, corresponding to about 2,400 t (this amount could be far higher in the case of important road networks). Animal-drawn carts for stone transport could carry 2 t at most (Bedon 1984), so that, even assuming that the forum paving was completed in a long time range, this option would entail a huge, unlikely number of journeys from the Euganean quarries. On the contrary, based on the structure of Roman shipwrecks previously discovered, the ships used for trachyte transport should have had a load capacity of about 25 t; although this might even be an underrated estimation, the hypothesis of stone transports by waterways and sea involving most of trachyte trades is definitely more robust.

8. Conclusions

Trachyte of the Euganean Hills used as building stone in Roman public infrastructures in Veneto was mostly extracted in four quarry localities: M. Merlo, M. Oliveto, Monselice and M. San Daniele.
Trachyte provenance was identified by the combined analysis of petrographic features, under the optical microscope, and major- and trace-element chemical composition of bulk rock and phenocrysts, determined by XRF and LA-ICPMS, respectively. Recognition of quarry locality was done following the provenance tracers discussed in Ch. 1. The results confirm the greater effectiveness of using LA-ICPMS and exploiting phenocryst composition – in particular that of mafic minerals – applying simple multivariate correlations for a precise and unbiased provenance identification of Euganean trachyte. This approach does not need any preliminary exploratory investigation, and is also independent from the petrographic or XRF analyses, which yield several drawbacks and lower accuracy. For LA-ICPMS very small amounts of sample are needed, e.g., a petrographic thin section, even undersized; this is highly advisable for archaeological materials, for which non-destructive or micro-destructive techniques are mandatory.
The provenance determinations described herein provide new information about the quarries active in the Roman times, the extent and development of their exploitation, the frequency of use of the materials extracted therein and the commercial and economic dynamics involving their supply for public works. The quarries of Monselice, M. Merlo and M. Oliveto are confirmed to be among the most exploited by the Romans, and M. San Daniele seems to have an analogous importance, contrarily to what found out in previous archaeometric studies.
Indications are also given with regard to the territorial organization of the Roman settlements in Veneto, their areas of political influence and ownership of quarries; these elements allow arguing a separate management of the Euganean quarries by the most important cities nearby, *Patavium* and *Ateste*, and possibly their competition.
Finally, broad insights into stone trades in northern Italy during the Roman age are provided. The preferential trade lines for the circulation of raw and finished quarry materials are discussed, considering the localization of the Euganean district in relation to the main water routes for transport and destination centers, the convenience of different means of transport and the amounts of trachyte required for public works. Most trades were organized by ship transports, taking advantage of the many rivers and channels of the Venetian Plain (the Adige and the Bacchiglione above all), the nearby Po river and the Adriatic Sea.

Acknowledgements

This study has benefitted by the valued contribution of Arturo Zara and Jacopo Bonetto (Uni. Padova) for the sampling and archaeological interpretation of the results, included in Arturo Zara's PhD dissertation referenced below.
The author thanks Klaus Simon and Burkhard Schmidt (Uni. Göttingen) for their support during the LA-ICPMS and micro-Raman analyses, respectively. Thanks are also due to Soprintendenza Archeologia del Veneto for kindly authorizing the sampling campaign.

References

Antonelli F., Bernardini F., Capedri S., Lazzarini L., Montagnari Kokelj E. (2004). Archaeometric study of protohistoric grinding tools of volcanic rocks found in the Karst (Italy-Slovenia) and Istria (Croatia). *Archaeometry*, 46 (4), 537–552

Antonelli F., Lazzarini L. (2010). Mediterranean trade of the most widespread Roman volcanic millstones from Italy and petrochemical markers of their raw materials. *Journal of Archaeological Science*, 37, 2081–2092

Antonelli F., Lazzarini L. (2012). The first archaeometric characterization of Roman millstones found in the Aquileia archaeological site (Udine, Italy). *Archaeometry*, 54 (1), 1–17

Bartoli O., Meli S., Bergomi M.A., Sassi R., Magaraci D., Liu D.Y. (2015). Geochemistry and zircon U-Pb geochronology of magmatic enclaves in trachytes from the Euganean Hills (NE Italy): further constraints on Oligocene magmatism in the eastern Southern Alps. *European Journal of Mineralogy*, 27, 161–174

Bedon R. (1984). *Les carrières et les carriers de la Gaule romaine*. Picard, Paris

Bondesan A., Fontana A., Mozzi P., Piovan S., Primon S. (2010. La geomorfologia del territorio dell'Annia. In: Rosada G., Frassine M., Ghiotto A.R., eds, *…viam Anniam influentibus palustribus aquis eververatam*. Canova, Treviso, 25–36

Buonopane A. (1987). Estrazione, lavorazione e commercio dei materiali lapidei. In: Buchi E., ed., *Il Veneto nell'età romana*. Banca Popolare di Verona, s.l., 1, 186–218

Buonopane A. (1992). La duplice iscrizione confinaria di Monte Venda (Padova). In: Gasperini L., ed., *Rupes Loquentes – Atti del convegno internazionale di studio sulle iscrizioni rupestri di età romana in Italia*, Roma, Bomarzo, Italy, 13–15 October 1989, 207–223

Capedri S., Grandi R., Venturelli G. (2003). Trachytes used for paving Roman roads in the Po Plain: characterization by petrographic and chemical parameters and provenance of flagstones. *Journal of Archaeological Science*, 30, 491–509

Capedri S., Venturelli G. (2003). Trachytes employed for funerary artefacts in the Roman Colonies Regium Lepidi (Reggio Emilia) and Mutina (Modena) (Italy): provenance inferred by petrographic and chemical parameters and by magnetic susceptibility. *Journal of Cultural Heritage*, 4, 319–328

Capedri S., Venturelli G. (2005). Provenance determination of trachytic lavas, employed as blocks in the Romanesque cathedral of Modena (Northern Italy), using magnetic susceptibility, and petrographic and chemical parameters. *Journal of Cultural Heritage*, 6, 7–19

Capedri S., Venturelli G., Grandi R. (2000). Euganean trachytes: discrimination of quarried sites by petrographic and chemical parameters and by magnetic susceptibility and its bearing on the provenance of stones of ancient artefacts. *Journal of Cultural Heritage*, 1, 341–364

Cattani M., Lazzarini L., Falcone R. (1997). Macine protostoriche dall'Emilia e dal Veneto: note archeologiche, caratterizzazione chimico-petrografica e determinazione della provenienza. *Padusa*, 31, 105–137

Cera G. (1995). Scali portuali nel sistema idroviario padano in epoca romana. In: Quilici L., Quilici Gigli S., eds, *Atlante tematico di topografia antica, Supplemento I: Agricoltura e commerci nell'Italia antica*. L'Erma di Bretschneider, Roma, 179–198

Chevallier R. (1976). *Roman Roads*. University of California Press, Berkeley

Davies H. (2008). *Roman Roads in Britain*. Shire, Oxford

Donati A. (2000). Scritture di Bologna romana: alcune riflessioni. *Atti e memorie della Deputazione di storia patria per le province di Romagna*, 51, 377–386

Grossi P., Zanco A. (2003). Miliari romani nel Nord Italia: materiali, provenienza, lavorazione. L'esempio dell'area Veneta e Friulana. *Quaderni di archeologia del Veneto*, 19, 192–202

Grossi P. (2007). Pietre miliari della VIII Regio: analisi litologiche, provenienza dei materiali e loro distribuzione. *Epigraphica*, 69, 181–207

Le Maitre R.W., ed. (2002). *Igneous rocks: a classification and glossary of terms*. 2nd ed. Cambridge University Press, Cambridge

Maritan L., Mazzoli C., Sassi R., Speranza F., Zanco A., Zanovello P. (2013). Trachyte from the Roman aqueducts of Padua and Este (north-east Italy): a provenance study based on petrography, chemistry and magnetic susceptibility. *European Journal of Mineralogy*, 25, 415–427

Matteazzi M. (2009). Costruire strade in epoca romana: tecniche e morfologie. Il caso dell'Italia settentrionale. *Exedra*, 1, 17–38

Milani L., Beccaluva L., Coltorti M. (1999). Petrogenesis and evolution of the Euganean Magmatic Complex, Veneto Region, North-East Italy. *European Journal of Mineralogy*, 11, 379–399

Mozzi P., Piovan S., Rossato S., Cucato M., Abbà T., Fontana A. (2010). Palaeohydrography and early settlements in Padua (Italy). *Il Quaternario*, 23 (2Bis), 387–400

Paton C., Hellstrom J., Paul B., Woodhead J., Hergt J. (2011). Iolite: Freeware for the visualisation and processing of mass spectrometric data. *Journal of Analytical Atomic Spectrometry*, 26, 2508–2518

Piccoli G., Sedea R., Bellati R., Di Lallo E., Medizza F., Girardi A., De Pieri R., De Vecchi G., Gregnanin A., Piccirillo E.M., Norinelli A., Dal Prà A. (1981). Note illustrative della Carta geologica dei Colli Euganei alla scala 1:25000 – II edizione. *Memore di Scienze Geologiche*, 34, 523–566

Piovan S., Mozzi P., Zecchin M. (2012). The interplay between adjacent Adige and Po alluvial systems and deltas in the late Holocene (Northern Italy). *Géomorphologie: Relief, Processus, Environnement*, 4, 427–440

Previato C. (2015). *Aquileia: materiali, forme e sistemi costruttivi dall'età repubblicana alla tarda età imperiale*. Padova University Press, Padova

Previato C., Bonetto J., Mazzoli C., Maritan L. (2014). Aquileia e le cave delle regioni alto-adriatiche: il caso della trachite euganea. In: Bonetto J., Camporeale S., Pizzo A., eds, *Arqueología de la construcción IV. Las canteras en el mundo antiguo: sistemas de explotación y procesos productivos*. CSIC, Mérida, 149–166

Previato C., Zara A. (2014). Il trasporto della pietra di Vicenza in età romana. Il relitto del fiume Bacchiglione. *Marmora*, 10, 59–78

Primon S., Ninfo A., Mozzi P., Piovan S., Abbà T. (2012). Indagine geoarcheologica di Montegrotto Terme attraverso il telerilevamento. In: Bassani M., Bressan A., Ghedini F., eds, *Aquae patavinae – Montegrotto Terme e il termalismo in Italia, aggiornamenti e nuove prospettive di valorizzazione*. Padova University Press, Padova, 55–74

Renzulli A., Antonelli F., Santi P., Busdraghi P., Luni M. (1999). Provenance determination of lava flagstones from the Roman 'Via Consolare Flaminia' pavement (central Italy) using petrological investigations. *Archaeometry*, 41 (2), 209–226

Renzulli A., Santi P., Nappi G., Luni M., Vitali D. (2002a). Provenance and trade of volcanic rock millstones from Etruscan-Celtic and Roman archaeological sites in Central Italy. *European Journal of Mineralogy*, 14, 175–183

Renzulli A., Santi P., Serri G., Luni M. (2002b). The Euganean trachyte flagstones ("basoli") used by the Romans along the mid-Adriatic coast (Marche, central Italy): an archaeometric study. *Periodico di Mineralogia*, 71, 189–201

Santi P., Renzulli A. (2006). Italian volcanoes as landmarks for the spreading of trade networks during the Etruscan and Roman periods: the millstones and flagstones case study. *Acta Vulcanologica*, 18 (1-2), 133–140

Sassi R., Mazzoli C., Spiess R., Cester T. (2004). Towards a better understanding of the fibrolite problem: the effect of reaction overstepping and surface energy anisotropy. *Journal of Petrology*, 45, 1467–1479

Simon K. (2015). *LA-ICP-MS transient signal quantification of NIST, USGS and MPI-DING glasses by ratioing, standardization, normalization and correction (RSNC)*, Unpublished. Geowissenschaftliches Zentrum, Georg-August-Universität Göttingen, Germany

Staccioli R.A. (2003). *The roads of the Romans*. The J. Paul Getty Museum, Los Angeles

Stefani M., Vincenzi S. (2005). The interplay of eustasy, climate and human activity in the late Quaternary depositional evolution and sedimentary architecture of the Po Delta system. *Marine Geology*, 222-223, 19–48

Stefani M., Zuppiroli M. (2010). The interaction of geological and anthropic processes shaping the urban growth of Ferrara and the evolution of the surrounding plain. *Il Quaternario*, 23 (2Bis), 355–372

Vergani R. (1994). Masegne e calchere: secoli di attività estrattiva. In: Rigon A., ed., *Monselice. Storia, cultura e arte di un centro "minore" del Veneto*. Canova, Monselice, 403–413

Whitney D.L., Evans B.W. (2010). Abbreviations for names of rock-forming minerals. *American Mineralogist*, 95, 185–187

Witcher R. (1998). Roman Roads: phenomenological perspectives on roads in the landscape. In: Forcey C., Hawthorne J., Witcher R., eds, *TRAC 97. Proceedings of the Seventh Annual Theoretical Roman Archaeology Conference*. Oxbow, Oxford, 60–70

Zara A. (2016). *La trachite euganea: approvvigionamento, impiego e diffusione in età romana*, PhD dissertation. Dipartimento dei Beni Culturali, Università degli Studi di Padova, Italy

Chapter 3

Weathering in the urban built environment

Abstract

Decay of trachyte employed as building stone in urban environment was investigated through the analysis of crusts and patinas detected on trachyte of the Euganean Hills used in the Renaissance city walls of Padova, in northern Italy. Mineralogical and microstructural characteristics of the alteration products, as well as major- and trace-element chemical composition, were determined by optical microscopy, SEM-EDS and X-ray mapping, XRPD, and LA-ICPMS. The findings are placed in direct correlation with quantitative environmental parameters, in particular concerning air quality and anthropic pollution sources. The influence of composition of the stone and other neighboring materials on specific weathering processes is also debated. The formation of crusts and patinas turns out to be mainly due to exogenous processes. Their enrichment in heavy metals and carbonaceous masses derives from emissions of particulate matter from fuel combustion related to road traffic and domestic heating and, secondarily, from industrial processes. Their crystalline matrix is typically formed by calcite, mainly derived from leaching of nearby mortar joints, or iron, released after iron-bearing mineral dissolution, both reprecipitated according to pH fluctuations. Gypsum layers are rarely observable instead. Generally, composition of the weathering crusts and patinas of Euganean trachyte proves to be an informative marker for the relevant environmental conditions and their evolution.

1. Introduction

Air quality is one of the most crucial factors affecting stone weathering in urban environment, where concentration of stoneworks is generally greater and, at the same time, human activities are more intense and diverse. The latter change in time and space, and so does their contribution to pollution. Time variations in quantity and quality of pollutant emissions depend especially on changes in fuel use (Brimblecombe & Camuffo 2003). SO_2 emissions used to represent a major concern but, during the last decades, they have considerably declined in Europe – by one or two orders of magnitude in cities – together with a generally improved air quality (Brimblecombe 2014). Nowadays, the higher concentration of other pollutants, like N oxides (NO_x), particulate matter (PM), and O_3, must be reassessed. Road transport, domestic heating, industry, and power plants are the main pollution sources in urban centers, but their relative importance has changed as well (Guerreiro et al. 2014).
The modern urban environment features a multi-pollutant scenario with a major incidence of airborne particulate, having high concentration of elemental C (soot) and volatile organic compounds (VOC), with fuel combustion from road traffic as the main contributor (Grossi & Brimblecombe 2007; Auras et al. 2013). This carbonaceous matter exhibits high specific surface area and contains heavy metals

and aluminosilicon particles, which act as catalysts and adsorbents for organic compounds (Saiz-Jimenez 2003). Pollutant interaction with stone preferentially occurs through short-range dry deposition. Overall, the well-known processes of crust formation are becoming less significant in favor of soiling, characterized by an increasing enrichment in organic C, i.e., aliphatic and polycyclic aromatic hydrocarbons (Saiz-Jimenez 1993; Sabbioni 1995; Charola & Ware 2002; Watt & Hamilton 2003). In urban environments, dry deposition is more important than wet deposition, but a notable danger is still represented by short drizzles, fog, and dew, which have higher pH, do not remove previous acid deposits, and provide sufficient moisture for their chemical activation (Camuffo et al. 1984; 1988; Camuffo 1995).

Most studies on the interaction between building stone and urban environment have been centered so far on weathering of carbonate rocks, their dissolution, and formation of gypsum crusts (Sabbioni 2003); other rock types have been investigated more rarely.

Deterioration of trachytic lavas has also received scarce attention in the literature, not only because of their generally good durability. In fact, their use is historically less common if compared to other volcanic rocks, i.e., tuffs above all, andesites, and basalts: these have been quarried in Europe, Latin America, Middle and Far East and so on, and employed by some of the most important ancient civilizations, like the Romans, Egyptians, Greeks, Incas, and Aztecs (Grissom 1990; St. Seymour et al. 2004). Trachyte use has not been such widespread, with an exploitation mostly limited to Europe, namely Italy, Germany, Czech Republic, and France, as well as the Azores and Canary Islands (Ch. 4).

Most studies on trachyte weathering have focused on coastal salt-aggressive environments, such as those of Venezia and Napoli in Italy, and the Azores islands. Several deterioration patterns have been observed, including scaling, powdering, exfoliation, blistering, differential erosion, and efflorescences. They result to be mainly due to cyclic processes of in-pore salt crystallization related to sea-salt supply. The phases involved are halite, gypsum, thenardite, and mirabilite and, in indoor environments, also trona and natron, linked to the external contribution of mortars (Prudêncio et al. 1998; Alves et al. 2000; Lazzarini et al. 2008; Langella et al. 2009). Only Lazzarini et al. (2008) have addressed in detail the on-site decay of trachyte of the Euganean Hills, subject of the present paper (Fig. 1).

Few studies have also been centered on trachyte used in inland continental climates, as in Czech Republic (Gillhuber et al. 2006) and Germany (Graue et al. 2013). In particular, Graue et al. (2013) have investigated weathering crusts of trachyte in industrial, urban and rural environments, showing how their thickness, grain size, and enrichment in heavy metals and other exogenous components well correlate with different degrees and sources of anthropogenic air pollution; the occurrence of gypsum crusts has been mainly related to external supplies of Ca and S, since trachyte is not a primary source for these elements.

In this paper, the problem of trachyte decay in urban environment is tackled investigating the mineralogical, microstructural and chemical characteristics of weathering crusts and patinas detected on trachyte of the Euganean Hills used in the Renaissance city walls of Padova, in northern Italy. Trachyte alteration is placed in direct correlation with quantitative environmental parameters, in particular concerning air quality and anthropic pollution sources. The influence of composition of the stone and other neighboring materials on specific weathering processes is also debated.

Fig. 1. Some of the most common decay patterns of Euganean trachyte used in Padova (for ashlars, flagstones and column bases), including scaling, flaking, blistering and differential erosion of groundmass and xenoliths.

2. The city walls of Padova

Padova has a composite wall system surrounding the historical district gone through millennia of history. Traces of several building phases have survived, indicating the raising of a first wall circuit in the Roman age. During the Middle Ages, at the end of the 12th century, a new broader circuit with defensive function was built, enlarged in the following decades and all through the 14th century. The Medieval wall perimeter was roughly followed in the Renaissance by the builders of *Serenissima Repubblica di Venezia* – an ancient state of northern Italy, existed from 697 to 1797 – for raising more modern walls, which today are those best preserved.

The dominion of *Serenissima* in Padova began in 1405, but the works for new defensive walls started one century later, during and after the war with the League of Cambrai. This alliance was formed in 1508 by the major European powers, attempting to hinder the political and military influence of Venezia in northern Italy. The difficulties encountered in defending Padova, the most important mainland city, and the ongoing technological military innovations forced *Serenissima* to plan the construction of a new fortification system. This started in 1513 and continued until half of the century, with the realization of walls with an 11 km perimeter, 19 bastions, 8 gates, and several bridges, protected by moats, rivers, and channels (Fig. 2). Several modifications of the original project occurred, as testified, for example, by the adoption of circular bastions or roundels at first, and the subsequent building of pentagonal bulwarks, more effective in curbing enemy approaching. What can be seen today, however, is the result of the extensive modifications and demolitions of several parts of the curtain walls and two gates occurred under urbanization pressure from the 19th century (Mazzi et al. 2002; Fadini 2013).

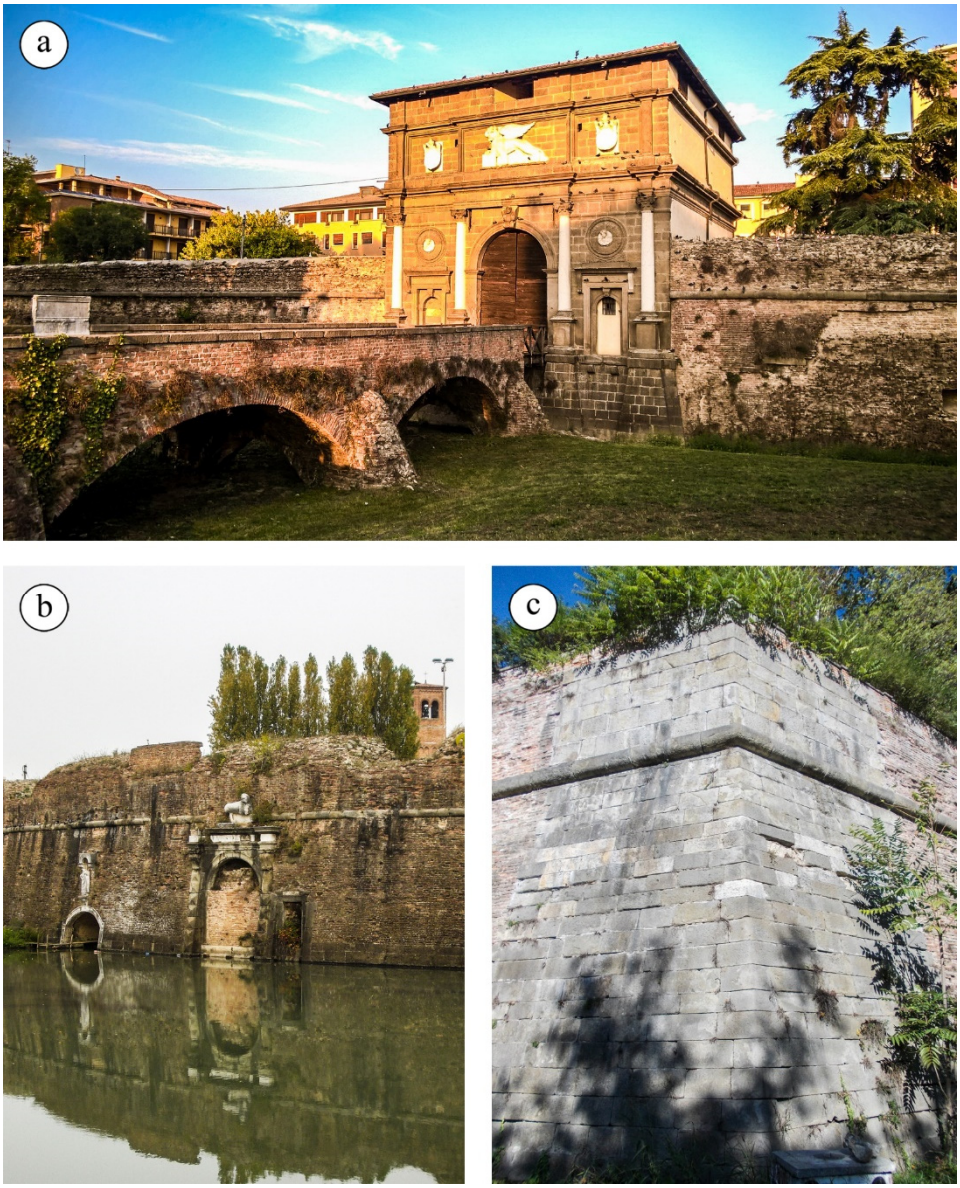

Fig. 2. The Renaissance city walls of Padova raised by *Serenissima Repubblica di Venezia*: **a)** Porta Savonarola gate, with a wall segment; **b)** Castelnuovo circular bastion with a water gate facing a channel; **c)** Cornaro pentagonal bastion.

The Renaissance wall system was built almost completely using bricks for the outer surfaces, with a core filled with rubble of bricks and stones consolidated with mortar. Trachyte was used not only as stone blocks in the core. It was employed for stringcourses, parapets, ashlars on angular ends of the bastions and other minor elements, as well as for building some of the gates (Porta Savonarola, Porta San Giovanni, Porta Santa Croce, and Porta Liviana-Pontecorvo).

A set of 22 trachyte samples were collected on four different segments of the Renaissance walls for analyzing their weathering crusts and patinas. Stringcourses on curtains and roundels as well as ashlars of an angled bastion were sampled, their localization being indicated in Fig. 3. During sampling, spots with different exposure were chosen; in the case of stringcourses, samples from the upper, frontal and lower surface were collected. To our knowledge, no cleaning restoration intervention has ever been carried out on the sampled stone elements.

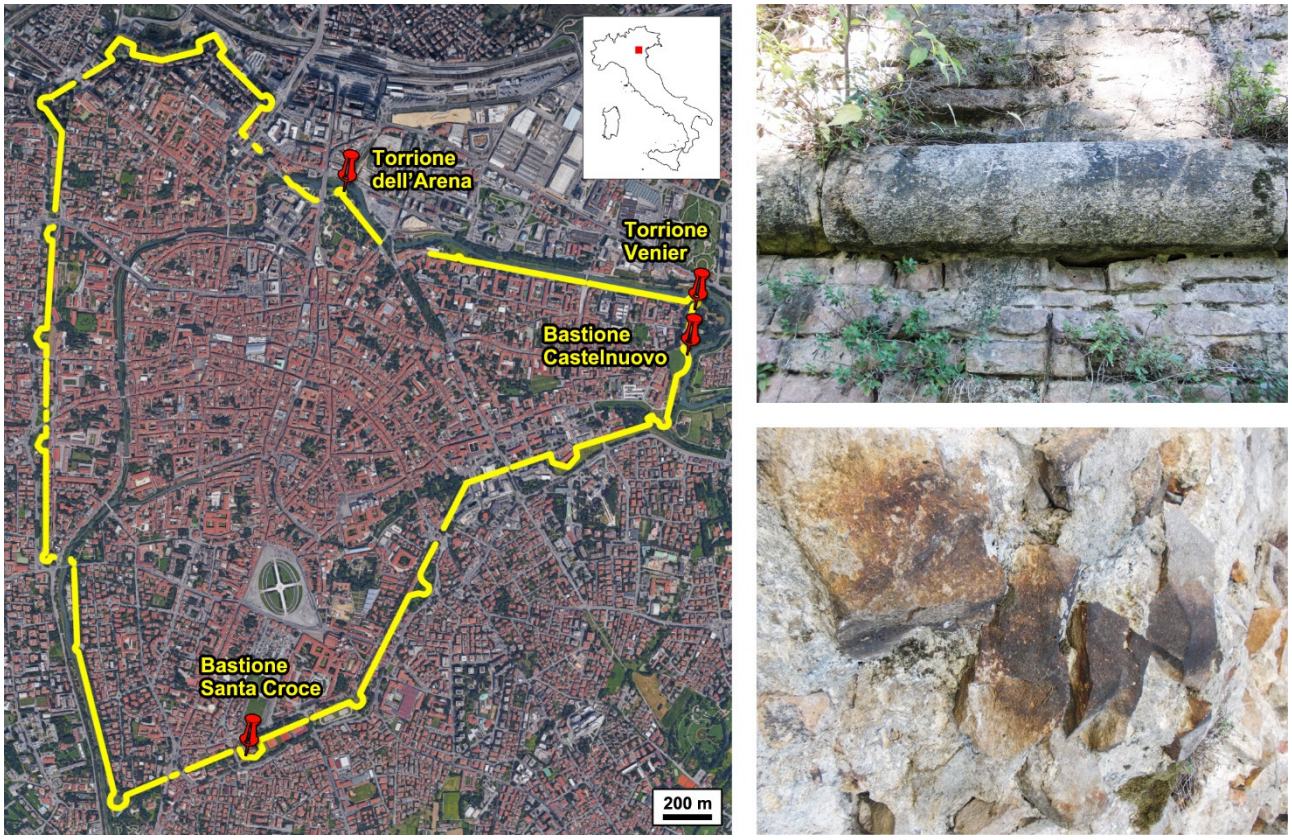

Fig. 3. The present-day circuit of the Renaissance city walls of Padova (satellite image from ©2016 Google), with sampling areas indicated, and two examples of weathering crusts and patinas on Euganean trachyte used for a stringcourse and as filling material in the wall core.

3. Euganean trachyte

The trachyte used in the Renaissance walls was extracted in the quarry district of the Euganean Hills, a group of hills located South-West of Padova. This is formed by a deep-water sedimentary succession of limestones and marls of the upper Jurassic–lower Oligocene, a Paleogene volcanic and hypabyssal series, and Quaternary detrital deposits. Trachytes are ascribable to a subvolcanic series dated to the lower Oligocene, and have acid to intermediate composition and moderate Na-alkaline affinity (Milani et al. 1999; Bartoli et al. 2015).

From a petrographic point of view, Euganean trachyte is a holocrystalline to hypocrystalline rock with porphyritic texture showing glomero- and cumuloporphyries of feldspars, namely anorthoclase, plagioclase, and sanidine, in diverse combination. Among the mafics, biotite is constantly present, and augite and kaersutite may be observed too. The accessory minerals typically comprise quartz, cristobalite, Ti-magnetite, ilmenite, apatite, and zircon; exceptionally, titanite, epidote, calcite, dolomite, siderite, monazite, and pyrite occur, whereas the content in secondary clay minerals is generally rather low or negligible. Pervasive migration fronts of Fe oxides and hydroxides and mafic xenoliths are sometimes visible as well. Groundmass is composed by prismatic alkali-feldspar microlites, frequently with fine-grained anhedral SiO_2 minerals and glass-bearing domains filling intercrystalline spaces; texture is usually felty, although preferred orientations are sometimes observable too (Ch. 1).

The exploitation of Euganean trachyte, still ongoing nowadays, started in Pre-Protohistory, but became more intense from the Roman times onwards. It has been widely used as carving and building stone in cultural heritage, in northern and central Italy and by its borders. Querns, mortars, cippi, milestones, steles, urns, tombstones, and sarcophagi comprise the most common artifacts crafted with trachyte all through the centuries. This material was widely used in the built environment too, as an instance for the admirable roads and other great infrastructures of the Roman age or the monumental architecture and construction from the Middle Ages and Renaissance. Indeed, with the rise of *Serenissima Repubblica di Venezia*, stone construction was given a substantial boost, and trachyte was largely employed in public buildings, churches, monasteries, monumental gates, defensive walls and private residences, as well as for paving squares and streets; the most striking examples can be admired in Padova and Venezia (Ch. 1 and references therein).

4. Experimental methods

The trachyte samples collected on the walls of Padova were analyzed in order to determine their mineralogical, microstructural and chemical characteristics, using the facilities of the Geoscience Center of Georg-August-Universität Göttingen.

Rock sections both parallel and perpendicular to the exposed surface were investigated with a polarized-light microscope and a field-emission scanning electron microscope (FE-SEM) FEI Quanta 200 FEG equipped with a ZrO/W Schottky field-emission gun and detector for energy-dispersive X-ray spectroscopy (EDS). In addition to usual observations and phase identifications, carried out on gold-coated samples, the SEM was used for acquiring X-ray elemental maps of selected cross sections, operating at 20 kV acceleration voltage, and scanning a grid of 512 x 400 pixels with a dwell time of 300 ms.

Powdery and incoherent samples were analyzed by X-ray powder diffraction (XRPD) with a Philips PW 1800 diffractometer equipped with Cu anode operating at 45 kV and 30 mA, measuring with scan steps of 0.02°2θ in the range 3–70°2θ and an integration time of 4 s.

Finally, analyses by laser ablation inductively-coupled plasma mass spectrometry (LA-ICPMS) were performed in order to determine major- and trace-element composition of both the altered layers and fresh host rock. The latter, prepared as polished samples embedded in epoxy, was analyzed with a Thermo Scientific Element 2 double-focusing magnetic-sector spectrometer coupled to a Resonetics Resolution 193 nm Ar-F excimer laser; data were acquired on profiles along 1.5 mm lines and average composition was calculated. Instead, the crust and patina samples were analyzed as they were, given the impracticality of preparing polished sections and analyzing the stratigraphy due to the limited thickness; for these samples, a Perkin Elmer ELAN DRC II quadrupole spectrometer was used coupled to a Lambda Physik COMPex 110 193 nm Ar-F excimer laser; data were acquired on profiles as long as the samples (centimetric size) and average composition was calculated. Both lasers operated with a 7 Hz repetition rate, 3 J/cm^2 fluence, 7 µm/s velocity, and using a spot size of 120 µm. Element concentrations were calculated with Iolite v2.5 software package, by a script based on the following procedure: the LA-ICPMS signal is first smoothed by ratioing to an appropriate denominator isotope present in the sample and standard (^{29}Si was used); the element ratios are standardized with NIST 610

glass reference material; then, they are normalized to oxides sum to reach 100%, including all the elements (Simon 2015).

5. Weathering analysis

5.1. Mineralogy and microstructure

Microscopic observations reveal that the thickness of the weathering crusts and patinas on the exposed surfaces is rather limited, often within few tens of µm, and only exceptionally may reach few hundreds of µm. Sometimes, powdery and incoherent deposits are also observed.
Almost all the samples have a high C content, responsible for the black-greyish color of many crusts and patinas. Subspherical carbonaceous particles may be isolated, grouped in small clusters (Fig. 4a), or form extensive layers covering trachyte surface more or less uniformly; depending on their thickness, these may display numerous fractures and microcracks (Fig. 4b). Soot represents a container for further accumulation of pollutants, indeed it may be rich in heavy metals, especially Pb, or include exogenous quartz, aluminosilicate minerals, chlorides, Al oxides etc.

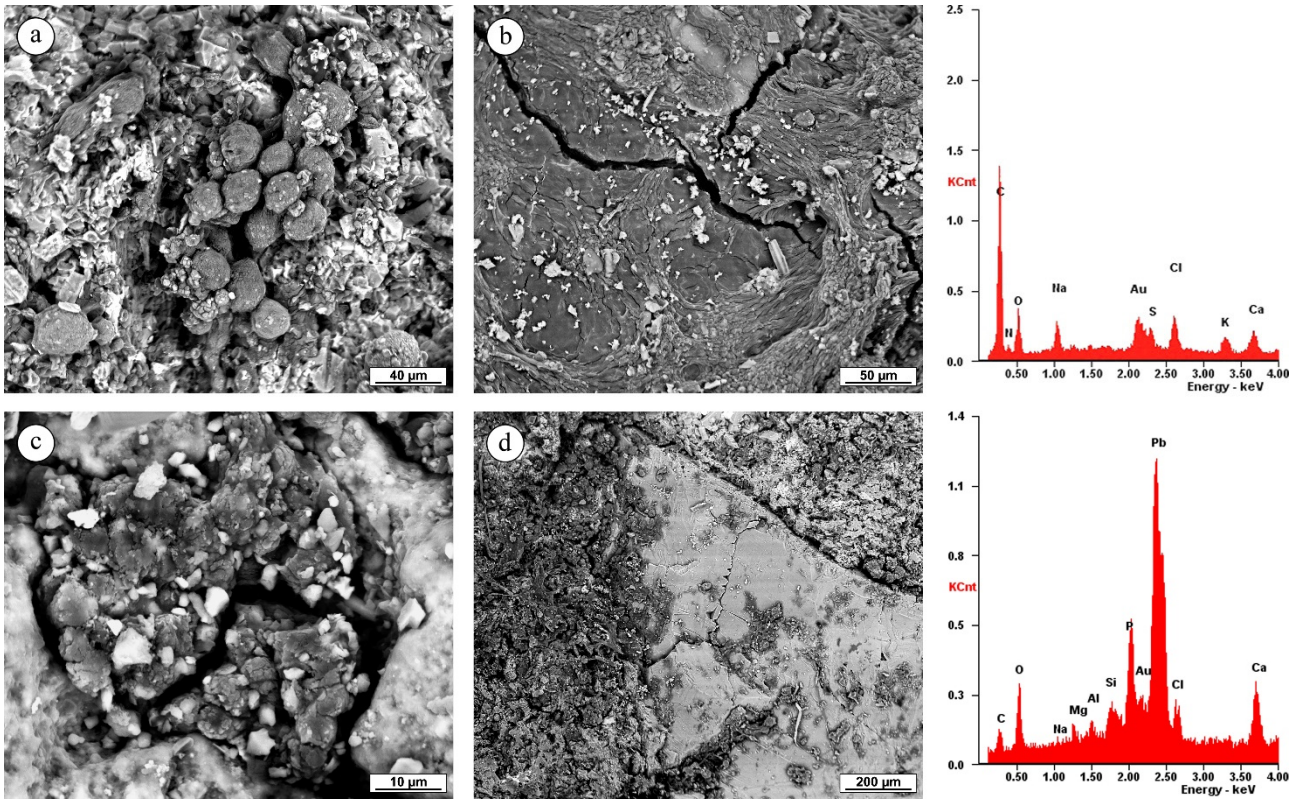

Fig. 4. SEM-BSE photomicrographs showing different features of the carbonaceous fraction (darker in the images) detected on the weathering crusts and patinas of Euganean trachyte and its microchemical composition by EDS measured on two different spots (signal from gold coating is also visible). **a)** Cluster of subspherical carbonaceous particles. **b)** Microcracked patina with crumbled fine-grained feldspars. **c)** Carbonaceous mass with Fe oxides, carbonates, and quartz. **d)** Aggregates of carbonaceous particles arranged along the edges and the internal fractures of a plagioclase phenocryst.

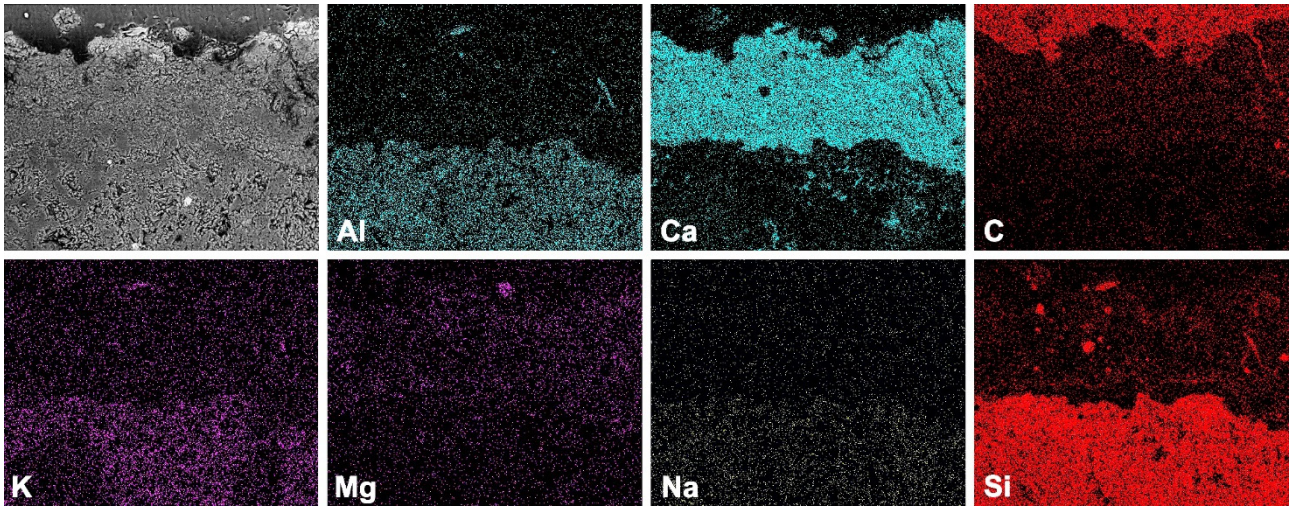

Fig. 5. SEM-EDS X-ray maps of a calcite crust of Euganean trachyte prepared as epoxy-embedded cross section, with the exposed surface displayed on the top (field size: 523.6 x 406.6 µm).

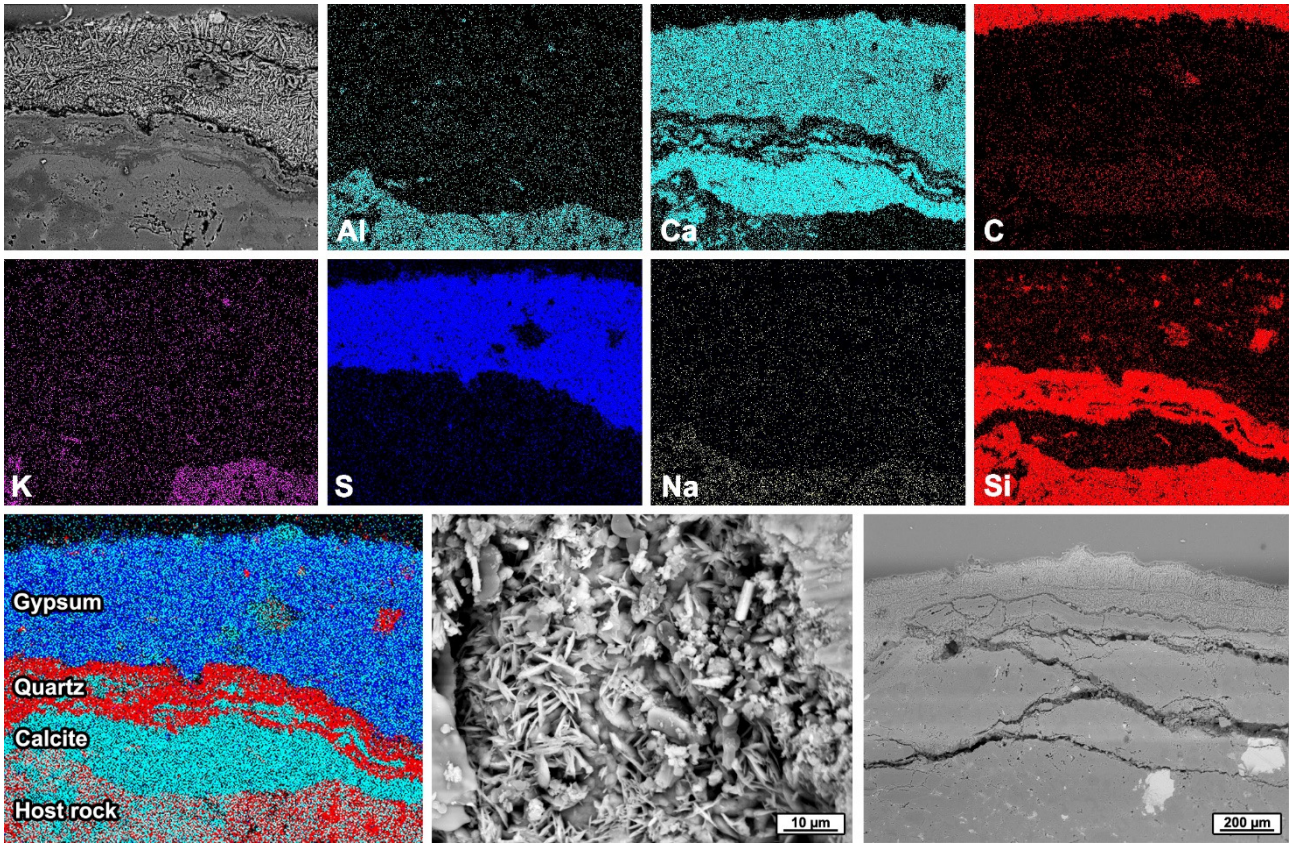

Fig. 6. SEM-EDS X-ray maps of a gypsum crust of Euganean trachyte prepared as epoxy-embedded cross section, with the exposed surface displayed on the top (field size: 524.5 x 407.3 µm). Details of the gypsum crystals and the fractured host rock beneath the crust are showed in the SEM-BSE photomicrographs.

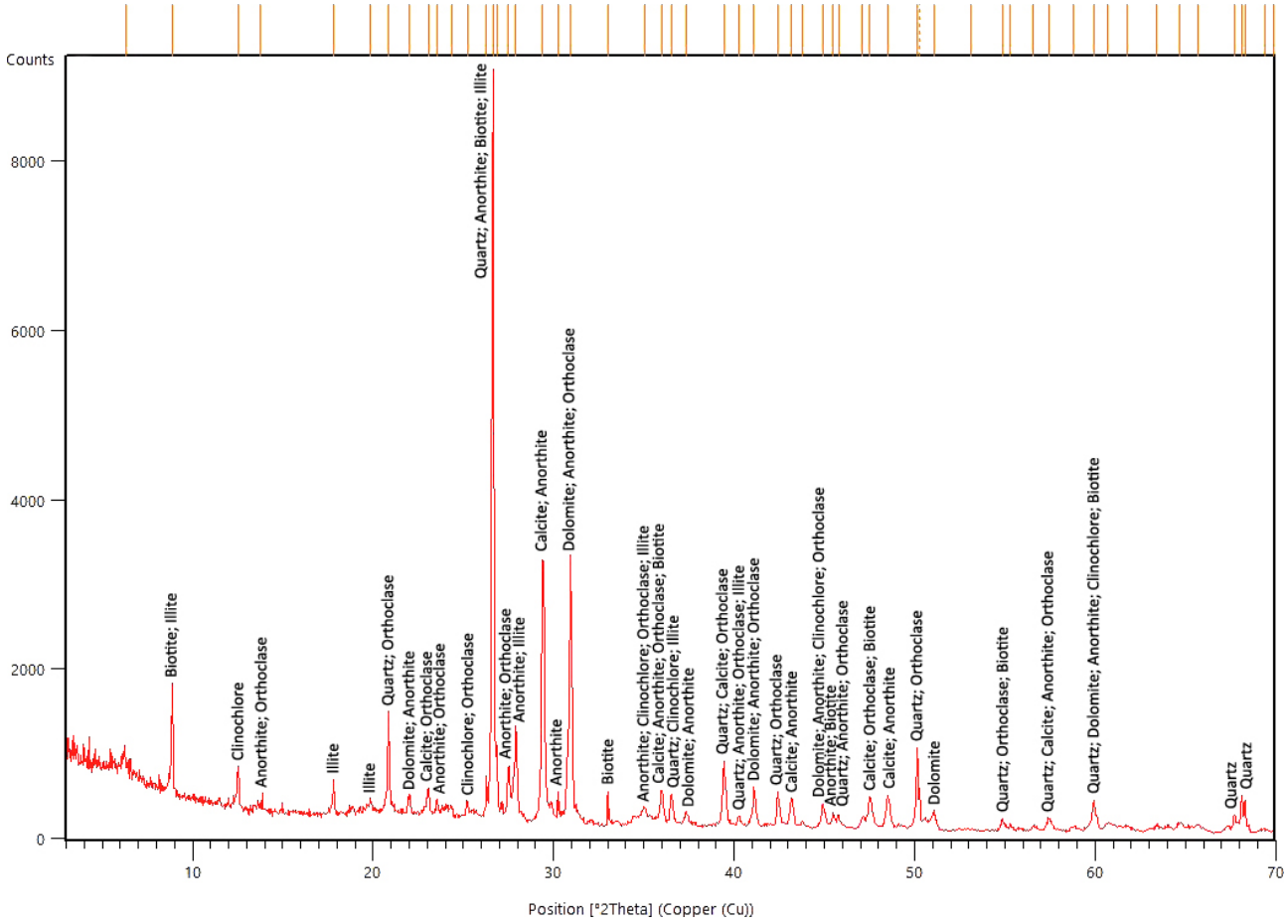

Fig. 7. XRPD spectrum of a powdery deposit on Euganean trachyte, showing a composition given mostly by quartz, calcite, and dolomite.

The airborne carbonaceous pollutants are frequently trapped in crusts formed by microcrystalline calcite and, secondarily, dolomite (Fig. 5). The high concentration of these phases cannot be traced back to trachyte composition, since they are originally present in low or negligible amount. A high content of quartz is often detected as well. The carbonaceous particles may be also associated with a matrix rich in Fe, present as oxides and hydroxides or in amorphous state, giving a general brown-reddish color, in possible combination with carbonates (Fig. 4c).

In the thinnest patinas, there are virtually no intermediate alteration layers between the host rock and the carbonaceous components, the adhesion of which occurs directly on the feldspars constituting the substrate; their fine grain size and crumbled appearance, which creates a porous surface favoring C deposition, suggests former processes of granular disintegration. C accumulates mainly on the groundmass or fine-grained phenocrysts, taking advantage of intercrystalline spaces and higher porosity, whereas large phenocrysts are less affected (Fig. 4d).

Gypsum crusts are detected on a sole sample, very close to a mortar splash by the joint of two trachyte blocks. Its collocation, on the lower side of a stringcourse, was a shelter against direct rainfall and washing out. The microscopic investigations reveal a complex stratigraphy (Fig. 6). The superficial layer is composed of a network of acicular or tabular gypsum crystals with rosette-like intergrowths, which embeds carbonaceous particles, but in rather low concentration. The second underlying layer

is composed of microcrystalline quartz, which is also observable in the gypsum layer, in lower amount. The third layer is constituted mostly by calcite, directly crystallized on the host rock. The presence of separate gypsum and calcite levels suggests a slow-rate alteration process, started with the crystallization and growth of a carbonate layer and its later, partial reaction with S, mostly limited to its outermost part. The gypsum layer represents a quite compact domain, whereas the underlying host rock shows a high degree of fracturing.
The XRPD analyses of powdery and incoherent deposits sampled on trachyte confirm the occurrence of some of the mineral phases detected through the SEM observations and microanalyses. Quartz, calcite, and dolomite are the major components, while the other identified phases comprise minerals from the host rock, like feldspars and biotite, or from their alteration, such as illite and chlorite (Fig. 7).

5.2. Major- and trace-element composition

The LA-ICPMS analyses of major elements (Table 1) substantially confirm the occurrence of two main alteration types, characterized by a high concentration of calcite and Fe. If the average composition of Euganean trachyte in Ch. 1 is taken as reference, the calcite crusts and patinas show an increase of CaO by a factor from 7 up to 60, corresponding to a maximum concentration of 86%. At the same time, a decrease in the content of SiO_2, Al_2O_3, Na_2O, and K_2O is always evident, up to a maximum of 87%, 93%, 97%, and 98%, respectively. A modest increase of MgO, associated with dolomite presence, is also noticeable. The different ratios between CaO and the feldspar-related elements reveal different degrees of alteration and homogeneity of the weathering layers, hence to what extent the silicate host rock has been obliterated by newly formed phases. As pointed out before, alterations with enrichments in carbonates and Fe may be associated but, when the latter is predominant, a Fe increase by a factor up to 6.5 is recorded, again with the contemporary depletion of the feldspar-related elements. Although a general surface sulphation is often evident, only in the gypsum crust a huge increase in SO_3 is reported, by a factor of 2487, corresponding to a concentration of 25%, which almost completely hides the silicate composition of the host rock, in association with the high content of CaO.
Further indications are given by the concentration of trace elements (a selection is reported in Table 2, while the complete dataset is included in Appendix 1). In comparison to the host rock, a remarkable enrichment in heavy metals of the crusts/patinas is evident (Fig. 8), especially in V, Cr, Ni, Cu, Zn, As, Cd, Sn, Sb, Pb, and Bi. As an instance, Pb results to be increased by a factor of over 1,700, while As, Cd, Sb, and Bi reach a factor of 370, 418, 230, and 1,661, respectively[1]. The highest absolute concentrations are reported for Cu, Zn, and Pb, equal to 1,009, 11,460, and 25,800 ppm, respectively. No significant mobilization of heavy metals into the host rock is detected (Török et al. 2011).
As also summarized in Fig. 9, when the host rock is shielded by thick, homogeneous and well-developed crusts, as those rich in calcite or gypsum, the near-surface concentration of heavy metals is lower on average, i.e., the absorption of pollutants is more limited. Calcite and gypsum tend to form microcrystalline domains more compact than the underlying host rock, so that mechanisms of dry and

[1] Except for Pb, the increase factors of the heavy metals were calculated comparing the LA-ICPMS analyses of the host rock, as the elements in question were not measured in the reference dataset of Ch. 1 used formerly.

Table 1. Major-element chemical composition expressed as oxide weight percent of representative samples of Euganean trachyte from the Renaissance city walls of Padova determined by LA-ICPMS, on both surface (i.e., weathering crust or patina) and host rock (inner part). The samples are divided by different types of alteration and sampling location as in Fig. 3 (SCR = Bastione Santa Croce; GAR = Torrione dell'Arena; CSN = Bastione Castelnuovo; FST = Torrione Venier).

Sample		SiO_2	TiO_2	Al_2O_3	Fe_2O_3	MnO	MgO	CaO	Na_2O	K_2O	P_2O_5	SO_3
Calcite-rich alteration												
SCR-01	Surface	8.57	0.02	1.14	0.58	0.04	1.49	85.85	0.17	0.12	0.69	0.38
	Host rock	63.69	0.12	18.09	0.76	0.01	0.14	4.40	6.18	4.56	0.04	0.45
GAR-03	Surface	52.04	0.17	13.40	3.98	0.31	1.21	16.29	3.28	0.83	3.21	1.18
	Host rock	67.17	0.09	18.08	0.91	0.00	0.20	1.51	5.75	5.70	0.12	0.10
CSN-03	Surface	55.10	0.40	11.59	3.51	0.09	1.51	15.60	3.00	0.97	1.42	2.93
	Host rock	65.78	0.11	18.31	2.04	0.01	0.35	1.03	5.82	5.63	0.04	0.06
SCR-05	Surface	58.50	0.19	13.81	3.31	0.05	0.72	10.42	2.77	0.55	1.22	0.44
	Host rock	67.89	0.30	15.96	1.97	0.02	0.59	1.69	5.26	5.21	0.17	0.12
Iron-rich alteration												
SCR-07	Surface	40.97	0.39	14.27	21.19	0.15	1.22	5.22	1.96	0.57	7.47	0.82
	Host rock	68.09	0.15	17.23	1.34	0.02	0.40	1.21	5.32	5.64	0.10	0.08
Weak alteration												
FST-07	Surface	66.20	0.13	17.71	2.99	0.12	0.33	3.73	5.07	0.91	0.72	0.65
	Host rock	69.08	0.06	16.46	0.84	0.01	0.12	2.01	5.20	4.33	0.07	0.11
Gypsum-rich alteration												
FST-05	Surface	5.44	0.01	0.41	0.11	0.00	0.17	66.07	1.34	0.12	0.58	24.87
	Host rock	70.62	0.23	14.93	1.29	0.01	0.32	1.05	4.01	6.32	0.03	0.19
Average composition of Euganean trachyte*		66.02	0.66	16.77	3.26	0.06	0.66	1.42	5.04	5.35	0.21	0.01

* Bulk-rock chemical composition determined by X-ray fluorescence and averaged among 86 fresh trachyte samples collected on the Euganean Hills in 40 different quarries and outcrops (Ch. 1).

Table 2. Trace-element chemical composition expressed as ppm of representative samples of Euganean trachyte from the Renaissance city walls of Padova determined by LA-ICPMS, on both surface (i.e., weathering crust or patina) and host rock (inner part). The samples are divided by different types of alteration and sampling location as in Fig. 3 (SCR = Bastione Santa Croce; GAR = Torrione dell'Arena; CSN = Bastione Castelnuovo; FST = Torrione Venier). Only a selection of the analyzed elements is showed (the complete dataset is included in Appendix 1).

Sample		V	Cr	Co	Ni	Cu	Zn	As	Cd	Sn	Sb	Σ REE	Pb	Bi
Calcite-rich alteration														
SCR-01	Surface	23.00	6.50	2.95	15.80	261.00	3660.00	25.80	10.50	13.70	6.29	48.95	176.60	0.92
	Host rock	3.49	2.32	0.68	1.58	12.09	57.50	2.40	0.17	1.58	0.25	123.34	8.24	0.05
GAR-03	Surface	87.20	115.00	14.70	75.20	865.00	1042.00	53.90	11.70	67.60	25.80	210.83	587.00	4.93
	Host rock	3.29	1.14	1.00	1.51	15.40	116.70	1.05	0.68	1.41	0.11	61.86	15.50	0.05
CSN-03	Surface	42.30	84.00	9.70	58.90	481.00	523.00	56.00	3.80	22.90	6.40	138.93	389.00	1.14
	Host rock	4.08	0.64	1.79	0.96	8.32	93.30	1.12	0.24	1.67	0.22	61.29	29.30	0.05
SCR-05	Surface	420.00	70.00	7.25	35.50	352.00	11460.00	55.40	8.85	50.50	32.60	199.78	25800.00	2.57
	Host rock	5.46	10.06	2.78	1.74	22.60	1582.00	1.98	0.50	3.74	0.27	236.71	8.39	0.05
Iron-rich alteration														
SCR-07	Surface	505.00	211.00	16.50	72.70	1009.00	6210.00	385.00	63.10	94.60	34.20	386.86	24900.00	45.50
	Host rock	2.99	0.79	1.60	1.50	30.00	65.80	1.04	0.15	0.92	0.17	130.32	8.21	0.03
Weak alteration														
FST-07	Surface	42.50	5.00	6.80	48.00	384.00	871.00	10.60	5.52	24.40	6.45	176.81	280.00	2.33
	Host rock	1.88	0.78	1.06	6.50	18.50	73.40	0.64	0.24	1.51	0.13	65.27	5.46	0.02
Gypsum-rich alteration														
FST-05	Surface	10.27	3.90	1.28	4.75	23.80	24.60	11.00	0.08	1.45	1.97	9.88	22.13	0.10
	Host rock	10.10	1.26	1.73	2.42	16.10	41.50	2.04	0.19	2.28	0.30	149.32	10.52	0.06
Average composition of Euganean trachyte*		23	3	3	2	23	103	*n/a*	*n/a*	*n/a*	*n/a*	*n/a*	15	*n/a*

* Bulk-rock chemical composition determined by X-ray fluorescence and averaged among 86 fresh trachyte samples collected on the Euganean Hills in 40 different quarries and outcrops (Ch. 1).

wet deposition of pollutants are hindered[2]. This is confirmed by a higher content of heavy metals on the stone parts exhibiting only a weak incipient alteration, maybe from a recently exposed surface (e.g., due to previous detachment of outer layers). On the other hand, non-uniform crusts, which do not entirely cover the host rock, represent an intermediate condition: storing of airborne carbonaceous particles and gathering of metallic pollutants are enhanced because of a relatively high porosity, given by a mix of disaggregated host rock and uneven, incomplete and scarcely adhering crystallization of newly formed phases; in this case, an enrichment in CaO, Fe_2O_3 and heavy metals is clear, but the compositional contribution of the silicate substrate is preserved.

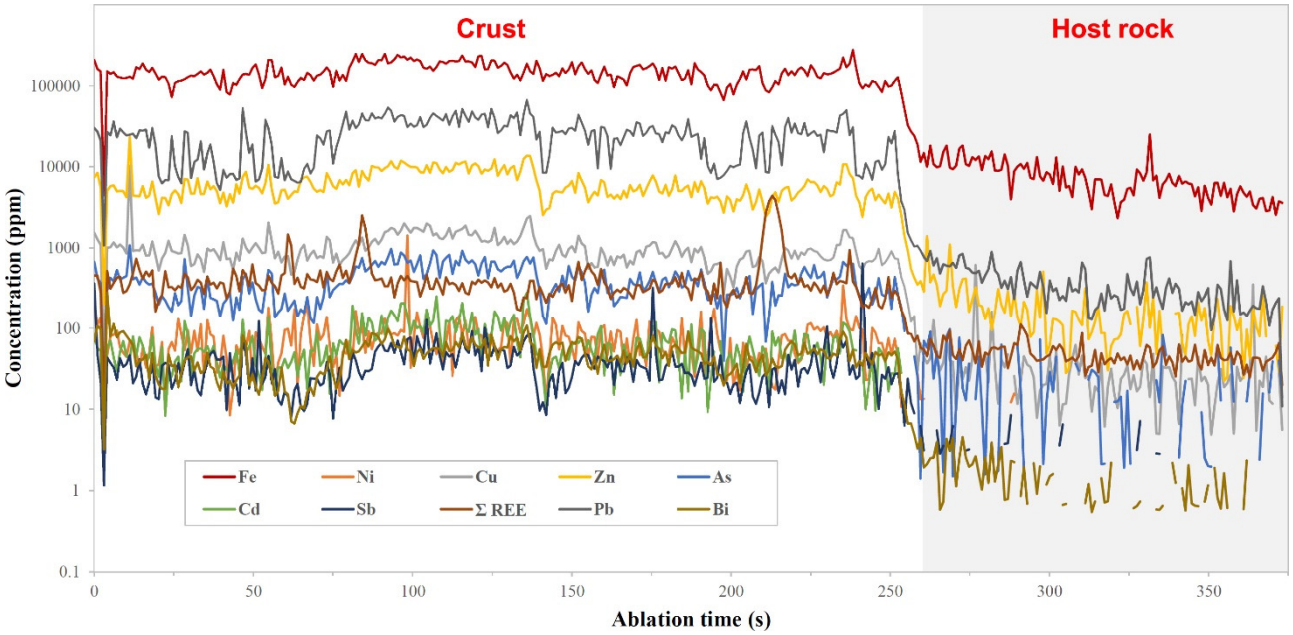

Fig. 8. Time-resolved LA-ICPMS spectrum obtained from a Fe-rich crust of Euganean trachyte, by a combined profile and spot analysis: crust surface was first ablated along a line and eventually drilled through, until reaching the host rock.

Finally, the relationship between trachyte sampling point and sample composition suggests the following considerations: the samples collected on frontal sides of stringcourses or ashlars feature a higher concentration of carbonates on average, thus indicating a major incidence of calcite-rich alteration on vertical surfaces; the samples collected on lower sides, including the gypsum crusts, display lower concentrations of heavy metals; no specific alteration trends dependent on the sampling site were recognized.

[2] The lowest content of heavy metals in the gypsum crusts is consistent with the scarce presence of carbonaceous particles and their role of vehicle for the accumulation of further pollutants. The abundance of heavy metals is remarkably lower than that measured on black crusts of other trachytes in urban and industrial environments, even in rural areas. Pb concentration, for example, is 22 ppm in Padova, whereas over 1800 ppm have been measured in several German cities. The heavy-metal concentration in the other crust types of Euganean trachyte, instead, is closer to that typical of European cities, which display for example a Pb content of few hundreds ppm up to 2000 ppm (Graue et al. 2013).

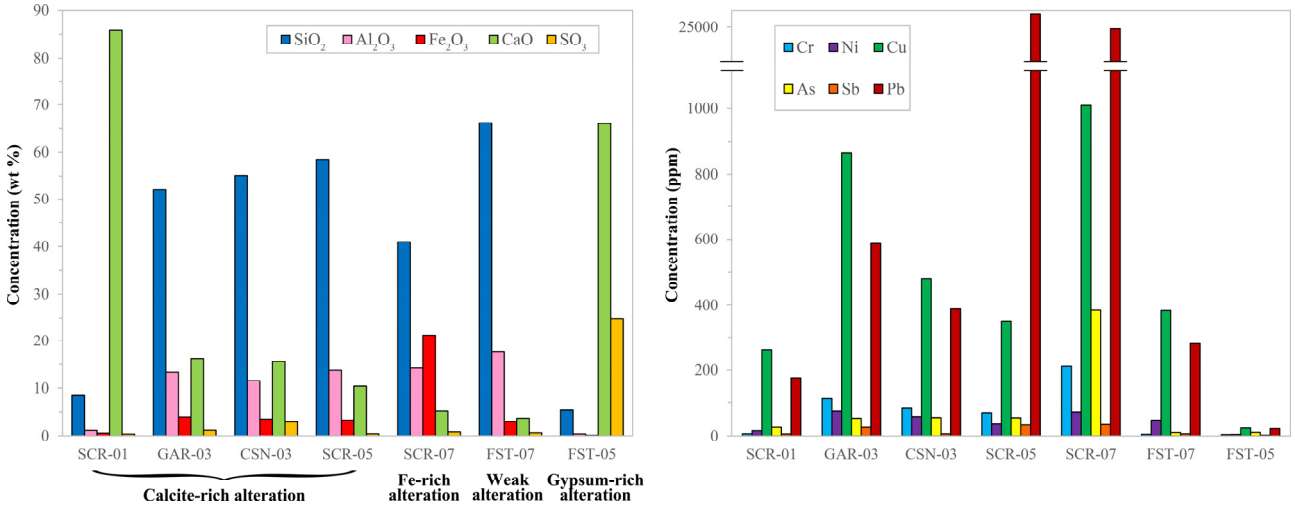

Fig. 9. Comparison of the major- and trace-element composition measured by LA-ICPMS on the weathering crusts and patinas of representative samples of Euganean trachyte. Sample names and compositions refer to Table 1 and Table 2.

6. Correlation with air quality

6.1. Environmental setting

In order to establish a correlation between trachyte alteration and air quality, it is necessary to describe the environmental setting the stone interacts with.

Padova is the seventh most populous city of northern Italy, with over 200,000 people and a population density of over 2,000/km^2. Located in the Veneto region, in the easternmost part of the Po Plain, it is about 20 km far from the Venetian Lagoon and 40 km from the coastline of the Adriatic Sea.

The climate is humid temperate ("Cfa" climate, according to Köppen classification). It features hot summers, with record maximum temperatures usually exceeding 35 °C, and mild to cold winters, when minimum temperatures may easily drop below 0 °C. The most humid period in the year is between fall and winter, whereas late-spring and summer months are the driest. Rainfall is concentrated during fall and spring, while winter has the lowest precipitation. Spring is usually the windiest season (data from ARPAV agency, Table 3).

Concerning air pollution (Table 4 and Table 5, ARPAV data), the concentration of virtually all the gaseous pollutants and PM dispersed in the air has significantly decreased in the last years. Although air quality in Padova does not change much locally (from one measurement station to another), it is expectedly more polluted by traffic areas or near industrial plants: the former present a concentration of NO_x increased by a factor of 1.5 if compared to that measured in background areas; near industrial plants, instead, the same increase in the concentration of SO_2 is registered, as well as an enrichment in heavy metals of the PM fraction, by a factor up to over 2.

Another important parameter is pH of rainfall, related to air pollution. There are no recent institutional data available, so an average value from 5.5 to 6 has to be assumed based on alternative sources: old measurements in Padova (Camuffo et al. 1988) and Venezia (RIDEP network, 1988), as well as recent

Table 3. Climatic parameters measured in Padova averaged from 2000 to 2015 (source: ARPAV).

Climatic parameter	Value	Climatic parameter	Value
Temperature (°C)		*Precipitation (mm)*	
Annual mean	14.5	Annual total	959
Annual mean min.	10.7	Lowest annual total	561
Annual mean max.	19.1	Highest annual total	1395
Lowest monthly mean & monthly mean min. (Month)	3.9 / 1.5 (January)	Lowest monthly total (Month)	58 (January)
Highest monthly mean & monthly mean max. (Month)	24.7 / 30.2 (July)	Highest monthly total (Month)	107 (November)
Relative humidity (%)		*Precipitation days*	
Annual mean	74	Annual total (≥ 1 mm)	84
Annual mean min.	53		
Annual mean max.	91	*Solar irradiance (MJ/m²)*	
Lowest monthly mean & monthly mean min. (Month)	65 / 43 (July)	Annual total (Legnaro, 1994–2015)	5005
Highest monthly mean & monthly mean max. (Month)	84 / 94 (November)	*Wind direction*	
		Annual mean	NE

Table 4. Concentration of air pollutants measured in Padova in different locations and expressed as hourly grand means, for gaseous pollutants, and daily grand means, for PM_{10}. The records comprise the following periods: for gaseous pollutants, from 2000 to 2015 (Background and Traffic stations) and from 2001 to 2015 (Industrial II station); for PM_{10}, from 2003 to 2015 (Background, Traffic and Industrial I stations) and from 2008 to 2015 (Industrial II station) (source: ARPAV).

Measurement station	CO	NO	NO_2	ΣNO_x	SO_2	O_3	PM_{10}		As	Cd	Ni	Pb	C_6H_6	$C_{20}H_{12}$
	mg/m³	µg/m³	µg/m³	µg/m³	µg/m³	µg/m³	µg/m³		ng/m³	ng/m³	ng/m³	ng/m³	µg/m³	ng/m³
Background														
Whole record	0.7	29.9	42.1	88.4	2.5	52.5	43.0		1.4	0.9	3.4	17.7	2.1	1.3
Last 5 years (2011–2015)	0.6	23.0	34.8	69.6	1.6	51.7	39.3		0.7	0.4	3.5	9.7	1.7	1.4
Traffic														
Whole record	0.8	53.2	53.0	132.6	2.4	45.2	43.4		1.5	1.0	3.8	17.4	3.3	1.3
Last 5 years (2011–2015)	0.4	29.8	44.0	89.8	2.4	45.6	36.8		0.8	0.5	3.6	9.7	3.6	1.2
Industrial I														
Whole record	*n/a*	*n/a*	*n/a*	*n/a*	*n/a*	*n/a*	43.0		1.5	1.3	6.7	45.2	*n/a*	1.2
Last 5 years (2011–2015)	*n/a*	*n/a*	*n/a*	*n/a*	*n/a*	*n/a*	37.9		1.0	0.5	4.1	21.3	*n/a*	1.3
Industrial II														
Whole record	0.7	35.0	42.2	95.9	3.7	39.4	37.2		0.9	0.5	3.0	10.0	*n/a*	1.1
Last 5 years (2011–2015)	0.6	26.6	38.7	79.6	1.8	43.0	36.0		0.9	0.5	3.0	9.3	*n/a*	1.3

PM_{10} composition

Industrial I: one station monitoring the emissions from a local steel mill;
Industrial II: two stations monitoring the emissions from a local waste-to-energy incinerator.

Table 5. Salt content, indicated by the concentration of selected anions, cations, and trace metals, and concentration of organic carbon (OC) and elemental carbon (EC) in the air in Padova, measured in $PM_{2.5}$ collected in the background station and expressed as daily means. The records comprise a short-term monitoring from January to March 2014 (source: ARPAV – Progetto PoAIR).

$PM_{2.5}$		Cl^-	SO_4^{2-}	NO_3^-	NH_4^+	Na	Mg	K	Ca	OC	EC
µg/m³	Composition	µg/m³	µg/m³	µg/m³	µg/m³	µg/m³	µg/m³	µg/m³	µg/m³	µg/m³	µg/m³
32.9		0.1	1.5	7.1	2.4	0.6	0.1	0.4	0.3	10.2	2.3

datasets from mountain localities in Veneto (CONECOFOR network and TESAF, University of Padova). For proposing this pH value, lower accuracy of old analyses, sampling location, and the general reduction of emissions during the last decades have been taken into account. The value indicated is typical to that of unpolluted rainwater, conventionally 5.6 (Steiger et al. 2014).
The most significant pollution sources in Padova – other than those typical of every city, like road traffic, domestic combustion etc. – are the only two major industrial plants in the city area, namely a waste-to-energy incinerator and a steel plant, about 3 km and 6 km far from downtown, respectively. A cement plant is also active at a distance of about 20 km in Monselice, responsible for higher NO_x emissions, however their long-range impact has proven to be almost irrelevant. Conversely, the influence of the industrial area of Venezia-Porto Marghera cannot be ruled out due to major emissions, which are also more easily transported to Padova by winds, having usually a NE direction. Venezia-Porto Marghera, located 30 km far from Padova, is one of the biggest coastal industrial zones in Europe. In its area of over 20 km^2, chemical, petrochemical and petroleum industries, refineries, thermal power stations, metallurgical industries, air separation and natural-gas processing plants, incinerators etc. are operational. The emissions comprise mainly SO_2, NO_x, CO, PM, and VOC, due principally to fuel use in the power stations, and partly to refining and chemical manufacturing processes, except for VOC, linked above all to the chemical and petroleum industry (ARPAV 2007; 2009; 2015).

6.2. Exogenous processes

The mineralogical and chemical identity of the alterations of Euganean trachyte can be related to air pollution, so that composition of the weathering crusts and patinas turns out to be a marker for the relevant environmental conditions and their evolution.
The enrichment in C and heavy metals can be traced back to the particulate deriving mostly from road traffic, emitted by diesel and gasoline-powered vehicles, and domestic combustion of woody biomass. These are the main sources of total suspended particulate (TSP) in Padova, according to the emission projections by ARPAV agency (ARPAV 2015b)[3] summarized in Fig. 10. A further major source of particulate is fuel-free industrial processes in the steel mill ("productive processes"); as indicated in Table 4, its emissions have a relatively high content of Pb, Ni, and As, so this can be directly related to the enrichment in heavy metals detected on the weathering crusts. By comparison, TSP produced by the local incinerator ("waste treatment and disposal") is almost negligible. If the contribution from the industrial area of Venezia-Porto Marghera is also considered, a further supply of carbonaceous pollutants and heavy metals can be identified mainly from the power stations, refinery, petroleum industries, and the related employment of fuels and machines. Conditions of high air humidity and precipitation and strong wind are the most favorable for pollutant dispersion, so that summer can be considered the least dangerous season. Carbonaceous and metallic particles act as catalysts, so their accumulation enhance further stone alteration and crust growth (Simão et al. 2006).

[3] INEMAR projections by ARPAV agency contain space- and time-based estimations of the yearly emissions in the atmosphere generated by several anthropic and natural activities that, given the complexity and amount of the possible sources, could not be all exactly calculated. The estimations are based on both real measured data and theoretical indicators, the latter inferred from statistical data and exploratory surveys concerning population, territory, economy, development etc. (ARPAV 2015b).

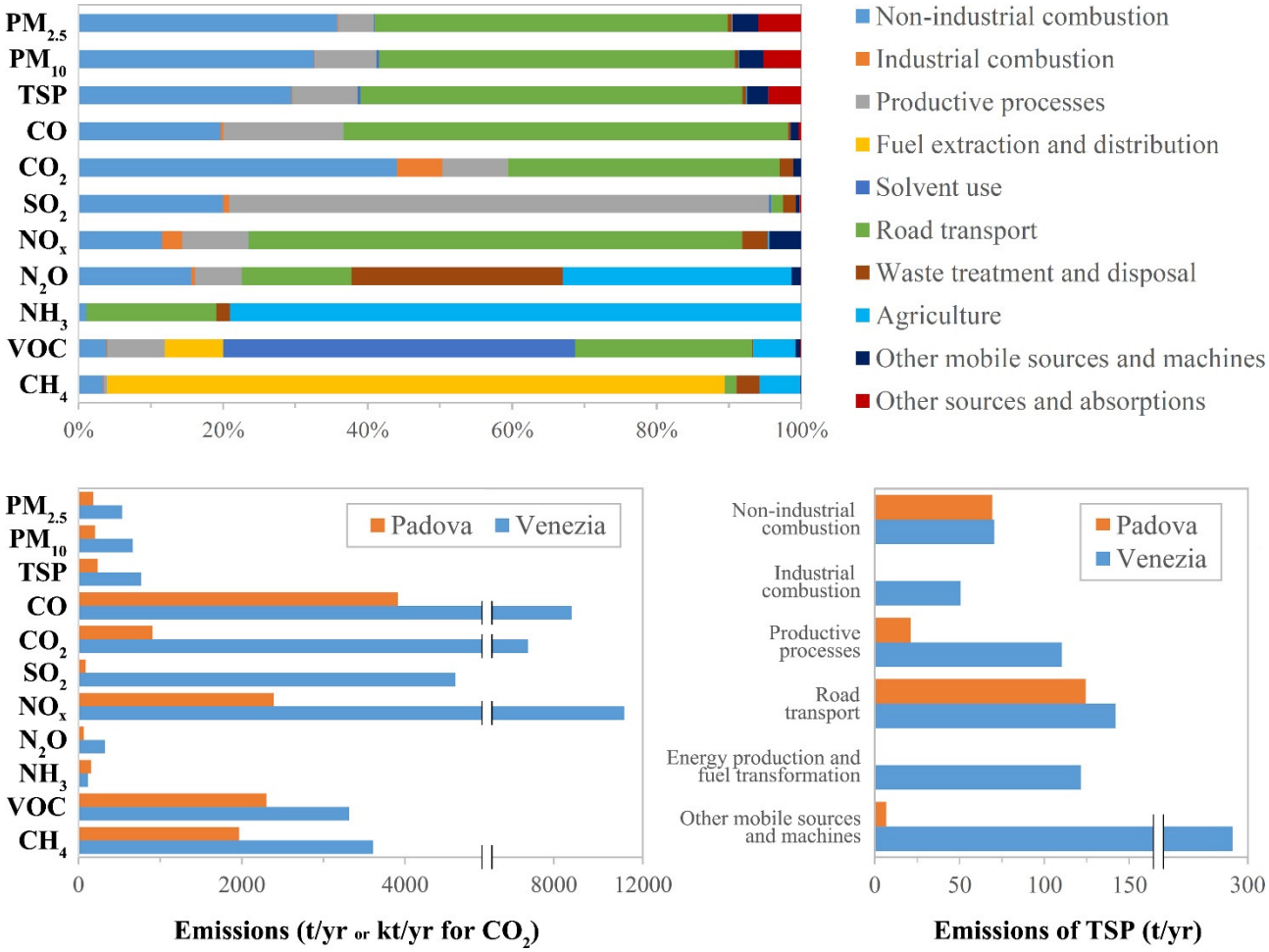

Fig. 10. Estimated emissions of the major air pollutants in Padova during 2010 by several macro-groups of anthropic and natural activities, and comparison with emissions calculated for Venezia in the same year, mainly deriving from the industrial area of Porto Marghera (INEMAR projections, ARPAV 2015b).

Among other exogenous processes contributing to the weathering of Euganean trachyte, it is worth mentioning the possible reactions leading to the formation of the carbonate crusts. A possible effect of Ca-rich airborne particles (Charola & Ware 2002) is not enough to explain such a high concentration of calcite and, secondarily, dolomite. The only plausible and consistent source is identified in lime and Mg-lime mortars used in the walls of Padova for joining trachyte blocks. In fact, Ca carbonate may be dissolved from mortars by acid solutions and reprecipitate in basic ones; calcite is less stable, i.e., its dissolution is faster, when pH is lower than about 5-6: dissolution rate increases with increasing H^+ activity, in high-acidity regime, or CO_2 partial pressure, in low-acidity regime (Fredd & Fogler 1998; Arvidson et al. 2003; Dolgaleva et al. 2005). As reported above, average pH of rainfall in Padova is around 5.5-6, just around the limit of calcite stability. This means that pH fluctuations[4]

[4] pH fluctuations of an aqueous solution can occur due to leaching of stones/mortars or solubilization of acid particles previously dry-deposited on their surface. Fluctuations also depend on the current general air quality and other large-scale factors: for example, a short drizzle or the initial stage of a rainfall are more acid, since the highly-soluble anthropogenic pollutants are first gathered; in a later stage, airborne alkaline agents reacting with slower kinetics and solubility – e.g., NH_3 from agricultural fertilizers, soil particles, wind-transported Saharan dust etc. – make water pH increase (Camuffo et al. 1984; 1988).

to higher acidity may increase leachability of Ca carbonate from mortars; the resulting solution containing leached $Ca(OH)_2$, thus an alkaline medium (Steiger et al. 2014), continues its short-range path, and may easily reach trachyte elements, wetting their surface and penetrating into pores; finally, calcite reprecipitates, taking advantage of the alkaline pH. Carbonate recrystallization episodes might be more common in summertime, whereas dissolution process possibly takes place more frequently during late fall and winter: in the cold season, atmosphere acidity is generally higher due to domestic heating and related emissions, and low temperatures increase calcite solubility (Deer et al. 2013); higher humidity and precipitation represent other favorable factors, as well as the recurrence of misty days, with fog being more acid than rainfall, with pH even below 4 (Charola & Ware 2002; Steiger et al. 2014).

The role of neighboring mortars acting as Ca source for trachyte weathering has been outlined by Graue et al. (2013) too. It seems to be confirmed also by other compositional features of the weathering crusts and patinas, especially concerning the high contents of quartz and formation of the gypsum crusts, very close to a mortar joint. These outcomes may be linked to a mortar aggregate rich in quartz and with trace impurities of sulfates, chlorides etc.

Alternatively, quartz might be also derived by Saharan dust, long-range transported from Africa by Sirocco: when this wind rises to pass over the Alps, the desert particles, composed of silicates and carbonates, are scavenged by rainfall (Camuffo et al. 1984; 1988).

On the other hand, the gypsum crusts might be also connected to anthropogenic air pollutants, i.e., to SO_2 oxidation and hydration and the well-known subsequent reaction of H_2SO_4 with a Ca carbonate substrate, in this case formed on trachyte after mortar leaching. The high degree of fracturing of the underlying host rock suggests an initial penetration of Ca-rich solutions in the outer pores, then producing crystallization pressures during water evaporation up to rock failure. Gypsum possibly formed after subsequent Ca loading and growing outwards of the carbonate crystallization layer. Concerning SO_2 supply, the most important contribution is given by the emissions of the steel mill. Anyway, the overall concentration of SO_2 is rather low in Padova and not comparable to that typical of big urban and industrial centers (Charola & Ware 2002), and presumably it was so even in the past. This – other than the carbonate-poor composition of trachyte – justifies the very limited extension of the gypsum crusts and their rare occurrence (Germinario et al. 2014). A hypothesis that can be completely discarded is the nucleation of gypsum directly from soot absorbing pollutants (Camuffo 1986), given its low concentration and, on the other hand, the large extension of the gypsum crusts.

Finally, it is worth reminding that no evident effect of interaction between trachyte and sea salts (Table 5) carried by wind or rainwater was noticed. The scant chlorides detected have to be traced back to mortar composition instead, as stated above.

6.3. Stone leaching

Some features of the weathering crusts and patinas of Euganean trachyte can be explained by intrinsic factors, in particular the Fe-rich alterations. Microscopic examinations disclosed an enrichment in fine-grained Fe oxides and hydroxides and amorphous Fe in the proximity of biotite phenocrysts and, secondarily, magnetite and ilmenite crystals (Fig. 11). This suggests Fe mobilization from mineral leaching and migration to surface, forming brown-reddish alteration layers. Leaching might have also

occurred at the expense of mafic xenoliths (Lazzarini et al. 2008) or oxidation fronts of Fe oxides/hydroxides, genetically linked to post-magmatic processes (Ch. 1). Leaching of biotite seems more likely, since solubility of magnetite and ilmenite is lower. Fe^{2+} release from the octahedral layers of biotite is strongly pH dependent: rate of dissolution linearly increases with decreasing pH, but the reaction is significant only for values lower than 4-5 (Acker & Bricker 1992; Bray et al. 2014; 2015). The environmental conditions leading to the formation of the Fe-rich crusts and patinas would be similar to those described for the calcite crusts, involving pH fluctuations around the limit of the stability field even of biotite; in this case, however, its lower leachability if compared to that of calcite requires a more acid environment for dissolution to get started. Finally, a minor contribution of PM to Fe enrichment of trachyte surfaces must be taken into account, however that is not the main source, as also confirmed by the absence of Fe compounds in the incoherent and powdery surface deposits of exogenous origin.

A leaching process of the host-rock has been supposed also with regard to dissolution of plagioclases and release of Ca^{2+} cations, as an alternative or concurrent mechanism of formation of the calcite crusts. In Euganean trachyte, plagioclase represents one of the main mineral phases, it has a prevalent oligoclasic-andesinic composition with an average CaO content of 6% (Ch. 1), so theoretically it is a possible source of Ca (Blum & Stillings 1995; White & Buss 2014). However, the overall CaO content of the bulk rock is rather low on average (1.4%, see Table 1). Additionally, in acid solutions, Ca leachability from plagioclase is quite low, especially taking calcite as a term of comparison or even Fe release from biotite (Snäll & Liljefors 2000; Brantley & Olsen 2014). Leaching is also facilitated in fine-grained crystals, whereas plagioclases are among the coarsest phenocrysts in Euganean trachyte, even reaching a centimetric size. Moreover, clay minerals, typically resulting from feldspar alteration, were detected only in minor amounts. For all these reasons, plagioclase cannot be considered the primary source of such a high concentration of carbonates in the crusts, although its contribution cannot be totally excluded.

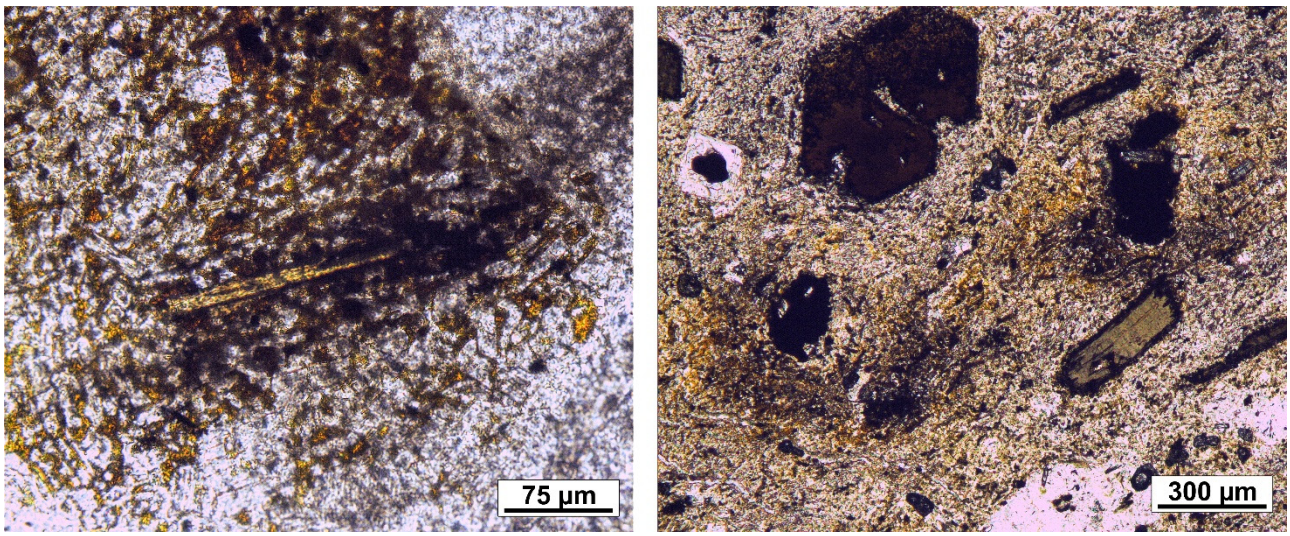

Fig. 11. Thin-section photomicrographs of samples of Euganean trachyte with Fe-rich crusts, showing dispersion of fine-grained Fe oxides/hydroxides or Fe in amorphous state around a biotite crystal **(left)** and two opaque minerals (i.e., magnetites or ilmenites) **(right)**, apparently indicating near-surface mineral leaching.

7. Conclusions

The crusts and patinas of Euganean trachyte related to urban weathering have mostly limited thickness and extension. They are rich in heavy metals and carbonaceous masses, which promote further accumulation of pollutants, mainly deriving from fuel use in road transport and domestic combustion and, secondarily, short- and medium-range industrial emissions. These products are typically embedded in matrixes rich in calcite or Fe (in oxides/hydroxides or amorphous state). The crusts and patinas also include grains of quartz, dolomite, and other minor components, such as metallic and alumosilicon particles, chlorides etc. The high concentration of carbonates cannot be traced back to host rock composition, and leaching of nearby lime mortars joints has been supposed as main source of Ca: this is dissolved, mobilized and then recrystallizes depending on local pH fluctuations. This process may also occur on seasonal basis. A secondary and very limited source of Ca can be represented by dissolution of plagioclases. A more likely intrinsic process of alteration affects biotite and other Fe-bearing minerals, through the pH-dependent leaching of Fe and its migration to surface. Other alteration types detected comprise powdery deposits and gypsum crusts, but they do not occur commonly. The latter possibly derive from the contribution of SO_2 pollutant, having a rather low concentration in the air though; alternatively, the presence of sulfate impurities in mortar aggregate and their leaching can be hypothesized. Anyway, the thickest, most homogeneous and well-developed crusts, rich in either calcite or gypsum, partially shield the host rock from further pollutant absorption.
From this study, it arises that most of the alteration products of Euganean trachyte are due to exogenous processes, whereas the stone itself does not have particular compositional features prone to trigger major dangerous mechanisms of decay. Generally, composition of the weathering crusts and patinas of Euganean trachyte proves to be an informative marker for the relevant environmental conditions and their evolution, with a strict link with air pollution and diverse anthropic pollution sources. Further studies are needed concerning trachyte-mortar interaction, in order to explore to what extent mortar affects stone surface alteration and in which microclimatic conditions, what is the mobilization potential of the leached components, and the influence of different mortar recipes.

Acknowledgements

The author thanks Klaus Simon, Kirsten Techmer and Klaus Wemmer (Uni. Göttingen) for their support during the LA-ICPMS, SEM and XRPD analyses, respectively. The author is very grateful to Hans Ruppert (Uni. Göttingen) for the helpful discussions on the results. Thanks are due to Comune di Padova for kindly authorizing sampling on the city walls and to Comitato Mura di Padova, in particular Fabio Bordignon, for providing information on the building phases and past conservation interventions. Finally, ARPAV agency is thanked for providing the climatic and air quality data, and Dario Camuffo (CNR-ISAC, Padova) and Michela Rogora (CNR-ISE, Verbania) for further information on local environmental parameters.

References

Acker J.G., Bricker O.P. (1992). The influence of pH on biotite dissolution and alteration kinetics at low temperature. *Geochimica et Cosmochimica Acta*, 56, 3073–3092

Alves C.A.S., Sequeira Braga M.A., Trancoso A. (2000). Saline pollution in trachyte monuments of the Azores Islands (Portugal). In: Fassina V., ed., *Proceedings of the 9th International Congress on Deterioration and Conservation of Stone*, Venezia, Italy, 19–24 June 2000, 225–233

Arvidson R.S., Evren Ertan I., Amonette J.E., Luttge A. (2003). Variation in calcite dissolution rates: a fundamental problem? *Geochimica et Cosmochimica Acta*, 67 (9), 1623–1634

ARPAV (2007). *Rapporto ambientale d'area di Porto Marghera – Bilancio ambientale 1998-2007*. ARPAV, Venezia

ARPAV (2009). *Tavolo tecnico cementifici – 1° rapporto tecnico*. ARPAV, Padova

ARPAV (2015a). *Monitoraggio della qualità dell'aria presso il Termovalorizzatore di San Lazzaro – Relazione tecnica*. ARPAV, Padova

ARPAV (2015b). *Inventario regionale delle emissioni in atmosfera INEMAR Veneto 2010 – Relazione generale*. ARPAV, Venezia

Auras M., Beer S., Bundschuh P., Eichhorn J., Mach M., Scheuvens D., Schorling M., von Schumann J., Snethlage R., Weinbruch S. (2013). Traffic-related immissions and their impact on historic buildings: implications from a pilot study at two German cities. *Environmental Earth Sciences*, 69, 1135–1147

Bartoli O., Meli S., Bergomi M.A., Sassi R., Magaraci D., Liu D.Y. (2015). Geochemistry and zircon U-Pb geochronology of magmatic enclaves in trachytes from the Euganean Hills (NE Italy): further constraints on Oligocene magmatism in the eastern Southern Alps. *European Journal of Mineralogy*, 27, 161–174

Blum A.E., Stillings L.L. (1995). Feldspar dissolution kinetics. In: White A.F., Brantley S.L., eds, *Chemical weathering rates of silicate minerals*. Mineralogical Society of America, Washington DC, Reviews in mineralogy, 31, 291–351

Brantley S.L., Olsen A.A. (2014). Reaction kinetics of primary rock-forming minerals under ambient conditions. In: Holland H.D., Turekian K.K., eds, *Treatise on geochemistry*, 2nd ed. Elsevier, Amsterdam, 7, 69–113

Bray A.W., Benning L.G., Bonneville S., Oelkers E.H. (2014). Biotite surface chemistry as a function of aqueous fluid composition. *Geochimica et Cosmochimica Acta*, 128, 58–70

Bray A.W., Oelkers E.H., Bonneville S., Wolff-Boenisch D., Potts N.J., Fones G., Benning L.G. (2015). The effect of pH, grain size, and organic ligands on biotite weathering rates. *Geochimica et Cosmochimica Acta*, 164, 127–145

Brimblecombe P. (2014). Environment and architectural stone. In: Siegesmund S., Snethlage R., eds, *Stone in architecture. Properties, durability*, 5th ed. Springer, Berlin, 317–347

Brimblecombe P., Camuffo D. (2003). Long term damage to the built environment. In: Brimblecombe P., ed., *The effects of air pollution on the built environment*. Imperial College Press, London, Air Pollution Reviews, 2, 1–30

Camuffo D. (1986). Deterioration processes of historical monuments. In: Schneider T., ed., *Acidification and its policy implications*. Elsevier, Amsterdam, 189–221

Camuffo D. (1995). Physical weathering of stones. *The Science of the Total Environment*, 167, 1–14

Camuffo D., Bernardi A., Zanetti M. (1988). Analysis of the real-time measurement of the pH of rainfall at Padova, Italy: seasonal variation and meteorological aspects. *The Science of the Total Environment*, 71, 187–200

Camuffo D., Del Monte M., Ongaro A. (1984). The pH of the atmospheric precipitation in Venice, related to both the dynamics of precipitation events and the weathering of monuments. *The Science of the Total Environment*, 40, 125–139

Charola A.E., Ware R. (2002). Acid deposition and the deterioration of stone: a brief review of a broad topic. In: Siegesmund S., Weiss T., Vollbrecht A., eds, *Natural stone, weathering phenomena, conservation strategies and case studies*. Geological Society, London, Special Publications, 205, 393–406

Deer W.A., Howie R.A., Zussman J. (2013). *An introduction to the rock-forming minerals*, 3rd ed. The Mineralogical Society, London

Dolgaleva I.V., Gorichev I.G., Izotov A.D., Stepanov V.M. (2005). Modeling of the effect of pH on the calcite dissolution kinetics. *Theoretical Foundations of Chemical Engineering*, 39 (6), 614–621

Fadini U., ed. (2013). *Mura di Padova. Guida al sistema bastionato rinascimentale*. In Edibus, Vicenza

Fredd C.N., Fogler H.S. (1998). The kinetics of calcite dissolution in acetic acid solutions. *Chemical Engineering Science*, 53 (22), 3863–3874

Germinario L., Andriani G.F., Laviano R. (2014). Petrography, mineralogy, chemical and technical properties of the building stone of Ostuni Cathedral (Italy): inferences on diagnostics and conservation. *Periodico di Mineralogia*, 83 (3), 379–400. doi: 10.2451/2014PM0021

Gillhuber S., Lehrberger G., Thuro K. (2006). Teplá trachyte weathering phenomena and physical properties of a rare volcanogenic building stone. In: *Proceedings of IAEG 2006 – Engineering geology for tomorrow's cities*, Nottingham, UK, 6–10 September 2006, 469, 1–11

Graue B. (2013). *Stone deterioration and replacement of natural building stones at the Cologne cathedral. A contribution to the preservation of cultural heritage*, PhD dissertation. Geowissenschaftliches Zentrum, Georg-August-Universität Göttingen, Germany

Graue B., Siegesmund S., Oyhantcabal P., Naumann R., Licha T., Simon K. (2013). The effect of air pollution on stone decay: the decay of the Drachenfels trachyte in industrial, urban, and rural environments – a case study of the Cologne, Altenberg and Xanten cathedrals. *Environmental Earth Sciences*, 69, 1095–1124

Grissom C.A. (1990). The deterioration and treatment of volcanic stone: a review of the literature. In: Charola A.E., Koestler R.J., Lombardi G., eds, *Proceedings of the International Meeting "Lavas and Volcanic Tuffs"*, Easter Island, Chile, 25–31 October 1990, 3–29

Grossi C.M., Brimblecombe P. (2007). Effect of long-term changes in air pollution and climate on the decay and blackening of European stone buildings. In: Přikryl R., Smith B.J., eds, *Building stone decay: from diagnosis to conservation*. London: Geological Society, Special Publications, 271, 117–130

Guerreiro C.B.B., Foltescu V., de Leeuw F. (2014). Air quality status and trends in Europe. *Atmospheric Environment*, 98, 376–384

Langella A., Calcaterra D., Cappelletti P., Colella A., D'Albora M.P., Morra V., De Gennaro M. (2009). Lava stones from Neapolitan volcanic districts in the architecture of Campania region, Italy. *Environmental Earth Sciences*, 59, 145–160

Lazzarini L., Antonelli F., Cancelliere S., Conventi A. (2008). The deterioration of Euganean trachyte in Venice. In: Lukaszewicz J.W., Niemcewicz P., eds, *Proceedings of the 11th International Congress on Deterioration and Conservation of Stone*, Torun, Poland, 15–20 September 2008, 153–163

Mazzi G., Verdi A., Dal Piaz V. (2002). *Le mura di Padova. Percorso storico-architettonico*. Il Poligrafo, Padova

Milani L., Beccaluva L., Coltorti M. (1999). Petrogenesis and evolution of the Euganean Magmatic Complex, Veneto Region, North-East Italy. *European Journal of Mineralogy*, 11, 379–399

Prudêncio M.I., Waerenborgh J.C., Gouveia M.A., Trindade M.J., Alves E., Sequeira Braga M.A., Alves C.A., Figueiredo M.O., Silva T. (1998). Degradation processes of trachytes in monument façades, Azores, Portugal. In: Arehart G.B., Hulston J.R., eds, *Water-Rock Interaction*. Balkema, Rotterdam, 391–394

Sabbioni C. (1995). Contribution of atmospheric deposition to the formation of damage layers. *The Science of the Total Environment*, 167, 49–55

Sabbioni C. (2003). Mechanisms of air pollution damage to stone. In: Brimblecombe P., ed., *The effects of air pollution on the built environment*. Imperial College Press, London, Air Pollution Reviews, 2, 63–106

Saiz-Jimenez C. (1993). Deposition of airborne organic pollutants on historic buildings. *Atmospheric Environment*, 27B (1), 77–85

Saiz-Jimenez C. (2003). Organic pollutants in the built environment and their effect on the microorganisms. In: Brimblecombe P., ed., *The effects of air pollution on the built environment*. Imperial College Press, London, Air Pollution Reviews, 2, 183–226

Simão J., Ruiz-Agudo E., Rodriguez-Navarro C. (2006). Effects of particulate matter from gasoline and diesel vehicle exhaust emissions on silicate stones sulfation. *Atmospheric Environment*, 40, 6905–6917

Simon K. (2015). *LA-ICP-MS transient signal quantification of NIST, USGS and MPI-DING glasses by ratioing, standardization, normalization and correction (RSNC)*, Unpublished. Geowissenschaftliches Zentrum, Georg-August-Universität Göttingen, Germany

Snäll S., Liljefors T. (2000). Leachability of major elements from minerals in strong acids. *Journal of Geochemical Exploration*, 71, 1–12

Steiger M., Charola A.E., Sterflinger K. (2014). Weathering and deterioration. In: Siegesmund S., Snethlage R., eds, *Stone in architecture. Properties, durability*, 5th ed. Springer, Berlin, 225–316

St. Seymour K., Sahin Guchan N., Lamera S., Hatziapostolou A., Kouli M., Vamvoukakis C. (2004). Romancing the stone: construction of monuments & works of art from volcanic rock. In: *Proceedings of the 7th Pan-Hellenic Geographical Conference of the Hellenic Geographical Association*, Mytilene, Lesvos, Greece, 14–17 October 2004, E1K164

Török Á, Licha T., Simon K., Siegesmund S. (2011). Urban and rural limestone weathering; the contribution of dust to black crust formation. *Environmental Earth Sciences*, 63, 675–693

Watt J., Hamilton R. (2003). The soiling of buildings by air pollution. In: Brimblecombe P., ed., *The effects of air pollution on the built environment*. Imperial College Press, London, Air Pollution Reviews, 2, 289–334

White A.F., Buss H.L. (2014). Natural weathering rates of silicate minerals. In: Holland H.D., Turekian K.K., eds, *Treatise on geochemistry*, 2nd ed. Elsevier, Amsterdam, 7, 115–155

Chapter 4

Petrophysical and mechanical properties, implications for decay and durability performance

Abstract

Euganean trachyte is a subvolcanic porphyritic rock extracted in northern Italy with an age-old tradition of use as dimension stone, historically linked, in particular, to the fervent building activity brought by the Roman Empire and, later on, Serenissima Repubblica di Venezia. The results of a comprehensive petrophysical and mechanical characterization of Euganean trachyte from the most representative quarries are discussed here, involving the following properties: density, porosity, water absorption, capillary water uptake, hygroscopic water adsorption, hydric/hygric dilatation, water vapor diffusion, thermal expansion, resistance to salt attack and abrasion. The different trachyte varieties, although belonging to the same quarry basin, exhibit a relatively wide array of technical performances, which are strongly dependent on pore volume, size, size distribution, shape, and degree of interconnection, controlling which modes of water transport and retention preferentially take place and at which rate. Therefore, indications are provided for evaluating durability performance of the stone, with a stress on water-driven weathering. Complementary information is finally given on the possible criteria followed in the antiquity for properly selecting the trachyte quarries to be exploited, and by a comparison with the properties of the most important trachytes extracted in Europe.

1. Introduction

Euganean trachyte is a subvolcanic porphyritic rock from the Euganean Hills (NE Italy), which has been exploited since Pre-Protohistory and widely used in cultural heritage, especially from the Roman times onwards, in northern and central Italy. Querns, mortars, cippi, milestones, steles, urns, tombstones, and sarcophagi comprise the most common artifacts crafted with trachyte all through the centuries. It has been historically used also as building stone, as an instance, in the admirable roads and other great infrastructures of the Roman age, or in the monumental architecture and construction from the Middle Ages and Renaissance, including churches, monasteries, public buildings, residences, defensive walls, gates, and squares (Fig. 1); these stoneworks were mainly linked to the fervent building activity brought first by Roman colonization and then by the rise of Serenissima Repubblica di Venezia (Ch. 1 and references therein). In the past decades, due to a drop in extraction activities for environmental safeguard, applications of this material have strongly reduced in number, mostly confined to claddings, pavings, and restorations of historical architecture. Nowadays, the Euganean Hills represent the most significant quarry district in Italy for the extraction of trachyte, which is also frequently exported, e.g., to Germany, Austria, Switzerland, Croatia, Netherlands, and Russia. Trachytic rocks are also exploited in other Italian regions, such as Sardinia, Lazio, Tuscany, and Campania, but

their commercial relevance is unquestionably minor (see e.g., Calvino 1966; Williams-Thorpe & Thorpe 1989; De Gennaro et al. 2000; Frulio et al. 2004; Langella et al. 2009).

While the petrological and geochemical aspects concerning Euganean trachyte have been deeply investigated (Bartoli et al. 2015; Ch. 1; and references therein), data about its performance and technical properties can be retrieved only in few papers. Regarding characterization of quarry materials, those by Calvino (1969) and Zantedeschi & Zanco (1993) are quite outdated and incomplete. More recent, detailed and thorough information has been provided by Graue et al. (2011), dealing with a broad analysis of moisture-related, thermal and strength properties. Additional findings have been reported

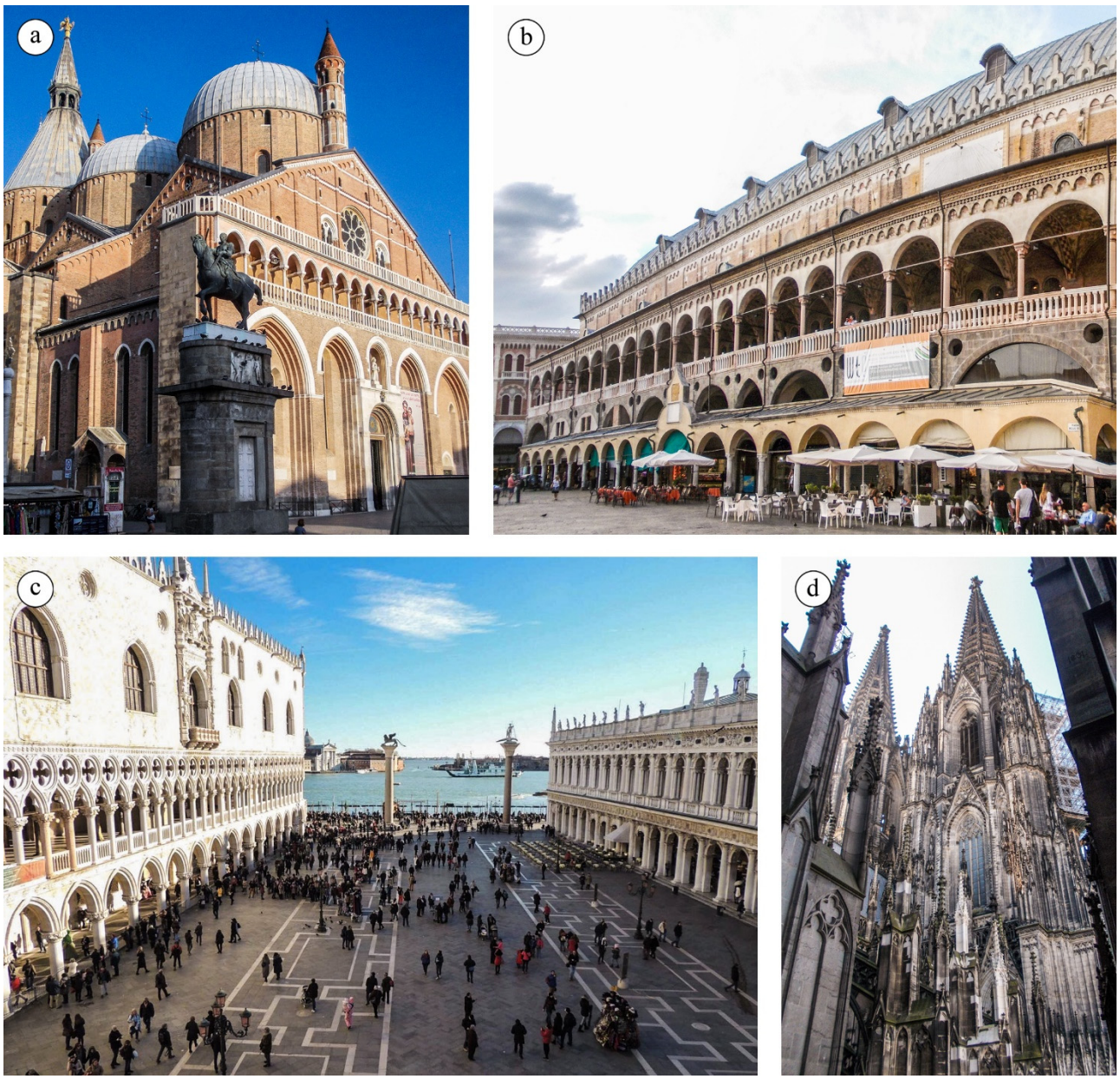

Fig. 1. Some examples of the historical use of Euganean trachyte in the built environment: **a)** Basilica of Sant'Antonio of Padova, 13–14th c., with trachyte pillars and buttresses, and the equestrian statue of Gattamelata by Donatello, 15th c., with trachyte base; **b)** Palazzo della Ragione, Padova, 13–14th c., with trachyte arcade; **c)** Piazza San Marco, Venezia, 12th–19th c., paved with trachyte; **d)** Cologne Cathedral, 13–19th c., with replacing ashlars in Euganean trachyte.

after sample testing of paving stones as well (Tomašić et al. 2000; Valluzzi et al. 2005). According to these studies and data provided by quarrying enterprises, Euganean trachyte can be classified as a strong or very strong material with medium porosity (Anon. 1979). Among its petrophysical properties, bulk density is about 2.4 g/cm^3, water absorption 2–5% of weight, and porosity 10% on average. Concerning mechanical properties, compressive strength is often comprised between 140 and 180 MPa (seldom below 120 MPa), flexural strength is around 10–20 MPa, tensile strength 4–5 MPa and abrasion resistance 3–5 mm of average wear by the Amsler test. One major flaw of the above-mentioned investigations regards the poor representativeness for the Euganean district, as many data refer only to a single trachyte type, namely from the active quarry of M. Merlo; in fact, as illustrated in Ch. 1, minero-petrographic and geochemical properties change among different trachyte varieties from different quarries, hence affecting their physico-mechanical performance. Neither direct nor indirect information has ever been provided about many other active or abandoned quarry localities, the latter being particularly important for historical reasons. Indeed, among the about 100 open pits for the extraction of trachyte detected in the Euganean area – 75 of them giving dimension stones (Calvino 1966) – only 4 are still active (near Montemerlo di Cervarese S. Croce and Zovon di Vo').

Durability and behavior in conditions of environmental stress represent another interesting topic directly related to the previous. So far, it has been addressed only referring to trachyte used mainly for pavings in coastal salt-aggressive environments. Ruling out few brief observations previously published (Calvino 1969; Valluzzi et al. 2005), the subject has been debated only by Lazzarini et al. (2008), who report flaking, powdering, exfoliation, blistering, and frame weathering ("*rahmenverwitterung*"), mainly linked to NaCl crystallization cycles in Venezia; moreover, differential erosion has been observed, due to dissolution of dark mafic inclusions.

This paper illustrates a comprehensive petrophysical and mechanical characterization of trachyte of the Euganean Hills, performed on different trachyte varieties used as dimension stones from the most representative quarry localities, currently or formerly exploited. The study is centered on the analysis of selected properties most affecting stone decay, with a stress on water-driven weathering, hence providing indications for evaluating durability performance. Particular attention is given to how different porosimetric properties affect mechanisms of water storing and, consequently, stone susceptibility to deterioration.

The present work aims at plugging the gap in the literature concerning the survey on the technical properties of Euganean trachyte and debating its long-time name of excellent and durable material with objective quantitative data. Complementary information is finally provided concerning the possible criteria followed in the antiquity for properly selecting the trachyte quarries to exploit, and by a comparison with the properties of the most important trachytes extracted in Europe.

2. Geological setting

The Euganean Hills are a group of hills South-West of the city of Padova (Veneto) in northeastern Italy, covering an area of about 110 km^2 entirely surrounded by the Venetian Plain. Here, a deep-water sedimentary succession of limestones and marls dated to the upper Jurassic–lower Oligocene is followed by a Paleogene volcanic and hypabyssal series, and by Quaternary detrital deposits. The volcanic activity, in particular, has been related to the South Alps orogeny and formation of the so-

called Venetian Tertiary Volcanic Province under extensional regime, and it developed over a 10 Ma time span during two distinct phases. The first one (upper Eocene–lower Oligocene) was associated with submarine basic and ultrabasic lavas with alkaline and subalkaline affinity, encompassing pillow and flow basalts, breccias, hyaloclastites, and tuffs. The second one (lower Oligocene) yielded mostly acid and intermediate subvolcanic rocks, at times combined with effusive and explosive products: rhyolites and trachytes with moderate Na-alkaline affinity are the most recurring rock types, while

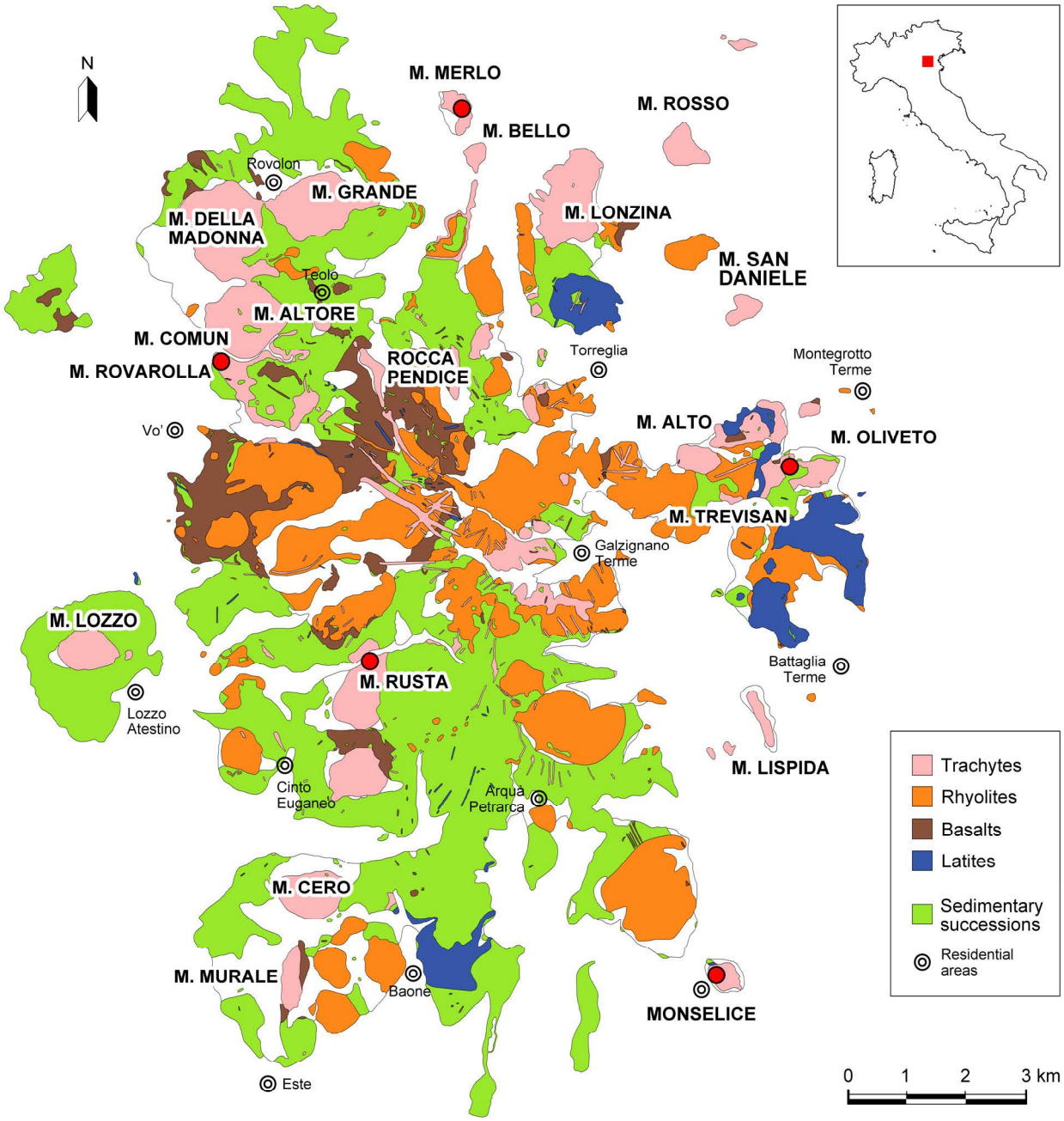

Fig. 2. Geological map of the Euganean Hills, indicating the sampled quarries with red dots. "M." in the proper name of the hills stands for "*Monte*" (mount).

latites and basalts subordinately occur (De Vecchi et al. 1976; De Pieri et al. 1983; Zantedeschi 1994; Cucato et al. 2011; Bartoli et al. 2015) (Fig. 2). This last differentiation was primarily connected to processes of fractional crystallization of mantle-derived basic melts, which took place in multiple shallow magma chambers formed due to block-faulting tectonics (Milani et al. 1999).

3. Methods

A set of trachyte samples collected from different Euganean quarry localities was firstly examined under the polarized light microscope for a preliminary petrographic study. It was then subjected to a petrophysical and mechanical characterization, in order to determine the following properties: density, water absorption, porosity, capillary water uptake, hygroscopic water adsorption, hydric and hygric dilatation, water vapor diffusion, thermal expansion, resistance to salt attack and abrasion. The measurements followed standard test methods with proper minor modifications, and were performed in the facilities of the Geoscience Center of Georg-August-Universität Göttingen, when not indicated otherwise.

Bulk density and matrix density were measured on cubic samples of 6.5 cm by buoyancy weighing, according to EN 1936 (2006), and the results were used to calculate forced water absorption under vacuum. Unforced water absorption at atmospheric pressure was indirectly calculated as well (Siegesmund & Dürrast 2014), using the value of degree of saturation from Graue et al. (2011).

Porosimetric properties were measured by two different methods. Firstly, mercury intrusion porosimetry (MIP) was performed on small fragments of about 1 g according to the standard ASTM D 4404-84 (1998), analyzing effective porosity, total porosity, pore radius, and pore-size distribution; pores with radius comprised between 0.004 and 63 μm were analyzed. Secondly, X-ray and back-scattered electron maps were acquired by micro X-ray fluorescence (μ-XRF) and scanning electron microscope with energy-dispersive spectroscopy (SEM-EDS), respectively, at the Department of Earth Sciences, University of Torino, and at the Department of Geosciences, University of Padova; the maps were then subjected to image analysis, treating no- or low-signal pixels as pores (Fig. 3), and calculating two-dimensional porosity and pore radius (Dal Sasso et al. 2014; Coletti et al. 2016). Map acquisition was performed at different resolutions with the two techniques: large areas of 20 cm^2 were analyzed by μ-XRF, giving information on pores from 73 μm up to millimetric size; instead, small areas of 0.3 to 1.2 mm^2 spotted in the rock groundmass were mapped by SEM-EDS, allowing the characterization and quantification of pores mainly of micrometric size, larger than 0.33 μm. Further details on the experimental conditions and technique of image analysis of μ-XRF and SEM-EDS maps can be retrieved in Ch. 1 and Germinario et al. (2016).

Capillary water uptake was determined by automated continuous weighing of cubic samples of 6.5 cm, along three orthogonal directions, according to EN 1925 (1999), and relative anisotropy in the water absorption coefficient was estimated.

Hygroscopic water adsorption and desorption were calculated on cylindrical samples, cut along different orthogonal orientations, with a length of 6.5 cm and a diameter of 2 cm, according to EN ISO 12571 (2000): the samples were placed in climatic chamber at constant temperature, 23 °C, and underwent a program of relative humidity (RH) increase from 25% to 95% and decrease down to 25% again; mass was measured every 10% step, after sample equilibration at constant RH.

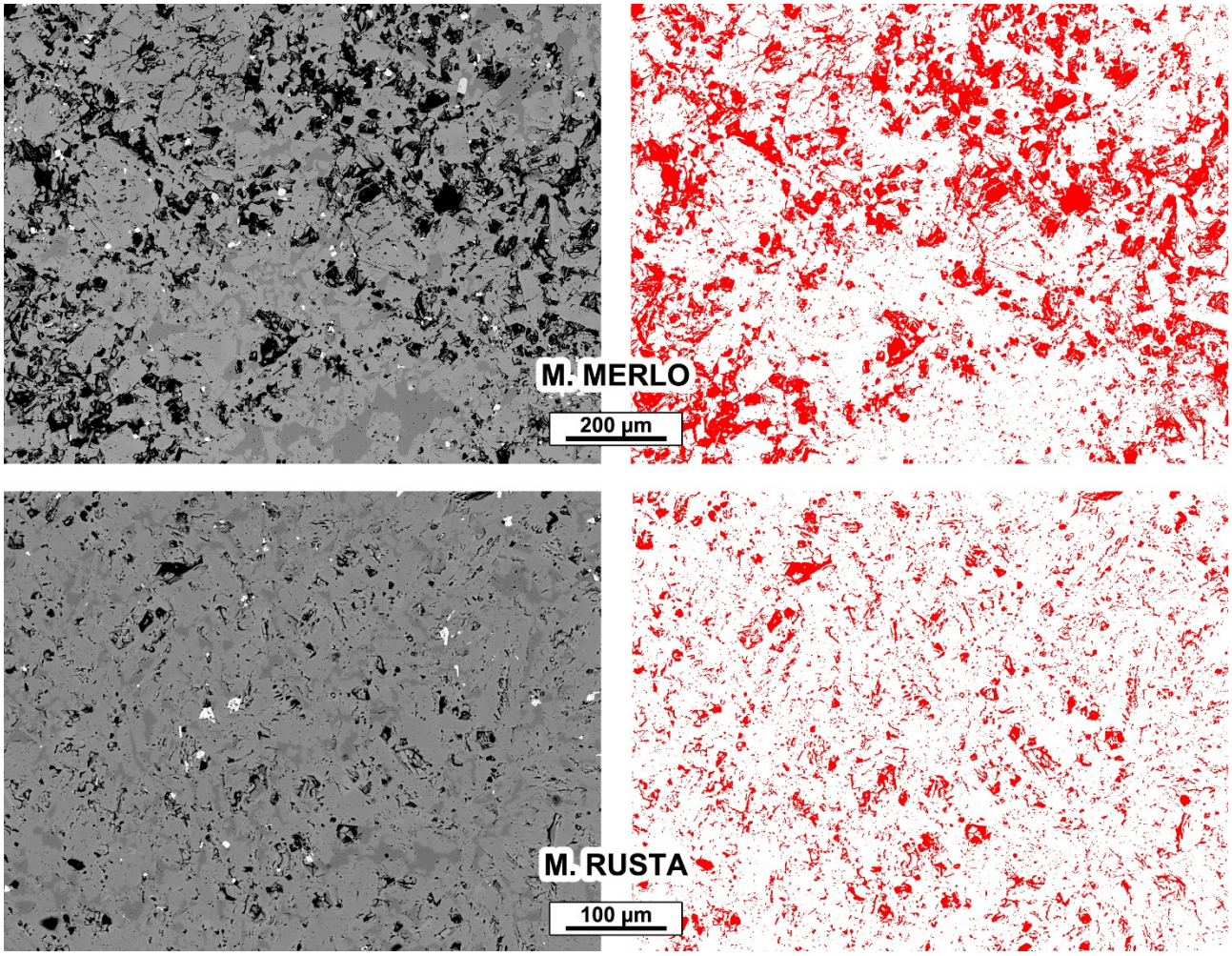

Fig. 3. Examples of back-scattered electron maps acquired by SEM-EDS on the groundmass of Euganean trachyte and relevant binary pore maps (pores in red), which were subjected to image analysis for determining porosimetric parameters. The samples of M. Merlo and M. Rusta trachytes show a porosity of 27.94% and 12.69%, respectively.

The same program of RH variations was applied to the same samples in order to determine hygric dilatation, following the standard EN 13009 (2000), while conditions of complete immersion in water and total sample saturation at atmospheric pressure were achieved to determine hydric dilatation compared to dry state; in both cases, length changes were registered by digital dilatometers, and relative anisotropy in the dilatation coefficients was estimated.

Water vapor diffusion was tested as suggested by EN ISO 12572 (2001) on disk-shaped samples, cut along different orthogonal orientations, with a thickness of 1 cm and a diameter of 4 cm: the samples were placed in climatic chamber at constant temperature, 23°C, and RH, 50%, performing the wet-cup test using distilled water, thus producing a vapor flow through the specimen from inside the holder (100% RH) to outside (50% RH); relative anisotropy in the water vapor resistance factors was finally estimated.

Concerning thermal properties, linear coefficient of thermal expansion was measured on cylindrical samples, cut along different orthogonal orientations, with a length of 5 cm and a diameter of 1.5 cm according to EN 14581 (2004); length changes were registered by digital dilatometers, during three

consecutive cycles of heating to 80 °C and cooling of each sample, both in dry and wet – i.e., partially immersed – conditions, and relative anisotropy in the expansion coefficients was estimated. Finally, thermally induced residual strains – related to the initial sample length – were quantified.
Resistance to salt attack was assessed following some of the indications in EN 12370 (1999). Two 6.5 cm cubic samples for each stone variety underwent a salt crystallization test with cycles planned as follows: 4 h total immersion in a 10% Na_2SO_4 aqueous solution, 16-20 h oven drying at 60 °C, 2 h cooling, and sample weighing.
Finally, abrasion resistance was determined on samples with size 7.1 x 7.1 x 2.5 cm, along different orthogonal directions, as outlined in EN 14157 (2004) and performing the Böhme test, at AMPA, University of Kassel. Abrasion wear on sample surface was also microscopically studied at the SEM.

4. Sampling and petrographic description

Considering the large number of quarries in the Euganean district, a choice of the most representative trachyte varieties to be sampled was necessary. The quarry localities of M. Merlo, Monselice, M. Oliveto, M. Rovarolla, and M. Rusta were selected, with the sampled quarries localized as in Fig. 2. The quarries of M. Merlo (Montemerlo di Cervarese S. Croce) and M. Rovarolla[1] (Zovon di Vo') are active and trachyte extraction is currently ongoing; instead, those of Monselice, M. Oliveto (Montegrotto Terme), and M. Rusta (Fontanafredda di Cinto Euganeo) are inactive and abandoned. The rock cropping out in these sites, according to the TAS (total alkali-silica) classification (Le Maitre 2002), can be chemically defined as trachyte, except for M. Rusta and M. Oliveto, where higher SiO_2 contents, in some cases, may shift the classification to rhyolite (Ch. 1).
The selection was done after a review of the petrographic features and bulk chemical composition of all the varieties of Euganean trachyte, indicated in Ch. 1. The chosen trachytes have different quantitative ratio of feldspars (i.e., anorthoclase, plagioclase, and sanidine), grain size, grain size distribution and groundmass texture (grain size and preferred orientations); their petrographic characteristics – virtually covering the entire petrographic variability of Euganean trachyte – are schematically showed in Fig. 4, together with their macroscopic and microscopic appearance. The sampled trachytes are also characterized by different chemistry, which is representative of different compositionally homogeneous groups of Euganean quarry localities, as pointed out in Ch. 1 by the principal component analysis (PCA) on major- and trace-element concentrations and the TAS diagram. Finally, the size of the quarry and its historical importance (Previato et al. 2014) were also taken into account for the sampling.

[1] Euganean trachyte extracted in the quarry localities of M. Rovarolla, M. Comun, and M. Altore is commercially known as "Zovonite", which is usually distinguished between "grey" and "yellow type", in relation to the presence of brownish-yellowish pervasive fronts of Fe oxidation. This distinction will be also followed in this paper.

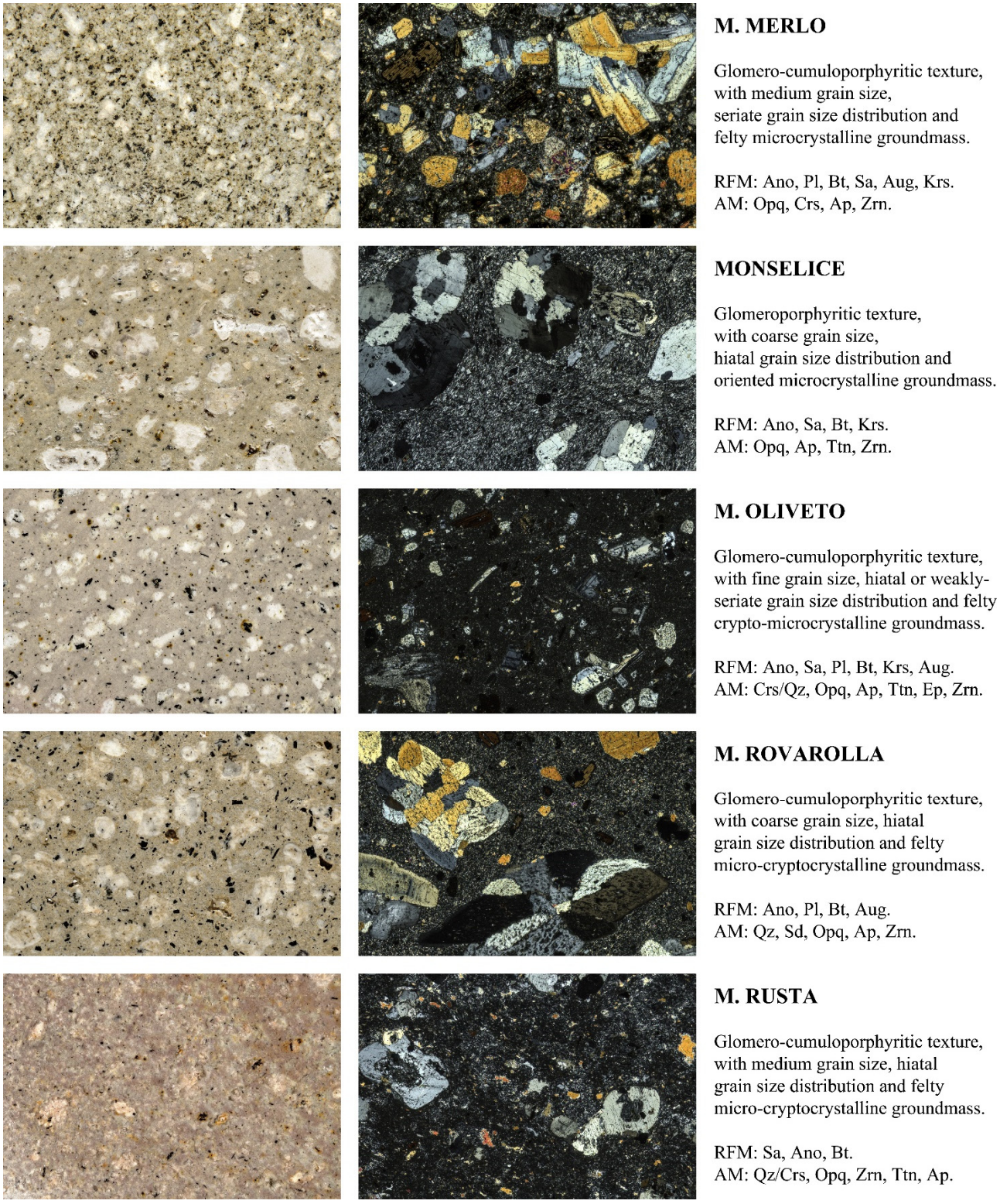

Fig. 4. Hand-specimen photos (5.8 x 3.8 cm) and thin-section photomicrographs in crossed-polarized light (1.4 x 0.9 cm) of the tested varieties of Euganean trachyte; relevant petrographic description is also embedded, using the following abbreviations for rock-forming minerals (RFM) and accessory minerals (AM), listed according to their abundance: Ano = anorthoclase; Ap = apatite; Aug = augite; Bt = biotite; Crs = cristobalite; Ep = epidote; Krs = kaersutite; Opq = opaques; Pl = plagioclase; Qz = quartz; Sa = sanidine; Sd = siderite; Ttn = titanite; Zrn = zircon. Anomalous interference colors are due to higher thickness of the sections (45 μm).

5. Technical properties

5.1. Density and porosity

The data of density and porosimetric properties are listed in Table 1 and Table 2.
Matrix density is affected by mineralogical composition. Considering the main phases in Euganean trachyte, the highest matrix density of M. Rovarolla and M. Merlo trachytes is explained by the larger amount of high-density minerals (Ch. 1), like biotite (~3 g/cm^3), iron oxides (~5 g/cm^3), and even plagioclase, which is slightly denser than the other feldspars.
Bulk density, instead, is also connected to rock porosity, other than mineralogical composition, since it is based on the volume of both voids and solids (Siegesmund & Dürrast 2014). A comprehensive evaluation of porosimetric properties is presented referring to the data of both MIP and image analysis of the µ-XRF maps, for pore radius from 0.004 to 63 µm and higher than 73 µm, respectively; in this way, the investigated pore-size range is extended, involving micropores (< 0.1 µm), capillary pores (0.1 µm–1 mm), and macropores (> 1 mm) (Klopfer 1985). M. Rovarolla trachyte has the highest bulk density and lowest effective porosity by MIP (7.67%), whereas Monselice trachyte is the least dense and most porous (14.04% by MIP, with maximum at 15%); for the latter, the large-pore fraction detected by µ-XRF has a considerable incidence too. The other varieties display intermediate values, although it is worth mentioning the notably higher groundmass porosity of M. Merlo trachyte, with intercrystalline voids up to 200 µm, evaluated by image analysis of the SEM-EDS maps (Fig. 3). Further details are provided by pore-size data and pore-size distributions (Fig. 5), which allow

Table 1. Mean values of density and porosimetric parameters determined by MIP on Euganean trachyte.

Quarry locality	Bulk density	Matrix density	Effective porosity	Total porosity	Mean pore radius	Median pore radius	Micropores	Capillary pores
	g/cm^3	g/cm^3	vol. %	vol. %	µm	µm	%	%
M. Merlo	2.38	2.64	11.16	14.31	0.049	0.310	24.84	75.17
Monselice	2.24	2.63	14.04	19.41	0.062	0.636	21.03	78.97
M. Oliveto	2.36	2.61	9.53	12.98	0.032	0.056	72.40	27.60
M. Rovarolla	2.46	2.66	7.67	10.17	0.039	0.136	41.62	58.38
M. Rusta	2.38	2.60	12.75	16.79	0.046	0.120	45.97	54.03

Classification of pore size according to Klopfer (1985): micropores are smaller than 0.1 µm, capillary pores are comprised between 0.1 and 1000 µm and macropores are larger than 1000 µm.

Table 2. Mean values of two-dimensional porosimetric parameters determined by image analysis of maps acquired by µ-XRF (for pores larger than 73 µm) and SEM-EDS (for pores in the rock groundmass larger than 0.33 µm) on Euganean trachyte.

Quarry locality	2D bulk porosity > 73 µm					2D groundmass porosity > 0.33 µm		
	Total porosity	Capillary pores	Macropores	Mean pore radius	Max. pore radius	Porosity	Mean pore radius	Max. pore radius
	area %	area %	area %	µm	µm	area %	µm	µm
M. Merlo	0.46	0.46	0.00	197.56	764.00	27.94	2.63	198.68
Monselice	3.69	1.43	2.26	430.61	3636.00	15.50	2.71	109.57
M. Oliveto	0.49	0.49	0.00	196.79	908.00	15.50	1.40	43.95
M. Rovarolla	0.66	0.17	0.49	354.22	2546.00	14.73	1.94	60.86
M. Rusta	1.80	1.47	0.33	357.41	2127.50	12.69	1.19	29.46

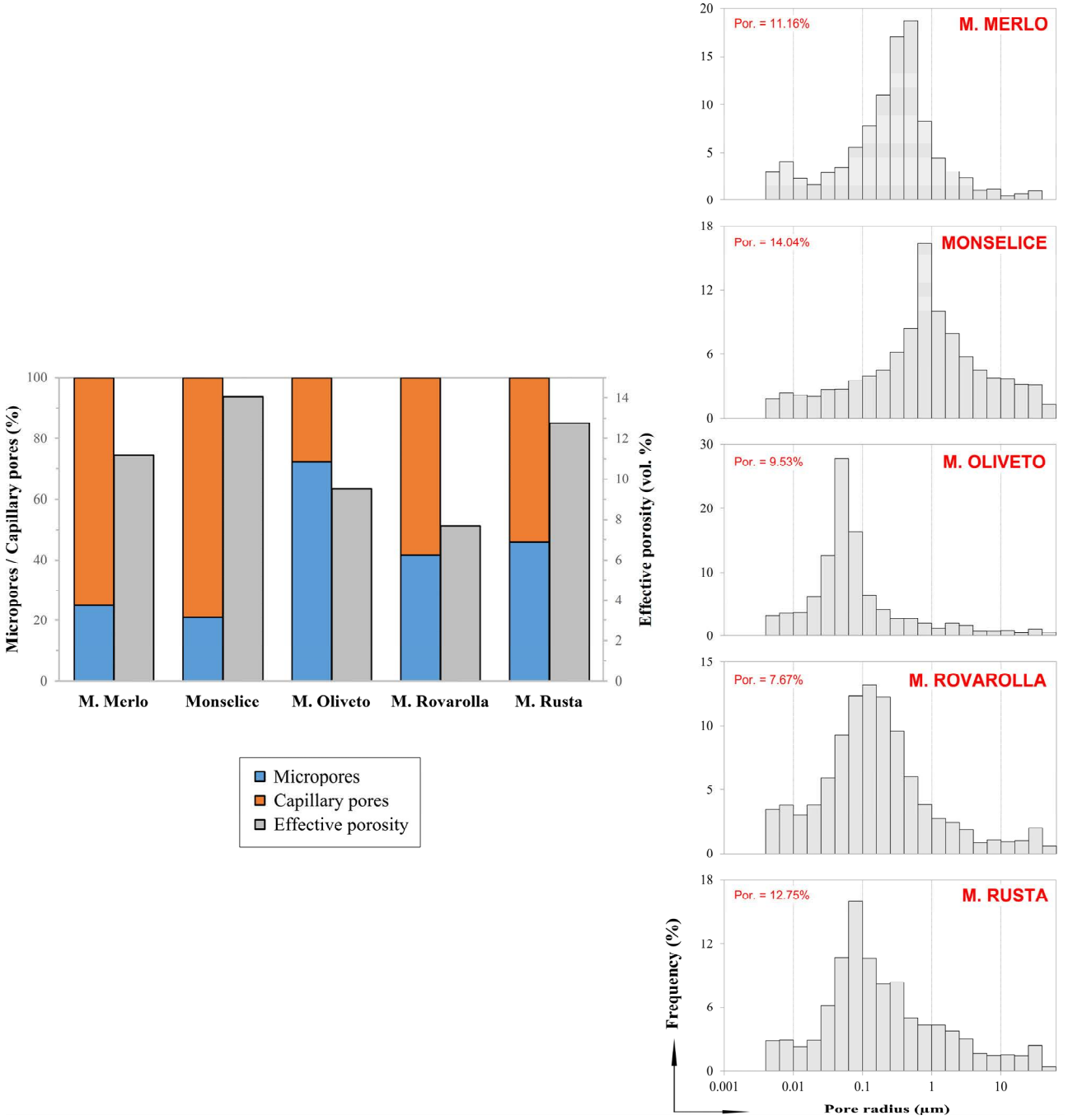

Fig. 5. Effective porosity, percentage of micropores and capillary pores, and representative pore-size distributions obtained by MIP on Euganean trachyte. Classification of pore size according to Klopfer (1985). Actual pore-radius range investigated by MIP between 0.004 and 63 µm.

identifying three main groups. The first includes large-pore trachytes from M. Merlo and Monselice, having a ratio micropores/capillary pores by MIP equal to 1:3 and 1:4, respectively; in Monselice, the largest size classes are particularly abundant, and this is supported by the µ-XRF analyses, which counted over 2% of macropores, with a radius up to 3.6 mm. The second group includes medium-pore trachytes, from M. Rovarolla and M. Rusta, with the two classes of micro- and capillary pores by MIP having approximately the same weight, the latter being slightly more numerous; in M. Rusta,

contrarily to Monselice, more capillary pores were detected over macropores in the large-pore fraction analyzed by μ-XRF. Finally, the third group comprises fine-pore trachyte from M. Oliveto, with a high amount of micropores (72.40%).

6.2. Water-related properties

A summary of the measured physical properties related to water transport and retention inside stone is given in Table 3 and Fig. 6. Only the results of the hygric dilatation tests have not been included, due to insufficient sensitiveness and precision of the adopted method of measurement.
Being water absorption in total immersion proportional to open porosity, the relevant considerations above apply here. However, these are only partially consistent with the behavior of the samples in capillary regime (Fig. 7). In particular, M. Rovarolla trachyte is characterized by the lowest water absorption both in total immersion (~2%) and capillary conditions (0.2 kg/m^2·√h). This correspondence is not applicable, in the most evident case, to Monselice. The fastest capillary water uptake is displayed by M. Rusta and M. Merlo trachytes (1.1 and 0.7 kg/m^2·√h, respectively).
Volume expansions in total immersion are generally quite contained, with a hydric dilatation coefficient mostly ranging from the minimum of 0.01 mm/m of M. Rovarolla trachyte to 0.18 mm/m of M. Rusta trachyte; M. Merlo represents an exception, with values up to 0.4 mm/m. As for dilatation rate, volume changes are the slowest for Monselice and even more for M. Oliveto (Fig. 7).
Referring to stone interaction with hygroscopic water, parallelisms can be found in the behavior of the different trachytes considering water vapor diffusion and hygroscopic adsorption. Water vapor resistance factor is by far the highest for M. Rovarolla, namely 126 with maximum of 144, whereas the range of variation is more limited among the other types, from 50 of M. Rusta to 74 of Monselice. M. Rovarolla and Monselice trachytes also show the lowest hygroscopic adsorption, equal to about 0.6% of weight at 95% RH. Further indications in this regard are provided by the adsorption and desorption curves in Fig. 8. From 75% RH mass increase starts to be faster, and from 85% to 95% RH a critical stage has been identified, described by an anomalously higher hygroscopic adsorption for all the trachyte types: in this range, half of total mass increase has been recorded for Monselice, M. Oliveto and M. Rovarolla trachytes. Differences in adsorption trends are observable for M. Merlo and M. Rusta: the former is involved in a significant hygroscopic adsorption already at low RH; the

Table 3. Mean values of water-related petrophysical properties determined on Euganean trachyte.

Quarry locality	Water absorption under vacuum	Water absorption at atmospheric P	Water absorption coefficient by capillarity	Max. hygroscopic adsorption (at 95% RH)	Hydric dilatation coefficient	Water vapor resistance factor (wet-cup method)
	wt %	wt %	kg/m^2·√h	wt %	mm/m	-
M. Merlo	4.13	2.93	0.710 (12%)	1.10	0.333 (31%)	59.64 (4%)
Monselice	6.75	4.79	0.347 (8%)	0.57	0.038 (16%)	73.75 (18%)
M. Oliveto	4.03	2.86	0.303 (6%)	1.35	0.087 (31%)	69.10 (7%)
M. Rovarolla	2.96	2.10	0.203 (14%)	0.64	0.032 (78%)	125.86 (26%)
M. Rusta	3.60	2.55	1.070 (26%)	1.39	0.184 (1%)	50.23 (7%)

- Anisotropy, expressed as percentage difference between the maximum and minimum value measured along different orthogonal directions of the same sample, is indicated in parentheses.
- Water absorption at atmospheric pressure is indirectly calculated using water absorption under vacuum and a constant value of degree of saturation, equal to 0.71 (Graue et al. 2011).

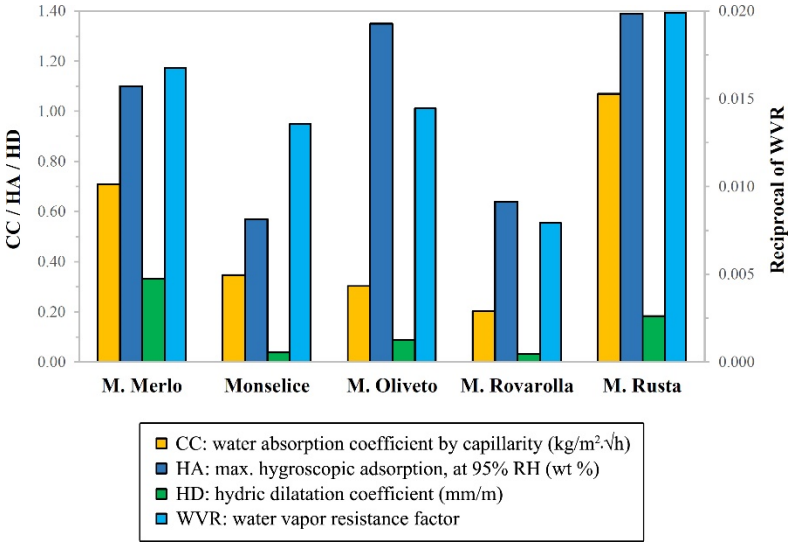

Fig. 6. Comparison of the main water-related properties measured on each variety of Euganean trachyte.

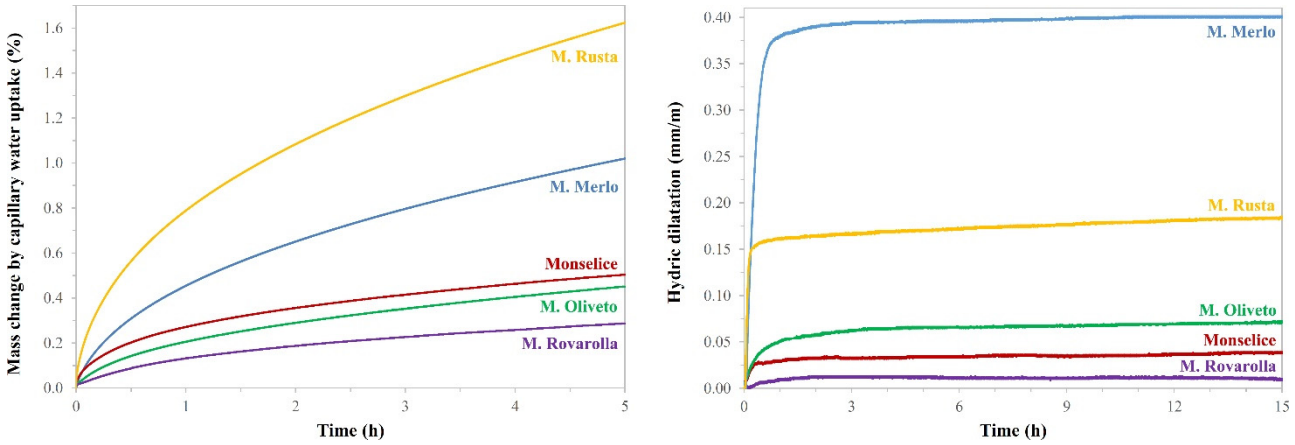

Fig. 7. Representative curves of capillary water uptake and hydric dilatation of Euganean trachyte, expressed as continuous time variations of mass and length (related to the original sample length), respectively.

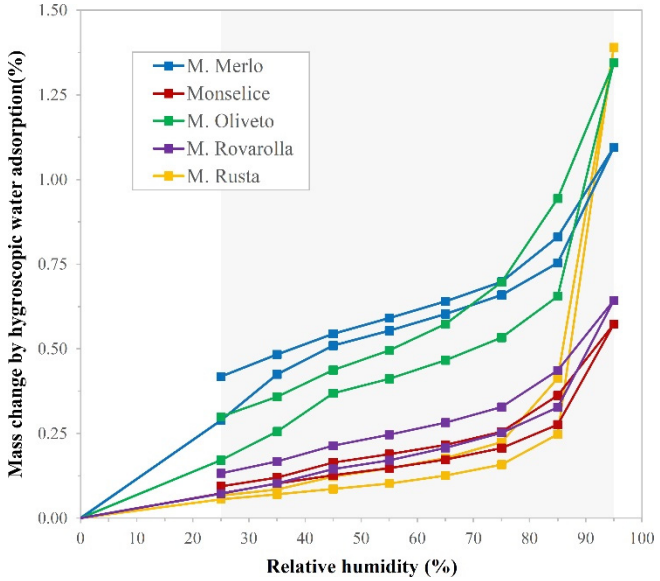

Fig. 8. Representative hygroscopic adsorption and desorption curves of Euganean trachyte, expressed as isothermal mass variations with changing relative humidity in the shaded range.

latter shows the lowest adsorption up to the critical stage 85-95% RH, during which mass increase dramatically becomes the highest among all the samples (82% of total mass increase). Hygroscopic desorption curves follow the relevant adsorption trends but exhibiting a certain degree of hysteresis, thus permanence of residual water stored in pores is noticeable, especially for M. Rovarolla and M. Oliveto.
A final remark concerns the degree of anisotropy displayed by the samples in the directional measurements of the water-related properties. M. Rovarolla trachyte gives the strongest orientation-dependent response, as it appears more frequently characterized by the presence of pervasive fronts of Fe oxidation and dark mafic xenoliths, having a porosity at times markedly different from that of the host rock (Lazzarini et al. 2008). Other texture anisotropies, such as microlite flow orientations in the groundmass of Monselice trachyte, seem not to have any significant influence.

5.3. Thermal expansion

Linear coefficient of thermal expansion is very similar among all the investigated stones, ranging from 5 to 6.5 10^{-6} °C^{-1} approximately (Table 4). No permanent volume changes are measured after the heating-cooling cycles, but with the test running in wet conditions residual strains are always detected, more pronounced for M. Merlo and M. Rusta trachytes (~0.09 mm/m). With the samples partially immersed in water, thermal expansion also turns out to increase, more prominently for Monselice and M. Rusta trachytes, by 20-30%.

5.4. Resistance to salt attack

The results of the salt crystallization test are summarized in Fig. 9. According to the trends of mass change, three groups of trachytes differently prone to decay are recognizable.
Trachytes from Monselice, M. Oliveto, and "grey type" from M. Rovarolla constitute the group opposing the greatest resistance to mechanical stresses induced by cyclic salt crystallization. Their mass decrease is slow and very gradual – except for the very last stage, in the case of M. Oliveto – and, at the end of the test, is either almost negligible or not higher than about 10%. The specimens tend to preserve most of their sharp edges, and localized small detachments occur mainly by scaling, peeling

Table 4. Mean values of thermal properties, in dry and wet (partially immersed) conditions, and abrasion resistance determined on Euganean trachyte.

Quarry locality	Linear coefficient of thermal expansion (dry)	Total residual strain (dry)	Linear coefficient of thermal expansion (wet)	Total residual strain (wet)	Volume loss by abrasion wear
	10^{-6} °C^{-1}	mm/m	10^{-6} °C^{-1}	mm/m	cm^3/50 cm^2
M. Merlo	5.55 (3%)	-	6.14 (10%)	0.094	18.06
Monselice	4.99 (15%)	-	6.05 (18%)	0.029	15.83
M. Oliveto	6.52 (15%)	-	7.00 (19%)	0.009	10.45
M. Rovarolla	6.03 (20%)	-	6.21 (12%)	0.019	10.45
M. Rusta	6.56 (3%)	-	8.49 (4%)	0.089	12.97

Anisotropy, expressed as percentage difference between the maximum and minimum value measured along different orthogonal directions of the same sample, is indicated in parentheses.

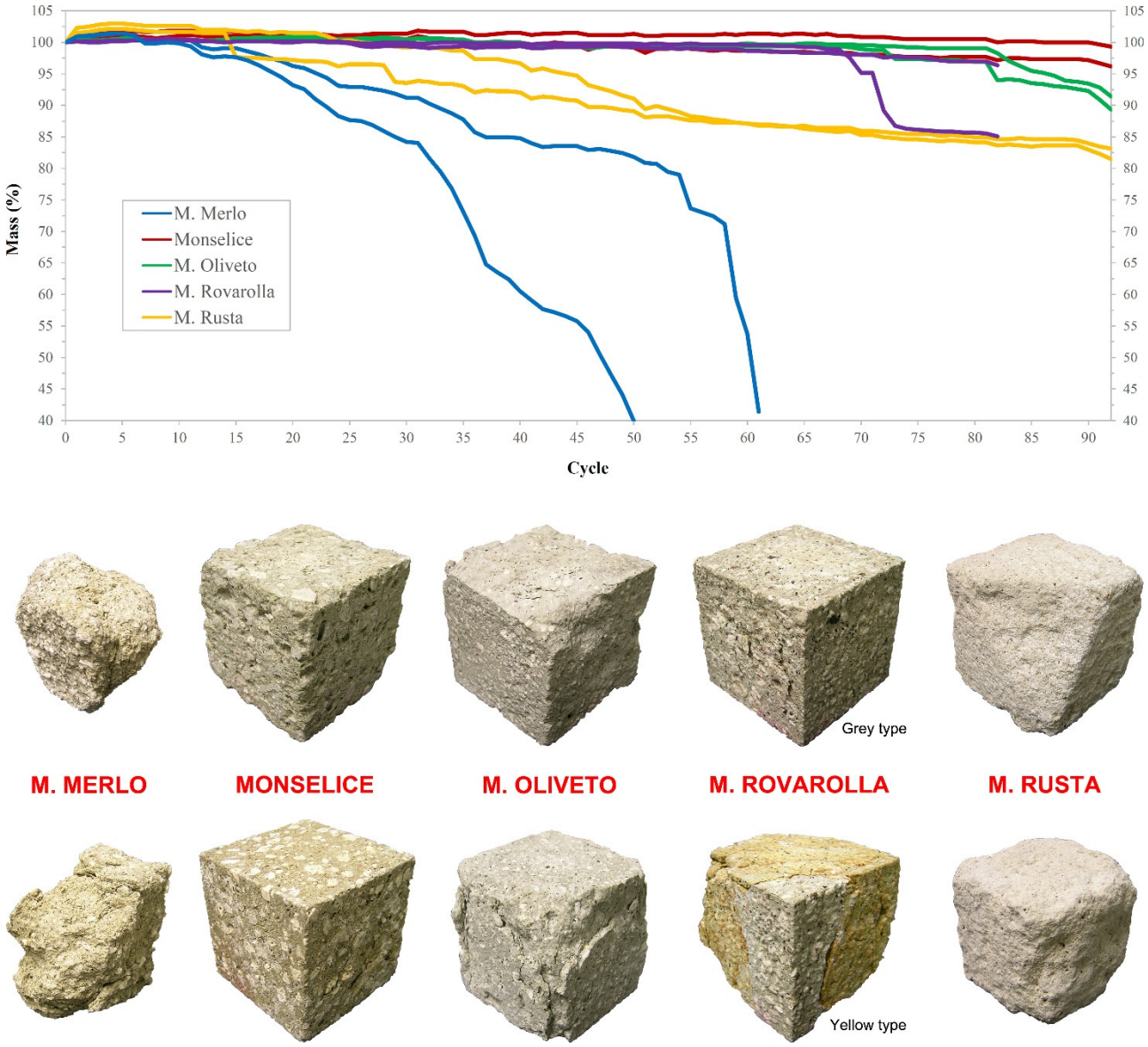

Fig. 9. Mass changes of Euganean trachyte during a salt crystallization test with 10% Na_2SO_4 aqueous solution. Macroscopic appearance of the tested cubic samples after the last cycle (92th for all the samples, except for M. Rovarolla, 82th, and M. Merlo, 50th and 61st) is also showed.

and blistering due to subflorescence development. A typical pattern observed on Monselice trachyte is the enlargement of the numerous natural macropores on the surface, progressively creating large cavities, and differential erosion on coarse feldspar phenocrysts, which are eventually removed. In M. Oliveto trachyte, fragmentation by chipping on the edges also takes place, whereas M. Rovarolla "grey type" trachyte displays a very slight selective erosion of the matrix.

On the other hand, M. Rovarolla "yellow type" trachyte and M. Rusta trachyte show a medium resistance to salt bursting. The main difference between the "grey" and "yellow type" from M. Rovarolla is that, during the test, the latter is affected by intensive fracturing and microcracking in the areas with higher concentration of Fe oxides and hydroxides, often following the weakness planes of Fe-rich fronts, resulting in quick localized deterioration; indeed, before the first point of failure, the trend

of sample mass decrease is totally consistent with that of the "grey type". M. Rusta trachyte, instead, is mainly involved in a pronounced erosion by rounding and powdering, with minor chipping, which leads to loss of the sharp edges, more evident from the 40th cycle; accelerated deterioration on pre-existing discontinuities, e.g., along natural fractures, causes material detachment already during the first cycles of salt attack.
Finally, trachyte from M. Merlo presents a relatively low resistance, exhibiting a mass decrease of about 60% already between the 50th and 60th cycle, approximately. However, many of the original shape characteristics turn out to be lost already from the 30th cycle, and finally deterioration progresses exponentially and very quickly. The typical decay pattern – which starts developing already during the first stage of the test – is differential erosion concentrated on the groundmass, which disintegrates and fractures, leaving feldspar phenocrysts out in relief; these last may detach from the substrate with prolonged stress. Peeling and scaling associated with subflorescences are also observable.

5.5. Abrasion resistance

Volume loss by abrasion wear is the lowest for M. Rovarolla and M. Oliveto trachytes (10.45 cm^3/50 cm^2) and the highest for M. Merlo trachyte (18.06): basically, lower the wear, higher the stone resistance to foot traffic (Table 4).
The microscopic investigation at the SEM of the wear effects on the surface disclosed the differences in decay acting preferentially on the groundmass and/or phenocrysts. As an instance, in M. Merlo trachyte abrasion produces an intense matrix disintegration (Fig. 10a), with resulting formation of numerous micrometric voids (Fig. 10b), which appear quite evenly distributed; phenocrysts seem only occasionally affected by mechanical damage, showing microcracks along weakness planes, e.g., in correspondence of twinning. On the other hand, Monselice trachyte represents an example of deterioration mainly concentrated on phenocrysts: selective disintegration starts especially with strong microcracking along phenocryst edges (Fig. 10c), and finally crystals get totally separated and removed from the surrounding groundmass (Fig. 10d).

6. Performance overview

On the basis of the results here presented, the performance of each trachyte type can be comprehensively debated, in particular its close link with porosimetric properties, as they control which modes of water transport and retention preferentially occur and at which rate. While macropores are involved in liquid water flow, capillary pores are responsible especially for processes of capillary water suction (Klopfer 1985), and micropores mainly for water vapor condensation. This can occur even when RH is lower than 100%, in dependence on pore size and according to the Kelvin equation; adsorption can start at a given RH inside all the pores with a radius equal or smaller than the critical radius determined by the Kelvin formula: generically, the smaller the pore, the lower the RH of condensation (Camuffo 1995; Germinario et al. 2015).
M. Merlo trachyte has a medium effective porosity, given mostly by capillary pores with a radius from 0.1 to 1 μm, so that a high amount of pores prone to capillary suction makes capillary water

uptake fast. This is favored by a well-interconnected pore network, as confirmed by the smallest difference between effective and total porosity by MIP, a fast and very high hydric dilatation – if compared to the other varieties – and the relatively low water vapor resistance factor. Since hydric/hygric dilatations are often attributed to swelling of clay minerals (Benavente et al. 2008), their occurrence might be assumed too (Tomašić et al. 2000; Koch 2006), linked to hydrothermal alteration processes. Conversely, the anomalously high hygroscopic water adsorption of M. Merlo trachyte at low RH seems not to find an exhaustive explanation based on the porosity data presented. In fact, capillary condensation can occur at 35% RH only in pores with a maximum radius of about 0.001 μm, and requires even smaller pores if RH is lower (Steiger et al. 2014). However, the lower limit of the investigated pores by MIP is 0.004 μm. Therefore, M. Merlo trachyte is possibly characterized by a large amount of sub-nanometric pores, not detected, responsible for the significant hygroscopic adsorption at low RH. This initial adsorption mainly involves multimolecular water layers, increasingly adhering to pore walls (Siegesmund & Dürrast 2014). This is also suggested by a small peak in the pore-size distribution in correspondence to the smallest size classes. The facilitated movement and retention of liquid water has also effects on thermal properties and resistance to salt attack. In fact, thermally induced residual strains are higher than for the other varieties, depending on the more pronounced dilatation this stone shows when soaked. Concerning the salt tests, resistance of M. Merlo trachyte is the lowest measured, with weathering especially concentrated in the groundmass due to its notably high and diffuse porosity, and probably also because of a low tensile strength (Graue et al. 2011). The major vulnerability of the groundmass is also confirmed by the pattern of abrasion wear, which is the most intense.

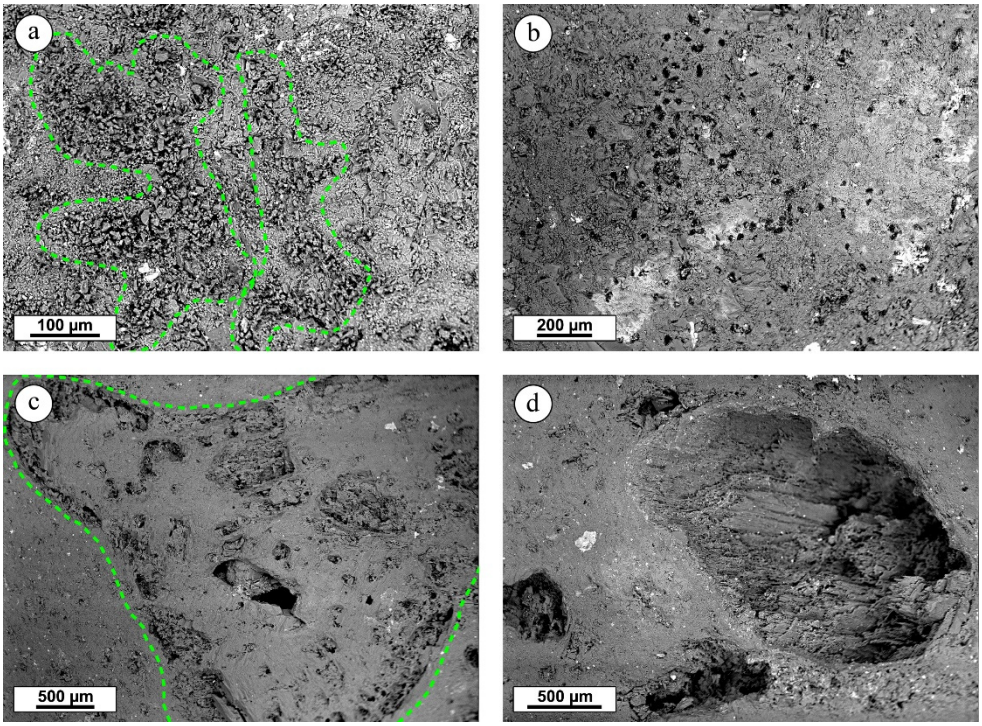

Fig. 10. Back-scattered electron maps acquired by SEM-EDS after the abrasion tests on the surface of samples of Euganean trachyte from: M. Merlo, with wear developing especially on the groundmass, showing **a)** partial crumbling (in the areas highlighted in green) and **b)** resulting formation of networks of voids (in black); Monselice, with wear affecting mostly phenocrysts, subjected to **c)** fracturing along the edges (highlighted in green) and **d)** subsequent detachment.

Monselice trachyte has the highest effective porosity and, similarly to M. Merlo trachyte, this is given mostly by capillary pores; mean pore size is evidently higher though, and a notable amount of macropores has to be taken into account as well. However, it is possible to hypothesize a very poor pore interconnection, since, despite the high porosity, water moves slowly inside this material, in both liquid and vapor state, and produces negligible changes in sample volume and mass: the values of capillary water uptake, hygroscopic adsorption, degree and rate of hydric dilatation, and vapor permeability are among the lowest recorded. Only water absorption in total immersion is not consistent: its relatively high value has to be traced back mainly to water stored in outer macropores, which are quickly filled and quickly drained as well, and virtually are not or barely involved in capillary water absorption or hygroscopic adsorption. The scarce pore interconnection and presence of numerous macropores also explain the typical alveolar-like decay pattern observed after salt attack: salt solution penetrates principally in the outer layers of the stone and first fills macropores, which are more frequently subjected to mechanical stresses when salt crystallizes (crystallization initially occurs in larger pores and only when these are full moves into smaller ones, Aires-Barros 2002); nevertheless, this never compromised greatly the sample integrity. Finally, Monselice trachyte shows one of the lowest values of abrasion resistance: pre-existing microcracks along phenocryst edges are preferentially activated by shear and tensile stresses (Strohmeyer & Siegesmund 2002) and, due to the coarse grain size, the high number of phenocrysts and their poor interlocking, mechanical weakening occurs more frequently and extensively.

M. Oliveto trachyte also denotes an excellent performance globally, but with important distinctions due to the different porosimetric properties. This trachyte has a relatively low effective porosity, the lowest mean pore size and the highest percentage of micropores, concentrated especially around 0.05 μm. Capillary water uptake and vapor permeability are as low as for Monselice, because of the significantly lower porosity and minor presence of capillary pores. Another difference lies in the higher hygroscopic adsorption; in particular, the prominent increase of moisture content between 85% and 95% RH totally matches the theory of capillary condensation, which occurs in the numerous micropores, having an average size small enough to allow condensation in that RH range. Micropores also favor a higher hydric dilatation, possibly due to water disjoining pressure inside small voids (Ruedrich et al. 2011), which is quite slow though. While this last characteristic suggests a poor pore interconnection, the relatively slow moisture desorption may indicate a bottle-neck shape of the pores. These last observations add further elements to explain the high resistance to salt attack, with salt solution penetration and crystallization limited to the outer layer of the samples. The good mechanical strength of this material is also confirmed by the highest abrasion resistance.

M. Rovarolla trachyte exhibited the best performance nearly for all the experimental tests. It has the highest bulk density and lowest effective porosity, characterized by an approximate bipartition between micropores and capillary pores, with a negligible amount of macropores. The values of water absorption, capillary water uptake, hygroscopic adsorption, hydric dilatation, and vapor permeability are practically always the lowest; consequently, the response to salt attack is excellent as well. However, as previously specified, the behavior of this stone has to be carefully revaluated in case pervasive fronts of Fe oxides and hydroxides occur, as they identify more porous and mechanically weaker domains (as also found out by Tomašić et al., 2000).

Finally, M. Rusta trachyte has a relatively high porosity, with a bipartition between the classes of micropores and capillary pores, with the second prevailing. The presence of a quite high number of

pores in both the size classes controlling the mechanisms of capillary suction and capillary condensation justifies the highest values displayed by M. Rusta trachyte of nearly all the water-related properties. Also thermally induced residual strains are relatively high, as described for M. Merlo. It is worth reminding the peculiar behavior in relation to hygroscopic adsorption, which is almost totally concentrated at very high RH. Indeed, most micropores have a radius around 0.05–0.1 μm, and in this

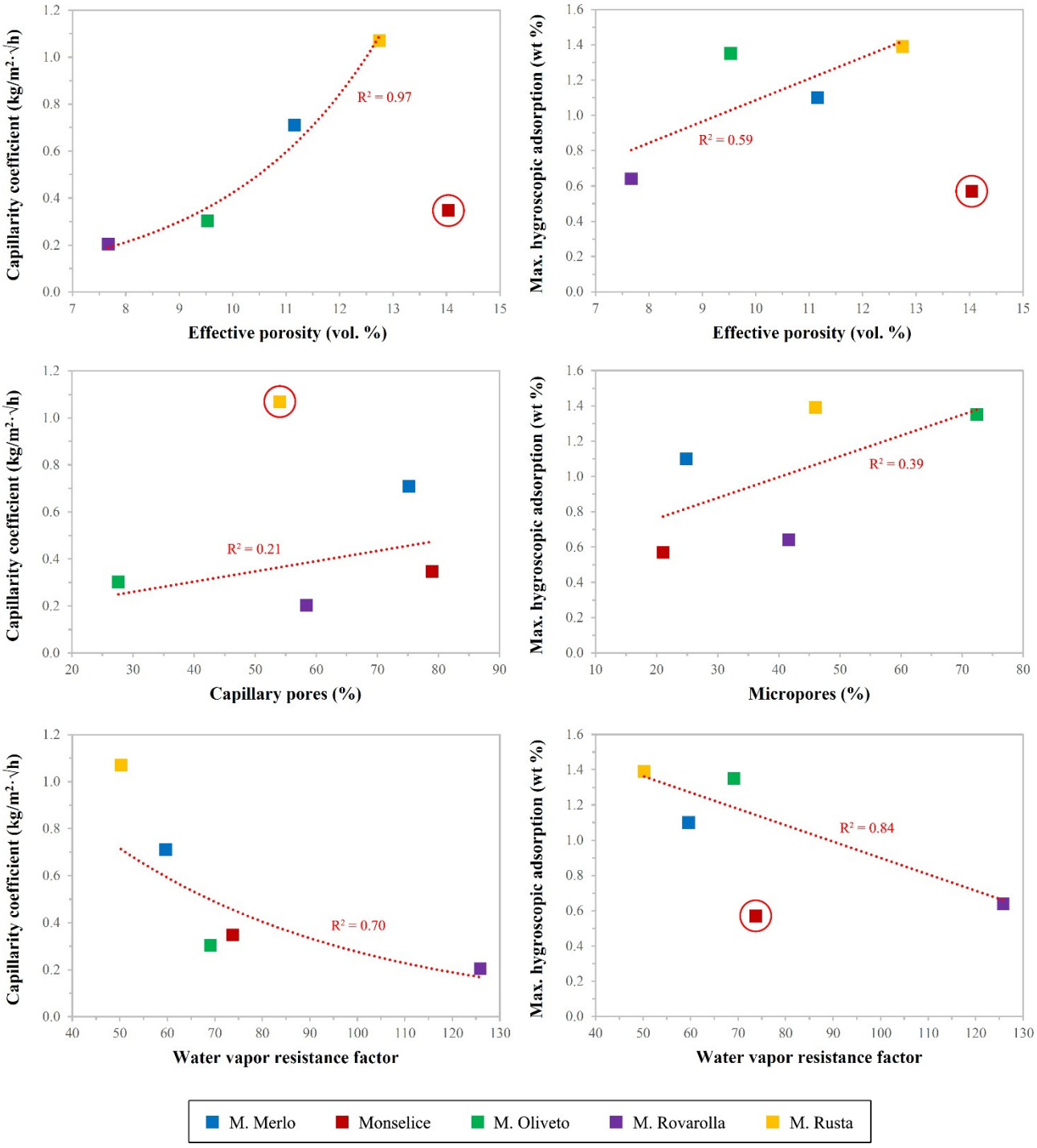

Fig. 11. Correlations among different water-related properties e porosimetric characteristics determined by MIP on Euganean trachyte (outliers not used for trendline interpolation are circled in red).

size class capillary condensation can start only at around 95% RH, when phenomena of water transport by capillary suction from filled micropores may join as well. The combination of these two mechanisms due to the mixed contribution of micropores and capillary pores also facilitates water vapor transmission. Although the performance showed by M. Rusta trachyte appears worse than that of M. Merlo trachyte, its resistance to salt attack is higher, due to a more compact groundmass and a generally finer grain size; in combination with a good pore interconnection, this might facilitate small-scale microcracking, leading to powdering and small detachments rather than removal of large volumes.
Some of the relationships between porosimetric and water-related properties are displayed in Fig. 11. Also on the basis of the previous observations, it results that simple porosity determination is not sufficient to predict accurately the physico-mechanical behavior of Euganean trachyte; considering the illustrative case of Monselice trachyte, a relatively high porosity does not necessarily indicate a bad performance. Other than effective porosity, one must consider also pore size, size distribution, shape and degree of interconnection, the possible contribution of pores out of the size range actually investigated, and the presence of particular microstructures and discontinuities – in phenocrysts, groundmass or bulk rock – creating microdomains with different mechanical properties.

7. Durability prediction and quality assessment

7.1. Susceptibility to decay

A durable stone should have low porosity, prevent processes of absorption/adsorption of liquid and vapor water and aqueous solutions, and preserve as much as possible its volume characteristics in case of hydric or thermal stresses.
Taking into consideration that and the evidences of this research, Euganean trachyte shows a better performance on average than tuffs, sandstones, and many limestones commercially available and used as dimension stones, but worse than most intrusive and metamorphic rocks, as well as some compact volcanites and carbonate rocks. Nevertheless, abrasion resistance – one of the most renowned characteristics of Euganean trachyte – is higher than that of many marbles, sandstones, limestones, tuffs, and shales and, in some cases, also comparable to a number of granites and other hard plutonic rocks (see Siegesmund & Dürrast 2014).
Among the tested trachyte varieties, those from M. Rovarolla, Monselice, and M. Oliveto surely represent the best quality materials, as it can be noticed when the petrophysical and mechanical data are considered together in a PCA (Fig. 12); this is also consistent with their high durability in salt-aggressive environment, indicated by the salt tests. Nevertheless, caution should be used for Monselice trachyte in conditions of possibly high abrasion wear, or for M. Oliveto trachyte when high RH, and consequently a strong increase in moisture content, comes into play. On the other hand, the results obtained on M. Merlo and M. Rusta trachytes indicate a lower durability. Considering water-driven weathering, partial or all-around direct contact with water may lead to stone damage to a greater extent, and more quickly.
Vulnerability to rising damp does subsist in many applications of Euganean trachyte, such as pavings, foundations, and static elements at ground level, but phenomena of capillary suction may also occur

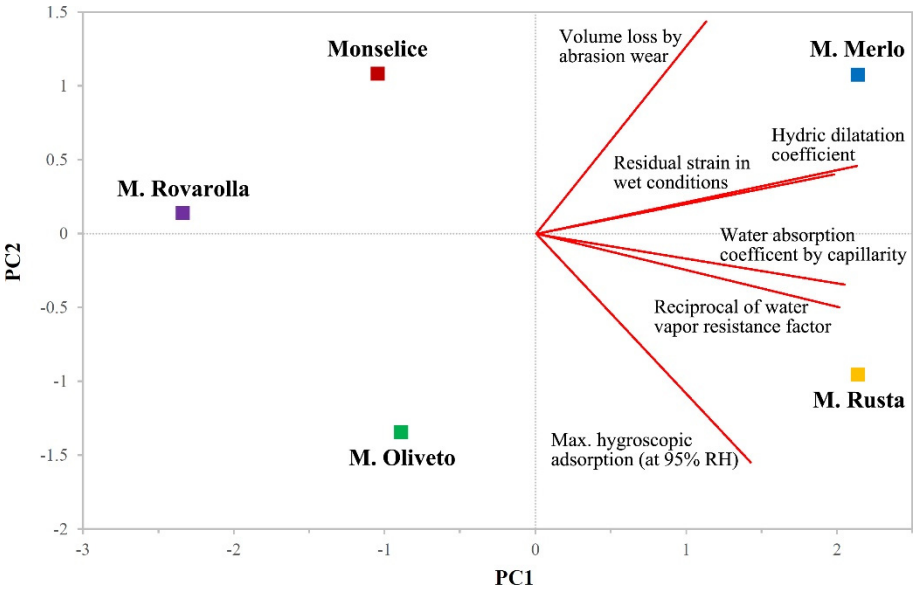

Fig. 12. Score and loading plot from PCA performed on some petrophysical and mechanical properties determined on Euganean trachyte, with PC1 and PC2 covering 69% and 21% of total variance, respectively.

Fig. 13. Piazza San Marco in Venezia, with trachyte paving partially flooded due to high tide ("*acqua alta*").

in many other contexts, for example simply when stone is wet by rainfall. Conditions of total immersion, instead, are met more rarely – a characteristic situation is "*acqua alta*" in Venezia when, due to exceptional high tides, many trachyte-paved squares and streets are completely flooded (Fig. 13) – but can frequently be resembled to heavy rainfall. Additionally, hygroscopic condensation must not be neglected. Among the numerous well-known water-driven processes, the most significant danger is the penetration of aqueous solutions containing and mobilizing soluble salts, from the ground, water or air. These salts, other than reacting with rock substrate, undergo cyclic crystallization/dissolution inside pores during stone drying/wetting phases (Arnold & Zehnder 1990), exerting a pressure on pore walls and, thus, rock solid matrix. When this mechanical stress exceeds rock tensile strength, because of further continuous salt loading, actual decay starts, progressively leading to diverse deterioration patterns (Vergès-Belmin 2010).

Those observed by Lazzarini et al. (2008) on trachyte-paved areas and exposed building foundations in Venezia, e.g., blistering, flaking, and powdering, were proven to be caused by crystallization of salts, most likely deriving from mechanisms of absorption of bulk and capillary sea water. The different decay types may be produced depending on trachyte pore distribution (more porous domains allow the salts to accumulate and raise more compact outer stone layers), grain size (fine grain size favors powdering) and presence of discontinuities.

7.2 Selection of trachyte in the antiquity

The historical, large exploitation and use of Euganean trachyte has opened the debate on the criteria followed by clients, quarrymen, and stonecutters for properly choosing quarries in the antiquity, especially during the Roman age, which can now be discussed based on the findings of this paper.
Considering the archaeological records for which provenance was constrained in the literature (Previato et al. 2014), trachytes from Monselice, M. Oliveto, and M. Merlo seem to be the most exploited historically. It arises that a targeted selection among different trachyte varieties was possibly carried out based on their final application and a knowledge of their different properties. It has been suggested, as an instance, that Monselice trachyte was preferentially used by the Romans for paving urban and extra-urban roads, because of its higher abrasion resistance linked to lower porosity, or that M. Merlo trachyte, other than being used for flagstones, was expressly chosen for harbor structures, because of its resistance to salt attack (see e.g., Capedri & Venturelli 2003; Previato et al. 2014). The results of the present research attest that these hypotheses are not correct.
In the antiquity, an empirical knowledge of the overall excellent durability of Euganean trachyte as dimension stone cannot be questioned, as its long-range, expensive trades demonstrate (Ch. 1). Nevertheless, the choice of the single quarries to exploit is probably to be traced back to mostly practical and commercial factors: accessibility and closeness to cities and main transport routes by land, river and sea, size of the outcrop and ease of exploitation, and presence of already open extraction faces, without forgetting private or public concessions for quarrying, also linked to political reasons. Obviously, quarries giving visibly bad materials were likely abandoned soon.

7.3. Comparison with other European trachytes

The quality assessment of Euganean trachyte as dimension stone can be concluded comparing the performance of other trachytes, inferred from data in the literature and databases, which are or have been exploited in Europe, i.e., in Germany (Drachenfels, Selters, and Reimerath), Czech Republic (Teplá), France (Massif Central, Chaîne des Puys), and off mainland, in Portugal (Azores: São Miguel and Terceira islands) and Spain (Canary Islands: Fuerteventura, Gran Canaria, La Gomera and Tenerife islands) (Zezza et al. 1995; Sequeira Braga et al. 2000; Hugues et al. 2005; Gillhuber et al. 2006; Silva et al. 2010; Graue et al. 2011; Graue 2013; Hernández Gutiérrez et al. 2014; Siegesmund & Dürrast 2014; Boivin et al. 2015; http://www.natursteinonline.de) (Fig. 14). For Euganean trachyte, the data of this paper were used, except for mechanical strength (see Introduction).
A comparison among bulk density, porosity, and compressive strength is proposed in Fig. 15. Euganean trachyte stands out for its noticeably higher mechanical strength, in view of a density more or less comparable with that of the other stones and, in some cases, a porosity even higher. As for other

properties, on which less data are available, water absorption is also quite similar among the different materials, ranging from 2 to 5% of weight on average, appearing higher for the trachytes with many capillary pores measured by MIP, such as those from Czech Republic and the Azores. On the other hand, hydric dilatation is always remarkably lower for Euganean trachyte: range of variation of the

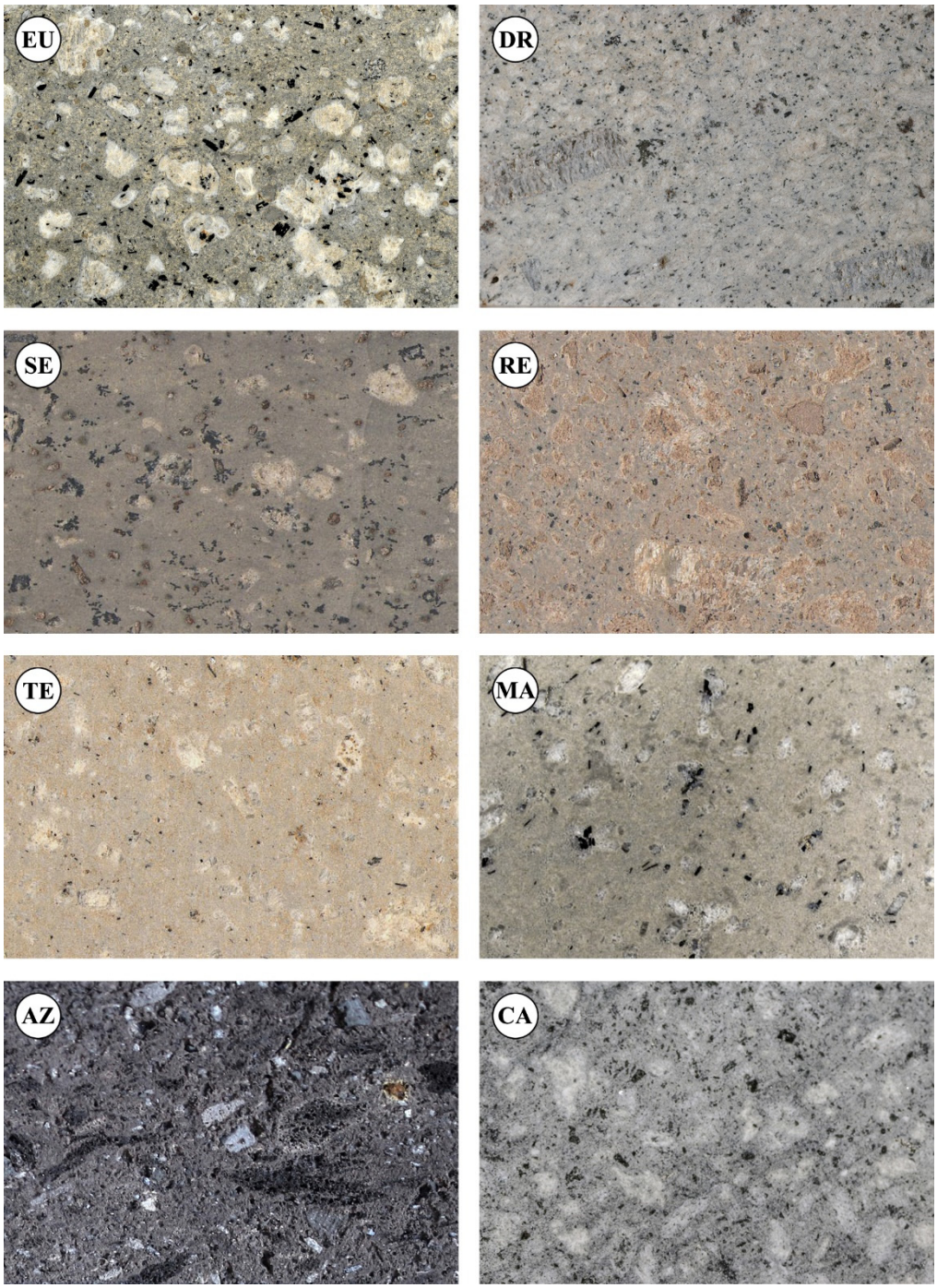

Fig. 14. Hand-specimen photos (5.0 x 3.4 cm) of Euganean trachyte (EU) and other trachytes exploited in Europe and used as dimension stones, known with the following denominations or provenances: Drachenfels (DR), Selters (SE), and Reimerath (RE), Germany; Teplá (TE), Czech Republic; Massif Central (MA), France; Azores (AZ), Portugal; Canary Islands (CA), Spain.

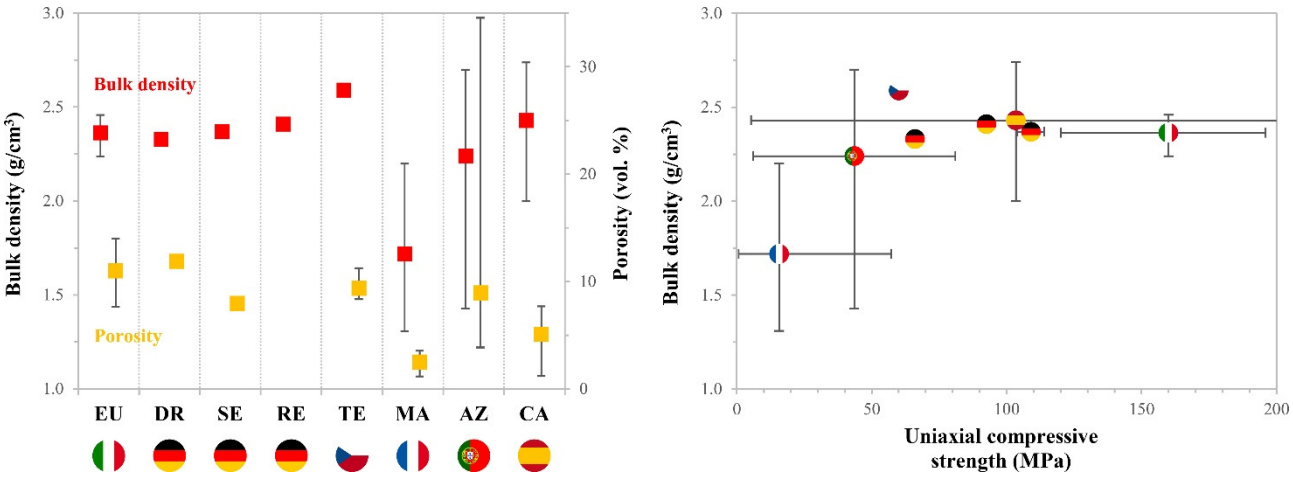

Fig. 15. Comparison of technical properties between Euganean trachyte (EU) and other trachytes exploited in Europe and used as dimension stones, known with the following denominations or provenances: Drachenfels (DR), Selters (SE), and Reimerath (RE), Germany; Teplá (TE), Czech Republic; Massif Central (MA), France; Azores (AZ), Portugal; Canary Islands (CA), Spain. The indicators mark mean values, while the bars show ranges of variation of the data considered, when available (refer to the text for references).

literature data is 0.236–0.253 mm/m for Drachenfels trachyte, 0.600–1.100 mm/m for Selters trachyte and 1.000–2.260 mm/m for trachyte from the Azores. The results of other petrophysical tests are not available except for Drachenfels trachyte, which generically shows a significantly worse performance than that of Euganean trachyte, referring to capillary water uptake, hygroscopic adsorption, and water vapor diffusion, as well as resistance to salt attack. Globally, based on the relatively small number of the literature data available (unfortunately, in several cases involving a fairly low number of properties, different experimental methods, and low statistics), trachyte of the Euganean Hills can be defined one of, or the best quality trachyte among those mentioned.

8. Conclusions

The different varieties of Euganean trachyte analyzed here exhibit a relatively wide array of technical performances, which are almost completely dependent on the diverse porosimetric characteristics. This applies, in particular, to the water-related properties, indicating which modes of water transport and retention preferentially take place and at which rate. Consequently, clues are given about the decay processes that would develop in presence of water or aqueous solutions, in particular cyclic crystallization/dissolution of soluble salts from ground water, rainfall or hygroscopic condensation during drying/wetting phases.

High porosity is not necessarily an indicator of bad durability performance for this stone, since the interaction with bulk, capillary or hygroscopic water can be regardless limited by a poorly interconnected pore network. On the other hand, pore size controls the favored interaction with water in either liquid or vapor state. A deep investigation of pore size, size distribution, shape and degree of interconnection, other than pore volume, is essential for correctly predicting the behavior in response to

weathering of such stones, extracted in the same quarry basin, having the same age and thus a similar mineralogical and chemical composition.
The findings might be extrapolated in order to predict the durability even of other varieties of Euganean trachyte not treated here and extracted in other quarry localities, based on strict petrographic and geochemical analogies. Nevertheless, any necessity of surveying for other trachyte types in the Euganean district does not subsist presently. In fact, the exploitation in few selected quarries, as currently happens at M. Merlo and M. Rovarolla, is sufficient to provide high quality materials, with due distinction, especially for the needs of architectural conservation and restoration.
In this regard, elements are provided for aiding quality assessment by conservators-restorers and building companies, and identifying the best performing materials, also proposing a comparison with other trachytes currently or historically extracted in Europe. Finally, possible criteria followed in the antiquity for selecting the trachyte varieties to be employed as carving and building stone are debated.

Acknowledgements

The author thanks Peter Machner and Martin Schmidt (Uni. Kassel) for the help during the abrasion tests. Thanks are also due to Luís Sousa (Uni. Trás-os-Montes e Alto Douro), Christian Knell and, in particular, Wanja Wedekind (Uni. Göttingen) for their support during the petrophysical tests. Finally, the author is grateful to Michelangelo Dalla Francesca (Cave Pietra Montemerlo s.r.l.) and Fabio Licenza (Trachite Euganea s.r.l.) for providing trachyte samples from M. Merlo and M. Rovarolla quarries, and to the following people for kindly sending the photographic material of the trachytes extracted in Europe: Pierre Boivin (Uni. Blaise Pascal), Cristina Carvalho (LNEG, S. Mamede de Infesta), Birte Graue (LWL, Münster), Luis Enrique Hernández Gutiérrez (Gobierno de Canarias, Santa Cruz de Tenerife), Reinhard Kögler (Deutsches Naturstein Archiv, Wunsiedel) and Maria Isabel Prudêncio (Uni. Lisboa).

References

Aires-Barros L. (2002). Modes and mechanisms of rock weathering. In: Galán E., Zezza F., eds, *Protection and conservation of the cultural heritage of the Mediterranean cities*. Swets & Zeitlinger, Lisse, 3–9

Anon. (1979). Classification of rocks and soils for engineering geological mapping. Part I: Rock and soil materials. *Bulletin of the International Association of Engineering Geology*, 19, 364–371

Arnold A., Zehnder K. (1990). Salt weathering on monuments. In: Zezza F., ed., *Atti del I Simposio Internazionale "La conservazione dei monumenti nel bacino del Mediterraneo"*, Bari, Italy, 7–10 June 1989, 31–58

ASTM D 4404-84 (1998). Standard test method for determination of pore volume and pore volume distribution of soil and rock by mercury intrusion porosimetry. In: *Annual book of ASTM Standards*, 04.08. ASTM, West Conshohocken, PA

Bartoli O., Meli S., Bergomi M.A., Sassi R., Magaraci D., Liu D.Y. (2015). Geochemistry and zircon U-Pb geochronology of magmatic enclaves in trachytes from the Euganean Hills (NE Italy): further constraints on Oligocene magmatism in the eastern Southern Alps. *European Journal of Mineralogy*, 27, 161–174

Benavente D., Cultrone G., Gómez-Heras M. (2008). The combined influence of mineralogical, hygric and thermal proper-ties on the durability of porous building stones. *European Journal of Mineralogy*, 20, 673–685

Boivin P., Miallier D., Cluzel N., Devidal J.L., Dousteyssier B. (2015). Building and ornamental use of trachyte in the center of France during antiquity: sources and criteria of identification. *Journal of Archaeological Science: Reports*, 3, 247–256

Calvino F. (1966). *Le cave dei Colli Euganei*. Consorzio per la valorizzazione dei Colli Euganei, Padova

Calvino F. (1969). Studi sulle proprietà tecniche della trachite da taglio di Montemerlo (Colli Euganei). *Memorie degli Istituti di Geologia e Mineralogia dell'Università di Padova*, 27, 3–39

Camuffo D. (1995). Physical weathering of stones. *The Science of the Total Environment*, 167, 1–14

Capedri S., Venturelli G. (2003). Trachytes employed for funerary artefacts in the Roman Colonies Regium Lepidi (Reggio Emilia) and Mutina (Modena) (Italy): provenance inferred by petrographic and chemical parameters and by magnetic susceptibility. *Journal of Cultural Heritage*, 4, 319–328

Coletti C., Mazzoli C., Maritan L., Cultrone G. (2016). Combined multi-analytical approach for study of pore system in bricks: how much porosity is there? *Materials Characterization*, 121, 82–92

Cucato M., De Vecchi G., Sedea R. (2011). Inquadramento geologico. In: Cucato M. et al., eds, *Note illustrative della Carta Geologica d'Italia alla scala 1:50.000, Foglio 147, Padova sud*. ISPRA, Padova, 27–31

Dal Sasso G., Maritan L., Salvatori S., Mazzoli C., Artioli G. (2014). Discriminating pottery production by image analysis: a case study of Mesolithic and Neolithic pottery from Al Khiday (Khartoum, Sudan). *Journal of Archaeological Science*, 46, 125–143

De Gennaro M., Calcaterra D., Cappelletti P., Langella A., Morra V. (2000). Building stone and related weathering in the architecture of the ancient city of Naples. *Journal of Cultural Heritage*, 1, 399–414

De Pieri R., Gregnanin A., Sedea R. (1983). Guida alla escursione sui Colli Euganei. *Memorie della Società Geologica Italiana*, 26, 371–381

De Vecchi G., Gregnanin A., Piccirillo E.M. (1976). Tertiary volcanism in the Veneto: magmatology, petrogenesis and geodynamic implications. *Geologische Rundschau*, 65 (1), 701–710

EN 12370 (1999). *Natural stone test methods – Determination of resistance to salt crystallisation*. CEN, Brussels

EN 13009 (2000). *Hygrothermal performance of building materials and products – Determination of hygric expansion coefficient*. CEN, Brussels

EN 14157 (2004). *Natural stone test methods – Determination of the abrasion resistance*. CEN, Brussels

EN 14581 (2004). *Natural stone test methods – Determination of linear thermal expansion coefficient*. CEN, Brussels

EN 1925 (1999). *Natural stone test methods – Determination of water absorption coefficient by capillarity*. CEN, Brussels

EN 1936 (2006). *Natural stone test methods – Determination of real density and apparent density, and of total and open porosity*. CEN, Brussels

EN ISO 12571 (2000). *Hygrothermal performance of building materials and products – Determination of hygroscopic sorption properties*. CEN, Brussels

EN ISO 12572 (2001). *Hygrothermal performance of building materials and products – Determination of water vapour transmission properties*. CEN, Brussels

Frulio G., Langiu M.R., Mameli P. (2004). L'impiego della trachite nelle architetture tra gli anni Venti e Cinquanta in Sardegna: tecniche costruttive e materiali tradizionali tra nuove tecnologie e modernità. In: Biscontin G., Driussi G., eds, *Architettura e materiali del Novecento: conservazione, restauro, manutenzione. Atti del convegno di studi*, Bressanone, Italy, 13–16 July 2004, 465–476

Germinario L., Andriani G.F., Laviano R. (2015). Decay of calcareous building stone under the combined action of thermoclastism and cryoclastism: a laboratory simulation. *Construction and Building Materials*, 75, 385–394. doi: 10.1016/j.conbuildmat.2014.11.035

Germinario L., Cossio R., Maritan L., Borghi A., Mazzoli C. (2016). Textural and mineralogical analysis of volcanic rocks by μ-XRF mapping. *Microscopy and Microanalysis*, 22, 690–697. doi: 10.1017/S1431927616000714

Gillhuber S., Lehrberger G., Thuro K. (2006). Teplá trachyte weathering phenomena and physical properties of a rare volcanogenic building stone. In: *Proceedings of IAEG 2006 – Engineering geology for tomorrow's cities*, Nottingham, UK, 6–10 September 2006, 469, 1–11

Graue B. (2013). *Stone deterioration and replacement of natural building stones at the Cologne cathedral. A contribution to the preservation of cultural heritage*, PhD dissertation. Geowissenschaftliches Zentrum, Georg-August-Universität Göttingen, Germany

Graue B., Siegesmund S., Middendorf B. (2011). Quality assessment of replacement stones for the Cologne Cathedral: mineralogical and petrophysical requirements. *Environmental Earth Sciences*, 63, 1799–1822

Hernández Gutiérrez L.E. (2014). *Caracterización geomecánica de las rocas volcánicas de las Islas Canarias*, PhD dissertation. Departamento de Biología Animal, Edafología y Geología, Universidad de La Laguna, Spain

Hugues T., Steiger L., Weber J. (2005). *Dressed stone. Types of stone, details, examples*. Institut für internationale Architektur-Dokumentation GmbH & Co. KG, Munich

Klopfer H. (1985). Feuchte. In: Lutz P. et al., eds, *Lehrbuch der Bauphysik*. Teubner, Stuttgart, 265–434

Koch R. (2006). Trachyte aus dem Colli Euganei, Norditalien. In: Schock-Werner B., ed., *Modellhafte Entwicklung von Konservierungskonzepten für den stark umweltgeschädigten Trachyt an den Domen zu Köln und Xanten*. Domverlag, Köln, 9–42

Langella A., Calcaterra D., Cappelletti P., Colella A., D'Albora M.P., Morra V., De Gennaro M. (2009). Lava stones from Neapolitan volcanic districts in the architecture of Campania region, Italy. *Environmental Earth Sciences*, 59, 145–160

Lazzarini L., Antonelli F., Cancelliere S., Conventi A. (2008). The deterioration of Euganean trachyte in Venice. In: Lukaszewicz J.W., Niemcewicz P., eds, *Proceedings of the 11th International Congress on Deterioration and Conservation of Stone*, Torun, Poland, 15–20 September 2008, 153–163

Le Maitre R.W., ed. (2002). *Igneous rocks: a classification and glossary of terms*. 2nd ed. Cambridge University Press, Cambridge

Milani L., Beccaluva L., Coltorti M. (1999). Petrogenesis and evolution of the Euganean Magmatic Complex, Veneto Region, North-East Italy. *European Journal of Mineralogy*, 11, 379–399

Previato C., Bonetto J., Mazzoli C., Maritan L. (2014). Aquileia e le cave delle regioni alto-adriatiche: il caso della trachite euganea. In: Bonetto J., Camporeale S., Pizzo A., eds, *Arqueología de la construcción IV. Las canteras en el mundo antiguo: sistemas de explotación y procesos productivos*. CSIC, Mérida, 149–166

Ruedrich J., Bartelsen T., Dohrmann R., Siegesmund S. (2011). Moisture expansion as a deterioration factor for sandstone used in buildings. *Environmental Earth Sciences*, 63, 1545–1564

Sequeira Braga M.A., Figueiredo M.O., Prudêncio M.I., Delgado Rodrigues J., Alves C.A.S., Costa D., Silva T., Trindade M.J., Waerenborgh J.C., Nasraoui M., Gouveia M.A. (2000). Trachyte stones in monuments of the São Miguel and Terceira Islands, Azores (Portugal). In: Fassina V., ed., *Proceedings of the 9th International Congress on Deterioration and Conservation of Stone*, Venezia, Italy, 19–24 June 2000, 235–245

Siegesmund S., Dürrast H. (2014). Physical and mechanical properties of rocks. In: Siegesmund S., Snethlage R., eds, *Stone in architecture. Properties, durability*, 5th ed. Springer, Berlin, 97–224

Silva J.B.P., Carvalho C., Caetano S.D., Gomes C. (2010). Natural stone from the Azores archipelago: relationship between lithology and physical-mechanical behaviour. In: Olalla C. et al., eds, *Volcanic Rock Mechanics*. Taylor & Francis Group, London, 125–131

Steiger M., Charola A.E., Sterflinger K. (2014). Weathering and deterioration. In: Siegesmund S., Snethlage R., eds, *Stone in architecture. Properties, durability*, 5th ed. Springer, Berlin, 225–316

Strohmeyer D. & Siegesmund S. (2002). Anisotropic technical properties of building stones and their development due to fabric changes. In: Siegesmund S., Weiss T., Vollbrecht A., eds, *Natural stone, weathering phenomena, conservation strategies and case studies*. Geological Society, London, Special Publications, 205, 115–135

Tomašić I., Vrkljan M., Helinger G., Bušić M., Tibljaš D. (2000). The persistence of trachyte-trachyandesite built into pedestrian-roadway construction. *Rudarsko-geološko-naftni zbornik*, 12, 89–98

Valluzzi M.R., Mazzoli C., Maritan L., Bianchini G., Andreoli F. (2005). Experimental analyses for the preservation of trachyte pavings in salt-controlled weathering conditions. In: Banthia N., Uomoto T., Bentur A., Shah S.P., eds, *Construction materials: proceedings of ConMat '05 and Mindness Symposium*, Vancouver, Canada, 22–24 August 2005, 1–10

Vergès-Belmin V., ed. (2010). *Illustrated glossary on stone deterioration patterns*. Monuments and Sites, XV. ICOMOS, International Scientific Committee for Stone (ISCS), Paris.

Williams-Thorpe O., Thorpe R.S. (1989). Provenancing and archaeology of Roman millstones from Sardinia (Italy). *Oxford Journal of Archaeology*, 8 (1), 89–117

Zantedeschi C. (1994). New Rb-Sr radiometric data from Colli Euganei (North-Eastern Italy). *Memorie di Scienze Geologiche*, 46, 17–22

Zantedeschi C., Zanco A. (1993). Distinctive characteristics of euganean trachytes for their identification in ancient monuments. *Science and Technology for Cultural Heritage*, 2, 1–10

Zezza U., Risso C., Fernandez Matran M.A. (1995). The trachyte of Fuerteventura: a new material of the Islas Canarias architecture. *Atti Ticinensi di Scienze della Terra*, 38, 193–204

Supplementary: Chapter 5

Textural and mineralogical analysis of volcanic rocks by μ-XRF mapping

Abstract

In this study, μ-XRF was applied as a novel surface technique for quick acquisition of elemental X-ray maps of rocks, image analysis of which provides quantitative information on texture and rock-forming minerals. Bench-top μ-XRF is cost-effective, fast and non-destructive, can be applied to both large (up to a few tens of cm) and fragile samples, and yields major and trace element analysis with good sensitivity. Here, X-ray mapping was performed with a resolution of 103.5 μm and spot size of 30 μm over areas of about 5 x 4 cm of samples of Euganean trachyte, a volcanic porphyritic rock from the Euganean Hills (NE Italy), traditionally used in cultural heritage. The relative abundance of phenocrysts and groundmass, as well as the size and shape of the various mineral phases, were obtained from image analysis of the elemental maps. The quantified petrographic features allowed identifying various extraction sites, revealing an objective method for archaeometric provenance studies exploiting μ-XRF imaging.

1. Introduction

The texture of a rock represents the geometric complexity of its constituents, i.e., crystals, grains, glass and pores, as defined by their size, shape, position, orientation and mutual spatial relationships. The description and quantification of texture is a key topic in petrology, as it provides information about petrogenetic processes and supports the development of physical models, texture being influenced by the growth rate, dissolution, movement and deformation of minerals during rock formation (Higgins 2006; Jerram & Kent 2006). Textural characteristics are also studied in a number of related disciplines, e.g., in archaeometry for information on how stone can resist deterioration (Steiger et al. 2014), or in engineering for inferring the quality of stone materials (Přikryl 2006; Ozturk & Nasuf 2013).

From a geometric viewpoint, texture is a three-dimensional property, so that its quantification by two-dimensional methods is indirect and requires extrapolation of data (Higgins 2000). Nevertheless, 2D methods are still frequently preferred, as sample and grain size is not strongly constrained, the necessary equipment is less expensive, and the analyses are non-destructive or micro-destructive (Jerram & Higgins 2007; Baker et al. 2012). Modern 2D methods rely on the extraction of textural information after automated analysis of digital images, acquired on a plane rock-sample surface with optical or electronic techniques. The former provides very cost-effective transmitted-light photos taken on thin sections with a polarizing microscope or image scanner, but resolution is often poor and, in most cases, image processing is slow and complex for rocks composed of many phases and crystals

(Tarquini & Armienti 2003; Tarquini & Favalli 2010). Segmentation may be difficult when different mineral phases with similar colors (under parallel polars) and interference colors (under crossed polars) are present in the same sample: in these cases, automatic attribution to a specific mineral phase is impossible, and assisted recognition is required to produce accurate data. Conversely, electronic techniques are based on scanning electron microscopy (SEM) or electron probe microanalysis (EPMA) to generate X-ray maps: chemical information is directly available and image analysis is fast, but acquisition may be extremely time-consuming, so it is usually applied only on millimetric or sub-millimetric surfaces. Back-scattered electron images may also be used, but phases with similar mean atomic numbers cannot easily be discriminated (Lindqvist & Åkesson 2001; Higgins 2006). Therefore, if mineralogy is a concern, X-ray maps are the most useful source of information, as they can also indirectly provide information on the modal composition of rocks, much more quickly than manual point counting under the optical microscope (Maloy & Treiman 2007).

Recent progress in X-ray optics has produced compact spectrometers for micro X-ray fluorescence (μ-XRF), once the prerogative of only a few synchrotron-based systems (Behrends & Kleingeld 2009; Mera et al. 2015). μ-XRF works on the same principles as standard XRF, but high-intensity, finely collimated X-ray beams are used. In bench-top instruments, the beam can reach a spot size of 10 μm and is usually generated by a polycapillary lens, a compact device composed of a bundle of curved, micrometric glass channels, through which photons are focused by multiple internal reflections. The secondary X-rays emitted by the sample are detected in energy-dispersion mode from discrete points, lines or areas, providing elemental maps. Detection limits are between 10 and 100 ppm for transition elements, and typically every element from Na (Z = 11) to U (Z = 92) can be measured (Janssens 2004; Behrends & Kleingeld 2009; Haschke et al. 2012; Vaggelli & Cossio 2012). The resolution achievable with μ-XRF is much lower than that of SEM or EPMA, but the advantages outweigh this disadvantage: the instrument is less expensive, analyses are faster, can be performed both in air and

Table 1. Petrographic features of trachyte samples microscopically observed on thin section.

Quarry locality	Sample	Quarry	Mineralogy	Texture
Monselice	MNS-01	1	Ano, Sa, Bt, Krs, Mag, Ilm, Ap, Ttn	Holocrystalline and porphyritic-glomeroporphyritic, with hiatal grain size and microcrystalline, trachytic-pilotaxitic matrix.
	MNS-05			
Monte Merlo	MRL-02	2	Ano, Pl, Sa, Bt, Krs, Aug, Crs, Mag, Ilm, Ap, Zrn, (Qz)	Holocrystalline and porphyritic-glomeroporphyritic-cumuloporphyritic, with seriate grain size and microcrystalline, felty matrix.
	MRL-03	3		
	MRL-05	4		
Monte Oliveto	OLV-01	5	Ano, Pl, Bt, Mag, Ilm, Ap, Ep, (Sa, Krs, Aug, Crs, Qz, Ttn)	Holocrystalline and porphyritic-glomeroporphyritic-cumuloporphyritic, with hiatal grain size and cryptocrystalline, felty matrix. In some cases, groundmass is locally oriented, with a trachytic-pilotaxitic texture.
	OLV-02			
	OLV-03	6		
	OLV-04			
	OLV-05	7		
	OLV-07			
	OLV-08	8		
	OLV-11	9		
	OLV-12			

Mineralogy reports mineral phases occurring in all samples from the same quarry locality (phases in brackets: not always present). Abbreviations for minerals according to (Whitney and Evans 2010): Ano = anorthoclase, Ap = apatite, Aug = augite, Bt = biotite, Crs = cristobalite, Ep = epidote, Ilm = ilmenite, Krs = kaersutite, Mag = magnetite, Pl = plagioclase, Qz = quartz, Sa = sanidine, Ttn = titanite, Zrn = zircon.

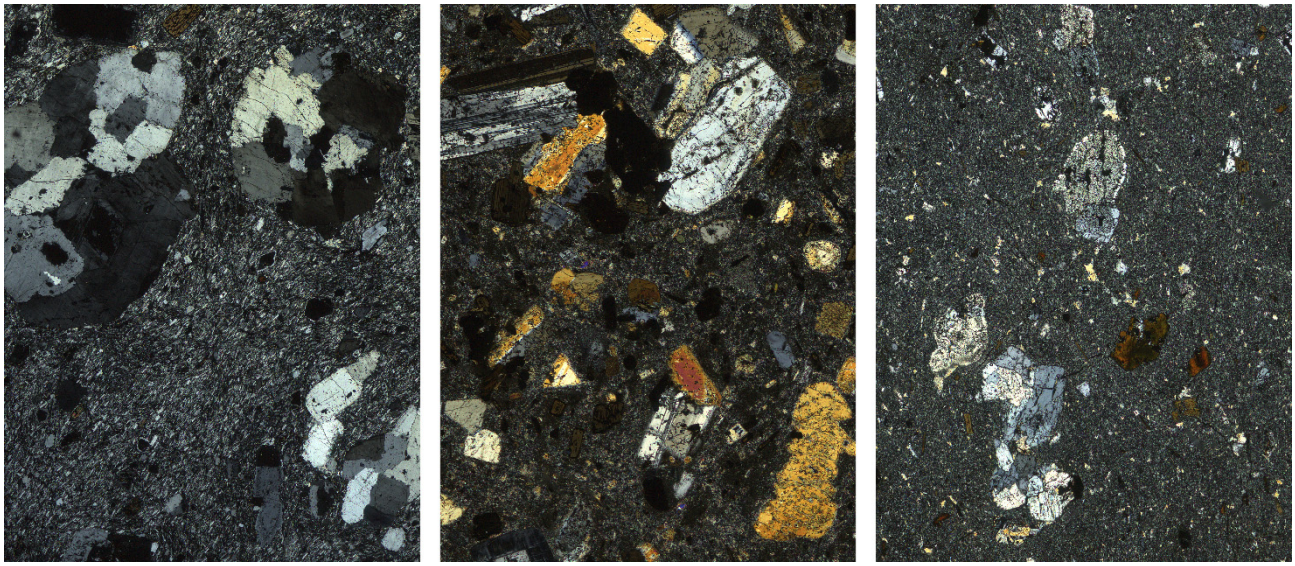

Fig. 1. Photomicrographs in cross-polarized light of samples MNS-01 **(left)**, MRL-03 **(center)** and OLV-01 **(right)**, taken at same magnification (field size: 9.71 x 13.07 mm). Anomalous interference colors of crystals are due to section thickness of 45 μm.

under vacuum, and are not affected by electronic charging effects (Higgins, 2006); large objects (up to a few tens of cm) can be analyzed and, although flat surfaces produce better results, no sample preparation is required. In addition, the latest advances in μ-XRF technology have led to the development of portable instruments and confocal spectrometers for 3D analysis (Malzer & Kanngießer 2005; Kanngießer et al. 2012). For all these reasons, μ-XRF is increasingly applied in archaeometric studies, in which non-invasive and non-destructive techniques are needed to analyze artistic and archaeological materials (Janssens et al. 2000; Rindby & Janssens 2002; Mantouvalou et al. 2011; Vaggelli et al. 2013; Angelici et al. 2015).

In this paper, μ-XRF mapping coupled with image analysis was tested for rapid acquisition of quantitative textural and mineralogical information on volcanic porphyritic rocks. The material analyzed was Euganean trachyte, quarried in the district of the Euganean Hills (Veneto, NE Italy) and widely used in cultural heritage. The possibility of applying μ-XRF imaging to archaeometric studies, with quantitative petrographic criteria to identify and discriminate quarry provenance, was also verified.

2. Materials

Euganean trachyte is a subvolcanic porphyritic rock that formed during the intermediate and acidic activity in the lower Oligocene in the area of the Euganean Hills (De Vecchi et al. 1976; Milani et al. 1999). This volcanic complex is the most important district in Italy for trachyte, which has been extensively quarried in more than 70 open pits, probably since the 7th century BC and still ongoing on a small scale. Historically, this activity has influenced the landscape and local economy but, above all, it represents the starting point of the widespread use of trachyte in the cultural heritage of northern and central Italy. In fact, from Roman times onwards, Euganean trachyte has been extensively used

as a building material in many monuments and infrastructures, as well as in common constructions and artefacts, thanks to its durability and excellent technical properties (Cattani et al. 1997; Renzulli et al. 1999, 2002a, 2002b; Capedri et al. 2000, 2003; Capedri & Venturelli 2003, 2005; Santi & Renzulli 2006; Antonelli & Lazzarini 2010, 2012; Maritan et al. 2013).
In this paper, 14 trachyte samples were analyzed, collected from nine quarries in Monselice, Monte Merlo and Monte Oliveto, the localities representing the main historical quarry sites in the Euganean district (Previato et al. 2014). These representative samples are a subset selected among 24 specimens collected in the above mentioned localities, after a detailed analysis by optical microscopy and SEM, which examined both textural and mineralogical variability within the same quarry and magmatic body. The results of preliminary petrographic characterization of the samples, carried out on separate thin sections under a polarizing microscope, are shown in Table 1 and Fig. 1. Attribution to the correct mineral phase was also confirmed by EPMA analyses, performed on all thin sections.

3. Methods

The samples were prepared in the form of 7 x 7 x 1 cm tiles and mapped on a smooth flat surface with an EDAX Eagle III XPL bench-top spectrometer, equipped as follows: X-ray tube with Rh anode; polycapillary lens for beam focusing on spots of 30 to 300 μm; Si(Li) energy-dispersive detector with Be window; large sample chamber, operating in air or under vacuum; motorized x-y-z sample staging; two cameras for sample viewing. The instrument and data were controlled by EDAX Vision 32 software. During map acquisition, a spot size of 30 μm and a resolution (step size) of 103.5 μm were used to analyze a 512 x 400 pixel grid, i.e., a total area of about 5 x 4 cm. The X-ray tube was operated at 40 kV and 1 mA, and a time constant of 2.5 μs and a dwell time of 200 ms were chosen. Count maps of the following elements were recorded: Na, Mg, Al, Si, P, S, K, Ca, Ti, Fe, Sr, Zr, Ba. Overall analytical time was about 18 hours for each automated overnight run. The Na maps proved to have a low signal/noise ratio. This problem could have been avoided with higher resolution or increased dwell time, but would have led to far longer analytical times.
The resulting maps (Fig. 2) were processed by digital image analysis with open-source software packages (ImageJ v1.48 and MultiSpec v3.4), in order to extract the relative abundances of the rock constituents, i.e., phenocrysts and groundmass, and the textural features of the various mineral phases. A pre-processing step of contrast/brightness adjustment and noise reduction preceded for each elemental map. The most significant maps from each sample were then superimposed and analysed as multispectral images, in which the various mineral phases were identified by their chemical composition and segmented according to manually defined training pixels. Lastly, classified images were obtained, after ECHO spectral/spatial classification with Fisher's linear discriminant algorithm; the classified images were subjected to color thresholding and, for each color-assigned constituent and phase, particle analysis was also performed. Quantitative textural and mineralogical data were extracted through calculation of the following descriptors of size and shape of each discrete grain: area, perimeter, Feret diameter, circularity and aspect ratio (the Feret diameter is the longest distance between any two points along the selected particle boundary, i.e., the maximum dimension of a grain; circularity is calculated as $4\pi \cdot \text{area}/\text{perimeter}^2$: a value of 1 indicates a perfect circle, values

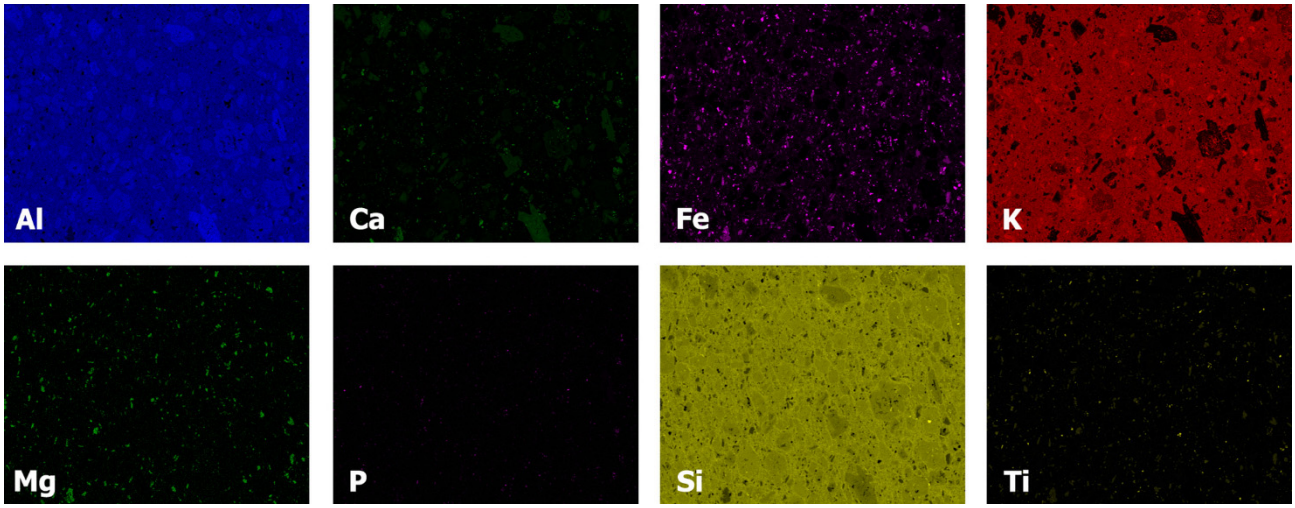

Fig. 2. X-ray maps of the most significant elements from one sample from Monte Merlo (field size: 5.30 x 4.14 cm).

approaching 0 denote an increasingly elongated shape; aspect ratio AR = Feret diameter/minimum Feret diameter: the ratio between the major and minor axes of an ellipse fitted to the selected particle boundary, thus expressing the average degree of elongation of that grain). It should be noted that a discrete grain, separated from the surrounding groundmass, is defined here according to the values of spot size and resolution chosen for the analyses. Lastly, petrographic parameters were statically processed by Principal Component Analysis (PCA) with the Statgraphics Centurion XVI software package.

4. Results and discussion

With the present experimental setup, data on crystals mostly above ~100 μm are given, which comprise, for each sample, the totality of phenocrysts (here defined as crystals distinctly larger – at least 5 times – than the grains of the groundmass). The smallest grain size measured was typically affected by the used resolution, but also by variable factors, such as orientation and shape of crystals and their spatial relationships with the position of mapping points and the chosen spot size.
Comparisons among representative classified images for each quarry locality (Fig. 3) clearly showed that trachytes from the various areas differ in terms of type, absolute and relative abundance and grain size of the phenocrysts, as well as the percentage of groundmass. This was confirmed by the porphyritic index (total percentage of phenocrysts) and the abundance of the various phases for each sample (Table 2).
Although a certain variability occurs in each quarry locality, trachytes from Monselice and Monte Merlo had a higher phenocryst-groundmass ratio than those from Monte Oliveto. Another main difference was feldspar content, while mafic and accessory minerals had random distribution. The trachyte from Monselice and Monte Merlo contained a higher feldspar fraction (total content) than that from Monte Oliveto, where this content was always lower than 22%. In addition, plagioclase was not

found in Monselice, although it does occur in the other two localities, the highest average concentration being in Monte Merlo (5.60%). Sanidine was found in almost all samples, although only in negligible amounts (less than 1%), except for the samples from Monselice and in two samples from Monte Merlo (MRL-03) and Monte Oliveto (OLV-12). PCA, performed on the percentages of the various mineral phases in the phenocrysts and the percentage of groundmass in each sample (Fig. 4a), showed that trachyte from the three localities can be discriminated on the basis of these parameters. According to the Mahalanobis distance, 100% of samples were correctly classified *a priori*, and none was assigned to a different group by the classification routine of discriminant analysis.

When the crystal-size distribution of feldspars was examined (Table 3, Fig. 5), the Monselice trachyte turned out to contain the largest feldspars, with a maximum area of about 40 mm^2 and maximum Feret diameter of about 10 mm, with grain size scattered over a rather broad but uneven range. The Monte Oliveto trachyte was characterized by fine-grained feldspars, mainly under 5 mm^2 and never exceeding 14 mm^2, and a Feret diameter mostly below 2 mm. The Monte Merlo trachyte showed intermediate characteristics, feldspars displaying seriate distribution from coarse- to fine-grained phenocrysts. PCA of the crystal-size distribution of the whole feldspar fraction, separating the concentrations of anorthoclase, plagioclase and sanidine (Fig. 4b), shows that trachytes from the three localities cluster according to the following parameters: high concentration of anorthoclase and coarser feldspars at Monselice; high content of fine-sized feldspars at Monte Oliveto; high plagioclase and intermediate-sized feldspars at Monte Merlo. Also in this case, discriminant analysis confirmed that the samples were correctly classified *a priori*, and none was assigned to a different group by the classification routine. Although grain-size properties proved to be efficient in discriminating the various quarrying localities, crystal shape turned out to be unsuitable for this purpose.

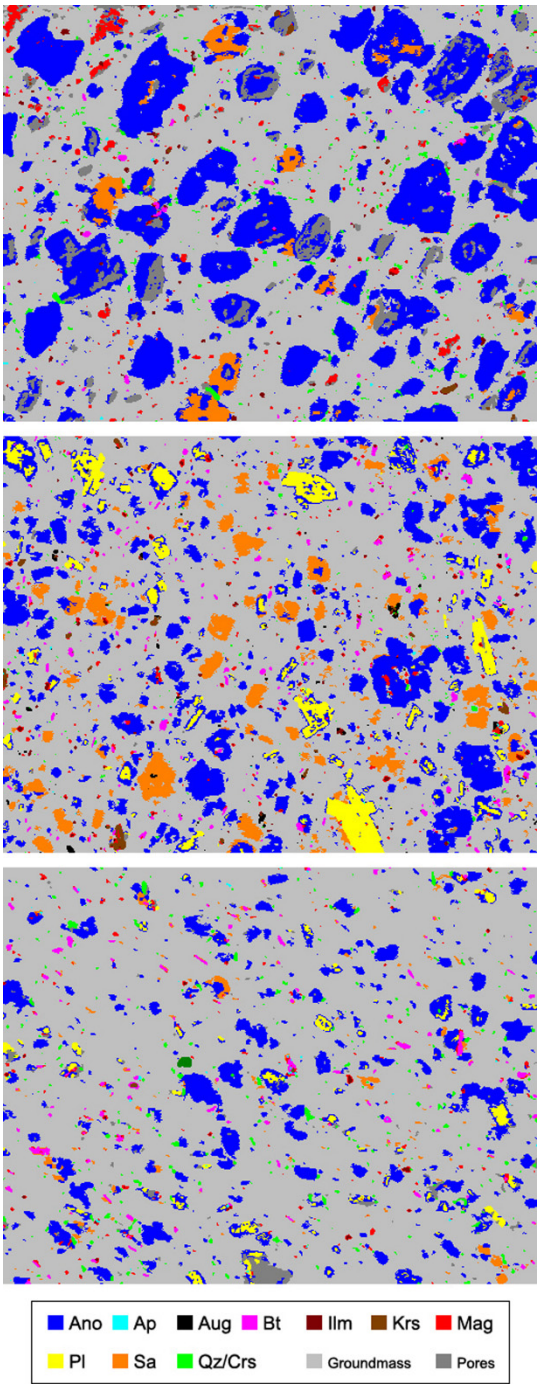

Fig. 3. Classified maps of samples MNS-01 **(top)**, MRL-03 **(center)** and OLV-01 **(bottom)** (field size: 5.30 x 4.14 cm). Colours not shown in legend: occasional phases. Abbreviations as in Table 1.

The textural and mineralogical quantitative information obtained from image analysis of the μ-XRF maps matched the previous qualitative observations under the microscope, but had greater statistical representativeness, since they were taken on areas twice as large as standard thin sections. In this

sense, although preliminary petrographic characterization may aid the processing of X-ray maps, it is not strictly necessary, provided that an approximate evaluation is made about the detectable mineral phases.

The petrographic differences observed among the trachytes subjected to μ-XRF suggested that the results could be applied to archaeometry, with the aim of proposing new parameters for identifying and discriminating the quarry of provenance for Euganean trachyte. Knowing exactly where the stone used in archaeological or historical objects was quarried provides clues about ancient trades, circulation of raw and finished stone materials and artefacts, quarry work and sources of stone supply.

Table 2. Percentage of mineral phases constituting phenocrysts, percentage of groundmass (GM) and porphyritic index (P.I., corresponding to percentage area of all phenocrysts), calculated after particle analysis.

Quarry locality	Sample	Feldspars				Mafic minerals			Accessory minerals					GM	P.I.
		Ano	Sa	Pl	Σ Fsp	Bt	Aug	Krs	Qz/Crs	Ilm	Mag	Ap	Others		
Monselice	MNS-01	29.08	2.39	0.00	31.47	0.25	0.00	0.15	1.04	0.37	1.48	0.04	0.00	65.19	34.81
	MNS-05	12.76	9.43	0.00	22.19	0.33	0.00	0.14	0.00	0.31	0.74	0.04	0.10	76.15	23.85
Monte Merlo	MRL-02	14.52	0.65	6.88	22.05	2.15	0.04	0.03	1.29	0.40	1.82	0.23	0.00	71.99	28.01
	MRL-03	15.93	6.01	4.46	26.40	1.03	0.30	0.32	0.23	0.31	0.75	0.05	0.00	70.59	29.41
	MRL-05	19.42	0.96	5.47	25.85	1.11	0.69	0.37	0.33	0.38	1.10	0.06	0.00	70.09	29.91
Monte Oliveto	OLV-01	9.80	0.97	1.22	11.99	0.88	0.00	0.01	1.14	0.09	0.58	0.08	0.07	85.16	14.84
	OLV-02	10.20	0.63	2.85	13.68	0.69	0.00	0.02	0.28	0.15	1.60	0.14	0.00	83.45	16.55
	OLV-03	13.67	0.25	2.44	16.36	0.71	0.00	0.00	1.81	0.17	0.49	0.17	0.00	80.29	19.71
	OLV-04	11.36	0.29	3.19	14.84	1.62	0.00	0.04	1.77	0.20	0.51	0.07	0.00	80.94	19.06
	OLV-05	11.08	0.61	1.77	13.46	0.29	0.00	0.00	6.30	0.25	0.36	0.23	0.00	79.10	20.90
	OLV-07	15.96	0.72	5.22	21.94	1.64	0.00	0.06	2.42	0.16	0.27	0.17	0.00	73.38	26.62
	OLV-08	15.99	0.00	5.06	21.05	1.19	0.00	0.00	0.62	0.25	0.19	0.11	0.00	76.59	23.41
	OLV-11	10.32	1.28	1.50	13.10	0.94	0.00	0.05	0.69	0.09	0.25	0.11	0.00	84.77	15.23
	OLV-12	4.28	6.03	0.91	11.22	0.29	0.05	0.00	0.65	0.04	0.19	0.05	0.00	87.50	12.50

Abbreviations of minerals as in Table 1. ΣFsp = total feldspars.

Table 3. Textural data of feldspars (anorthoclase, plagioclase and sanidine considered together) calculated after particle analysis.

Quarry locality	Sample	Feret diameter (mm)					Area (mm^2)						Perim. (mm)	Circ.	AR
		Mean	Max	$d_{<2}$ (%)	d_{2-8} (%)	$d_{>8}$ (%)	Mean	Max	a_{1-5} (%)	a_{5-10} (%)	a_{10-30} (%)	$a_{>30}$ (%)			
Monselice	MNS-01	1.12	10.77	85.56	13.73	0.71	1.07	40.00	60.24	18.07	18.07	3.61	3.52	0.69	1.85
	MNS-05	1.40	10.37	82.67	16.67	0.67	1.28	41.15	67.86	23.81	5.95	2.38	4.72	0.62	1.90
Monte Merlo	MRL-02	0.85	6.15	90.63	9.37	0.00	0.41	15.37	85.05	12.15	2.80	0.00	2.38	0.71	1.94
	MRL-03	1.02	7.99	87.96	12.04	0.00	0.63	26.96	83.90	8.47	7.63	0.00	3.01	0.66	1.93
	MRL-05	1.31	9.69	84.72	15.15	0.13	0.83	34.94	80.34	13.68	5.13	0.85	3.87	0.62	2.02
Monte Oliveto	OLV-01	0.75	6.95	92.11	7.89	0.00	0.29	10.21	95.31	3.13	1.56	0.00	1.98	0.74	1.95
	OLV-02	0.86	4.13	90.32	9.68	0.00	0.39	7.63	97.67	2.33	0.00	0.00	2.32	0.75	1.85
	OLV-03	0.91	7.13	91.87	8.13	0.00	0.41	13.86	84.42	12.99	2.60	0.00	2.44	0.74	1.89
	OLV-04	0.80	7.46	93.56	6.44	0.00	0.37	13.20	86.36	10.61	3.03	0.00	2.13	0.73	1.90
	OLV-05	0.74	5.12	93.57	6.43	0.00	0.34	6.90	90.28	9.72	0.00	0.00	1.95	0.78	1.85
	OLV-07	0.80	8.53	92.88	7.04	0.08	0.38	13.28	88.78	9.18	2.04	0.00	2.14	0.78	1.84
	OLV-08	0.88	7.83	91.10	8.90	0.00	0.43	9.61	92.92	7.08	0.00	0.00	2.62	0.73	1.88
	OLV-11	1.04	4.88	88.04	11.96	0.00	0.56	7.22	93.83	6.17	0.00	0.00	2.91	0.72	1.89
	OLV-12	0.90	5.51	92.72	7.28	0.00	0.43	6.57	93.65	6.35	0.00	0.00	2.50	0.75	1.76

Feret diameter values subdivided into three classes (lower and upper limits of intermediate class at 2 and 8 mm); area values higher than 1 mm^2 subdivided into four classes (with limits at 5, 10 and 30 mm^2) and relative percentage frequency calculated. Perimeter (perim.), circularity (circ.) and aspect ratio (AR) values are averaged.

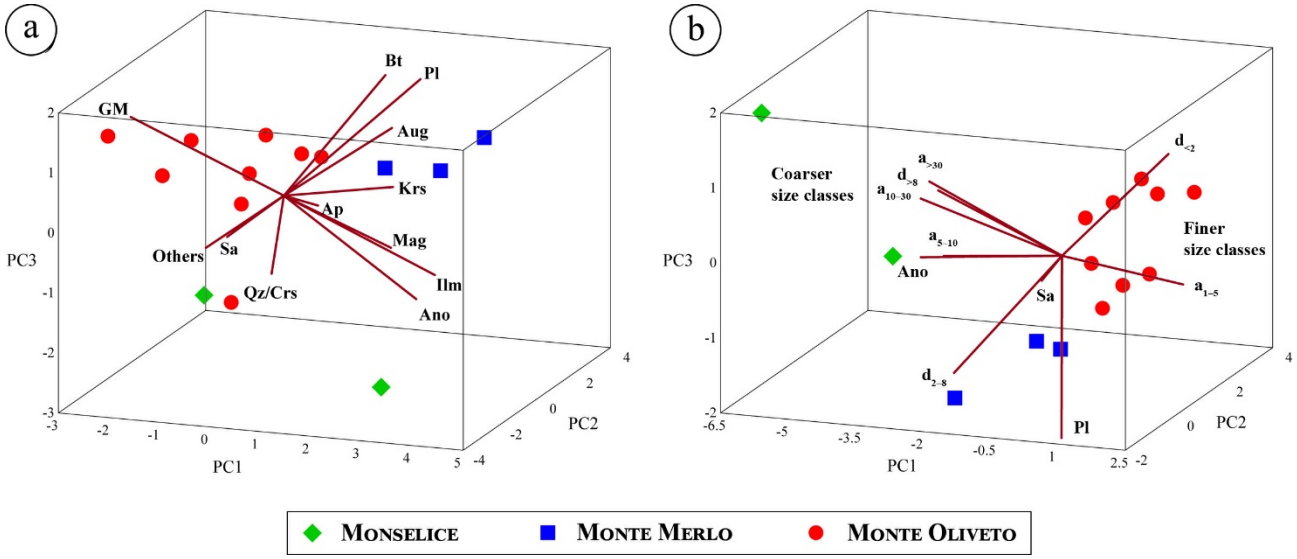

Fig. 4. Score and loading plots from PCA on: **a)** modal composition of all samples (variables as in Table 2, excluding P.I.), PC1, PC2 and PC3 covering 35%, 26% and 12% of total variance, respectively; **b)** crystal-size data of feldspars of all samples (Feret diameter and area classes as in Table 3) and percentages (anorthoclase, plagioclase and sanidine, as in Table 2), with PC1, PC2 and PC3 covering 65%, 15% and 10% of total variance, respectively.

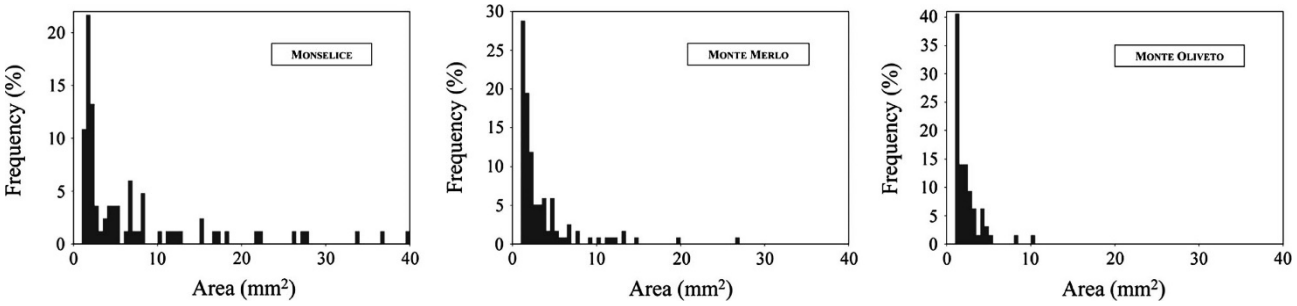

Fig. 5. Frequency histograms of crystal-size distribution of feldspars, based on areas larger than 1 mm^2 for each particle analyzed, calculated for samples MNS-01 **(left)**, MRL-03 **(center)** and OLV-01 **(right)**.

It can also aid reconstruction of the territorial organization of settlements and, lastly, can provide useful indications about the most suitable materials for restoration. The Euganean trachytic rocks are very similar in both bulk chemical composition and macroscopic and microscopic characteristics. This is why the most traditional methods used in provenance studies, such as XRF analyses or thin-section observations, are not sufficient to differentiate the rocks from various outcrops and quarrying localities. Recent studies do demonstrate that the discrimination criteria generally accepted in the literature are partially unreliable (Maritan et al. 2013). The problem is further complicated by the widespread use of trachyte and the existence of many ancient quarries in the Euganean Hills. In this regard, PCA on both textural and mineralogical data extracted by μ-XRF imaging was aimed at verifying the validity of the discriminating parameters inferred from the raw results.

5. Conclusions

Complete petrographic characterization of samples of Euganean trachyte, obtained from image analysis of X-ray maps, clearly shows the advantages of bench-top μ-XRF mapping as a non-destructive technique for textural and mineralogical quantitative analysis of porphyritic rocks, provided that their grain size matches the resolution limits of the spectrometer used. Given this, if modal analysis is the only concern, μ-XRF can also be extended to rocks with equigranular textures and with multiple minerals of the same phase in mutual contact.

Although it does not introduce really new analytical possibilities, the potential of μ-XRF mapping for imaging – more than for spot analyses, for which it has mostly been used so far – are promising, and are enhanced by cost-effective instrumentation, low detection limits, short analysis times, and the possibility of analyzing also large fragile objects. Thanks to these characteristics, μ-XRF exceeds the possibilities of SEM and EPMA, which can still serve as preparatory techniques when higher resolution, sensitivity or accuracy are required.

The application of μ-XRF to archaeometric provenance studies is only one of its potential uses. However, the quality of the results from the main historical quarries of Euganean trachyte encourages extending this type of research to the entire Euganean district, in order to create a complete reference database. This is a novel alternative approach to classic provenance studies of stone, traditionally performed according to chemical or microchemical properties, without taking texture into account.

References

Angelici D., Borghi A., Chiarelli F., Cossio R., Gariani G., Lo Giudice A., Re A., Pratesi G., Vaggelli G. (2015). μ-XRF analysis of trace elements in lapis lazuli-forming minerals for a provenance study. *Microscopy and Microanalysis*, 21, 526–533

Antonelli F., Lazzarini L. (2010). Mediterranean trade of the most widespread Roman volcanic millstones from Italy and petrochemical markers of their raw materials. *Journal of Archaeological Science*, 37, 2081–2092

Antonelli F., Lazzarini L. (2012). The first archaeometric characterization of Roman millstones found in the Aquileia archaeological site (Udine, Italy). *Archaeometry*, 54 (1), 1–17

Baker D.R., Mancini L., Polacci M., Higgins M.D., Gualda G.A.R., Hill R.J., Rivers M.L. (2012). An introduction to the application of X-ray microtomography to the three-dimensional study of igneous rocks. *Lithos*, 148, 262–276

Behrends T., Kleingeld P. (2009). Bench-top micro-XRF - a useful apparatus for geochemists? *Geochemical News*, 138, 1–5

Capedri S., Grandi R., Venturelli G. (2003). Trachytes used for paving Roman roads in the Po Plain: characterization by petrographic and chemical parameters and provenance of flagstones. *Journal of Archaeological Science*, 30, 491–509

Capedri S., Venturelli G. (2003). Trachytes employed for funerary artefacts in the Roman Colonies Regium Lepidi (Reggio Emilia) and Mutina (Modena) (Italy): provenance inferred by petrographic and chemical parameters and by magnetic susceptibility. *Journal of Cultural Heritage*, 4, 319–328

Capedri S., Venturelli G. (2005). Provenance determination of trachytic lavas, employed as blocks in the Romanesque cathedral of Modena (Northern Italy), using magnetic susceptibility, and petrographic and chemical parameters. *Journal of Cultural Heritage*, 6, 7–19

Capedri S., Venturelli G., Grandi R. (2000). Euganean trachytes: discrimination of quarried sites by petrographic and chemical parameters and by magnetic susceptibility and its bearing on the provenance of stones of ancient artefacts. *Journal of Cultural Heritage*, 1, 341–364

Cattani M., Lazzarini L., Falcone R. (1997). Macine protostoriche dall'Emilia e dal Veneto: note archeologiche, caratterizzazione chimico-petrografica e determinazione della provenienza. *Padusa*, 31, 105–137

De Vecchi G., Gregnanin A., Piccirillo E.M. (1976). Tertiary volcanism in the Veneto: magmatology, petrogenesis and geodynamic implications. *Geologische Rundschau*, 65 (1), 701–710

Haschke M., Rossek U., Tagle R., Waldschläger U. (2012). Fast elemental mapping with micro-XRF. *Advances in X-ray Analysis*, 55, 286–298

Higgins M.D. (2000). Measurement of crystal size distributions. *American Mineralogist*, 85, 1105–1116

Higgins M.D. (2006). *Quantitative textural measurements in igneous and metamorphic petrology*. Cambridge University Press, New York

Janssens K. (2004). X-ray based methods of analysis. In: Janssens K., Van Grieken R., eds, *Non-destructive microanalysis of cultural heritage materials*. Comprehensive Analytical Chemistry, Vol. XLII. Elsevier, Amsterdam, 129–226

Janssens K., Vittiglio G., Deraedt I., Aerts A., Vekemans B., Vincze L., Wei F., Deryck I., Schalm O., Adams F., Rindby A., Knöchel A., Simionovici A., Snigirev A. (2000). Use of microscopic XRF for non-destructive analysis in art and archaeometry. *X-Ray Spectrometry*, 29, 73–91

Jerram D.A., Higgins M.D. (2007). 3D analysis of rock textures: quantifying igneous microstructures. *Elements*, 3, 239–245

Jerram D.A., Kent A.J.R. (2006). An overview of modern trends in petrography: textural and microanalysis of igneous rocks. *Journal of Volcanology and Geothermal Research*, 154, 7–9

Kanngießer B., Malzer W., Mantouvalou I., Sokaras D., Karydas A.G. (2012). A deep view in cultural heritage – confocal micro X-ray spectroscopy for depth resolved elemental analysis. *Applied Physics A*, 106, 325–338

Lindqvist J.E., Åkesson U. (2001). Image analysis applied to engineering geology, a literature review. *Bulletin of Engineering Geology and the Environment*, 60, 117–122

Maloy A.K., Treiman A.H. (2007). Evaluation of image classification routines for determining modal mineralogy of rocks from X-ray maps. *American Mineralogist*, 92, 1781–1788

Malzer W., Kanngießer B. (2005). A model for the confocal volume of 3D micro X-ray fluorescence spectrometer. *Spectrochimica Acta Part B*, 60, 1334–1341

Mantouvalou I., Wolff T., Hahn O., Rabin I., Lühl L., Pagels M., Malzer W., Kanngiesser B. (2011). 3D micro-XRF for Cultural Heritage objects: New analysis strategies for the investigation of the Dead Sea scrolls. *Analytical Chemistry*, 83, 6308–6315

Maritan L., Mazzoli C., Sassi R., Speranza F., Zanco A., Zanovello P. (2013). Trachyte from the Roman aqueducts of Padua and Este (north-east Italy): a provenance study based on petrography, chemistry and magnetic susceptibility. *European Journal of Mineralogy*, 25, 415–427

Mera M.F., Rubio M., Pérez C.A., Galván V., Germanier A. (2015). SR μXRF and XRD study of the spatial distribution and mineralogical composition of Pb and Sb species in weathering crust of corroded bullets of hunting fields. *Microchemical Journal*, 119, 114–122

Milani L., Beccaluva L., Coltorti M. (1999). Petrogenesis and evolution of the Euganean Magmatic Complex, Veneto Region, North-East Italy. *European Journal of Mineralogy*, 11, 379–399

Ozturk C.A., Nasuf E. (2013). Strength classification of rock material based on textural properties. *Tunnelling and Underground Space Technology*, 37, 45–54

Previato C., Bonetto J., Mazzoli C., Maritan L. (2014). Aquileia e le cave delle regioni alto-adriatiche: il caso della trachite euganea. In: Bonetto J., Camporeale S., Pizzo A., eds, *Arqueología de la construcción IV. Las canteras en el mundo antiguo: sistemas de explotación y procesos productivos*. CSIC, Mérida, 149–166

Přikryl R. (2006). Assessment of rock geomechanical quality by quantitative rock fabric coefficients: limitations and possible source of misinterpretations. *Engineering Geology*, 87, 149–162

Renzulli A., Antonelli F., Santi P., Busdraghi P., Luni M. (1999). Provenance determination of lava flagstones from the Roman 'Via Consolare Flaminia' pavement (central Italy) using petrological investigations. *Archaeometry*, 41 (2), 209–226

Renzulli A., Santi P., Nappi G., Luni M., Vitali D. (2002a). Provenance and trade of volcanic rock millstones from Etruscan-Celtic and Roman archaeological sites in Central Italy. *European Journal of Mineralogy*, 14, 175–183

Renzulli A., Santi P., Serri G., Luni M. (2002b). The Euganean trachyte flagstones ("basoli") used by the Romans along the mid-Adriatic coast (Marche, central Italy): an archaeometric study. *Periodico di Mineralogia*, 71, 189–201

Rindby A., Janssens K. (2002). Microbeam XRF. In: Van Grieken R.E., Markowicz A.A., eds, *Handbook of X-Ray Spectrometry*. Marcel Dekker, New York, 631–718

Santi P., Renzulli A. (2006). Italian volcanoes as landmarks for the spreading of trade networks during the Etruscan and Roman periods: the millstones and flagstones case study. *Acta Vulcanologica*, 18 (1-2), 133–140

Steiger M., Charola A.E., Sterflinger K. (2014). Weathering and deterioration. In: Siegesmund S., Snethlage R., eds, *Stone in architecture. Properties, durability*, 5th ed. Springer, Berlin, 225–316

Tarquini S., Armienti P. (2003). Quick determination of crystal size distributions of rocks by means of a color scanner. *Image Analysis & Stereology*, 22, 27–34

Tarquini S., Favalli M. (2010). A microscopic information system (MIS) for petrographic analysis. *Computer & Geosciences*, 36, 665–674

Vaggelli G., Cossio R. (2012). μ-XRF analysis of glasses: a non-destructive utility for cultural heritage applications. *Analyst*, 137, 662–667

Vaggelli G., Lovera V., Cossio R., Mirti P. (2013). Islamic glass weights from Egypt. A systematic study by non-destructive μ-XRF technique. *Journal of Non-Crystalline Solids*, 363, 96–102

Whitney D.L., Evans B.W. (2010). Abbreviations for names of rock-forming minerals. *American Mineralogist*, 95, 185–187

General conclusions

A new petrographic and geochemical database for trachyte of the Euganean Hills, based on samples from 40 different quarries, has been established in support of archaeometric provenance studies, serving as reference for identifying the extraction site of trachyte used in artifacts and structures of archaeological and historical significance. The criteria for provenance recognition introduced here are alternative to those available from the literature, which have demonstrated to be incomplete, partly unreliable or inaccurate. The new provenance tracers are based on a multianalytical investigation of the quarry samples that involved optical microscopy, SEM and EDS mapping, μ-XRF mapping, XRF, EPMA, and LA-ICPMS, supported by techniques of multivariate statistical analysis.

The most useful petrographic provenance tracers principally include quantitative data about mineralogical composition and textural features of phenocrysts and groundmass, determined by image analysis of μ-XRF and SEM-EDS chemical maps, in particular: abundance and grain size distribution of feldspar phenocrysts, phenocrysts-groundmass ratio, content of SiO_2 phases in the groundmass, and arrangement and grain size of microlites in the matrix. On the other hand, the geochemical provenance tracers involve composition of bulk rock and phenocrysts, determined by XRF and LA-ICPMS, respectively.

In general, differences of petrographic features and bulk-rock composition among trachytes from different Euganean quarries are subtle, so that their precise discrimination may be rather problematic. In addition, the analysis of those properties needs samples to be representative and large enough, a major drawback when dealing with archaeological materials, the sampling of which may be restricted to very small portions, in some cases also having altered surfaces. For these reasons, petrographic observations of thin sections or XRF analyses – the most traditional methodologies previously used – might not be sufficient to solve provenance problems univocally, even when combining the two techniques. Nevertheless, the novel approach considering quantitative petrographic parameters from image analysis of X-ray elemental maps, in comparison with conventional qualitative examinations, considerably improves the reliability of petrography-based provenance determination.

Alternatively, LA-ICPMS analysis at the mineral scale has proven to be a precise, accurate, and highly sensitive method for autonomously recognizing virtually all the Euganean quarry localities, using composition of phenocrysts, especially of biotite and, secondarily, augite, kaersutite, and magnetite. Linear combinations of major- and trace-element concentrations analyzed on these phases, calculated by a statistical discriminant analysis, have been used to build binary and ternary plots, indicating reference quarry clusters for provenance recognition. Quarry clustering achieved with LA-ICPMS is definitely more precise and effective than that based on the XRF data, especially if analyses of different phases are cross-matched. Moreover, the amount of material required for LA-ICPMS is very limited: at best, even few fine-grained crystals of a single diagnostic phase might be sufficient, and this is a great advantage in the study of cultural heritage, when non-destructive or micro-destructive techniques are mandatory. Finally, although LA-ICPMS may work as a stand-alone technique,

one could choose to couple a petrographic examination, in this case a single thin section of suitable thickness (40-50 μm) would be needed.
The provenance study of Roman infrastructures, involving six former Roman cities in Veneto where Euganean trachyte was used as building stone (mostly from the 1st century BCE to the 1st century CE), has allowed the effectiveness of the new provenance tracers to be tested. LA-ICPMS analysis of major- and trace-element composition of phenocrysts, performed on thin section, was supported by traditional XRF analysis of bulk rock and examination of petrographic features under the optical microscope. In this way, the independence of LA-ICPMS from the other techniques and any other preliminary exploratory analysis has been verified, and confirmed.
Indeed, the LA-ICPMS results, especially those obtained on mafic minerals (the sole biotite composition provides most of the information required), have led to a precise, univocal and autonomous identification of the quarry localities where Euganean trachyte was extracted by the Romans. It has been possible to distinguish even the archaeological samples sharing very similar mineralogical, textural and bulk-chemical characteristics, but extracted in different sites. On the other hand, the above-mentioned drawbacks of microscopic observations on thin section and XRF analyses have arisen again, leading to uncertain provenance determinations.
This study also gives interesting archaeological information, about the quarries active in the Roman times, extent and development of their exploitation, frequency of use of the materials extracted therein, and the commercial and economic dynamics involving their supply for public works. Moreover, indications are given with regard to the territorial organization of the Roman settlements in Veneto, their areas of political influence, and ownership and competition of quarries. A connection has been found between specific quarry localities and the Roman settlements in which trachytes extracted therein were preferentially used. This allows arguing a separate management of the Euganean quarries by the most important cities nearby. The quarries were presumably owned by the city authorities, but conceded as usufructuary properties to single private citizens or societies of publicans.
Finally, this study provides broad insights into ancient trades in northern Italy during the Roman age. The main trade lines for the circulation of raw and finished quarry materials are discussed, considering the localization of the Euganean district in relation to the main transport routes and destination centers, the convenience of different means of transport, and the amounts of trachyte required for public works. Most trades were organized by ship transports taking advantage of the many rivers and channels of the Venetian Plain (especially those flowing very close to the Euganean quarries), the nearby Po river, and the Adriatic Sea. Land transports were slower, more expensive, and far smaller loads could be carried.
The second main study subject of the present research concerns the investigation of weathering and durability of Euganean trachyte in the built environment. Generally, understanding stone provenance of archaeological and historical materials and examining the cause-effect relationships of their decay are among the most debated topics in archaeometry. From one side, social, cultural and commercial dynamics around ancient materials can be investigated; on the other, it is possible to comprehend the link between their widespread use and properties, and their vulnerability in the modern environment. Following these goals, the research continued focusing on the weathering analysis of Euganean trachyte.
The response of trachyte to environmental stresses has been examined in urban environment, where concentration of stoneworks is relatively high and their conservation threat more significant. A set of

trachyte samples was collected on the Renaissance city walls of Padova (16th century), for analyzing weathering crusts and patinas, i.e., their mineralogical and microstructural characteristics, and major- and trace-element chemical composition, by optical microscopy, SEM and EDS mapping, XRPD, and LA-ICPMS.

Trachyte alteration can be placed in direct correlation with quantitative environmental parameters, in particular concerning air quality and anthropic pollution sources. The crusts and patinas on the exposed surfaces are rich in heavy metals and carbonaceous masses, mainly deriving from particulate matter emitted in Padova due to fuel use in road transport and domestic combustion. A secondary source of particulate matter is represented by short- and medium-range industrial emissions, i.e., in Padova and in the industrial area of Venezia-Porto Marghera, one of the biggest coastal industrial zones in Europe, 30 km far.

The pollutants are entrapped in a crystalline matrix usually rich in calcite or iron, present as oxides/hydroxides or in amorphous state, also including minor amounts of quartz, dolomite, and other components (metallic and alumosilicon particles, chlorides, etc.). The high concentration of carbonates cannot be traced back to host rock composition. The only plausible and consistent source is identified in neighboring lime and Mg-lime mortars used in the walls of Padova for joining trachyte blocks. In fact, calcium carbonate may be dissolved by acid solutions and reprecipitate in basic ones. Local pH fluctuations, also occurring on seasonal basis, may favor mechanisms of cycling leaching, short-range mobilization, and recrystallization of calcium carbonate from mortars. With regard to intrinsic alteration processes, the enrichment in iron of the weathering crusts and patinas is dependent on the leaching of this element from iron-bearing minerals of trachyte, and its migration to surface, where it forms brown-reddish layers. Indeed, microscopic examinations disclosed an enrichment in fine-grained iron oxides and hydroxides and amorphous iron in the proximity of biotite phenocrysts and, secondarily, magnetite and ilmenite.

Other less common alteration types detected comprise powdery deposits and gypsum crusts. The thickest, most homogeneous and well-developed crusts, rich in either calcite or gypsum, partially shield the host rock from further pollutant absorption.

From this study, it arises that most of the alteration products of Euganean trachyte are due to exogenous processes, whereas the stone itself does not have particular compositional features prone to trigger major dangerous mechanisms of decay. Generally, composition of the weathering crusts and patinas of Euganean trachyte proves to be an informative marker for the relevant environmental conditions and their evolution.

In order to further explore the properties affecting the weathering behavior of Euganean trachyte, quarry samples from the most representative extraction localities were subjected to a comprehensive petrophysical and mechanical characterization, involving: density, porosity, water absorption, capillary water uptake, hygroscopic water adsorption and desorption, hydric and hygric dilatation, water vapor diffusion, thermal expansion and residual strains, resistance to salt attack and abrasion resistance. Particular emphasis was placed on the characterization of porosimetric properties, by mercury intrusion porosimetry and image analysis of μ-XRF and SEM-EDS X-ray maps; this allowed getting information about a pore size range extended from nanometric to millimetric scale.

The different varieties of Euganean trachyte exhibit a relatively wide array of technical performances, which are almost completely dependent on the diverse porosimetric characteristics. This applies, in particular, to the water-related properties, indicating which modes of water transport and retention

preferentially take place and at which rate. High porosity is not necessarily an indicator of bad durability, since the interaction with bulk, capillary or hygroscopic water can be regardless limited by a poorly interconnected pore network. On the other hand, pore size controls the favored interaction with water in either liquid or vapor state: while macropores are involved in liquid water flow, capillary pores are responsible especially for processes of capillary water suction, and micropores mainly for water vapor condensation. Therefore, a deep investigation of pore size, size distribution, shape and degree of interconnection, other than pore volume, turns out to be essential for correctly predicting the weathering behavior of different varieties of Euganean trachyte.

Clues are given about the decay processes that would develop in presence of water or aqueous solutions, in particular cyclic crystallization/dissolution of soluble salts from ground water, rainfall or hygroscopic condensation, during drying/wetting phases. In this regard, the experiments of salt crystallization outline diverse deterioration patterns, related to the different porosimetric properties, mechanical strength, textural characteristics, and presence of discontinuities: scaling, peeling, blistering, differential erosion (on phenocrysts or groundmass), microcracking, powdering, etc.

The improved knowledge of the technical properties of Euganean trachyte also allows arguing the possible criteria followed by clients, quarrymen, and stonecutters for properly choosing the quarries to exploit in the antiquity, especially during the Roman age. Finally, additional elements for aiding quality assessment of Euganean trachyte and identifying the best performing materials are provided by a comparison with the physico-mechanical properties of the most important trachytes currently or historically extracted in other European countries (Germany, Czech Republic, France, Portugal, and Spain). Euganean trachyte can be defined one of, or the best quality trachyte, having a performance even better than that of many tuffs, sandstones, and limestones commercially available and used as dimension stones.

Appendices

The appendices mentioned in the text, listed below with the relevant captions, are freely available for download on the following website: http://geo.geoscienze.unipd.it/phd-dissertation. Alternatively, they can be requested by email: luigi.germinario@gmail.com.

Chapter 1

Appendix 1. Coordinates of the sampling point where each quarry sample of Euganean trachyte was collected.

Appendix 2. Bulk-rock chemical composition of Euganean trachyte determined by XRF for all the samples (quarry number and localization as in Fig. 2); major elements are expressed as oxide weight percent, LOI as weight percent, trace elements as ppm and concentrations below detection limit indicated by "b.d.".

Appendix 3. Score and loading plot from PCA performed on bulk-rock chemical composition of Euganean trachyte determined by XRF for all the samples, with PC1 and PC2 covering 37% and 16% of total variance, respectively (quarry number and localization as in Fig. 2, symbols as in Table 1). All the measured elements were considered, since none of them showed anomalous concentrations, which might be detected after weathering, or crystallization of secondary phases; this was verified examining the compositional variation matrix and variance of each element, namely the "τ.i" value (Buxeda i Garrigós 1999; Buxeda i Garrigós & Kilikoglou 2003).

Appendix 4. Chemical composition of the main mineral phases in Euganean trachyte determined by LA-ICPMS; major elements are expressed as oxide weight percent, trace elements as ppm and concentrations below detection limit indicated by "b.d." (for data about all the major elements see Table 5). Different spot analyses on the same sample (quarry number and localization as in Fig. 2) are indicated with progressive numbers and small letters, with outlier samples excluded. Each worksheet contains the results of different phases and average values of the reference materials.

Appendix 5. Complementary binary scatterplots for provenance recognition of Euganean trachyte, based on simple concentrations of major and trace elements of the main mineral phases determined by LA-ICPMS, using the isotopes in Appendix 4. Each worksheet contains the most significant plots for different phases. Quarry symbols as in Table 1.

Chapter 2

Appendix 1. List of the samples of Euganean trachyte collected from Roman infrastructures in Veneto, reporting sampling site, type of infrastructure, sampled element and dating. Uncertain dating is generically indicated as "Roman age".

Appendix 2. Summary of the petrographic features of the archaeological samples of Euganean trachyte, with their possible provenance determined accordingly. Abbreviations of minerals according to Whitney & Evans (2010): Ano = anorthoclase; Ap = apatite; Aug = augite; Bt = biotite; Cal = calcite; Crs = cristobalite; Ep = epidote; Krs = kaersutite; Opq = opaque mineral; Pl = plagioclase; Qz = quartz; Sa = sanidine; Ttn = titanite; Zrn = zircon.

Appendix 3. Bulk-rock chemical composition of the archaeological samples of Euganean trachyte determined by XRF, with their possible provenance determined accordingly; major elements are expressed as oxide weight percent, LOI as weight percent, trace elements as ppm and concentrations below detection limit indicated by "b.d.".

Appendix 4. Chemical composition of phenocrysts of biotite, kaersutite, augite, Ti-magnetite, sanidine and anorthoclase in the archaeological samples of Euganean trachyte determined by LA-ICPMS, with their possible provenance determined accordingly; major elements are expressed as oxide weight percent, trace elements as ppm and concentrations below detection limit indicated by "b.d.". Different spot analyses on the same sample are reported, excluding outliers. Each worksheet contains the results of different phases and average values of the reference materials.

Appendix 5. V/Sc and Co/Sc complementary scatterplots for provenance recognition of Euganean trachyte using chemical composition of biotite (Ch. 1), determined on the archaeological samples by LA-ICPMS, using the isotopes in Appendix 4. For each sample (symbols as in Fig. 6), concentrations are averaged from multiple analyses. The fields indicated by dotted lines and the name of the quarry locality, drawn according to the position of the relevant quarry samples in Ch. 1, overlap or are very close to those of other localities: they cannot be used for univocal provenance attribution, but serve as reference for checking the position of unknown samples in multiple plots.

Chapter 3

Appendix 1. Trace-element chemical composition expressed as ppm of representative samples of Euganean trachyte from the Renaissance city walls of Padova determined by LA-ICPMS, on both surface (i.e., weathering crust or patina) and host rock (inner part). The samples are divided by different types of alteration and sampling location as in Fig. 3 (SCR = Bastione Santa Croce; GAR = Torrione dell'Arena; CSN = Bastione Castelnuovo; FST = Torrione Venier).